A SYSTEMS-INTEGRATION APPROACH TO OPTIMIZING THE WATER-ENERGY NEXUS IN ENERGY SURPLUS PROCESSES

A Dissertation

by

KERRON JUDE GABRIEL

Submitted to the Office of Graduate and Professional Studies of
Texas A&M University
in partial fulfillment of the requirements for the degree of

DOCTOR OF PHILOSOPHY

Chair of Committee,	Mahmoud El-Halwagi
Co-Chair of Committee,	Patrick Linke
Committee Members,	Sam M. Mannan
	Hisham Nasr-El-Din
Head of Department,	M. Nazmul Karim

December 2014

Major Subject: Chemical Engineering

ABSTRACT

The objective of this research was to develop novel tools for systematically optimizing the benefits of the water-energy nexus in processes with surplus energy. The developed approach consists of the following problems: (1) screening of the processes to identify potential for cogeneration of water and power, (2) development of a flexible water generating process, (3) synthesis of the integrated water and power generating facility and (4) thermoeconomic analysis of the integrated process.

In the screening problem, a targeting and benchmarking approach was used to identify the limits of the process for producing water and power from surplus energy. Various designs of the process were explored to compare the effects of process change on the overall targets for water and power generation.

For the water generating process problem, a new mathematical formulation was proposed for the thermal desalination of saline water. The new formulation consisted of a mass flowrate decoupling approach that reduced the overall mass and energy balances to a linear programming (LP) problem. This approach was used to develop novel and flexible Multi-effect distillation with thermo vapor compression (MED-TVC) processes that balanced the tradeoff between economics and thermal efficiency.

In the synthesis problem, an integrated water and power generating facility was developed based on the excess heat sources from the process. The synthesis approach incorporated the use of four building blocks: (a) Total site analysis to identify appropriate steam level connections in the process, (b) heat exchange network synthesis for producing steam and boiler feed water utilities from excess process heat, (c) turbine network development for power generation and (d) water generation and integration via direct recycle.

In the thermoeconomic analysis, the integrated facility from the synthesis approach was evaluated and optimized to maximize the intrinsic balance of the water-energy nexus. The analysis utilized extensive literature sources, fundamental chemical engineering practices as well as mathematical programming techniques to yield insightful conclusions.

The Gas-to-liquids process was strategically used as the case study to demonstrate the developed methodologies due to its ability to produce not only fuels and synthetic lubricants but potable water and power as part of its commodity portfolio.

DEDICATION

To my family: parents and siblings

ACKNOWLEDGEMENTS

I would like to thank my academic advisor Dr. Mahmoud M. El-Halwagi for his unwavering guidance, support and encouragement throughout this journey. He has contributed greatly to both my professional and personal development and I consider myself fortunate to have such a remarkable human being for an advisor during my master's and doctoral programs.

I am also grateful to Dr. Patrick Linke for providing his thoughts and insights for developing Chapter IV as well as Dr. Mannan and Dr. Nasr-El-Din for serving on my committee and sharing their suggestions for improving the quality and inclusiveness of this research work.

Thanks also go to my friends, colleagues, department faculty and staff for greatly enriching my experience at Texas A&M University. A special thank you to my dear friend Mohamed Noureldin for joining me on this journey as we navigated through the ebb and flow of graduate school; an experience that I am sincerely grateful for in our drive for professional success and overall development.

Finally, thanks to my parents, Judy Perichan-Gabriel and Dominic Gabriel as well as my siblings Kerryn Hinds and Kevorn Gabriel for their unconditional love, support and encouragement throughout my career. I am eternally grateful to my mother for her inspirational words which have helped to guide my decisions and foster a sense of humility and appreciation for my numerous blessings.

Financial support from Qatar National Research Fund (a member of Qatar Foundation), NPRP grant no. 4-1191-2-468 is gratefully acknowledged.

NOMENCLATURE

Abbreviations

ASPEN	Advanced Simulator for Process Engineering
CC	Capital Cost
DCC	Direct Capital Cost
HRS-TN	Heat recovery System- Turbine network
MINLP	Mixed Integer Nonlinear Program
OC	Operating Cost
RAM	Random Access Memory
SC	Soft Cost
TAC	Total Annualized Cost
TAP	Total Annual Profits
TCI	Total Capital Investment
TOC	Total Operating Cost

Defined sets

HPS	Set of hot process streams
US	Set of utility streams
SOURCE	Set of water sources
SINK	Set of water sinks
IMPURITY	Set of water impurities
N	Number of effects
Nc	Number of components

Defined indices

i	Temperature interval (Chapter II), Effect number (Chapter III), Heat exchange network hot process stream or Effect number (Chapter IV)
j	Utility stream stage
k	Component
m	Water source
n	Water sink

Subscripts and superscripts

a	Subscript denoting actual exit conditions
BF	Subscript denoting brine flashing
BFW	Subscript/ Superscript denoting boiler feed water stream
brine	Subscript denoting brine stream
c	Subscript/superscript denoting condensate stream
cond	Subscript/superscript denoting down condenser
DS	Subscript denoting de-superheater
EX	Subscript denoting exit conditions
exh	Subscript denoting exhaust conditions
extract	Subscript denoting extract conditions
f	Superscript denoting saturated water conditions
f '	Superscript denoting saturated water conditions in brine flashing
f ''	Superscript denoting saturated water conditions in distillate flashing
feed	Subscript denoting feed
header	Subscript denoting header conditions
is	Subscript denoting isentropic conditions
MED	Superscript referring to multi-effect distillation unit
mot	Subscript denoting motive
perm	Superscript referring to permeate stream
RO	Superscript referring to reverse osmosis unit
s	Subscript denoting salt
s'	Subscript denoting salt in brine flashing
sat	Subscript denoting saturated conditions
turb	Subscript denoting turbine unit
v	Superscript denoting vapor conditions
v'	Superscript denoting vapor conditions in brine flashing
v''	Superscript denoting vapor conditions in distillate flashing
vac	Superscript denoting vacuum conditions
WHB	Superscript denoting waste heat boiler unit

Units

ft	feet
GJ	Gigajoule
hr	hour
lb	pounds
kg	kilogram
kW	kilowatts
m	meter
MMBtu	Million British thermal units
ton	a metric weight, equal to 2,000 pounds
tonne	a metric weight, equal to 1,000 kilograms
yr	year

Variables

A_i	Heat transfer area in *i*th effect
A_{ij}	Area for heat transfer between *i*th HPS and *j*th US
$\overline{A}\left(\overline{\pi}\right)$	Membrane permeability
B_i	Brine flow from *i*th effect
BPE	Boiling point elevation
$\frac{\overline{C}_{fc}}{C_f}$	Log mean concentrate-side to feed concentration ratio in RO unit
D_i	Distillate mass flowrate from *i*th flash pot
Dr	Mass flowrate of entrained steam from final effect
DR	Design ratio for turbine
$DT_{i,j}^{in}$	Inlet temperature difference exponent between *i*th HPS and *j*th US
$DT_{i,j}^{out}$	Outlet temperature difference exponent between *i*th HPS and *j*th US
F	Flowrate
F_{pump}	Flowrate to pump

f_{ij}	Flowrate of *j*th utility stream for *i*th hot process stream cooling
f_j^c	Flowrate of condensate at *j*th utility stage conditions
$F_j^{BFW,boiler}$	Flowrate of boiler feed water from *j*th stage to boiler
$F_j^{stm,furnace}$	Flowrate of saturated steam from *j*th stage to furnace
FCp_i	Flowrate-heat capacity for *i*th hot process stream (HPS)
FF	Fouling factor of RO unit
G_n	Water flowrate from *n*th sink
h_s	Enthalpy of salt
h_w	Enthalpy of saturated water
H	Enthalpy of stream
$H_{BF,i}$	Enthalpy of stream associated with brine flashing in *i*th effect
H_{DS}	Enthalpy of steam from de-superheater
H_{EX}	Enthalpy of stream at exiting conditions
H_i	Enthalpy of stream in *i*th effect or flashing pot
H_{mot}^v	Enthalpy of motive steam to multi-effect distillation
H_{sat}	Enthalpy of stream at saturated conditions
H_{sea}^{salt}	Enthalpy of salt in feed seawater
H_{sea}^{water}	Enthalpy of water in feed seawater
ΔH_j	Enthalpy difference of *j*th utility stream stage
L	Plant life
$LMTD$	Logarithmic mean temperature difference
$\dot{m}$	Mass flowrate of stream
M	Mass flowrate of stream
$\dot{m}_{DESAL}$	Mass flowrate of desalinated water
$\dot{m}_{brine,EX}^{salt}$	Mass flowrate of salt in exiting brine stream
$\dot{m}_{brine,EX}^{water}$	Mass flowrate of water in exiting brine stream

$\dot{m}_{pot,i}^{stm}$	Mass flowrate of steam from flashing distillate in *i*th pot
$\dot{m}_{sea}^{BYPASS}$	Mass flowrate of bypass stream for cooling excess preheated seawater
$\dot{m}_{sea}^{PRE}$	Total preheated seawater
$\dot{m}_{sea}^{TOTAL}$	Total feed seawater to system
$\dot{m}_{sea,in}^{salt}$	Mass flowrate of salt in feed seawater to *i*th effect
$\dot{m}_{sea,in}^{water}$	Mass flowrate of water in feed seawater to *i*th effect
$\dot{m}_{sea,i}^{salt}$	Mass flowrate of salt from seawater in *i*th effect
$\dot{m}_{sea,i}^{stm}$	Mass flowrate of steam from seawater in *i*th effect
$\dot{m}_{sea,i}^{water}$	Mass flowrate of saturated water from seawater in *i*th effect
N	Number of effects
NEA_i^{brine}	Non-equilibrium allowance of flashing brine in *i*th effect
NEA_i^{flash}	Non-equilibrium allowance of flashing distillate in *i*th pot
NM	Number of modules
pf	Concentration polarization factor
P_f	Feed pressure to RO unit
P_p	Permeate pressure from RO unit
P^{Sink}	Sink pressure stream
P^{Source}	Source pressure of stream
PW_{pump}	Pumping power for stream
$\overline{\Delta P}_{fc}$	Average concentrate-side system pressure drop for RO unit
q_{ij}	Heat exchange between *i*th hot process stream and *j*th utility stream stage
Q	Heat exchanger duty
Q_i^{EVAP}	Evaporator duty in *i*th effect
Q_i^{sens}	Sensible heating duty of seawater in *i*th effect
Q_i^{vap}	Vaporizing duty of seawater in *i*th effect

Q^{PRE}	Preheating duty of seawater
Q_{xs}	Excess cooling duty
$\overline{R}$	Average salt rejection of RO unit
S	Steam mass flowrate
SM	Module surface area of RO unit
T	Temperature
T_{sea}^{hot}	Temperature of preheated seawater
T_i^{eff}	Temperature of brine in *i*th effect
T_i^{flash}	Temperature of flashed distillate in *i*th pot
$TH_{i,j}$	Inlet temperature of *i*th hot process stream (HPS) at *j*th utility stream (US) stage
$TCIN_j$	Inlet temperature of *j*th utility stream
$TCOUT_j$	Outlet temperature of *j*th utility stream
TIN_i	Inlet temperature of *i*th hot process stream (HPS)
$TOUT_i$	Outlet temperature of *i*th hot process stream (HPS)
$SUMDT_{i,j}$	Sum of temperature differences exponent between *i*th HPS and *j*th US
TCF	Temperature correction factor or RO unit
ΔT_i^{losses}	Temperature loss of saturated steam from *i*th effect
ΔT^{eff}	Temperature difference between effects
$\Delta T_{Cool\ fluid}$	Operating temperature difference of cooling fluid
U	Heat transfer coefficient of heat exchanger
U_{ij}^{HEN}	Heat transfer coefficient between *i*th HPS and *j*th US
U_i^{eff}	Heat transfer coefficient of evaporator of *i*th effect
V_i	Vapor flow from *i*th effect
W_m	Water flowrate from *m*th source
$w_{m,n}$	Water flowrate from *m*th source to *n*th sink
W_{shaft}	Shaft work of turbine

X	Salt concentration in feed to RO unit
X_i^{MAX}	Maximum concentration of brine in *i*th effect
Y	Recovery of RO unit
$y_{m,k}$	Concentration of *k*th impurity in *m*th water source
$z_{n,k}^{in}$	Allowable concentration of *k*th impurity in *n*th water sink
ρ	Density of fluid
π_f	Osmotic pressure of seawater feed to RO unit
λ	Latent heat of vaporization

Parameters

Cp	Specific heat capacity
C_{power}	Cost of power
C_{water}	Cost of water
T^{EX}	Exiting temperature streams
T_{sea}^{avg}	Average preheated seawater temperature
T_{sea}^{MAX}	Maximum seawater discharge temperature
$T_{sea,pre}^{MAX}$	Maximum preheated seawater temperature
$\Delta T_{\min}^{HEX}$	Minimum heat exchange approach temperature
X_{sea}^{IN}	Concentration of seawater
$z_{n,k}^{\max}$	Maximum allowable concentration of *k*th impurity in *n*th water sink
$z_{n,k}^{\min}$	Minimum allowable concentration of *k*th impurity in *n*th water sink
η	Unit efficiency

TABLE OF CONTENTS

Page

Page

LIST OF FIGURES

Page

Page

LIST OF TABLES

Page

Page

Page

CHAPTER I
INTRODUCTION

The water-energy nexus continues to gain traction around the world as the implications of the relationship bolsters the notion that regional and global economic sustainability cannot consider both resources independently. The production phases of energy in its various forms require large volumes of water while the extraction, treatment and distribution of water for various human uses then treatment and return of the waste water to the environment, require some quantity of energy. This inextricable link cannot be ignored as population and economies continue to grow and expand respectively.

Historically, water and energy system interactions have been considered on a case-by-case basis with no holistic and systematic approach to identifying the opportunities or impacts of the link. This is the case with the recent and aggressive development of domestic unconventional oil and gas which have resulted in significant volumes of water being used for production spurred on by hydraulic fracturing and improved horizontal drilling technologies. While the demand for these valuable energy resources has promoted growth in that industry, the associated water implications have resulted in a complex national discussion on the future sustainability of the activity.

In addition to the oil and gas industry, there are many other factors that affect the water-energy balance. These include climate change as well as population migration to areas that are already water stressed but provide economic advantages. Such activities will continue to affect the management strategies for supplying both water and energy resources. In addition, governmental regulations such as zero liquid discharge in some regions may impact the sustainability of expanding industrial activities.

These factors present many challenges though they also provide research opportunities that can transform the future of industries heavily vested in water-energy systems.

The objective of this research is to develop a novel methodology for systematically identifying and optimizing the water-energy nexus for generation of both resources.

The procedure consists of the following steps: (1) screening of processes to identify potential for cogeneration of water and power, (2) development of novel configurations for which water can be generated via desalination technologies, (3) synthesis of integrated water and power cogeneration facilities and (4) thermoeconomic analysis of the integrated process. The approach is demonstrated using the Gas-to-liquid (GTL) process that has gained interest due to its application in monetizing the abundant domestic shale gas. The first step and second step are developed in chapter II and III respectively while the third and fourth will be addressed in chapter IV.

CHAPTER II

TARGETING OF THE WATER-ENERGY NEXUS IN GAS-TO-LIQUID PROCESSES: A COMPARISON OF SYNGAS TECHNOLOGIES*

2.1 Introduction

The growing global population and expansion of economies continue to have a direct effect on the demand for energy and water resources. The increasing energy demand coupled with more stringent environmental regulations and depleting crude oil reserves have prompted interest in seeking cleaner and abundant alternatives for energy supply such as natural gas. According to the International Energy Agency (IEA) [1], the demand for natural gas is expected to grow to more than 50% by 2035, thus overtaking the coal global energy share. This increased usage of natural gas will come from many different sources depending on regional political environments, technological advancements in recovery and holistic cost of gas field development. The choice of developing these gas resources is mostly a function of the available markets and financial investments in converting the gas to market-ready products.

The current exportation of natural gas to markets is commonly done via pipeline and liquefaction (LNG). The growing cost of transportation fuel and increasing gap in the cost of crude oil and gas on energy content basis has promoted the evaluation of FT-based GTL processes. The GTL process presents a viable option for gas producing countries to diversify their exportation portfolio [2]. This chemical liquefaction technique produces sulfur free transportation fuels with a high cetane number suitable for blending or as a direct fuel for combustion engines [3,4].

The FT-based GTL process employs three major stages: the synthesis gas (syngas) production section, the FT reaction section, and the FT product upgrading section. Within each section, the process design and operational philosophy can vary depending on the requirements for marketable products [5]. In specific, the syngas production section is of utmost importance since it supplies the rest of the process with the desired composition for operation. The available technologies for achieving this desired composition are partial oxidation (POx), steam methane

---

reforming (SMR) and autothermal reforming (ATR) which is a thermodynamic combination of the former two technologies. These syngas production configurations have been successfully implemented by various industrial entities [6-8], though there is little understanding of the heuristics in utilizing any of the configurations and the water-energy implications on the rest of the process.

Previous studies have been done to evaluate the potential for carbon dioxide capture and conversion to GTL products [9]. Other works have evaluated optimal carbon dioxide removal unit locations in the GTL process to minimize product loss and effects of inerts on FT reactor operation [10]. In previous studies, detailed simulations of the GTL process with a selected design for heat recovery and power generation have been done [11]. In other studies a basic representation of the GTL process with a single syngas technology choice has been developed, along with heat integration and economic insights [12].

A study by Martinez et al. [13] provided benchmarks and macroscopic insights into the overall water and energy requirements of the GTL process based on various syngas production technology choices. In contrast, the typical approach to evaluating GTL processes has been to select a syngas technology route followed by heuristic selection of FT catalyst and basic upgrading philosophy. This approach provides a singular view of the water and energy implications of the GTL process given the availability of three different syngas technologies. The objective of this paper is to evaluate the GTL process for various syngas technologies as it relates to heat, mass, power and greenhouse gas emissions. It differs from previous research [13] in that it incorporates targets for power generation and adds fresh water production via a multi-effect distillation (MED) desalination technology. In addition, the greenhouse gas footprint is evaluated as a function of emissions from the process itself and from fuel combustion as well as credits from power production.

2.2 Process background

The GTL process can be divided into three sections, namely synthesis gas production and conditioning, FT reaction, and FT product upgrading and separation. The interrelationship of each section within the overall GTL process scheme is shown in Figure 1. Apart from the individual sections, there are numerous possibilities for recycling of material to achieve maximum natural gas conversion and energy utilization.

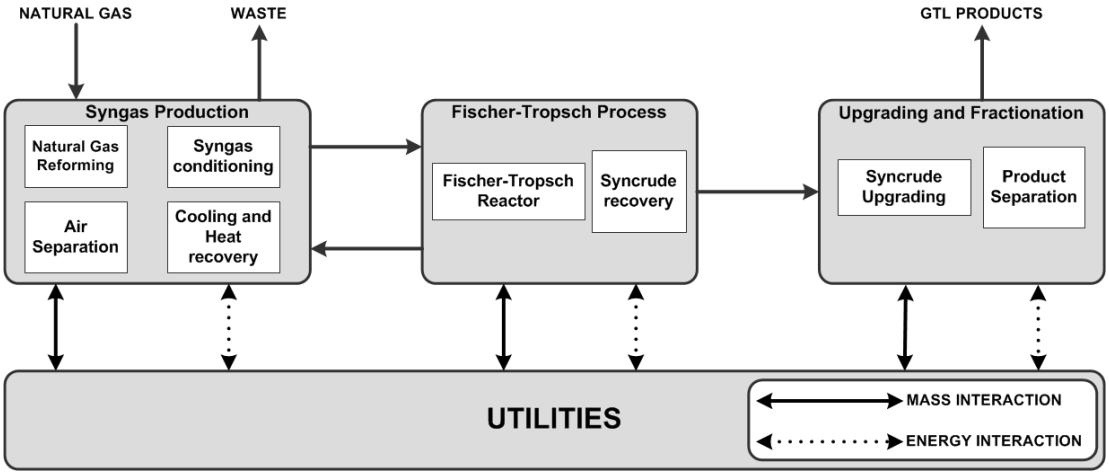

Figure 1 Overall Gas-to-Liquids block flow diagram

2.2.1 Natural gas cleaning

The catalysts for most industrial gas reforming processes are nickel-based. These catalysts can be easily poisoned by sulfur and halogen containing compounds [14]. To remove these compounds, a two-step process is employed. The process involves the hydrogenation of the natural gas to remove traces of unsaturated hydrocarbons and to convert sulfur compounds into hydrogen sulfide. The halogen-containing compounds are hydrogenated to their corresponding hydrogen acids. The hydrogenation step is conducted using NiMo / Al_2O_3 or CoMo / Al_2O_3 catalyst, after which hydrogen sulfide is easily removed to extremely low levels via the use of ZnO in the second step. The process is normally carried out at 350 – 400°C [5].

2.2.2 Natural gas reforming

Natural gas is converted to synthesis gas via two main reforming operations, steam reforming and adiabatic oxidative reforming. The inherent difference between both concepts is the approach to supplying energy for the reactions. The steam reforming process is a nickel based catalytic process that requires externally supplied heating to drive the reaction. Adiabatic oxidative reforming can be either catalytic or non-catalytic, with the use of heat generated from the partial oxidation reaction [15]. For the steam reforming reaction, Equations 1 - 2 describe the endothermic conversion of natural gas to synthesis gas in the presence of carbon dioxide.

$$CH_4 + H_2O \longleftrightarrow CO + 3H_2, \qquad \Delta H_{298K} = +206\ kJ \cdot mol^{-1} \tag{1}$$

$$CH_4 + CO_2 \longleftrightarrow 2CO + 2H_2, \qquad \Delta H_{298K} = +247\ kJ \cdot mol^{-1} \tag{2}$$

Similar reactions for the partial oxidation of methane to synthesis gas are given by Equation 3 [16].

$$CH_4 + 0.5O_2 \longleftrightarrow CO + 2H_2, \qquad \Delta H_{298K} = -36\ kJ \cdot mol^{-1} \tag{3}$$

The combination of the steam reforming and partial oxidative reactions yields a special approach to methane reforming known as autothermal reforming. In this case there is partial combustion of the hydrocarbon feed to balance the endothermic requirements of the steam reforming reactions. This partial combustion reaction is given by Equation 4.

$$CH_4 + 1.5O_2 \longleftrightarrow CO + 2H_2O, \qquad \Delta H_{298K} = -519\ kJ \cdot mol^{-1} \tag{4}$$

In all processes, the water gas shift reaction takes place which is given by Equation 5.

$$CO + H_2O \longleftrightarrow CO_2 + H_2, \qquad \Delta H_{298K} = -41\ kJ \cdot mol^{-1} \tag{5}$$

The final composition of the synthesis gas is dependent on a thermodynamically equilibrated combination of all the above-mentioned reactions.

2.2.3 Synthesis gas conditioning

The synthesis gas produced from natural gas is typically sulfur free and requires no additional sulfur removal processes. In contrast, syngas contains carbon dioxide (CO_2), which may require removal steps depending on the design of the FT gas loop. The process of CO_2 removal operates under the basic principle of selective absorption. In industry the process is mainly called acid gas removal, and is widely used in petroleum refineries. There are two types of acid gas removal processes namely chemical absorption and physical absorption. Both techniques have their merits, though for this study the chemical absorption route was chosen. For the chemical absorption route, Diethanolamine (DEA) is used as the absorption solvent. The previous study by Martinez et al. [13] did not consider the detailed simulation of CO_2 removal unit, which may represent a significant heat sink for amine regeneration.

The composition of the syngas from each reforming technology is different, thus requiring various adjustments or conditioning steps to meet the H_2:CO requirements of the FT reaction section. The workhorse for this conditioning step is the water gas shift (WGS) reaction for syngas compositions below the requirements of the FT reaction. For compositions above the FT requirements, a combination of membrane and adsorbent techniques were assumed for this work.

2.2.4 Fischer-Tropsch reaction

The Fischer Tropsch (FT) reaction is an overall process for converting synthesis gas (carbon monoxide and hydrogen) to synthetic crude oil (syncrude). The FT synthesis reaction is highly exothermic with an average heat release of 140 – 160 kJ.mol^{-1} converted CO [5]. It can be described by the two main reactions given by Equations 6 - 7.

$$\text{Alkenes: } nCO + 2nH_2 \longleftrightarrow (CH_2)_n + nH_2O \quad (6)$$

$$\text{Alkanes: } nCO + (2n+1)H_2 \longleftrightarrow H(CH_2)_n H + nH_2O \quad (7)$$

The product distribution of the syncrude can be modeled using the Anderson-Schulz-Flory (ASF) distribution shown by Equation 8.

$$x_n = (1-\alpha)\cdot\alpha^{(n-1)} \quad (8)$$

Where x_n represents the molar fraction of each carbon number (n) and the alpha (α) value is the chain growth probability, which is a direct measure of the likelihood for a FT catalyst to catalyze chain propagation, as opposed to chain termination. Despite the mathematical simplicity of Equation 8, studies have shown that there is deviation of the syncrude composition from the ideal ASF distribution [17-19]. In this case multiple alpha values are used to describe the syncrude composition [20].

There is a strong dependence of the alpha value on both catalyst type and operating conditions. The catalyst type plays a more dominant role in the overall alpha value. This has led to a number of studies investigating the performance of various catalysts types in the overall FT reaction [21-26]. Of the various potential catalyst types only Iron (Fe) and Cobalt (Co) based catalyst are commercially used. Both catalyst types have different hydrogenation activities, with Fe being more active than Co. This results in the products of Fe based catalyst being more olefinic and containing oxygenates [5] in comparison to products from Co based catalyst, which are more paraffinic. In addition, Fe based catalyst can catalyze the WGS reaction while Co based catalyst show little activity for this reaction. This feature provides a wider operating range for the Fe based catalyst in terms of syngas composition, and thus has tremendous implications on the gas loop design [25]. The choice of catalyst therefore depends on the desired products and downstream refining capabilities.

The operating conditions of the FT synthesis process can be manipulated to effect changes in the ASF distribution. Increasing temperature results in an increase in hydrogenation as well as product desorption rates from catalysts. The dominating process is the desorption rate, which

results in a net increase in chain termination to less hydrogenated products such as alkenes and oxygenates [5]. This equates to a lower alpha (α) value. In addition, higher operating pressures promote reactant adsorption to catalyst, thus increasing observed α-value of the catalyst.

There are several reactor designs that can be implemented for FT synthesis. The most recent industrial implementations incorporate slurry bed and tubular fixed bed designs [6,8]. For these reactor designs there are two commercially accepted operating temperature ranges, namely Low Temperature FT (LTFT) and High Temperature FT (HTFT). Their corresponding temperature ranges are 220 – 240ºC and 300 – 350ºC respectively. In addition, the typical operating pressure range is 2 – 2.5 MPa [2,27].

The observed alpha value has a direct effect on the H_2:CO usage ratio. As illustrated by Equations 6 - 7, longer chain hydrocarbons would have a usage ratio closer to 2 with an increasing value expected for shorter chain hydrocarbons. The syngas composition should therefore be close to the usage ratio so as not to affect the FT reactor performance during synthesis.

2.2.5 Syncrude refining

The upgrading or refinery design for the GTL process can be simple or complex depending on the desired end products. For this study we have followed the philosophy of the Sasol Oryx GTL plant in producing only intermediate products and LPG [5]. As such, the refinery design consists of only a hydrocracking unit for upgrading long chain paraffinic compounds. For the hydrocracking process, there are a number of studies that focus on detail modeling of the numerous reactions that simultaneously occur [28-32]. For this study we have assumed a normal distribution model that may serve to describe the reactions. The objective of the model is to simply quantify the magnitude of heating and cooling requirements for the process. Previous works by Martinez et al. [13] do not consider this section of the process simulation, which may have an effect on the overall energy integration potential.

For the simplified model, we assume that all C_{20}^{+} hydrocarbons are cracked into smaller chain molecules. The products from the cracking process follow an ideal normal distribution. Equations 9 - 11 provide an example of a cracked long chain molecule.

$$C_{20}H_{42} + H_2 \longrightarrow 2C_{10}H_{22} \quad (9)$$

$$C_{20}H_{42} + H_2 \longrightarrow C_9H_{20} + C_{11}H_{24} \quad (10)$$

$$C_{21}H_{44} + H_2 \longrightarrow C_{10}H_{22} + C_{11}H_{24} \quad (11)$$

The normal distribution curve for the products is truncated at a standard deviation of four (4), which represents four (4) carbon numbers above and four (4) carbon numbers below the mean product from hydrocracking.

2.3 Problem statement

Given a GTL process with three different technologies for syngas production and common downstream processing units, it is desired to develop targets for maximum heat and mass integration, as well as power and water production. The issues to be addressed are as follows:

- What are the opportunities for heat and mass integration for each syngas technology? How do the opportunities differ for each technology?
- What are the power and water generation opportunities for each technology?
- What are the water usage implications of each technology based on process and cooling requirements?
- What are the GHG emission implications of each technology choice?
- What basic design philosophies can help improve performance of each technology?

2.4 Methodology and approach

For this study, special attention has been devoted to the design of the GTL process, thus expanding on the opportunities for integration and insights for possible investor decisions. The hierarchal approach used here for obtaining targets and benchmarking the GTL process is given by the following steps:

- Develop the overall GTL flow sheet for all three syngas technology cases from literature and public data sources.
- Simulate each GTL flow sheet using ASPEN Plus and PROMAX
- Extract hot and cold stream data and apply thermal pinch analysis
- Develop basic integrated power and water generation flow sheet
- Utilize excess heat from alternative GTL process sources and thermal pinch analysis to determine the power and water generation targets. An LP formulation is used for this procedure.
- Identify final minimum heating and cooling for each GTL flow sheet and use mass integration techniques to establish overall water management targets.

2.5 Process development

There has been a shift in the commercial use of Fe-based catalyst to Co-based catalysts due to improved yields and upgraded product properties [28]. Employing various FT reactor designs as well as FT gas loop configurations has had some impact on liquid product yield, though the choice of syngas technology plays a more dominant role when identifying process integration opportunities. For this work, we consider a constant design for the FT reaction section and syncrude upgrading section, and evaluate the effects of the various syngas production technologies on the overall benchmarks for heat and mass integration as well as power and water generation. We assume a natural gas feed with the characteristics shown in Table 1.

The base case flow sheets with the three syngas production technologies, namely Autothermal reforming (ATR), Partial Oxidative reforming (POx) and Steam methane reforming (SMR), were developed and simulated using ASPEN Plus. The SRK – Kabadi-Danner (SRKKD) thermodynamic property package was used to account for the liquid-liquid interactions in hydrocarbon-water systems. For each technology the syngas ratio was selected as 2.15. This value corresponds to the H_2:CO usage ratio for a Co-based LTFT reaction [33]. In addition, the GTL liquid product capacity was set as 50,000 bbl/day, which would yield a suitable return on investment [12].

Table 1 Natural gas conditions for this study

Component	**Composition** (mol%)
Methane	95.39
Ethane	3.91
Propane	0.03
Carbon dioxide	0.59
Nitrogen	0.08
Temperature [^{o}F]	79
Pressure [psia]	310

2.5.1 Syngas production flowsheet

The syngas production section consists of three main unit operations, namely the saturator, pre-reformer and reformer. The natural gas fed to the syngas production unit is first compressed to reforming reactor pressure, then heated to 300 ^{o}F before transfer to the saturator, where the natural gas is saturated with process water [34]. This unit is followed by the pre-reformer, which is used to convert long chain hydrocarbons into CO, H_2 and CH_4. This unit operation provides a preventative measure for coke formation in the reforming unit [5,35]. The exiting stream from the pre-reformer is mixed with recycled FT tail gas, saturated high pressure (HP) steam at reformer pressure and carbon dioxide and then heated in a fired heater before sending to the reforming unit. The ratio of steam or carbon dioxide addition would depend on the type of reformer being employed. For this study CO_2 is assumed to be obtained from the CO_2 removal unit, and not from outside of the process as in previous studies [13]. These steps represent the general process flow of the syngas production section. The standardized syngas unit configuration for all reformer choices is illustrated in Figure 2.

2.5.1.1 Autothermal reforming (ATR) option

For the ATR base case configuration, the reformer pressure was set to 435 psia, in agreement with industrial practice [5]. The stream exiting the pre-reformer is combined with FT tail gas and HP steam and sent to the fired heater. This heated stream is sent to the gas reforming unit, where compressed oxygen is also fed at an O_2 to Carbon ratio of 0.6. The reformer is operated adiabatically, and the outlet temperature is controlled to 1949 ^{o}F by adjusting the heat input from the fired heater. The syngas ratio from the reformer is adjusted to 2.15 by manipulating the steam to carbon ratio before the fired heater. The exhaust from the reformer is sent to a heat recovery and cooling unit in the syngas conditioning section, where process water is separated out in a vapor-liquid separator. The conditioning section is used to adjust the syngas composition to meet FT requirements. Its process flow steps are described in a later section.

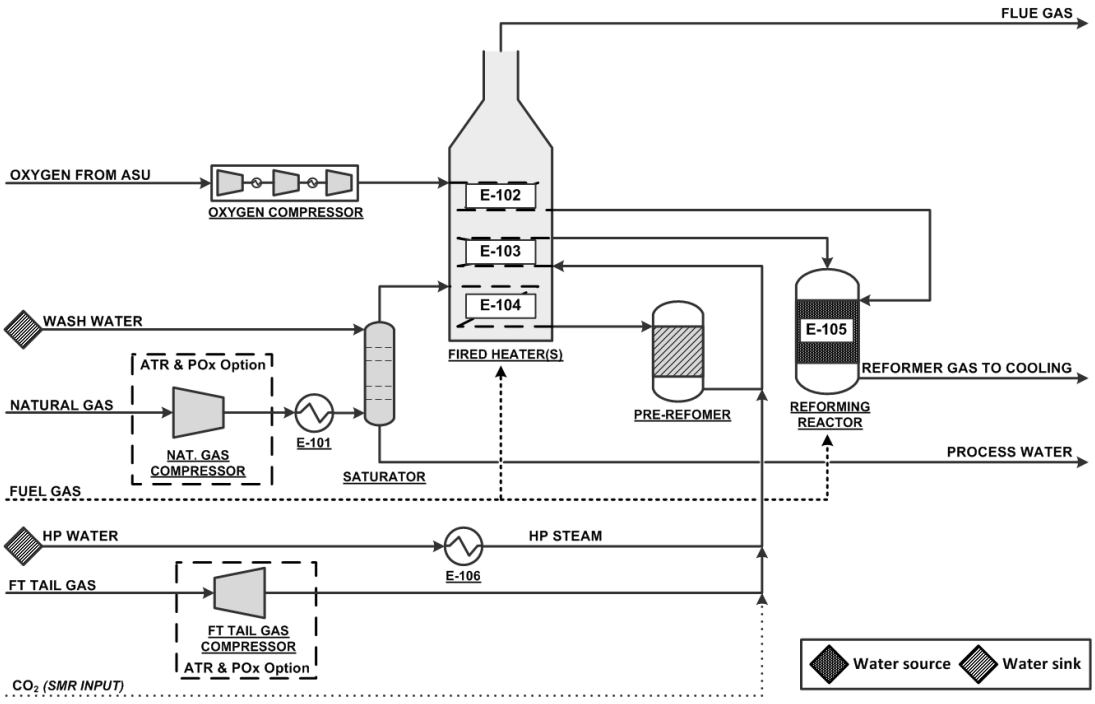

Figure 2 Standardized Syngas production unit

2.5.1.2 Partial Oxidative reforming (POx) option

For the POx base case configuration, the reformer pressure was set to 435 psia, which also corresponds to industrial practice [5]. The stream exiting the pre-reformer is combined with FT tail gas and sent to the fired heater. This combined stream is sent to the gas reforming unit, where compressed oxygen is also fed at an O_2 to Carbon ratio of 0.65. The reformer is operated adiabatically, adjusting in this case the outlet temperature to 2372 ^{o}F with the heat obtained from the fired heater. The exhaust from the reformer is treated as in the previous case. The cooled syngas ratio is below the 2.15 value required by the FT reaction, but it is adjusted in the subsequent conditioning section.

2.5.1.3 Steam methane reforming (SMR) option

For the SMR base case configuration, the reformer pressure was set to 300 psia [5]. The operating pressure of the SMR reactor is lower since the reaction is favored by these conditions. The natural gas compressor is therefore not needed, though a downstream syngas compressor would be required. The stream exiting the pre-reformer is combined with FT tail gas, HP steam and carbon dioxide and sent to the fired heater. The steam is added at a H_2O to carbon ratio of

2.5, while the carbon dioxide addition is given by the conditioning section. The CO_2 is added to reduce the H_2:CO ratio of the syngas. This combined stream is sent to the gas reformer operated at 1600ºF. The endothermic SMR reaction is maintained isothermally via external heating from fuel gas. The exhaust from the reformer is treated as in the previous case. The syngas ratio is above the 2.15 value required by the FT reaction, but is adjusted in the subsequent conditioning section.

For all syngas production configurations and reforming options, the saturator was rigorously modeled using the RADFRAC block in ASPEN Plus, while the pre-reformer and reformer were modeled as Gibbs minimization reactions using the RGIBBS block. The process water leaving the vapor-liquid separator is sent to the waste water pretreatment unit. This unit is illustrated in Figure 3 and incorporates the use of distillation columns that are rigorously modeled with the RADFRAC block in ASPEN Plus. The pretreated water leaving this unit is considered to have minimal impurities and will be used later in the water integration approach.

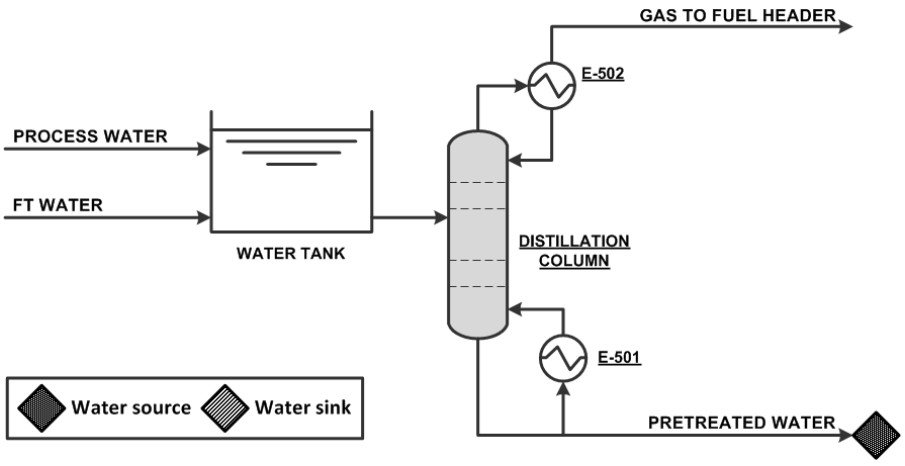

Figure 3 Waste-water pretreatment section for GTL process

2.5.2 Syngas conditioning

The syngas H_2:CO ratio from each reforming technology is evidently different and requires various conditioning methods. For all reforming options, a CO_2 removal unit was used to reduce overall inert concentrations in the feed to the FT reactor. For the CO_2 removal unit the typical industrial design for a diethanolamine (DEA) based chemical absorption process was used. For this process, the syngas is fed to an absorption column where DEA is fed counter-currently to chemically react with the CO_2 gas. The rich amine stream leaving the bottom of the absorption column is sent to a stripping column where CO_2 is removed to reproduce a lean amine stream. The stripped CO_2 stream leaving the stripping column is saturated with water and represents the major loss of water in this process. Make-up water is added to the lean amine stream to maintain its concentration (30 wt %), after which it is further cooled and recycled to the absorption column.

The process was modeled in PROMAX, with estimates for DEA recirculation flow rate and process operating conditions given by literature [36].The flow sheet is illustrated in Figure 4. The removed CO_2 is vented to the atmosphere or recycled to the syngas production unit depending on the reforming technology choice. For the SMR base case, the input CO_2 represents 50% of the removed CO_2 from the total syngas stream.

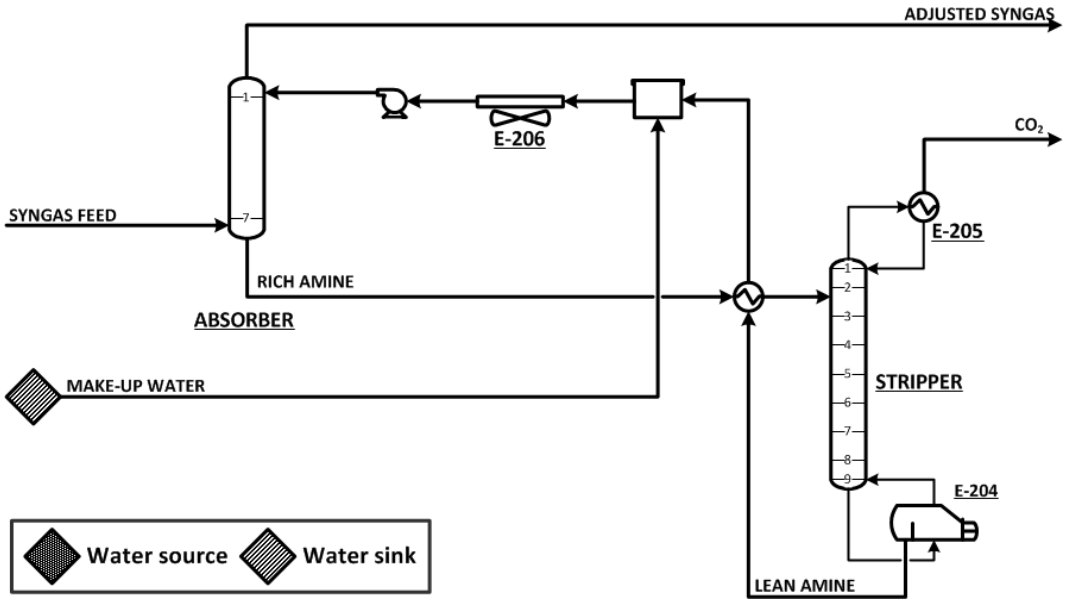

Figure 4 PROMAX simulation of **c**arbon-dioxide removal system using Diethanolamine (DEA)

For the SMR base case with a syngas H_2:CO ratio higher than the required 2.15 value, this study assumes that the syngas can be adjusted via the separation of hydrogen at 50°C using a series of membranes [37,38]. In ASPEN Plus this is modeled as a combination of component splitters, mixers and splitter blocks. The hydrogen rich gas is assumed to contain 98% hydrogen and 2% of methane, carbon monoxide, nitrogen and water combined. This hydrogen-rich gas is then sent to a Pressure swing adsorption (PSA) unit to recover hydrogen for use in other sections of the process. The PSA is modeled as a component splitter block in ASPEN Plus. The PSA is assumed to recover 87% of the hydrogen with a purity of 99.99% [39,40]. The PSA tail gas is sent to the fuel header.

For the POx base case with a lower syngas ratio than the required 2.15 value, this study utilizes the WGS reaction to increase hydrogen composition. The syngas is first heated to 572°C, after which it is co-fed with steam to a WGS reactor. The steam flow rate is manipulated to adjust the syngas ratio to the desired 2.15 value. The WGS reactor is modeled as a REQUIL block in ASPEN Plus. For hydrogen supply to the rest of the process, a small stream of the adjusted syngas is separated and sent to a PSA unit. The performance and modeling of the PSA unit is similar to that described for the SMR base case.

For the ATR base case, the syngas H_2:CO ratio is at the required 2.15 value due to upstream process adjustments. For this case there is no need for a hydrogen adjustment step. For hydrogen supply to the rest of the process, a similar procedure as that applied for the POx case is utilized. The overall flow sheet for the syngas conditioning section with all options is illustrated in Figure 5.

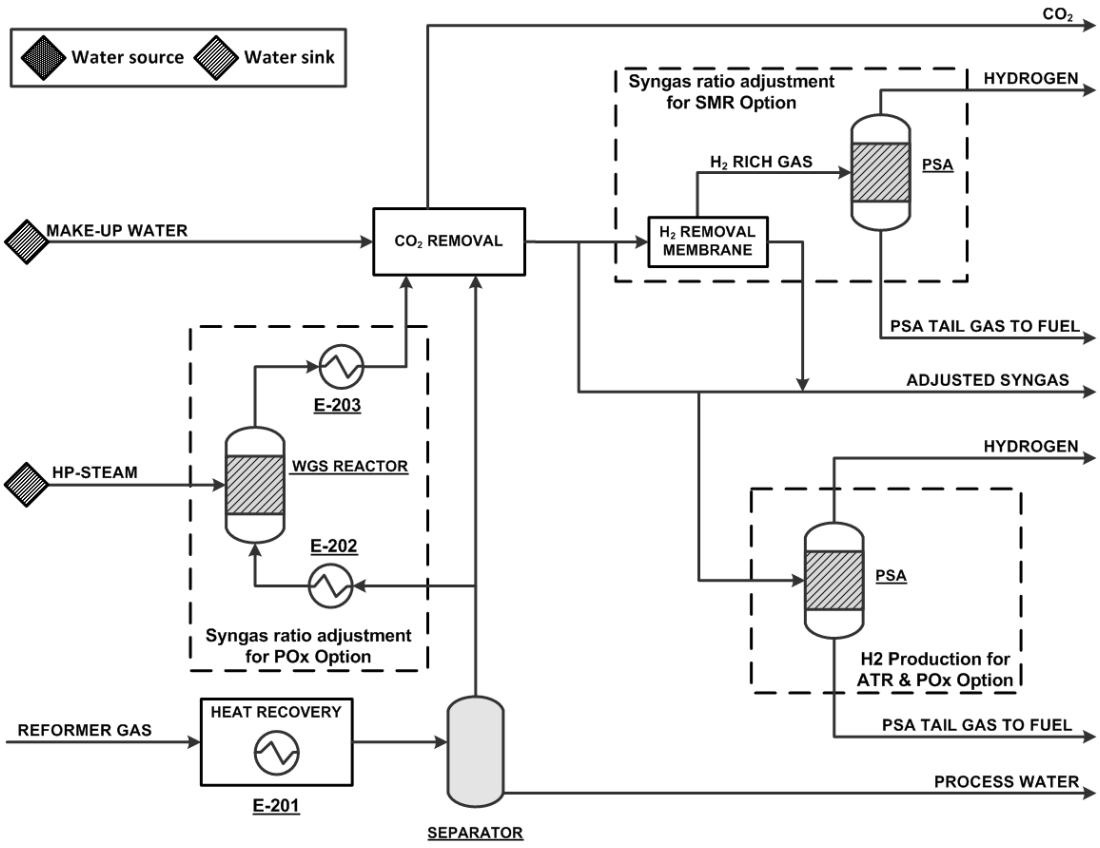

Figure 5 Syngas conditioning section

2.5.3 Fischer-Tropsch reaction

The FT reaction section is common to all syngas configurations. The reactor is chosen to be a slurry bed reactor operating at 428 ^{o}F and 363 psia [41,42] with a Co-based catalyst having an α-value of 0.92 [42,43]. For this high alpha value, the product distribution is expected to be mostly paraffinic with a carbon number range of one (C1) to one hundred (C100). Due to convergence issues with ASPEN Plus C30+ hydrocarbons are lumped [12]. The α-value is used along with Equation 8 to reverse calculate the stoichiometric coefficients of all the paraffinic hydrocarbons from C1 to C100, which are subsequently adjusted for the C30+ lumping assumption. A RSTOIC block is used to model the FT reactor in ASPEN Plus with a per pass conversion of 70% [35,44].

In this study the adjusted syngas is fed directly to the FT reactor without preheating, since the high exothermic nature of the reaction coupled with high heat transfer rate of the slurry bed

reactor ensures quick temperature equilibration [5]. For the SMR option, a syngas compressor is used to increase the feed pressure to FT reactor conditions. The FT reactor is operated isothermally by producing medium pressure steam (MPS) to remove heat generated by the highly exothermic reaction [42]. The FT reactor vapor is sent to a heat recovery and cooling unit, after which it is sent to a three phase separator to remove condensed hydrocarbons and process water. The vapor leaving the three phase separator, namely the FT tail gas, is sent to the syngas unit and fuel header at a 1:1 ratio. The process water leaving the three phase separator is sent to the waste water pretreatment unit as illustrated in Figure 3. The condensed hydrocarbon stream and liquid wax stream from the FT reactor are sent to the syncrude refining section. The overall FT synthesis section is illustrated in Figure 6.

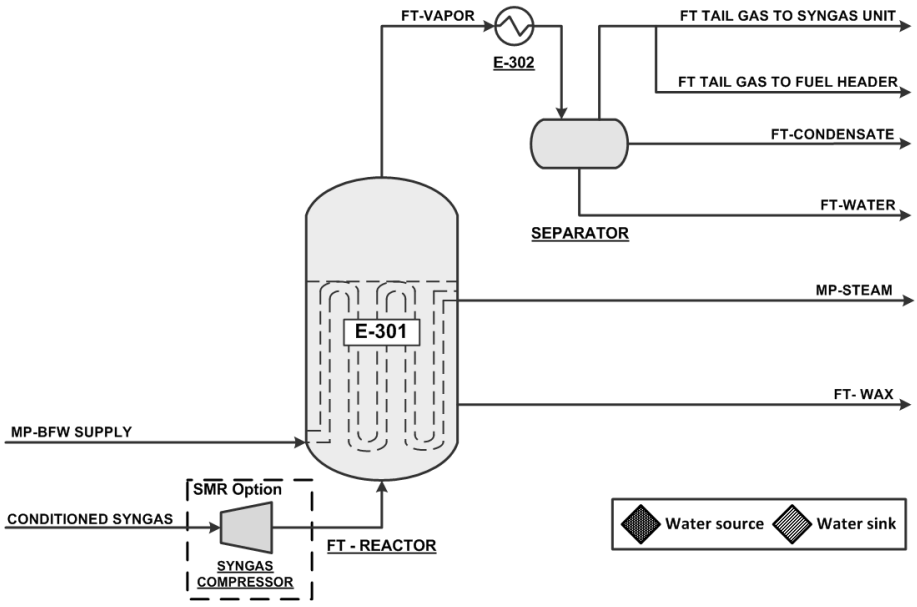

Figure 6 The FT synthesis and product recovery section

2.5.4 Syncrude refining

The syncrude refining section receives both condensed hydrocarbons (FT-condensate) and liquid wax (FT-wax) streams. These two streams are combined, pumped to the hydrocracker reactor pressure of 1015 psia and heated to 662 ^{o}F. The heated feed is co-fed with recycled wax and hydrogen gas at reactor pressure [45]. The typical per pass conversion of the hydrocracker is

65% [30,46,47]. The product from the hydrocracker is cooled to 400 °F and sent to a vapor-liquid separator. The vapor product is further cooled to 122 °F and sent to a flash tank operating at 55 psia to recover as much hydrogen for recycle. The liquid streams from both separators are combined, heated in a fired heater and sent to the fractionation column as partial vapor feed. The hydrogen rich gas leaving the cold separator is combined with fresh hydrogen from the syngas conditioning section, compressed and sent to the hydrocracker. Some of the hydrogen rich gas from the cold separator is purged to prevent inert build up in the gas loop.

The fractionation column is rigorously modeled using the RADFRAC block in ASPEN Plus. The column bottom vapor feed comes from the preceding fired heater. The condenser is designed to produce both vapor and liquid distillate, and is operated at a set temperature of 302 °F. The liquid distillate is cooled to 122 °F and represents the final GTL liquid product. The unconverted waxy bottoms stream is pumped and recycled to the hydrocracker [45]. The vapor distillate stream is sent to the fuel gas header. The overall syncrude refining section is illustrated in Figure 7.

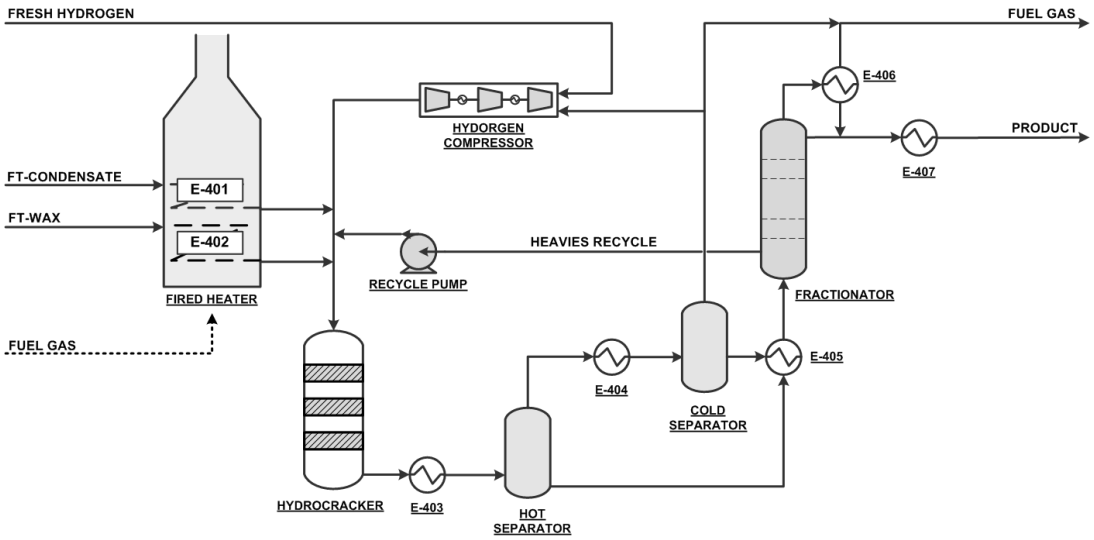

Figure 7 Syncrude upgrading and product fractionation section

2.6 Power and water generation

For this study, a thermal pinch analysis was done to identify the minimum process heating and cooling requirements. The minimum cooling requirement of the process is reduced by producing superheated steam at 1500 psia and 596 ^{o}F [48]. This steam is let down through a back pressure steam turbine to produce power for the GTL process. The turbine is assumed to have an isentropic efficiency of 70%. The overall generation efficiency is assumed to be 90%. This value includes the mechanical, generation and transmission efficiency. Any excess power is sent to the grid. The exhaust steam at 1 atmosphere is sent to a multi-effect distillation (MED) unit for water production. The capacity of the MED unit is 280,000 m^3/day (12,860 tons/ hr) which is typical for a commercial scale desalination plant. Any excess exhaust steam not utilized by the MED unit is cooled to boiler feed water conditions. Figure 8 illustrates the proposed design for the integrated power and water generation process. For this study the heating and electrical energy required by the MED to produce desalinated water is 1.8 kWh/ton and 115 Btu/lb respectively [49].

To determine the flow rate of the superheated steam a simple linear programming (LP) formulation is used. The formulation is shown below and solved to optimality via the use of the LINGO® software.

$$\max \sum_{i=1}^{n} H_{stm,i} \tag{12}$$

$$R_i = H_{hot,i} + R_{i-1} - H_{cold,i} - H_{stm,i} \tag{13}$$

$$H_{stm,i} = \dot{m}_{stm} \times \Delta h_i \tag{14}$$

$$R_i \geq 0 \tag{15}$$

$H_{hot,i}$: Hot streams' heat into interval "i"

$H_{cold,i}$: Cold streams' heat removal from interval "i"

R_i : Residual heat from interval "i"

$H_{stm,i}$: Heat into steam from interval "i"

$\dot{m}_{stm}$: Mass flow of steam

Δh_i : Enthalpy change for steam in interval "i"

For this study, we recognize that there is potential for greater heat recovery in the form of steam production at lower pressure levels; however, without neighboring plants or processes to utilize it, there is no value or incentive for production.

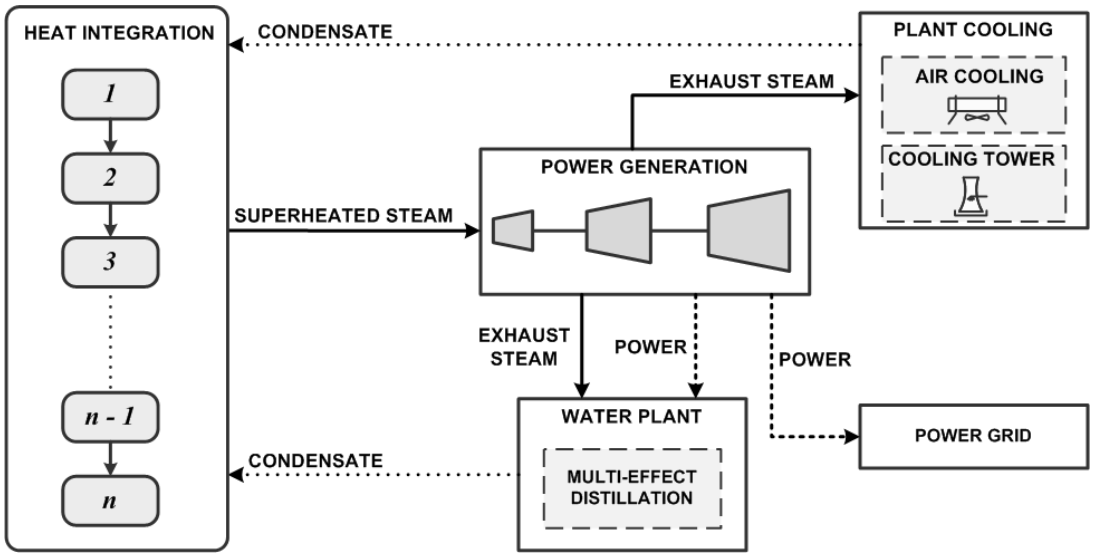

Figure 8 Integrated power and water generation process

2.7 Heat, mass and power integration overview

The interconnectivity of all units in the GTL production process has been detailed in the previous sections. The streams to be heated and cooled within the process are identified and used to target minimum heating and cooling requirements via thermal pinch analysis. In addition to process hot streams, the analysis considers excess heat from fuel gas, obtained from various sections of the GTL process. The utility cooling requirement can be reduced via the production of steam, for simultaneous power and water generation as illustrated in Figure 8. For this study, we consider air cooling and cooling water as utility cooling options.

The power sinks are identified and integrated with the power source via a direct allocation method. Other techniques for power targeting and allocation are outlined by El-Halwagi et al [50]. Finally, the water sources and sinks from each GTL process section have been identified in Figures 2 – 7. The allocation of water sources to sinks is performed via a direct recycle method to identify the overall water target for each GTL process configuration. Other rigorous methods

are presented by El-Halwagi et al. and Gabriel and El-Halwagi[51,52]. The macroscopic heat, mass and power integration interactions, within the combined GTL and water desalination process is illustrated in Figure 9.

The focus of this work is to identify performance targets for the GTL process. While there are unique power and water targets, there are numerous alternatives for implementation. These implementations can be obtained via the methods and techniques outlined by El-Halwagi; Biegler, Grossmann, and Westerberg; Seider et al.; Smith; Towler and Sinnott [53-57].

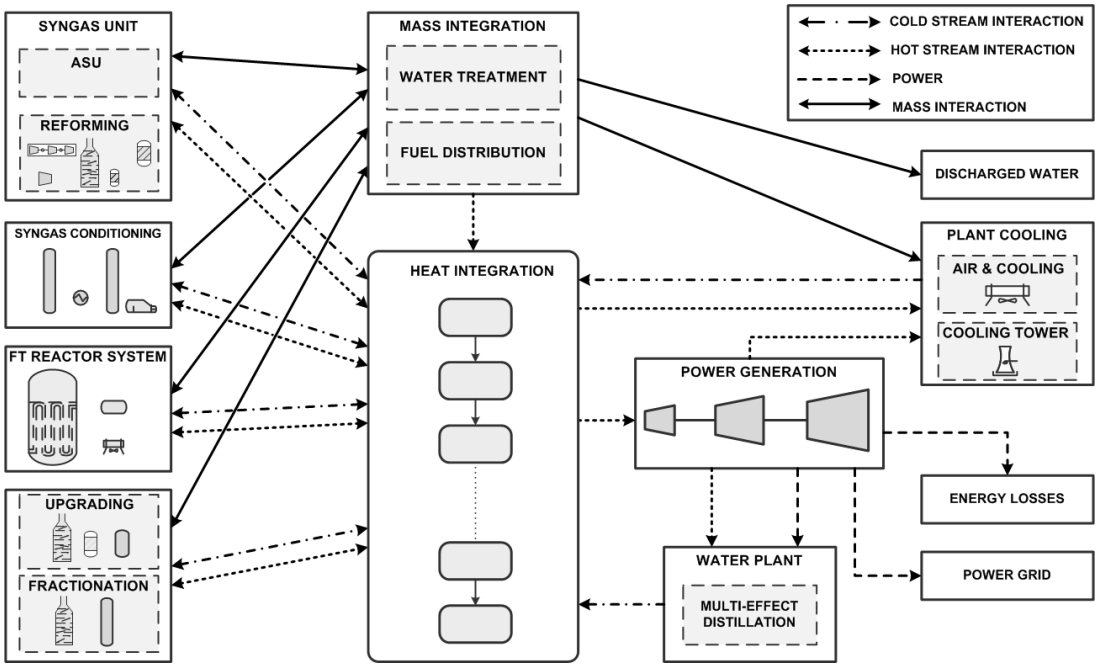

Figure 9 A macroscopic view of the heat, mass and power relationships within the GTL plant

2.8 Results and discussion

2.8.1 Process mass balance

The modeling and simulation of the three proposed GTL processes highlighted the differences in the input requirements and output flows. Table 2 illustrates such differences. An immediate analysis of the mass flows for both ATR and POx based configurations indicates their close similarity in terms of natural gas usage. This point highlights the similarity in carbon efficiency for GTL processes with either technology. In contrast, the natural gas usage by the SMR based GTL process is significantly higher than the two other configurations. This is most likely due to a lower conversion of methane to carbon monoxide and hydrogen in the SMR reactor. A lower conversion in the reforming reactor would result in more methane being lost to the fuel header at the 50% split point of the FT tail gas.

Further evaluation of the material inputs and outputs for the syngas section indicates that the proposed POx based GTL process is more efficient in utilizing water for syngas production. A similar evaluation on the carbon dioxide emissions highlights that ATR has the lowest carbon footprint without carbon credits from power production and/or cogeneration. It should be noted that the FT water flow rate would be similar for all configurations. This is directly due to all oxygen atoms in the converted carbon monoxide leaving the system as water, while the carbon atoms ideally leave as GTL liquid product. Therefore, the pretreated water can be used as an indicator for comparing water production from the syngas production section. The data from the mass balance provides macroscopic key performance indicators for the GTL process, and are shown in Table 3.

Table 2 Overall mass balance of GTL process

Stream (lb/hr)	ATR	POx	SMR
Input			
Saturator water feed	102,381	102,652	125,678
HP Steam	455,267	112,393	3,586,600
CO_2 removal make-up water	8,862	11,046	28,690
Natural gas feed	953,276	955,806	1,170,198
Oxygen feed	1,171,340	1,256,520	-
Total	2,691,126	2,438,418	4,911,166

Table 2 (*continued*)

Stream (lb/hr)	ATR	POx	SMR
Output			
GTL product	531,019	530,977	531,252
Carbon dioxide	371,674	432,356	642,010
Fuel gas	377,893	358,224	719,464
Pretreated water	1,410,540	1,116,860	3,018,440
Total	2,691,126	2,438,418	4,911,166

Table 3 Key performance indicators (KPI) for GTL process

KPI		ATR	POx	SMR
Nat. Gas conversion	[SCF/bbl GTL]	10,352	10,379	12,708
Net water [a]	[lb/bbl GTL]	405	428	-347
Carbon dioxide [b]	[lb/bbl GTL]	450	453	732
Oxygen	[lb/bbl GTL]	562	603	-

[a] Water losses due to evaporative cooling not considered
[b] Carbon credits due to power generation not considered

2.8.2 Heat Integration and targeting

The data for hot and cold streams, as well as isothermal heating and cooling requirements, were extracted from the simulation and are shown in Tables 4-6. A thermal pinch analysis was performed to determine the minimum heating and cooling requirements for each process configuration.

Table 4 Stream data for ATR-based GTL process

Stream Heat exchanger	**Duty** (MMBtu/hr)	$\mathbf{T_{supply}}$ (^oF)	$\mathbf{T_{target}}$ (^oF)
Syngas production			
E-101	93	138	300
E-102	49	212	392
E-103	263	581	787
E-104	395	342	700
E-105	-	-	-
E-106	458	79	453
Syngas conditioning			
E-201	-4002	1949	122
E-202	-	-	-
E-203	-	-	-
E-204	1093	-	254
E-205	-444	-	122
E-206	-497	173	122
FT Reaction			
E-301	-2550	-	428
E-302	-1051	428	122
Upgrading			
E-401	55	140	662
E-402	65	430	662
E-403	-191	705	400
E-404	-3	404	122
E-405	266	402	733
E-406	240	-	302
E-407	-55	302	122
Water pretreatment			
E-501	124	-	230
E-502	-0.2	-	227

Table 5 Stream data for POx-based GTL process

Stream Heat exchanger	Duty (MMBtu/hr)	T_{supply} (^oF)	T_{target} (^oF)
Syngas production			
E-101	93	138	300
E-102	52	212	392
E-103	318	590	892
E-104	332	223	700
E-105	-	-	-
E-106	113	79	453
Syngas conditioning			
E-201	-3999	2372	122
E-202	628	122	572
E-203	-753	637	122
E-204	1272	-	254
E-205	-517	-	122
E-206	-578	173	122
FT Reaction			
E-301	-2554	-	428
E-302	-1042	428	122
Upgrading			
E-401	55	140	662
E-402	65	430	662
E-403	-191	705	400
E-404	-3	404	122
E-405	265	402	733
E-406	240	-	302
E-407	-55	302	122
Water pretreatment			
E-501	95	-	230
E-502	-0.2	-	227

Table 6 Stream data for SMR-based GTL process

Stream Heat exchanger	Duty (MMBtu/hr)	T_{supply} (^oF)	T_{target} (^oF)
Syngas production			
E-101	151	79	300
E-102	-	-	-
E-103	1758	476	1000
E-104	414	212	700
E-105	8448	-	1600
E-106	3602	79	453
Syngas conditioning			
E-201	-7812	1600	122
E-202	-	-	-
E-203	-	-	-
E-204	3777	-	254
E-205	-1535	-	122
E-206	-1715	173	122
FT Reaction			
E-301	-2590	-	428
E-302	-1105	428	122
Upgrading			
E-401	57	138	662
E-402	64	430	662
E-403	-191	705	400
E-404	-3	404	122
E-405	266	402	734
E-406	240	-	302
E-407	-55	302	122
Water pretreatment			
E-501	283	-	230
E-502	-0.4	-	227

A grand composite curve (GCC) was also developed for each configuration to highlight any opportunities for heat recovery for power and water generation. Figures 10 -12 represent the GCC for each syngas configuration.

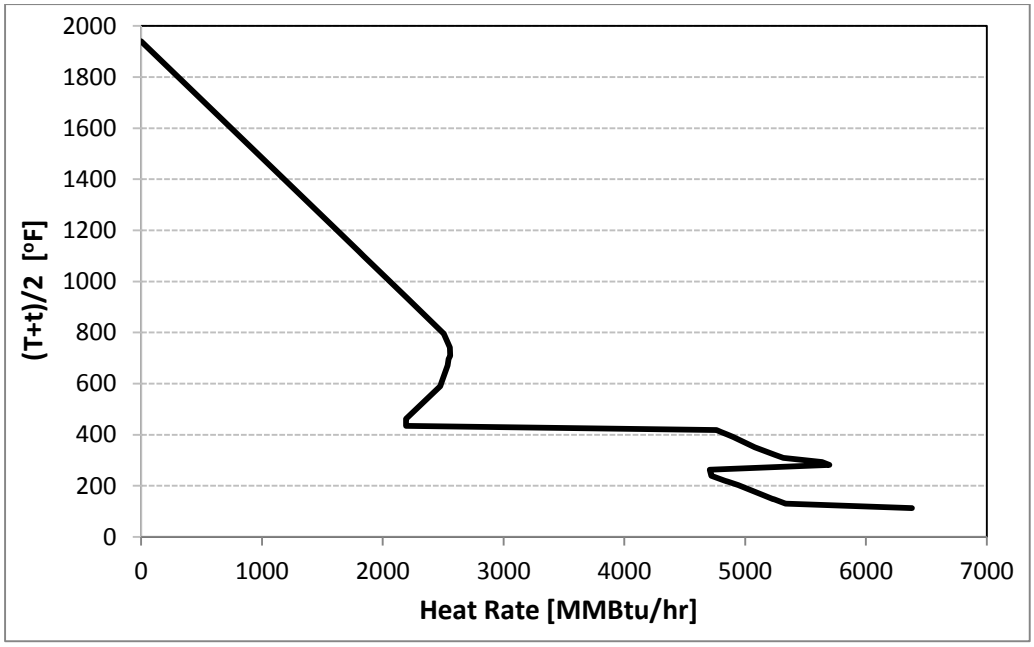

Figure 10 Grand composite curve (GCC) for ATR-based GTL process before power and water generation

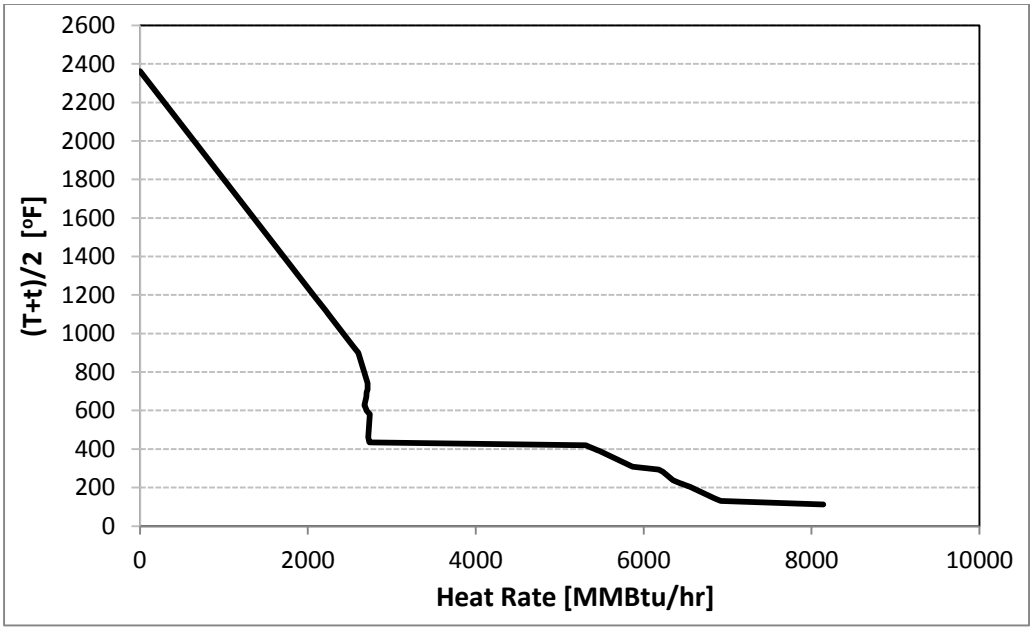

Figure 11 Grand composite curve (GCC) for POx-based GTL process before power and water generation

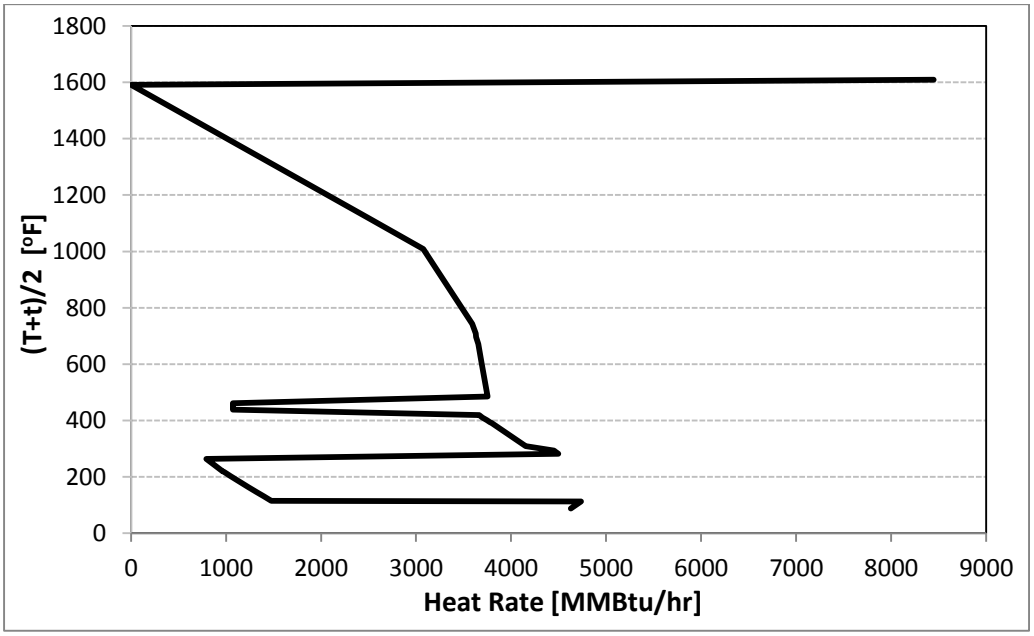

Figure 12 Grand composite curve (GCC) for SMR-based GTL process before power and water generation

Table 7 Minimum heating and cooling requirements of GTL process for different syngas technologies

Parameter	ATR	POx	SMR
Minimum heating [MMBtu/hr]	-	-	8448
Minimum cooling [MMBtu/hr]	6313	8121	4630

The results shown in Table 7 highlight that the minimum heating for the ATR and POx based GTL processes are zero, while that of the SMR based configuration is 8,448 MMBtu/hr. The SMR minimum heating is as a direct result of the isothermal energy required for the highly endothermic reforming reaction. In contrast, the results show that the SMR based configuration has the lowest minimum cooling requirements of 4,630 MMBtu/hr.

2.8.3 Power and water generation

An evaluation of the grand composite curves for each GTL process configuration indicates a potential for power and subsequent water production. In this evaluation we consider the fuel gas as an additional source of heating for all configurations. The flow rate of available fuel gas is given in Table 2 in the mass balance section. The heat from this source is considered a high level heat source, and as such would appear at the top of the cascade diagram.

In the case of the SMR based GTL process, some of the fuel gas would be used for minimum heating, while the remainder would be passed down the energy levels to be recovered in the form of superheated steam. The power and water generation as well as CO_2 credits are shown in Table 8.

Table 8 Performance and requirements of GTL process after power and water generation

Parameter		ATR	POx	SMR
Power generated	[MW]	417	436	188
Available low grade heat [a]	[MMBtu/hr]	5,208	5,439	2,354
MED water generated	[tons/hr]	12,860	12,860	10,233
CO_2 credits [b]	[lb/bblGTL]	244	255	110
Minimum heating	[MMBtu/hr]	-	-	-
Minimum cooling [c]	[MMBtu/hr]	5,185	6,632	3,733

[a] Represents available heat from back pressure turbine exhaust
[b] Represents the CO_2 credits from producing power
[c] Considers the cooling required for unused low grade heat from turbine

The results shown in Table 8 indicate that the SMR based configuration has the lowest power generation potential. These results do not take into consideration the GTL process power requirements for compressors and other energy-intensive units. Table 9 shows this comparison of required power and produced power for all configurations. For this study we only consider the power requirements of compressors and the air separation unit (245 kWh/ton O_2) [58], where applicable. The pumping requirements were neglected except for that required for the cooling water circuit, which was derived from literature [36].

The final minimum cooling after heat recovery for power and water generation represents a gross cooling requirement. Further evaluation of the minimum cooling reveals a need for various cooling levels. For this study we used two cooling mediums, namely air cooling and evaporative cooling via a cooling water circuit. The air cooling method has a power requirement and the cooling water approach has both power and water implications. Table 10 shows the power and water implications of both cooling methods based on factors derived from literature [36].

Table 9 Comparison of power required and produced in the GTL process

Unit (MW)	**ATR**	**POx**	**SMR**
Air separation unit	130	140	-
Nat. gas compressor	8.4	8.4	-
Oxygen compressor	69.2	74.2	-
Carbon dioxide compressor	-	-	20.8
FT tail gas compressor	2.9	2.8	-
Syngas compressor	-	-	19.2
Hydrogen compressor	3.2	3.2	3.3
Multi-effect distillation	23.3	23.3	18.6
Total	237	252	62
Net Power [a]	180	184	127

[a] Power requirements for air and cooling water based cooling not considered

Table 10 Power and water implications of satisfying the minimum cooling

Parameter		ATR	POx	SMR
Air cooler	[MMBtu/hr]	4,157	5,418	501
Cooling water	[MMBtu/hr]	1,028	1,215	3,232
Power required	[MW]	5.6	7.0	4.8
Evaporative losses [a]	[tons/hr]	514	607	1,616

[a] Rule of thumb metric: 1 lb evaporated water / 1000 Btu/hr of evaporative cooling

The grand composite curves (GCC) for each GTL configuration indicates that SMR has the lowest minimum cooling requirement. Upon segregation into air cooling and evaporative cooling requirements, it is clear that ATR has the lowest minimum evaporative cooling needs. Therefore, the ATR configuration choice has the lowest impact with regards to evaporative losses. An overall analysis of the power requirements and GHG emission effect for each syngas alternative is shown in Table 11. The overall water implications are discussed in a later section.

The power integration for this study is based on a direct allocation method. A possible implementation for the allocation of power to each unit is illustrated in Figure 13, for the ATR based process. Similar diagrams can be developed for the POx and SMR based configurations.

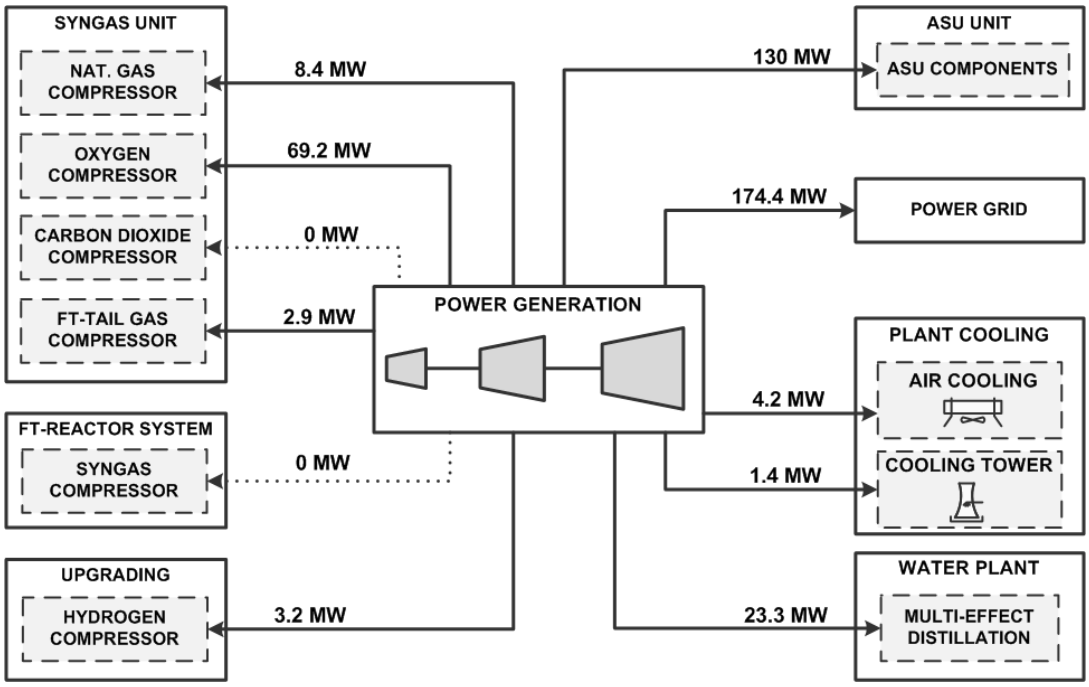

Figure 13 Direct allocation of power for all GTL process sinks

Table 11 Overall performance of GTL process with different syngas technologies

KPI		ATR	POx	SMR
Export Power	[kWh / bbl]	84	85	58
CO_2 footprint	[lb/ bbl GTL]	206	198	621

2.8.4 Water management

At this stage of the targeting analysis, all water sources and sinks are clearly identified and an overall mass integration approach can be used to minimize water usage. For this targeting approach, we use a direct recycle technique to identify the minimum water requirement or maximum production of water for each configuration. Table 12 shows the composition of combined water from the GTL process to the pretreatment section. This work considers that the water from the syngas production and FT synthesis section contains minimal total dissolved solids (TDS) and no catalyst fines. The study also neglects oxygenate formation in the FT reactor and as such, FT water only contains oily matter to be removed. Using ASPEN Plus and the SRK

– Kabadi-Danner (SRKKD) thermodynamic package, a water stream with less than 0.1 ppm of oily matter and less than 1 ppb of dissolved gases was obtained from the rigorously simulated pretreatment distillation columns. The TDS for water from the MED was assumed to be 10 ppm which can be achieved commercially [59]. In addition, there is minimal oil in the MED generated water due to the absence of this contaminant in the seawater feed. Table 13 shows the typical requirement for TDS and oily matter for process water and boiler feed water [60]. For this study we use process water as makeup for the cooling tower and CO_2 removal unit, and boiler feed water as makeup for the natural gas saturator and to produce steam for the reforming reactor. The source and sink data are shown in Tables 14- 17.

Table 12 Composition (ppm) of various components in water to pretreatment section for different syngas technologies

Component	**Contaminant concentration [ppm]**		
	ATR	**POx**	**SMR**
Carbon monoxide	3.1	3.3	1.7
Carbon dioxide	87.8	23.1	258.0
Hydrogen	1.6	1.7	1.2
Methane	28.5	23.8	32.6
Ethane	1.9	2.5	0.7
Propane	2.1	2.7	0.8
Oil (C_4+)	7.0	9.9	3.0
TDS	0.06	0.08	0.04

Table 13 Quality specifications for process water and boiler feed water [60]

Quality specification		**Process water**	**Boiler feed water**
Oily matter	[mg/L]	1.0	1.0
TDS	[mg/L]	500.0	2.0

Table 14 Water integration sink data for GTL process

Sink	Flow Rate [tons/hr] ATR	Flow Rate [tons/hr] POx	Flow Rate [tons/hr] SMR	Max. inlet conc. of Oil [mg/L]	Max. inlet conc. of TDS [mg/L]
Natural gas saturator	51	51	63	1.0	2.0
Cooling tower	514	607	1,616	1.0	500
CO_2 removal unit	4	6	14	1.0	500
Natural gas reformer	228	56	1,793	1.0	2.0

Table 15 Water integration source data for ATR based GTL process

Source	Flow Rate [tons/hr] ATR	Conc. of Oil [mg/L]	Conc. of TDS [mg/L]
Pretreated water	705	0.100	0.06
MED generation	12,860	0.001	10.00

Table 16 Water integration source data for POx based GTL process

Source	Flow Rate [tons/hr] POx	Conc. of Oil [mg/L]	Conc. of TDS [mg/L]
Pretreated water	558	0.100	0.08
MED generation	12,860	0.001	10.00

Table 17 Water integration source data for SMR based GTL process

Source	Flow Rate [tons/hr] SMR	Conc. of Oil [mg/L]	Conc. of TDS [mg/L]
Pretreated water	1,509	0.100	0.04
MED generation	10,233	0.001	10.00

The source-sink data in Tables 14 through 17 are used to target the minimum water requirement for the GTL process. Table 14 shows the final comparison of all syngas options regarding their individual total water impact. Figure 14 illustrates a single water integration implementation for the ATR based configuration with sink contaminant specifications given by Table 14.

The results indicate that the proposed ATR based configuration has the greatest potential for producing excess water, while the SMR based configuration exhibits the lowest potential for water production. The latter insight corroborates the findings of previous studies [13].

Table 18 Water production potential of GTL process with different syngas technologies

Stream (tons/hr)	**ATR**	**POx**	**SMR**
Input			
Saturator water feed	51	51	63
HP Steam	228	56	1,793
CO_2 removal make-up water	4	6	14
Evaporative losses	514	607	1,616
Output			
Pretreated water	705	558	1,509
MED generation	12,860	12,860	10,233
Net Water	12,768	12,698	8,256

A basic evaluation of the overall water flows indicates that the general GTL process is a net producer of water, whether directly or indirectly, from desalination processes. This highlights the potential for large natural gas reserves to serve as both an energy source, as well as an indirect water source. It represents the ideal benefits of the water-energy nexus in GTL processes for water scarce regions rich in natural gas reserves.

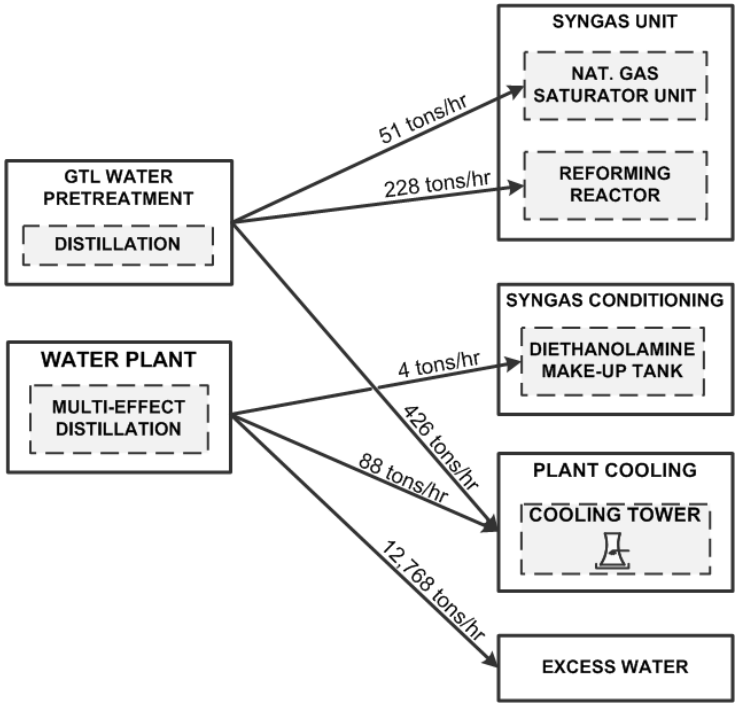

Figure 14 Water source-sink diagram for the ATR based configuration

2.9 Summary

An evaluation of the basic Gas-to-liquid (GTL) process has been conducted to identify targets for heat ad mass integration, as well as power and water generation. Three syngas production technologies, namely autothermal reforming (ATR), partial oxidative reforming (POx) and steam methane reforming (SMR), were included in the evaluation to assess the implications of technology choice on these targets. Of the three syngas technology choices, ATR was deemed to have the highest potential for overall performance, followed by POx and then SMR, based on potential water production.

Previous studies have indicated that SMR-based GTL plants are the most efficient in terms of natural gas usage. In contrast we have identified SMR-based GTL plants to be the most inefficient when no external supply of CO_2 is considered as an additional carbon source for GTL production. The base case results show that it has the highest CO_2 production of 621 lb CO_2/bbl GTL product, as well as the lowest power and fresh water generation values of 58 kWh/ bbl GTL and 3.96 tons water/ bbl GTL respectively. For similar key performance indicators (KPI), the base case ATR and POx configurations had values of 206 lb CO_2/bbl and 198 lb CO_2/bbl

respectively, 84 kWh/ bbl GTL and 85 kWh/ bbl GTL respectively, as well as 6.13 tons water/ bbl GTL and 6.10 tons water/ bbl GTL respectively.

The results for the SMR base case GTL process indicate that technologies for monetizing stranded natural gas via the SMR route would be intrinsically disadvantaged by the net requirement for process water. The results also show that both ATR and POx configurations display attractive KPIs, and as such the choice of one technology over the other is a matter of operational experience and flexibility.

CHAPTER III
OPTIMIZATION OF MULTI-EFFECT DISTILLATION PROCESS USING A LINEAR BASED ENTHALPY MODEL

3.1 Introduction

The global demand for an economical and reliable supply of water continues to increase as populations grow and standard of living improves. This demand for water resources has prompted countries to explore alternate routes for supplying this vital resource. In particular, many countries have shifted their focuses to the use of seawater desalination as a means of reliably providing high-quality water from a seemingly limitless water resource. In fact, numerous countries in the Middle East as well as Spain and Greece have already advanced in their use and dependency on desalination technologies to supply water for their growing populations and expanding economies.

The current water supply from existing desalination plants will be outpaced by the expected demand from growing countries thus there is a need to add new installations to address this supply-demand disparity. These new plants would utilize either thermal or membrane technologies depending on numerous factors such as seawater salinity, capital cost and many other regionally dependent decision variables. It has been estimated that by 2016, global water supply utilizing desalination technologies would grow to more than 60% from its 2010 recorded value [61]. In particular, thermal desalination techniques are expected to continue to dominate the market in Gulf Corporation Countries (GCC) due to their reliability, low cost of energy in the region as well as high salinities that complicate the use of membrane-based technologies. This continued approach to supplying fresh water would require improvements in both multi-effect distillation (MED) and multi-stage flash distillation (MSF) plants from an overall energy efficiency and capital cost perspective. The latter requirement is expected though the former represents a step forward to reduce carbon footprint within an ever expanding industrial sector.

There have been numerous studies over the past two decades geared towards addressing the performance of thermal desalination technologies. Various approaches have been proposed and implemented to optimize and improve the thermal efficiency and capital requirements of this important technology. In specific, there has been a shift in focus towards MED technology due to improved performance and reliability over MSF-based desalination [59]. For MED technology, parametric studies have been done to investigate the influence of the many operating and

equipment design variables on the overall performance of the plant [62-66]. These variables include but are not limited to the total number of effects, the top and bottom brine temperatures, incoming seawater salinity and the temperature of the heating steam. While these studies have provided key insights into the operation and performance improvement opportunities for MED plants, their ability to find optimal solutions has been limited due to the use of highly non-linear mathematical formulations.

This chapter proposes a novel formulation for the modeling of the mass and energy balances of effects in thermal desalination processes. The modeling approach is utilized in the optimization of the MED process due to its increased interest over MSF technology. Although many linear based models are gross approximations of the actual nonlinear relationships, the proposed model is able to capture the accuracy of original nonlinear formulations within the specified ranges. In addition, the linear based modeling approach reduces numeric complexities that have required the use of exhaustive iterative methods and stochastic programming methods that do not guarantee globally optimal solutions.

3.2 Literature survey

There have been numerous contributions towards the improvement of thermal desalination processes via simulation, parametric analysis, thermoeconomic and thermodynamic optimization. In earlier studies, Aly [67] evaluated the performance of multiple-effect distillation (MED) and mechanical vapor compressor (MED-MVC) configurations using generally accepted thermodynamic models for the MEE process. El-Dessouky et al. [68] evaluated the multiple-effect distillation with thermo-vapor compression (MED-TVC) process using a simple thermodynamic model which assumed a constant heat transfer area, constant physical properties of water and an absence of preheaters. Their study highlighted the advantages of this configuration over other thermal desalination systems. Hanbury [69] also developed simple models that assumed a linear decrease in heat transfer coefficient, unequal effect temperature differences and equal thermal load transfer per effect from the second effect and upwards. Model results were also successfully compared with industrial data. Wade [70], Darwish et al. [71] economically evaluated the MSF, MED-TVC and MED-MVC thermal desalination processes and concluded that their competitiveness with reverse osmosis (RO) technology is contingent on low energy costs. Morin [72] performed similar analyses on low temperature MED with similar conclusions. Hamed et al. [73] evaluated the MED, MED-TVC and MED-MVC systems via second law thermodynamics and concluded that the MED-TVC process had the least exergy destruction. In addition, they

determined that exergy losses decrease for increased number of effects, higher entrainment ratios, lower top brine temperatures as well as steam heating temperatures. Lambert et al. [74] linearized some of the non-linear equations governing the MED process and solved using an iterative Gaussian elimination technique. In this formulation, boiling point elevation and salinity were included. Al-Shayji et al. [75] utilized artificial neural networks (ANNs) as a modeling approach to analyzing and optimizing MSF processes. Dahdah et al. [76] developed a structural optimization model for determining novel configurations of hybrid MED-MSF thermal desalination systems. The model assumed a constant specific heat capacity that is independent of temperature and salinity as well as a constant latent heat of vaporization that is independent of pressure. Their model also neglects the use of the non-equilibrium allowances as well as uses a constant boiling point elevation for each effect. Sayaadi et al. [77,78] utilized a meta heuristic based optimization approach to determine the optimal thermoeconomic configuration of a MED-TVC process. Other works have focused on the optimization of the physical structure of the MED process via exhaustive iterative methods [62,79-82]. Studies that neglect economics have sought to maximize distillate production and or minimize overall exergy losses [78,83,84].

Over the past decade, greater research efforts have focused on improving the thermal performance of the MED-TVC process [85]. This interest has been as a result of the reuse of compressed vapor as heating steam which significantly reduces overall motive steam requirement as well as boiler capacity and capital cost [86]. In addition, the use of steam ejectors has represented an advancement for the vapor compression strategy due to its simple design and lack of moving parts [87].

In general, most of the existing thermal desalination models have utilized highly nonlinear thermophysical correlations to describe and optimize the operation and economics of the desalination process. As such there has been a justifiable tradeoff between complexity of model and purpose. For models aimed at optimizing geometry of a fixed design, iterative methods have been employed while models targeting novel configurations have utilized stochastic optimization approaches. Based on the increased interest in the MED-TVC process, this study introduces a new model for evaluating and optimizing thermal desalination processes with emphasis on the MED-TVC design.

3.3 MED-TVC process description

The MED-TVC configuration adopted in this work is based on the parallel feed forward design described by El-Dessouky et al.[82]. In this design, the brine leaving each effect (*i*) is introduced into the brine pool of the subsequent effect (*i+1*). The difference in operating temperature and pressure between the effects results in the flashing of a small portion of the introduced brine. This produced vapor is added to the vapor formed from boiling of fed seawater in effect (*i*) thus enhancing overall system productivity and thermal efficiency.

Figure 15 illustrates the overall MED-TVC configuration. As shown, the system is an aggregation of *n* repeating effects with *n-1* distillate flashing boxes. In addition, each effect has a vapor space for vapor liquid disengagement, a demister to remove any entrained seawater droplets, an evaporator, seawater feed lines / spray nozzles and a brine pool. The effects are numbered from 1 through n in the direction of the falling pressure and consequent vapor flow direction. Seawater is introduced into each effect at a controlled and equal rate depending on the heating provided to the first effect.

For the first effect, compressed vapor from the last effect is introduced into the tube side and used to sensibly heat and boil a portion of the fed seawater using its available latent heat. The vapor formed from boiling is sent to the tube side of the second effect where sensible heating and boiling also occurs to produce vapor for the third effect. This is repeated until the n^{th} effect.

The condensed vapor from effects 1 to (*n* -1) is introduced into the corresponding distillate flashing box, where the reduced operating pressure results in the flashing of a small amount of vapor. This flashing process reduces the temperature of the overall distillate pool in that section. The flashed off vapor is introduced into the tube side of the next effect along with the vapor from boiling seawater as well as flashing brine in that effect.

The vapor from the last effect is routed to the down condenser where it is partially condensed using a controlled flow of seawater. The remaining vapor is entrained by the steam ejector which compresses it the desired pressure using motive steam. In a similar fashion, the brine leaving the last effect is cooled to the desired temperature using a controlled flow of seawater. The resulting warm exiting seawater stream from both cooling processes are combined then divided into two parts; the first represents the feed seawater stream which is evenly distributed among the effects while the second represents the cooling seawater stream that is rejected back to the sea. Based on environmental restrictions, the cooling seawater stream is combined with fresh seawater so as not to exceed the allowable temperature limit on discharged

cooling seawater. An overall heat balance indicates that most of the heat load introduced into the system via motive steam, is rejected to the cooling seawater.

The final component of the MED-TVC system is the steam ejector which provides most of the performance improvements for the MED system by reducing overall heating steam requirements. It consists of a nozzle, mixing chamber and diffuser. The design of the ejector can be for choked or un-choked flow depending on the supply conditions of the motive steam, entrained vapor conditions as well as the desired properties of the ejector exhaust. For this study, the superheated exhaust from the steam ejector is de-superheated using distillate from the flash boxes.

3.4 Problem description

3.4.1 Motivation

The thermal performance of the MED-TVC process is reflected in the gain output ratio (GOR) which compares the total flowrate of desalinated water to that of the input motive steam. This GOR is considered a key performance indicator (KPI) for the system and is intrinsically linked to the quality of the motive steam. In addition, the heat supplied to the process via motive steam is removed by pumping large volumes of seawater as a cooling utility.

In general, the steam supply and quality as well as power consumption requirements for pumping can have a significant influence on the design and overall economics of the process. As a result, the interesting optimization problem for the MED-TVC process is not only determining the optimal configuration for improved thermal performance but to also incorporate economics as the overall objective function.

The current models used for evaluating and optimizing thermal desalination systems involve the use of highly nonlinear, non-convex equations that link heat and mass balances to the varying salinities in the process. The general formulation for the heat balance incorporates the use of a multiplicative relationship among flows, specific heat capacities and effect operating temperatures. In this formulation, both flow and heat capacities are functions of salinity while specific heat capacity is in itself a thermophysical property. Conceivably, the heat balance is a product of many unknown variables which can be difficult to solve deterministically for a timely and optimal solution.

In most studies on the optimization of thermal desalination processes, authors have adopted two approaches; include basic assumptions or variable search ranges to reduce or eliminate the effects of the nonlinear relationships or optimize the process around a fixed design. While both

approaches yield valuable insights for the process, there is currently no flexible model that is solved deterministically for both configuration and operational optimization with inclusion of all identified thermodynamic limitations. As a result there is a need to develop a new mathematical formulation that can optimally identify novel configurations and operational parameters for thermal desalination plants. In general, the new formulation would be useful in identifying integration opportunities for thermal desalination plant with process that can supply both steam and power such as dual purpose power plants. I addition, a robust but simple model would be useful in real time optimization (RTO) of existing plants.

3.4.2 Problem statement

It is desired to develop a systematic approach for identifying the economically optimal design of the MED-TVC desalination process for possible coupling with various options for steam and power sources. In developing the optimal MED-TVC configuration, the following variables should be determined:

- The equipment size of effect evaporators, seawater feed preheaters and trim coolers
- The number of effects
- The sources and flowrates of de-superheating water feed for of the steam ejector exhaust
- The required flowrate of feed seawater
- The flowrate of entrained vapor in the steam ejector
- The motive steam consumption and gain output ratio (GOR)
- The distribution of seawater preheating via the hot brine stream, distillate stream and condensing vapor from the last effect
- The preheat temperature of the feed seawater
- The power requirements for pumping

For the problem, the operating temperature range of the MED-TVC, temperature of feed, mass flowrate of product water and feed seawater total dissolved solids (TDS) concentration are clearly defined. In addition, environmental constraints on brine discharge concentration and seawater discharge temperatures are also given.

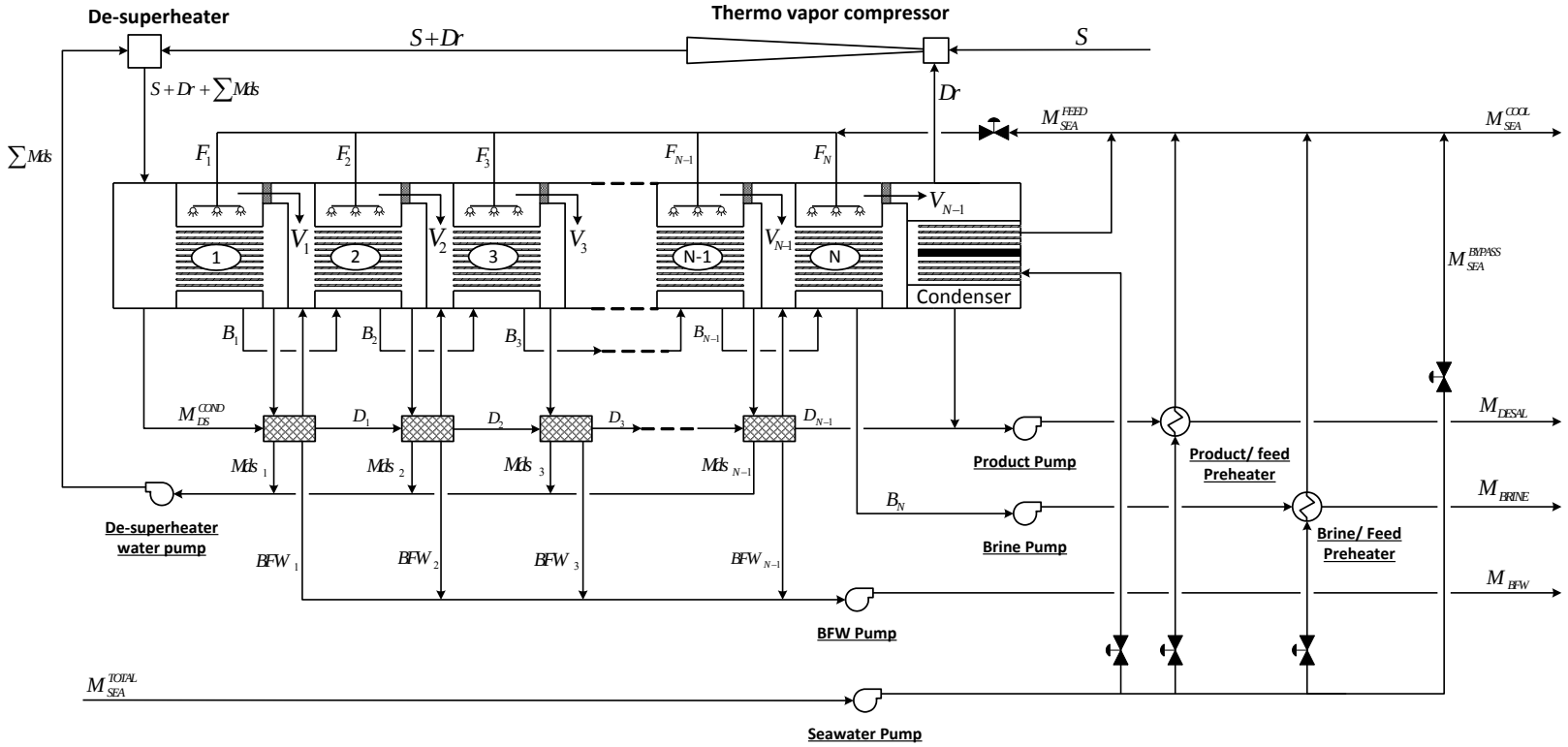

Figure 15 Overall base case process flow diagram for multi-effect distillation with thermo vapor compression (MED-TVC)

3.5 Mathematical formulation

The thermal desalination process can be described and optimized using a mass balance, heat balance and pre-specified cost functions. The formulation foe the model used include highly nonlinear, nonconvex equations that may be difficult to solve using deterministic solvers. In specific, the component balance on the system is represented by the product of and unknown flowrate and salinity. This introduced bilinear terms into the formulation that may require various techniques for finding globally optimal solutions. In addition, the heat balance on the system consists of the product of an unknown flowrate, specific heat capacity and operating temperature. In this case, the flowrate and specific heat capacities are functions of salinity while the heat capacity in itself a thermophysical property. As a result, the heat balance represents a highly nonlinear formulation.

In recent studies, the degree of nonlinearity in the heat balance has been reduced by assuming a linear temperature profile for the operation of the MED-TVC [88-90]. This study utilizes this assumption and adopts a new approach whereby mass flowrates of water and salt are decoupled to create a mass and energy balance model that is less nonlinear. In addition, thermodynamic losses and novel flow routing options are considered in the overall formulation.
The developed models in the literature include the assumption of steady state operation, constant heat transfer area in each effect, negligible heat losses to the surroundings as well as zero salt in the distillate. The following sections discuss the formulation of the model developed for this work and highlight the differences from other previously adopted approaches.

3.5.1 Model for MED balances

The previous models developed for the MED energy balances typically utilized specific heat capacities for pure water and brine that were governed by complex nonlinear correlations. These correlations are both salinity and temperature dependent thus requiring simultaneous calculations of mass and energy balances due to their interdependency. This formulation may be difficult to solve since the heat flow is a multiplicative function of an unknown brine flow, unknown specific heat capacity and unknown final temperature. Equations 16 - 19 describe the mass and heat balance formulation adopted by previous studies.

3.5.1.1 Current mass and energy balance for MED process

Effect mass balances

$$F_i + B_{i-1} = V_i + B_i \tag{16}$$

$$V_{i-1} = \dot{m}^{stm}_{brine,i-1} + \dot{m}^{stm}_{sea,i-1} \quad (17)$$

$$X^{IN}_{sea} F_i + X_{brine,i-1} B_{i-1} = X_{brine,i} B_i \quad (18)$$

Effect heat balances

$$\dot{m}^{stm}_{sea,i-1}\lambda_{i-1} + \dot{m}^{stm}_{brine,i-1}\lambda_{i-1} + \dot{m}^{stm}_{pot,i-1}\lambda'_{i-1} = F_i Cp \cdot \left(T^{eff}_i - T^{hot}_{sea}\right) + \dot{m}^{stm}_{sea,i}\lambda_i \quad (19)$$

3.5.1.2 Proposed linear-based enthalpy model for MED process

As a result, earlier solution algorithms utilized exhaustive iterative methods to optimize the designs of thermal desalination processes [79]. In addition, an assumption for constant temperature differences between effects helped to reduce solving times by fixing one of the dependent variables in the complex specific heat capacity correlation [88-90].

For this work we consider seawater as binary mixture of salt and water therefore the specific enthalpy of the mixture at constant temperature and pressure can be described by Equation 20 [91,92]. In essence the adopted model is linearly dependent on both pure water enthalpy and salt enthalpy. This approach takes advantage of the fact that:

1. At the operating salinity of the MED system (0 – 120,000 ppm), the overall seawater enthalpy is mainly dependent on pure water enthalpy
2. An assumed constant temperature difference between effects allows for the formulation of a linear model for the overall mass and energy balances thus significantly reducing solving times for novel MED designs

$$h_{sw} = \left(1 - x_s\right) \cdot h_w + x_s h_s \quad (20)$$

Where h_w, h_{salt} and x_s represent the specific enthalpy of water and salt respectively and the salinity taken as a mass fraction. For this equation the enthalpy of the pure water $\left(h_w\right)$ and salt $\left(h_{salt}\right)$ are nonlinear functions though by assuming a constant temperature difference between effects and a desired top brine temperature, the enthalpies of the pure water and salt are fixed for each effect with the only manipulated variable being the salinity. The linear enthalpy relationship can also be rewritten in terms of overall mass flowrates of pure water and salt thus Equation 21 is valid for the overall heat balance.

$$\dot{m}_{sw} h_{sw} = \dot{m}_w h_w + \dot{m}_s h_s \quad (21)$$

Where $\dot{m}_{sw}$, $\dot{m}_w$ and $\dot{m}_s$ are the mass flowrates of seawater, water and salt respectively. The use of Equation 21 for the energy balances provides the modeling benefit of decoupling the

flows of water and salt thus reducing numerical difficulties when optimizing for MED topologies, novel stream routings and overall system economics.

The correlation for pure water enthalpy was developed using the IAPWS-IF97 formulation for the thermodynamic properties of water and steam [93]. The correlation for the salt enthalpy was developed using the IAPWS-2008 formulation for the thermodynamic properties of seawater [94] in conjunction with the IAPWS-IF97 formulation. The developed correlations for pure water enthalpy and salt enthalpy as functions of temperature are given by Equations 22 and 23 respectively. In the desired operating range of the MED system (0 – 120 g/kg salinity and 40 – 120 ^{o}C), the overall seawater enthalpy using these developed correlations has a ± 0.63% maximum deviation from the IAPWS 2008 and a ± 0.13% maximum deviation from the correlations presented by Sharqawy et al. [95]. In addition the maximum deviation for the full range of investigation (0 – 120 g/kg salinity and 0 – 120 ^{o}C) was ±3.42% from the IAPWS 2008 which is comparable in performance with the correlation from Connors [96] and better than that presented by Millero [92].

Pure water enthalpy

$$h_w = 0.5812899 + 4.152796(T) + 3.548276\times10^{-4}(T)^2 \tag{22}$$

Salt enthalpy

$$h_s = -18.31445 - 2.009888(T) + 3.443001\times10^{-2}(T)^2 - 2.095227\times10^{-4}(T)^3 \tag{23}$$

The developed enthalpy correlation for pure water was taken at 1 atm and has similar accuracy to other correlations developed by Mandani et al. [97]. It can be used when evaluating the heat balance of the system at atmospheric pressures; for example in seawater preheating. In contrast, the energy balances of the MED system are at vacuum conditions and as such enthalpy correlations for saturated water and steam are required. These are given by Equations 24 and 25 with correlation coefficients of 0.9999 and 0.9995 respectively, as compared to the IAPWS-IF97 [93].

Pure saturated water enthalpy

$$h_w^{sat,vac} = 2.302797 + 4.111306(T^{sat}) + 5.786723\times10^{-4}(T^{sat})^2 \tag{24}$$

Pure saturated steam enthalpy

$$h_{stm}^{sat,vac} = 2495.172 + 2.047401(T^{sat}) - 2.471814\times10^{-3}(T^{sat})^2 \tag{25}$$

3.5.2 Mass and energy balance for evaporation effects

In each evaporation effect there are two simultaneous operations occurring namely heating and vaporization of seawater feed as well as flashing of entering brine from the previous effect. For this model formulation, we have decoupled the mass and energy balances for both operations by utilizing the linear based energy balance model described in the previous section. Based on the flows described in Figure 15, the overall mass balance for each effect is given by Equation 26.

$$F_i + B_{i-1} = V_i + B_i \tag{26}$$

Where, F_i, B_i and V_i represent the seawater feed to effect (*i)*, brine and vapor flow from effect (*i)* respectively. In addition, the represented vapor flow (V_i) consists of vapor formed from seawater feed and flashing brine from the previous effect. Each effect operates at a constant temperature difference from the previous effect. The constant temperature difference is a function of the first and last effect's desired seawater boiling temperature and is given by Equation 27 [88-90].

$$\Delta T^{eff} = \frac{T_1^{eff} - T_N^{eff}}{N-1} \tag{27}$$

Where T_1^{eff} and T_N^{eff} represent the seawater boiling temperature in the first and last effect and *N*, the number of effects. For this formulation, the number of effects (*N*) represents a parameter in the overall formulation. A looping algorithm is used to traverse through the allowable number of effects from the minimum (N_{min}) to the maximum (N_{max}) to determine the optimal configuration. Since the model is linearly based, this task is accomplished in a short time.

3.5.2.1 Seawater heating and vaporization

With the flow of water and salt decoupled for this model formulation, the overall mass balance for the heating and vaporization of feed seawater is given by Equations 28 – 30.

$$\dot{m}_{sea,in}^{water} + \dot{m}_{sea,in}^{salt} = \dot{m}_{sea,i}^{stm} + \dot{m}_{sea,i}^{water} + \dot{m}_{sea,i}^{salt} \tag{28}$$

$$\dot{m}_{sea,in}^{water} = \left(1 - X_{sea}^{IN}\right) \cdot \rho_{sea} F^{FEED} \tag{29}$$

$$\dot{m}_{sea,in}^{salt} = X_{sea}^{IN} \rho_{sea} F^{FEED} \tag{30}$$

In Equation 28, the first two terms represent the separate flow of water and salt in the seawater fed to each effect. The corresponding water and salt component balance for this operation is given by Equations 31 and 32.

$$\dot{m}_{sea,in}^{water} = \dot{m}_{sea,i}^{stm} + \dot{m}_{sea,i}^{water} \quad (31)$$

$$\dot{m}_{sea,in}^{salt} = \dot{m}_{sea,i}^{salt} \quad (32)$$

For the energy balance on the heating and vaporization of seawater feed, there are three heat flows into the system boundary; energy from the condensing steam in the evaporator, energy inflow from the fed seawater and energy from seawater preheating operations. The energy outflows are the saturated steam, saturated water and heated salt stream. This overall energy balance is given by Equation 33.

$$Q_i^{EVAP} + \dot{m}_{sea,in}^{water} H_{sea}^{water} + \dot{m}_{sea,in}^{salt} H_{sea}^{salt} + \frac{Q_{sea}^{PRE}}{N} = \dot{m}_{sea,i}^{stm} H_i^{v} + \dot{m}_{sea,i}^{water} H_i^{f} + \dot{m}_{sea,i}^{salt} H_i^{s} \quad (33)$$

The first term in Equation 33 represents the evaporation duty which is used to sensibly heat the seawater to saturation conditions as well as vaporize a portion of the water. This distribution of heat duty is given by Equation 34.

$$Q_i^{EVAP} = Q_i^{vap} + Q_i^{sens} \quad (34)$$

The heat associated with vaporizing water in the seawater is given by Equation 35.

$$Q_i^{vap} = \dot{m}_{sea,i}^{stm}\left(H_i^{v} - H_i^{f}\right) \quad (35)$$

The enthalpy of the steam $\left(H_i^{v}\right)$ is calculated using Equation 35 and the saturation temperature of the effect given by Equation 36. The enthalpy of the saturated water $\left(H_i^{f}\right)$ and heated salt $\left(H_i^{s}\right)$ are determined using the effect temperature $\left(T_i^{eff}\right)$ and Equation 24 and Equation 23 respectively. For Equation 36, the boiling point elevation $\left(BPE_i^{eff}\right)$ for each effect is calculated using correlations by Sharqawy et al. [95].The BPE correlation is nonlinear and dependent on both salinity and temperature therefore for this work, an expected BPE is calculated for each effect. This BPE value is based on the expected salinity in each effect and the operating effect temperature which is already known. The expected salinity is updated after each optimization run to ensure an accurate calculation of the BPE value.

$$T_i^{v} = T_i^{eff} - BPE_i^{eff} \quad (36)$$

The overall heat balance for the seawater can be described by Equations 33 – 35 thus negating the need for a redundant energy balance for the sensible heating of seawater.

3.5.2.2 Brine flashing

The mass and energy balance on the brine flowing across effects is taken as a separate system from the heating and vaporization of inlet seawater. By utilizing a similar mass flowrate decoupling approach, the overall mass balance for the brine flow across effects is given by Equation 37.

$$\dot{m}_{brine,i-1}^{water} + \dot{m}_{brine,i-1}^{salt} + \dot{m}_{sea,i-1}^{water} + \dot{m}_{sea,i-1}^{salt} = \dot{m}_{brine,i}^{water} + \dot{m}_{brine,i}^{salt} + \dot{m}_{brine,i}^{stm} \quad (37)$$

In Equation 37, the first two terms represent the water and salt associated with the flashed brine in the previous effect. The subsequent third and fourth terms represent the water and salt associated with the brine stream formed after heating and vaporization of the seawater from the previous effect. This mass balance concept is illustrated in Figure 16.

Based on the overall mass balance, the corresponding water and salt component flows are given by Equations 38 and 39.

$$\dot{m}_{brine,i-1}^{water} + \dot{m}_{sea,i-1}^{water} = \dot{m}_{brine,i}^{water} + \dot{m}_{brine,i}^{stm} \quad (38)$$

$$\dot{m}_{brine,i-1}^{salt} + \dot{m}_{sea,i-1}^{salt} = \dot{m}_{brine,i}^{salt} \quad (39)$$

The energy balance on this flashing brine stream is given by Equation 40.

$$\dot{m}_{brine,i-1}^{water} H_{i-1}^{f'} + \dot{m}_{brine,i-1}^{salt} H_{i-1}^{s'} + \dot{m}_{sea,i-1}^{water} H_{i-1}^{f} + \dot{m}_{sea,i-1}^{salt} H_{i-1}^{s} = \dot{m}_{brine,i}^{water} H_{i}^{f'} + \dot{m}_{brine,i}^{salt} H_{i}^{s'} + \dot{m}_{brine,i}^{stm} H_{i}^{v'} \quad (40)$$

For the non-equilibrium flashing operation, the enthalpy associated with brine that flashed in the previous effect is denoted as $H_{i-1}^{f'}$ and $H_{i-1}^{s'}$, for water and salt respectively. These enthalpy values are calculated using the brine flashing temperature determined from Equation 41. Similarly, the enthalpy of the produced steam from the flashing brine is denoted as $H_i^{v'}$ and calculated using the flashing temperature of the brine $\left(T_i^{brine}\right)$.

$$T_i^{brine} = T_i^{eff} + NEA_i^{brine} \quad (41)$$

The difference in brine flashing temperature $\left(T_i^{brine}\right)$ and effect temperature $\left(T_i^{eff}\right)$ is the non-equilibrium allowance $\left(NEA_i^{brine}\right)$ given by Equation 42 and developed by [Miyatake et al. [98].

$$NEA_i^{brine} = \frac{33 \cdot \left(T_{i-1}^{eff} - T_i^{eff}\right)^{0.55}}{T_i^{v}} \quad (42)$$

The salinity of the brine leaving each effect is constrained to a maximum value to prevent scaling [63]. This maximum allowable salinity can be calculated using correlations adopted by

Ettouney et al. [82]. The maximum salinity constraint is given by Equation 43 and is applied to the last effect for a brine salinity discharge limit $\left(X_N^{MAX} = X_{brne}^{MAX}\right)$.

$$\frac{\dot{m}_{sea,i}^{salt} + \dot{m}_{brine,i}^{salt}}{\dot{m}_{sea,i}^{salt} + \dot{m}_{brine,i}^{salt} + \dot{m}_{sea,i}^{water} + \dot{m}_{brine,i}^{water}} \le X_i^{MAX} \tag{43}$$

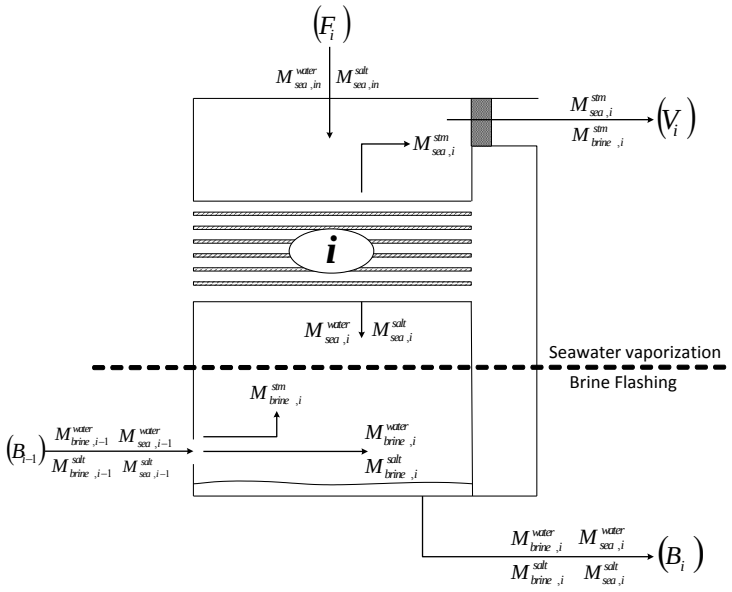

Figure 16 Diagram showing stream flow for seawater boiling and brine flashing in each effect

3.5.2.3 Effect evaporator

The heat supplied to the effect evaporators represents the latent heat released from condensing steam produced from vaporizing seawater, flashing brine and distillate flashing. The mass balance for the effect evaporator is given by Equations 44 – 45 and illustrated in Figure 17.

$$V_{i-1} + \dot{m}_{pot,i-1}^{stm} = \dot{m}_i^c \tag{44}$$

$$V_{i-1} = \dot{m}_{brine,i-1}^{stm} + \dot{m}_{sea,i-1}^{stm} \tag{45}$$

Based on the mass balance, the corresponding general heat balance on the effect evaporator is given by Equation 46 for the first effect and Equation 47 for effect 2 to N.

$$Q_1^{EVAP} = \dot{m}_{DS}^{stm}\left(H_{DS}^{v} - H_{DS}^{c}\right) \tag{46}$$

$$Q_i^{EVAP} = \dot{m}_{sea,i-1}^{stm} H_{i-1}^{v} + \dot{m}_{brine,i-1}^{stm} H_{i-1}^{v'} + \dot{m}_{pot,i-1}^{stm} H_{i-1}^{v''} - \left(\dot{m}_{sea,i-1}^{stm} + \dot{m}_{brine,i-1}^{stm} + \dot{m}_{pot,i-1}^{stm}\right) \cdot H_{i-1}^{c} \quad (47)$$

For Equation 47, the enthalpy of the flashing distillate $\left(H_i^{v''}\right)$ is determined using the flashing temperature derived from Equation 48 [82] and Equation 25. This flashing temperature is higher than the vapor saturation temperature by the non-equilibrium allowance given by Equation 49 [82].

$$T_i^{flash} = T_i^{v} + NEA_i^{flash} \quad (48)$$

$$NEA_i^{flash} = \frac{0.33 \cdot \left(T_{i-1}^{c} - T_i^{v}\right)}{T_i^{v}} \quad (49)$$

The enthalpy of the condensed vapors $\left(H_i^{c}\right)$ is calculated using the condensing temperature given by Equation 50 and the saturation liquid enthalpy given by Equation 24.

$$T_i^{c} = T_i^{v} - \Delta T_i^{losses} \quad (50)$$

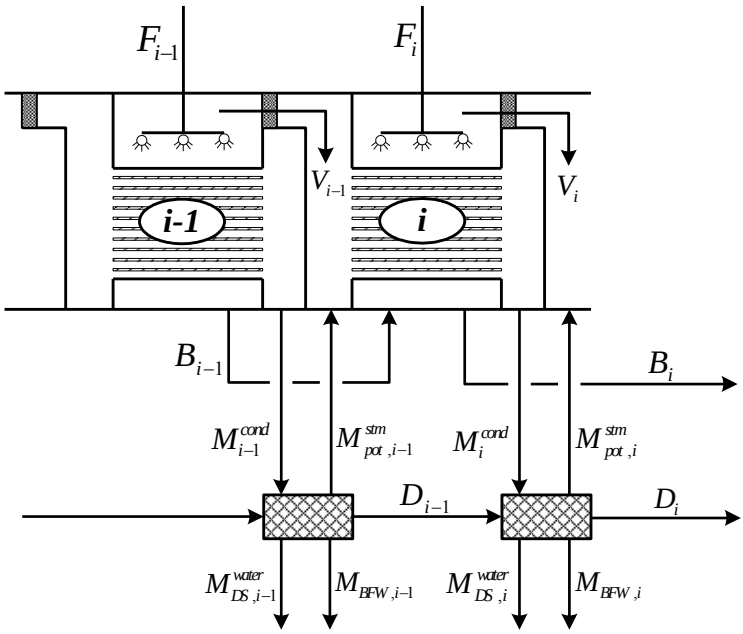

Figure 17 Diagram showing flow arrangement between effects and associated flash pots

The temperature losses used in Equation 50 is a direct result of the pressure drop across the demister, transfer line and condenser tubes of the evaporator in the subsequent effect. For this study we have taken the overall pressure drop to be constant across effect resulting in a varying temperature loss due to the non-linear relationship between saturation pressure and temperature. The chosen constant pressure drop is taken as 10 cmH_2O as suggested in literature [62].

3.5.3 Flash pot balances

The condensed vapor produced from each effect is mixed with condensate from the previous effect and sent to a flash pot. The general mass and energy balance on the flash pot is given by Equations 51 – 53.

$$D_{i-1} + \dot{m}_i^c = \dot{m}_{pot,i}^{stm} + \dot{m}_{DS,i}^{water} + \dot{m}_{BFW,i} + D_i \qquad \forall i = 2,3...,(N-1) \qquad (51)$$

$$\dot{m}_i^c = \dot{m}_{sea,i-1}^{stm} + \dot{m}_{brine,i-1}^{stm} + \dot{m}_{pot,i-1}^{stm} \qquad (52)$$

$$D_{i-1} H_{i-1}^{f''} + \dot{m}_i^c H_{i-1}^c = \dot{m}_{pot,i}^{stm} H_i^{v''} + \left(\dot{m}_{DS,i}^{water} + \dot{m}_{BFW,i} + D_i\right) \cdot H_i^{f''} \qquad (53)$$

In Equation 53, the enthalpy for the flashed liquid $\left(H_i^{f''}\right)$ is calculated using Equation 24 and the flashing temperature $\left(T_i^{flash}\right)$ described by Equation 48.The mass and energy balance across the flash pot for the first effect is different due to the lack of flashing brine, saturated water from a preceding flashing pot and water takeoff for de-superheating steam ejector exhaust steam. The mass and energy balance for this flash pot is then given by Equations 54 – 55 and illustrated in Figure 18.

$$\dot{m}_{DS}^{stm} + \dot{m}_{DS}^c = \dot{m}_{pot,1}^{stm} + \dot{m}_{BFW,1} + D_1 \qquad (54)$$

$$\dot{m}_{DS}^{stm} H_{DS}^c + \dot{m}_{DS}^c H_{DS}^f = \dot{m}_{pot,1}^{stm} H_1^{v''} + \left(\dot{m}_{BFW,1} + D_1\right) \cdot H_1^{f''} \qquad (55)$$

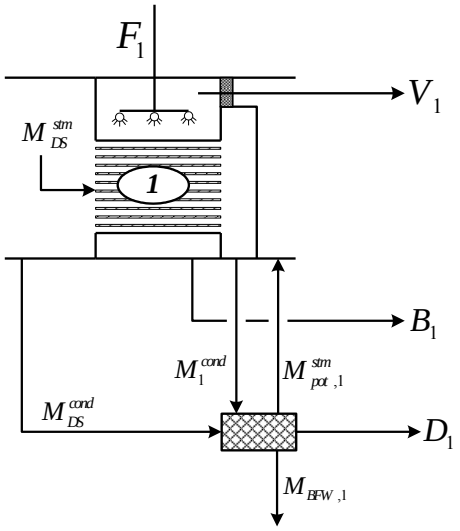

Figure 18 Diagram showing flow arrangement between effect one and associated flash pot

3.5.4 Steam ejector balance

The steam ejector represents the section of the process that significantly improves its thermal efficiency over the conventional MED design. The adopted model for the steam ejector is that developed by El-Dessouky [82]. It is a semi-empirical model that was developed using field data collected for over 35 years and relates the vapor entrainment ratio (mass of entrained vapor to motive steam) to the entrained vapor pressure (P_{ent}), motive steam pressure (P_{mot}) and ejector exhaust pressure (P_{exh}). This relationship is given by Equation 56 for the entrainment ratio (ε) and is valid for compressions ratios (Cr) greater than 1.81 and less than 6.

$$\varepsilon = 0.65 Er^{-1.54} P_{ent}^{1.72} P_{cxh}^{0.0679} \frac{\left(22.82 + 0.000421 P_{mot}^{1.34}\right)}{\left(9.32 + 0.128 P_{cxh}^{1.14}\right)} \tag{56}$$

$$Er = \frac{P_{mot}}{P_{ent}} \tag{57}$$

$$Cr = \frac{P_{exh}}{P_{ent}} \tag{58}$$

The entrainment vapor pressure (P_{ent}), ejector exhaust pressure (P_{exh}) and steam motive pressure (P_{mot}) are measured in kPa. The equation is valid for $\varepsilon \le 4$ and 100 kPa $\le P_{mot} \le 3500$

kPa. To calculate the pressure of the last effect for the purpose of determining the entrainment ratio, a correlation for saturated pressure under vacuum conditions was developed for this study. The correlation range is 0.7 to 1 bar and has a correlation coefficient of 0.9943 as compared to the IAWPS-IF97 Industrial formulation [93]. The correlation is given by Equation 59.

$$T_i^v = 101.52 \cdot \left(P_i^{eff}\right)^{0.3365} \tag{59}$$

Using the entrainment ratio for the steam ejector, the entrained vapor from the last effect is given by Equation 60 and illustrated in Figure 15.

$$Dr = \varepsilon \cdot S \tag{60}$$

For current MED-TVC models there are different approaches to relating structural changes in the MED design to the operational requirements of the steam ejector. For this study we have fixed the exhaust pressure so that the saturation temperature of the vapor is more than the operating temperature of the first effect by ΔT^{eff} [78].

3.5.5 De-super heater balance

The steam ejector exhaust is at superheated conditions and is cooled to saturated conditions using distillate feed from the flashing pots. For this study, the source of this distillate feed is optimized to maximize the distribution of heat supplied across effects thus improving unit economics. The mass balance on the de-superheater is given by Equation 61 and illustrated in Figure 19 while the heat balance is developed for both the steam ejector and de-superheater. The latter approach to the heat balance assumes that there are no heat losses across the steam ejector unit hence an energy balance across this unit is not required. The energy balance across both units is given by Equation 62.

$$S + Dr + \sum_{i=1}^{N} \dot{m}_{DS,i}^{water} = \dot{m}_{DS}^{stm} + \dot{m}_{DS}^{c} \tag{61}$$

$$S \cdot H_{mot}^{v} + Dr \cdot H_{N}^{v} + \sum_{i=1}^{N} \dot{m}_{DS,i}^{water} H_{i-1}^{f''} = \dot{m}_{DS}^{stm} H_{DS}^{v} + \dot{m}_{DS}^{c} H_{DS}^{f} \tag{62}$$

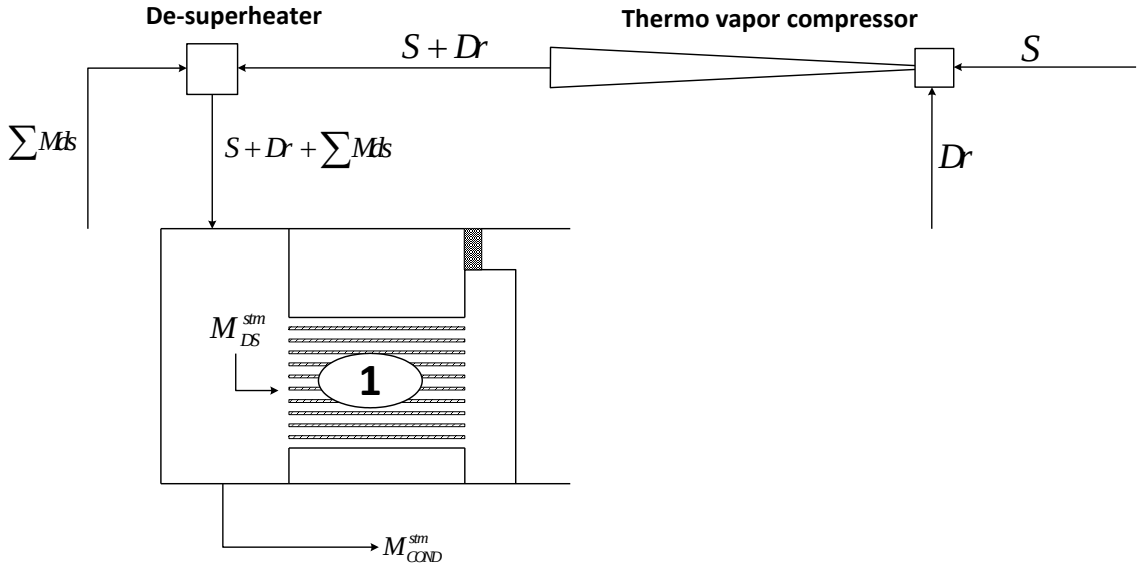

Figure 19 Diagram showing flow arrangement for steam eject and de-superheater

3.5.6 Seawater preheating balances

The remaining steam not entrained by the steam ejector is cooled in the condenser which simultaneously preheats some of the seawater before it is routed to each effect. This preheating scheme is also adopted for the cooling of total brine and distillate discharge. The amount of preheating done by each hot stream is optimized based on the minimum cost of heat exchanger area required for the overall preheating and cooling option. Figure 15 shows the possible options for preheating the seawater based on this design logic. The mass and energy balances for cooling these streams are given by Equations 63 – 70.

The condenser balance is given by:

$$V_N = \dot{m}^{stm}_{sea,N} + \dot{m}^{stm}_{brine,N} \tag{63}$$

$$\dot{m}^{stm}_{sea,N} = Dr + \dot{m}^{stm}_{cond} \tag{64}$$

$$\dot{m}^{stm}_{cond} H^{v}_{N} + \dot{m}^{stm}_{brine,N} H^{v'}_{N} - \left(\dot{m}^{stm}_{cond} + \dot{m}^{stm}_{brine,N}\right) \cdot H^{c}_{N} = Q^{COND}_{total} \tag{65}$$

$$Q^{COND}_{total} = Q^{COND}_{pre} + Q^{COND}_{xs} \tag{66}$$

The brine cooling balance is given by:

$$\dot{m}^{water}_{brine,N} + \dot{m}^{salt}_{brine,N} + \dot{m}^{water}_{sea,N} + \dot{m}^{salt}_{sea,N} = \dot{m}^{water}_{brine,EX} + \dot{m}^{salt}_{brine,EX} \tag{67}$$

$$\dot{m}_{BRINE} = \dot{m}^{water}_{brine,EX} + \dot{m}^{salt}_{brine,EX} \tag{68}$$

$$\dot{m}^{water}_{brine,N} H^{f'}_{N} + \dot{m}^{salt}_{brine,N} H^{s'}_{N} + \dot{m}^{water}_{sea,N} H^{f}_{N} + \dot{m}^{salt}_{sea,N} H^{s}_{N} = \dot{m}^{water}_{brine,EX} H^{f}_{EX} + \dot{m}^{salt}_{brine,EX} H^{s}_{EX} + Q^{BRINE}_{total} \tag{69}$$

$$Q^{BRINE}_{total} = Q^{BRINE}_{pre} + Q^{BRINE}_{xs} \tag{70}$$

The enthalpy of the exiting water $\left(H^{f}_{EX}\right)$ and salt $\left(H^{s}_{EX}\right)$ in the brine are calculating using the exit temperature determined by Equation 71.

$$T^{EX} = T^{MAX}_{sea} + \Delta T^{HEX}_{\min} \tag{71}$$

The distillate cooling balance is given by:

$$D_{N-1} + \dot{m}^{c}_{N} + \dot{m}^{stm}_{cond} + \dot{m}^{stm}_{brine,N} = \dot{m}_{DESAL} \tag{72}$$

$$D_{N-1} H^{f''}_{N-1} + \dot{m}^{c}_{N} H^{c}_{N-1} + \left(\dot{m}^{stm}_{cond} + \dot{m}^{stm}_{brine,N}\right) \cdot H^{c}_{N} = \dot{m}_{DESAL} H^{f}_{EX} + Q^{DIST}_{total} \tag{73}$$

$$Q^{DIST}_{total} = Q^{DIST}_{pre} + Q^{DIST}_{xs} \tag{74}$$

The seawater feed used in the brine and distillate preheaters as well as condenser is heated to an unknown hot temperature $\left(T^{hot}_{sea}\right)$. This optimal temperature is dictated by the economic tradeoff associated with the capital cost for preheater and condenser surface area. The energy balance on the seawater for this cooling purpose is given by Equations 75 – 76 while the constraint on the seawater temperature is given by Equations 77 – 78. In Equation 78, the last term, $\Delta T^{cond}_{\min}$, represents the minimum allowed temperature difference for the condenser.

$$\dot{m}^{PRE}_{sea} Cp^{avg} \cdot \left(T^{hot}_{sea} - T^{IN}_{sea}\right) = Q^{COND}_{total} + Q^{DIST}_{total} + Q^{BRINE}_{total} \tag{75}$$

$$N \cdot \left(\dot{m}^{water}_{sea,in} + \dot{m}^{salt}_{sea,in}\right) \cdot Cp^{avg} \cdot \left(T^{hot}_{sea} - T^{IN}_{sea}\right) = Q^{COND}_{pre} + Q^{DIST}_{pre} + Q^{BRINE}_{pre} \tag{76}$$

$$T^{hot}_{sea} \le T^{EFF}_{N} - \Delta T^{HEX}_{\min} \tag{77}$$

$$T^{hot}_{sea} \le T^{c}_{N} - \Delta T^{cond}_{\min} \tag{78}$$

A portion of the preheated seawater is sent to the effects while the remainder is discharged to sea after it is cooled to the maximum allowable return temperature. This is done via mixing with fresh seawater from a bypass line. The scheme for this is shown in Figure 15. The energy balance on this bypass flow is given by Equation 79 with the total seawater intake determined using Equation 80.

$$\dot{m}^{BYPASS}_{sea} Cp^{avg} \cdot \left(T^{MAX}_{sea} - T^{IN}_{sea}\right) = Q^{COND}_{xs} + Q^{DIST}_{xs} + Q^{BRINE}_{xs} \tag{79}$$

$$\dot{m}_{sea}^{TOTAL} = \dot{m}_{sea}^{PRE} + \dot{m}_{sea}^{BYPASS} \tag{80}$$

For Equations 75, 76 and 79, the average specific heat capacity $\left(Cp^{avg}\right)$is determined using the seawater salinity and average temperature given by Equations 81 – 82.

$$T_{sea}^{avg} = \frac{T_{sea}^{IN} + T_{sea,pre}^{MAX}}{2} \tag{81}$$

$$T_{sea,pre}^{MAX} = T_N^c - \Delta T^{HEX}_{\min} \tag{82}$$

3.5.7 Heat transfer area

The heat transfer area for each effect consists of sensible heating and vaporization area. Equations 83 – 85 are used to calculate these areas for each effect.

$$Q_i^{vap} = A_i^{vap} U_i^{eff} \left(T_{i-1}^c - T_i^{eff}\right) \tag{83}$$

$$Q_i^{sens} = A_i^{sens} U_i^{eff} \left(LMTD\right)_i^{sens} \tag{84}$$

$$\left(LMTD\right)_i^{sens} = \frac{T_i^{eff} - T_{sea}^{hot}}{\ln\left(\frac{T_{i-1}^c - T_{sea}^{hot}}{T_{i-1}^c - T_i^{eff}}\right)} \tag{85}$$

To reduce numerical difficulties within the optimization framework, the LMTD for the sensible heating area is calculated using Equation 86 which is an approximation developed by Chen [99].

$$\left(LMTD\right)_i^{sens} = \left[\left(T_{i-1}^c - T_{sea}^{hot}\right)\cdot\left(T_{i-1}^c - T_i^{eff}\right)\cdot\left(T_{i-1}^c - \frac{T_{sea}^{hot} + T_i^{eff}}{2}\right)\right]^{1/3} \tag{86}$$

For the brine and distillate preheater as well as condenser, Equations 87 – 89 are used to calculate the heat transfer areas while Equations 90 – 92 are used for LMTD calculations respectively.

$$Q_{total}^{BRINE} = A_{brine} U_{brine} \left(LMTD\right)_{brine} \tag{87}$$

$$Q_{total}^{DIST} = A_{dist} U_{dist} \left(LMTD\right)_{dist} \tag{88}$$

$$Q_{total}^{COND} = A_{cond} U_{cond} \left(LMTD\right)_{cond} \tag{89}$$

$$\left(LMTD\right)_{brine} = \left[\left(T_N^{eff} - T_{sea}^{hot}\right)\cdot\left(T^{EX} - T_{sea}^{IN}\right)\cdot\left(\frac{T_N^{eff} + T^{EX} - T_{sea}^{hot} - T_{sea}^{IN}}{2}\right)\right]^{1/3} \tag{90}$$

$$(LMTD)_{dist} = \left[\left(T_N^c - T_{sea}^{hot}\right) \cdot \left(T^{EX} - T_{sea}^{IN}\right) \cdot \left(\frac{T_N^c + T^{EX} - T_{sea}^{hot} - T_{sea}^{IN}}{2} \right) \right]^{1/3} \quad (91)$$

$$(LMTD)_{cond} = \left[\left(T_N^c - T_{sea}^{hot}\right) \cdot \left(T_N^c - T_{sea}^{IN}\right) \cdot \left(T_N^c - \frac{T_{sea}^{hot} + T_{sea}^{IN}}{2} \right) \right]^{1/3} \quad (92)$$

3.5.8 Boiler duty and pumping power

The boiler duty for steam production can vary depending on the optimal selection of boiler feed water sources from the process. Therefore Equation 93 is used to calculate this duty for feeds from different sources with different enthalpies.

$$Q_{boil} = {}^{1}\!/_{\eta_{boil}} \left(S \cdot H_{mot}^{v} - \sum_{i=1}^{N} \dot{m}_{BFW,i} H_i^{f''} \right) \quad (93)$$

For the pumping power requirements at the MED facility, Equation 94 is used. The pressure head requirement of each pump is assumed to be the difference between destination and source pressures. For the seawater intake pump this pressure difference is taken as that required for overcoming the pressure drop of the pretreatment section, solids removal, preheaters, feed nozzles and typical line losses. For the distillate pump, this study assumes discharge into a 10 m high storage tank open to atmosphere.

$$PW_{pump,j} = {}^{1}\!/_{\eta_{pump}} 0.1 \cdot \left(P_j^{Sink} - P_j^{Source}\right) F_{pump,j} \quad (94)$$

3.6 Economic analysis

The optimization of the MED-TVC process involves a tradeoff between the gain output ratio (GOR) and specific heat transfer area. The former is the ratio between the produced desalinated water and the required motive steam while the latter represents the total heat transfer area required per flowrate of desalinated water. Some studies have sought to optimize this tradeoff between both variables by applying various metrics [76] thus avoiding the addition of nonlinear cost functions into an already complex optimization framework. While this approach is useful, solutions obtained from the method may be economically suboptimal. As such an economic based optimization approach is required to simultaneously balance process topology and operation to minimize the overall cost of desalinated water.

For this study, correlations that account for direct capital costs as well as operating and maintenance costs are used to quantify the various process tradeoffs. The direct capital costs represent the expenditures that are directly associated with the construction of the MED plant;

cost incurred for the purchasing of process equipment [54]. To account for other capital costs incurred due to project engineering services, project development, financing and contingency, a percentage of the direct capital cost is used based on literature on desalination plants [59,100-104].

The operating costs are categorized as variable and fixed. The variable operating costs are those associated with the purchase of power, steam, chemicals and other requirements that are hinged to the varying production rate of desalinated water. Fixed operating costs represent expenditures that are required for the operation of the plant but are independent of the varying production rate. In many cases, these costs are related to the nameplate capacity of the plant or taken as a factor of the direct capital cost. For this study, both operating cost categories are estimated based on available data from literature [59,100-106]. In addition, maintenance costs are taken as a subset of the fixed operating cost.

A key component in the operating cost of the MED process is the price of motive steam. In some studies, a fixed cost of steam is used [78] while in others, the cost of the boiler and natural gas cost are used [106]. For this study the cost of the boiler and natural gas is used to determine the steam cost. The boiler cost as a function of operating pressure, superheated temperature and heat transferred is taken from the work by Al-Azri et al [107].

The total capital investment (TCI) for the MED plant is incurred before steady operation. As such it is compared to the operating costs by annualizing it based on the useful plant life. In addition, the operating costs are scaled to a yearly basis to evaluate it in relation to the annualized capital cost also referred to as the annualized fixed cost (AFC). The total operating cost (TOC) and annualized fixed cost (AFC) are used to determine the total annualized cost (TAC) which in this study is minimized to determine the optimal cost of desalinated water within a given set of conditions. Table 19 shows the TAC objective function and corresponding correlations used to determine its value.

Table 19 Summary of economic equations

Category	Equation	
Total annualized cost	$\min TAC = \frac{1}{L} TCI + TOC$	(95)
Total capital investment	$TCI = DCC + SC + CC_{contingency}$	(96)
Direct capital costs	$DCC = CC_{Site} + CC_{Intake} + CC_{\Pr etreatment} + CC_{Pipe} + CC_{Boiler}$ $+ CC_{Ejector} + CC_{De-\sup erheater} + CC_{Flash\ pot} + CC_{Heat\ exhangers}$ $+ CC_{Pump} + CC_{Post\ treatment} + CC_{waste\ disposal} + CC_{Building}$ $+ CC_{Electircal} + CC_{Auxiliary} + CC_{Start-up}$	(97)
Site Preparation	$CC_{Site} = 432 \times F^{FEED}$	(98)
Intake	$CC_{Intake} = 1964 \times F^{FEED}$	(99)
Pretreatment	$CC_{\Pr etreatment} = 2700 \times F^{FEED}$	(100)
Piping	$CC_{Piping} = 1370 \times F^{FEED}$	(101)
Boiler	$CC_{Boiler} = 3.13 \times N_P N_T Q_{boil}^{0.77}$ $N_P = 1.015 \times 10^2 \times P_{gauge} + 0.6$ $N_T = 4.63 \times 10^{-7} T_{sh}^2 + 6.28 \times 10^{-4} T_{sh} + 1$	(102)
Steam ejector	$CC_{Ejector} = 1949 \times (S + Dr)^{0.3}$	(103)
De-superheater	$CC_{De-\sup erheater} = 40745 \times \left(\dot{m}_{DS}^{cond}\right)^{0.3}$	(104)
Distillate flashing pot	$CC_{Pot} = \sum_{i=1}^{N} 40745 \times \left(\dot{m}_i^{cond} + D_{i-1}\right)^{0.3}$	(105)
Heat exchangers	$CC_{Heat\ exchangers} = CC_{Evaporators} + CC_{Condenser} + CC_{Brine} + CC_{Distillate}$	(106)
Evaporators	$CC_{Evaporators} = \sum_{i=1}^{N} 93.3 \times \left(A_i^{vap} + A_i^{sens}\right)^{0.7}$ $CC_{Condenser} = 93.3 \times \left(A_{cond}\right)^{0.7}$ $CC_{Brine} = 91 \times \left(A_{brine}\right)^{0.7}$ $CC_{Distillate} = 91 \times \left(A_{dist}\right)^{0.7}$	(107)
MED Pumps	$CC_{MED\ pumps} = 3516 \times \left(PW_{pumps}\right)^{0.65}$; $if\ PW_{pumps} \le 224\,kW$ $CC_{MED\ pumps} = 50000 + 234.5 \times PW_{pumps}$; $if\ PW_{pumps} \ge 224\,kW$	(108)
Post treatment	$CC_{Post\ treatment} = 785.5 \times F^{FEED}$	(109)
Waste disposal	$CC_{Waste\ disposal} = CC_{Solids} + CC_{Brine\ disposal}$	(110)
Solids removal	$CC_{Solids} = 432 \times F^{FEED}$	(111)

Table 19 (*continued*)

Category	Equation	
Brine disposal	$CC_{Brine\ disposal} = 1296 \times F^{FEED}$	(112)
Buildings	$CC_{Buildings} = 49.4 \times F^{DESAL} + 1728 \times F^{FEED} + 12185$	(113)
Electrical	$CC_{Electrical} = 11140 \times \left(F^{DESAL}\right)^{0.65}$	(114)
Auxiliary process equipment	$CC_{Auxiliary} = 785.5 \times F^{FEED}$	(115)
Start-up	$CC_{Start-up} = 785.5 \times F^{FEED}$	(116)
Soft costs	$SC = CC_{Financing} + CC_{Permitting}$	(117)
Project financing	$CC_{Financing} = 0.04 \times DCC$	(118)
Permitting	$CC_{Permitting} = 0.1 \times DCC$	(119)
Contingency	$CC_{Contingency} = 0.05 \times DCC$	(120)
Total operating costs	$TOC = VOC + FOC$	(121)
Variable operating costs	$VOC = OC_{Intake} + OC_{\Pr etreatemnt} + OC_{Gas} + OC_{Boiler} + OC_{Power} + OC_{Post\ treatment} + OC_{Service} + OC_{Chemicals} + OC_{Brine\ disposal}$	(122)
Intake	$OC_{Intake} = 495 \times PWC \times PW_{pumps}$	(123)
Pretreatment	$OC_{\Pr etreatment} = 33.7 \times PWC \times PW_{pumps}$	(124)
Natural gas	$OC_{Gas} = 8.76 \times 10^{-3}\, NGC \times Q_{boil}$	(125)
Boiler auxiliaries	$OC_{Boil} = 2.63 \times 10^{-3}\, NGC \times Q_{boil}$	(126)
Power	$OC_{Power} = 8760 \times PWC \times PW_{pumps}$	(127)
Post treatment	$OC_{Post\ treatment} = 458.7 \times PWC \times PW_{pumps}$	(128)
Service facilities	$OC_{Service} = 337 \times PWC \times PW_{pumps}$	(129)
Chemicals	$OC_{Start-up} = 1576.8 \times F^{DESAL}$	(130)
Brine disposal	$OC_{Start-up} = 315.4 \times F^{FEED}$	(131)
Fixed operating costs	$FOC = OC_{Labor} + OC_{Main} + OC_{Environemnt} + OC_{Indirect} + OC_{Spare}$	(132)
Labor	$OC_{Labor} = 473 \times F^{DESAL}$	(133)
Maintenance	$OC_{Main} = 631 \times F^{FEED}$	(134)
Environment	$OC_{Environment} = 50.5 \times F^{FEED}$	(135)
Indirect	$OC_{Indirect} = 757 \times F^{FEED}$	(136)
Equipment sparing	$OC_{Spare} = 0.01 \times DCC$	(137)

3.7 Optimization methodology

There are few studies on the optimization of MED processes that use a purely deterministic approach. For this study, the MED process model has been formulated as a mixed integer nonlinear program (MINLP) in which the objective function constitutes the minimization of the total annualized cost (TAC) described by Equations 95 – 137. To illustrate the tradeoffs of model variables, the problem is solved by using discrete steps. In each step, the number of effects, motive steam pressure and desired desalinated water flowrate are fixed prior to optimization while the minimal TAC is determined. This step is repeated for a varying number of effects at a fixed desalination water flowrate and steam pressure thus developing a single optimal cost profile for that steam pressure. In essence, the MINLP problem is decomposed into separate NLP problems that can be conceivably solved to global optimality using a deterministic solver.

To illustrate the outlined methodology a base case MED-TVC process with restrictions on de-superheater water and boiler feed water sources is optimized. These restrictions are based on the outlined configuration adopted by Sayaadi et al. [77]. The base case is then rerun to allow for the various flow options as well as evaluate effects of changes in other operating conditions. The input parameters for the model are shown in Table 20. These parameters are similar to those used in literature [81,100,102,103,106,108]. In specific, the natural gas and power cost are based on typical values expected in the Middle East; the main location for most thermal desalination plants [105,109].

Table 20 Input data and parameters used in MED process evaluation

Parameter	Symbol / Expression	Value
Capacity of MED (L/s)	F^{DESAL}	231.48[a]
Minimum number of effects	$N_{\min}$	4
Maximum number of effects	$N_{\max}$	16
Motive steam pressure (bar)	P_{mot}	2.4
Temperature of sea water inlet (°C)	T_{sea}^{IN}	25
Salinity of seawater inlet (ppm)	X_{sea}^{IN}	34,483[b]
Salinity limit on brine discharge (ppm)	$X_{brine}^{\max}$	71,800
Operating temperature of first effect (°C)	T_1^{EFF}	70
Operating temperature of last effect (°C)	T_N^{EFF}	40
Coolant seawater reject temperature (°C)	T_{sea}^{MAX}	30
Pump efficiency (%)	η_{pump}	80
Boiler efficiency (%)	η_{boil}	75
Seawater line pressure head (bar)	$P_{sea}^{\sin k} - P_{sea}^{source}$	2.0
Distillate storage pressure (bar)	$P_{distilalte}^{\sin k}$	2.0
Plant life (yrs)	L	20
Natural gas cost ($/GJ)	NGC	1.90 [c]
Power cost ($/kWh)	PWC	0.05

[a] Flow equivalent to 20,000 m^3/day
[b] Salinity for typical seawater
[c] Heating cost equivalent to $2.00 /MMBtu

3.8 Results and discussion

The optimization of the MED-TVC process was carried out using LINGO and run on a desktop PC (Intel® Core™ Duo, 2.27 GHz, 4 GB RAM, 64-bit operating system). The results from the optimization of the base case indicated that the minimal cost of desalinated water was $ 1.71/m^3 which is within the range of cost found in literature [59,101,102,110-114]. The optimal number of effects was 12, using the cost estimates outlined in this study. The data for the optimized process is shown in Table 21 and Table 22. The optimal area requirements for the base case highlight important contradictions in the typical approach to optimizing these systems. Some authors have suggested that an equal heat transfer area in each effect is preferable due to the cost savings associated with purchasing identical units [68,115]. These results highlight that this approach would only serve to add excess surface area to each effect which may have been eliminated to improve process economics. Studies that minimize heat transfer area in isolation as an approach to improving process economics are suboptimal designs. In fact the minimum water cost can yield suboptimal values of GOR and specific heat transfer area. This competing tradeoff is illustrated in Figure 20 and Figure 21 for the base case system.

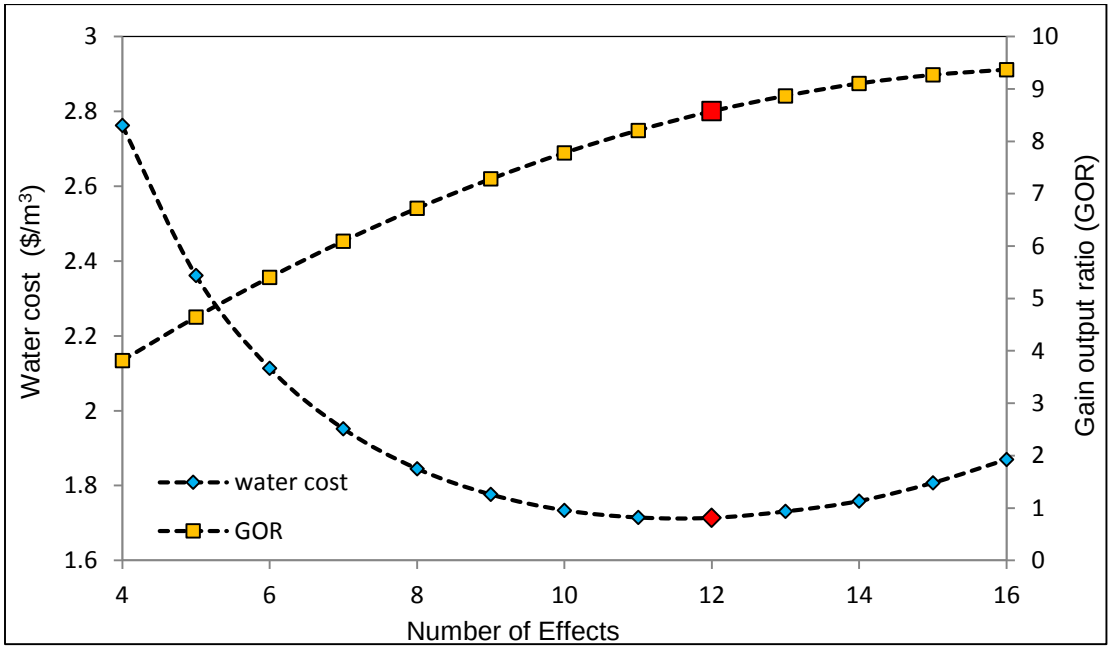

Figure 20 Tradeoff between gain output ratio (GOR) and minimum water cost

The model formulation presented in this study allows for the novel routing of auxiliary streams such as boiler feed water and de-superheating water as options to improve thermal efficiency and process economics. In allowing these options as an addition to the base case, the process economics are significantly improved. For these added optimization variables, the optimal process configuration data is given in Table 23 and Table 24.

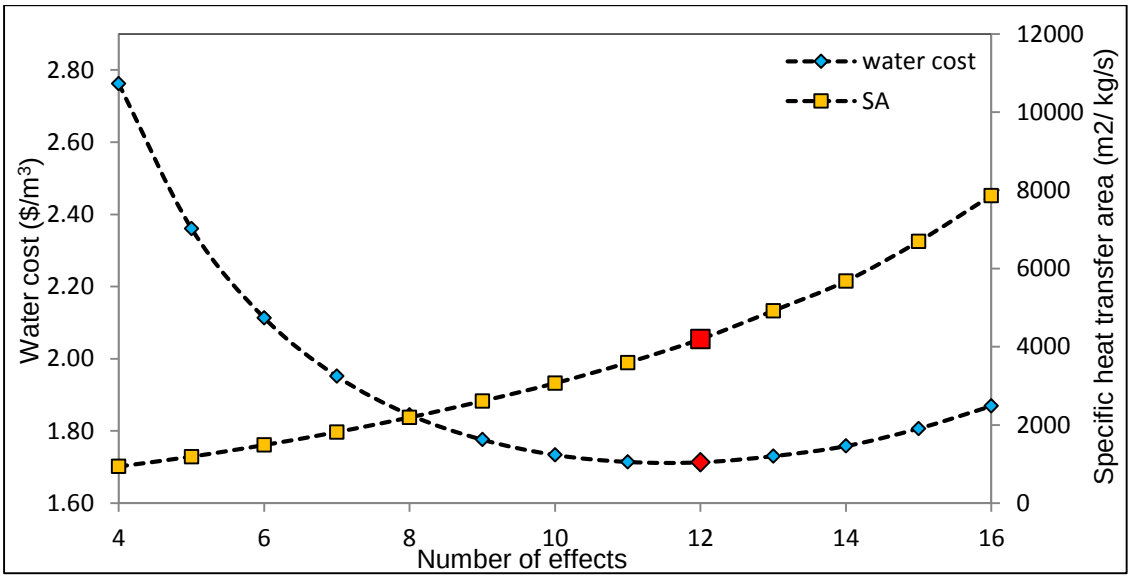

Figure 21 Tradeoff between specific heat transfer area (SA) and minimum water cost

The results immediately indicate that the process is improved via a significantly large flowrate of de-superheating water. This flow routing is unconventional but highlights a potentially novel option for improving the MED process. In this configuration, some of the steam ejector exhaust is used to heat de-superheating water to saturated conditions before sending to the flash pot associated with the first evaporator. This in essence allows for the distribution of heat to the second evaporator via distillate flashing as opposed to the conventional approach. The decision to utilize this configuration is not intuitive though in recognition of the salinity limits on each effect, the strategy is warranted. For the MED system, there are two opposing factors that results in this novel flow configuration. The first is the increasing allowable salinity from the first to last effect. The second is the decreasing availability of latent heat from the first to the last effect. The heat input to each effect is used to vaporize water from the fed seawater thus a decreasing heat input results in a simultaneous decrease in effect salinity. As such an optimal configuration with no salinity constraints would aim to maximize heat input in the first effect resulting in a salinity gradient that ends at the environmentally allowable discharge value. In contrast, an introduction of salinity limits that are below the optimal salinity, results in the need to redistribute heat from earlier effects to meet salinity constraints. The effect of the different scenarios on the concentration profile of the MED-TVC is illustrated in Figure 22.

Table 21 Data for optimized base case MED-TVC process with flow restrictions on boiler feed and de-superheater feed sources

Parameter		Effect 1	Effect 2	Effect 3	Effect 4	Effect 5	Effect 6	Effect 7	Effect 8	Effect 9
Effect boiling temperature	[°C]	70.0	67.3	64.5	61.8	59.1	56.4	53.6	50.9	48.2
Effect vapor production	[kg/s]	27.8	24.4	21.5	19.2	17.4	16.3	15.6	15.6	16.1
Effect brine flow	[kg/s]	33.7	70.7	110.6	152.9	196.9	242.1	287.9	333.8	379.1
Flash pot vapor production	[kg/s]	0.18	0.14	0.26	0.36	0.45	0.54	0.61	0.68	0.75
De-superheater water flow	[kg/s]	-	-	-	-	-	-	-	-	-
Boiler feed water flow	[kg/s]	26.9	-	-	-	-	-	-	-	-
Maximum effect salinity [a]	[ppm]	62764	66778	71259	76244	81774	87888	94625	102026	110130
Brine salinity	[ppm]	62764	59786	57298	55274	53646	52358	51368	50643	50161
Effect duty	[GJ/hr]	239	211	186	165	149	137	129	125	126
Effect area	[m^2]	15285	19367	17314	15644	14387	13576	13250	13462	14286

[a] Maximum allowable effect salinity based on correlation adopted from study by El-Dessouky et al. [82]

Table 21 (*continued*)

Parameter		Effect 10	Effect 11	Effect 12
Effect boiling temperature	[°C]	45.5	42.7	40.0
Effect vapor production	[kg/s]	17.2	18.8	20.9
Effect brine flow	[kg/s]	423.4	466.1	506.6
Flash pot vapor production	[kg/s]	0.82	0.90	-
De-superheater water flow	[kg/s]	-	1.20	-
Boiler feed water flow	[kg/s]	-	-	-
Maximum effect salinity [a]	[ppm]	118975	128603	139051
Brine salinity	[ppm]	49906	49870	50049
Effect duty	[GJ/hr]	130	140	153
Effect area	[m^2]	15841	18321	22070

Table 22 Data for optimized base case MED-TVC process with flow restrictions on boiler feed and de-superheater feed sources

Parameter		Value
Feed Flow	[kg/s]	61.4
Preheated feed temperature	[^{o}C]	33.3
Power usage	[kWh/m^3]	1.60
Condenser duty	[GJ/hr]	134.7
Brine/ Feed preheater duty	[GJ/hr]	73.8
Distillate/Feed preheater	[GJ/hr]	37.0
Seawater coolant flow	[kg/s]	4111
Total seawater flow	[kg/s]	4848
Water recovery	[%]	32.4%
Gain output ratio		8.6
Water cost	[$/m^3]	1.71

Table 23 Data for optimized base case MED-TVC process without flow restrictions on boiler feed and de-superheater feed sources

Parameter		Effect 1	Effect 2	Effect 3	Effect 4	Effect 5	Effect 6	Effect 7	Effect 8	Effect 9
Effect boiling temperature	[^{o}C]	70.0	67.3	64.5	61.8	59.1	56.4	53.6	50.9	48.2
Effect vapor production	[kg/s]	15.9	19.4	21.9	20.5	19.4	18.6	18.2	18.2	18.4
Effect brine flow	[kg/s]	21.0	38.4	53.4	69.9	87.4	105.6	124.3	143.1	161.5
Flash pot vapor production	[kg/s]	5.63	4.36	0.17	0.27	0.37	0.46	0.55	0.63	0.71
De-superheater water flow	[kg/s]	-	860.57	-	-	-	-	-	-	-
Boiler feed water flow	[kg/s]	23.9	-	-	-	-	-	-	-	-
Maximum effect salinity [a]	[ppm]	62764	66778	71259	76244	81774	87888	94625	102026	110130
Brine salinity	[ppm]	60504	66018	71259	72669	72619	72070	71450	70958	70697
Effect duty	[GJ/hr]	138	163	180	168	158	151	146	144	145
Effect area	[m^2]	8775	16728	19971	19716	19030	18700	18770	19302	20391

[a] Maximum allowable effect salinity based on correlation adopted from study by El-Dessouky et al. [82]

Table 23 (*continued*)

Parameter		Effect 10	Effect 11	Effect 12
Effect boiling temperature	[°C]	45.5	42.7	40.0
Effect vapor production	[kg/s]	19.0	20.0	21.2
Effect brine flow	[kg/s]	179.4	196.4	212.1
Flash pot vapor production	[kg/s]	0.79	0.88	0.00
De-superheater water flow	[kg/s]	-	-	-
Boiler feed water flow	[kg/s]	-	-	-
Maximum effect salinity [a]	[ppm]	118975	128603	139051
Brine salinity	[ppm]	70725	71081	71800
Effect duty	[GJ/hr]	148	154	162
Effect area	[m^2]	22188	24949	29154

Table 24 Data for optimized base case MED-TVC process without flow restrictions on boiler feed and de-superheater feed sources

Parameter		Value
Feed Flow	[kg/s]	36.9
Preheated feed temperature	[°C]	33.1
Power usage	[kWh/m^3]	1.49
Condenser duty	[GJ/hr]	141.3
Brine/ Feed preheater duty	[GJ/hr]	30.2
Distillate/Feed preheater	[GJ/hr]	36.3
Seawater coolant flow	[kg/s]	4032
Total seawater flow	[kg/s]	4475
Water recovery	[%]	54.0%
Gain output ratio		9.7
Water cost	[$/$m^3$]	1.54

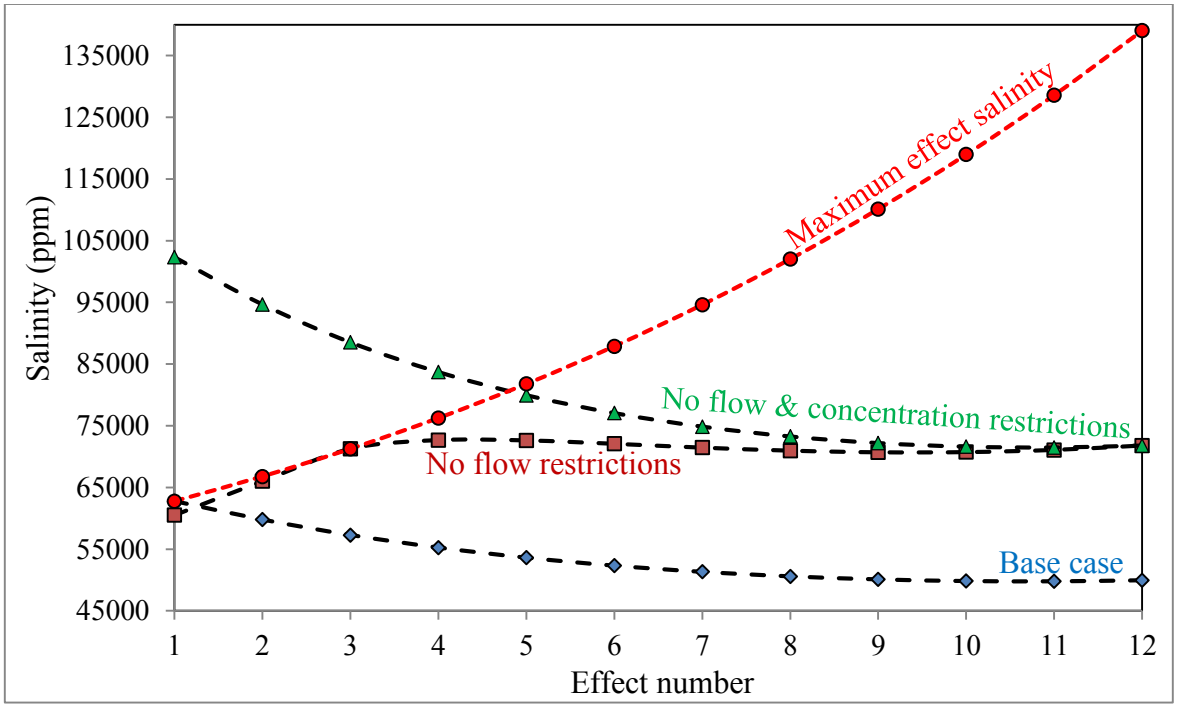

Figure 22 Comparison of various configuration and operational constraints on minimizing water cost

3.8.1 Investigating effects of motive steam pressure

The motive steam pressure to the MED-TVC process is a required decision variable that can be influenced by many factors. Commercial MED processes have used a range of pressures that may be suboptimal for the given MED configuration. Considering that the latent heat of vaporization of water decreases with increasing pressure, it is conceivable that the thermal performance of the MED-TVC process decrease with increased steam pressure. Therefore the choice of a higher steam pressure would be for steam ejector stability as well availability. This tradeoff of steam pressure to minimal water cost is highlighted in Figure 23 and Figure 24.

3.8.2 Desalinated water flow effects on cost

It is well known that the cost of any product from a process decreases as the scale of operation increases. This is due to the advantages of the economies of scale. Therefore it is easy to accept that the cost of desalinated water increases as the scale of operation increases. The results from varying the water flow rate corroborate this advantage as shown in Figure 25 though non-intuitively, the optimal number of effects decreases as the plant capacity decreases. This is

shown in Figure 26 and can have numerous implications when developing multi-train processes. The determination of the optimal number of effects for each train becomes a nontrivial decision and cannot be based on simple multiplication or reduction of existing technology.

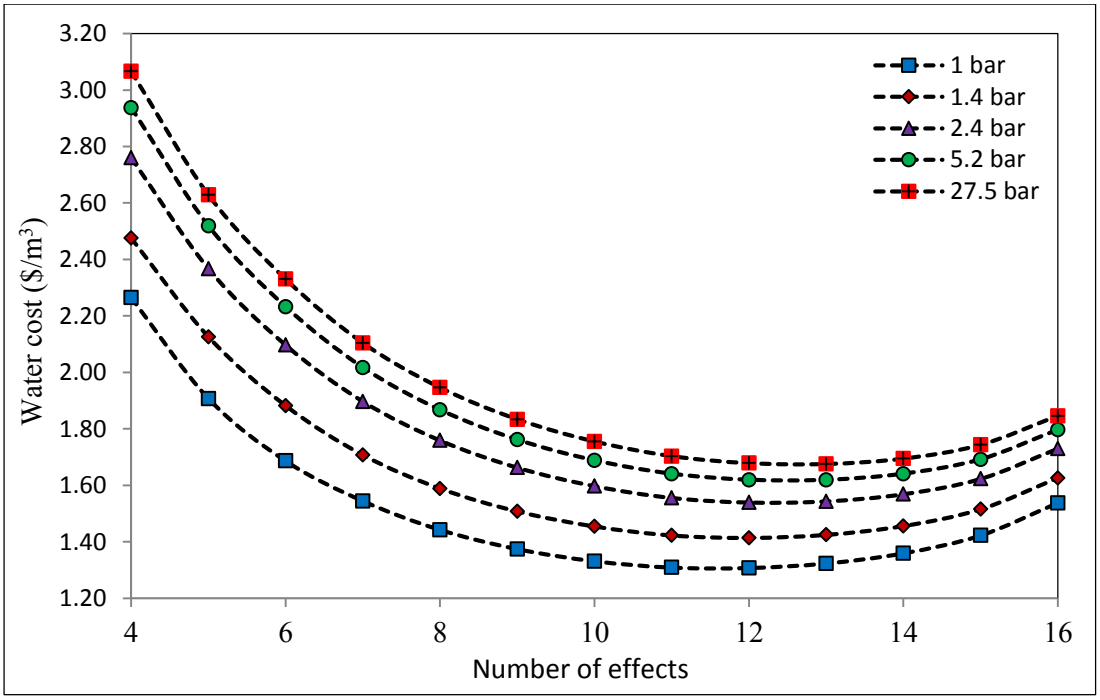

Figure 23 Effects of steam supply pressure on the minimum water cost

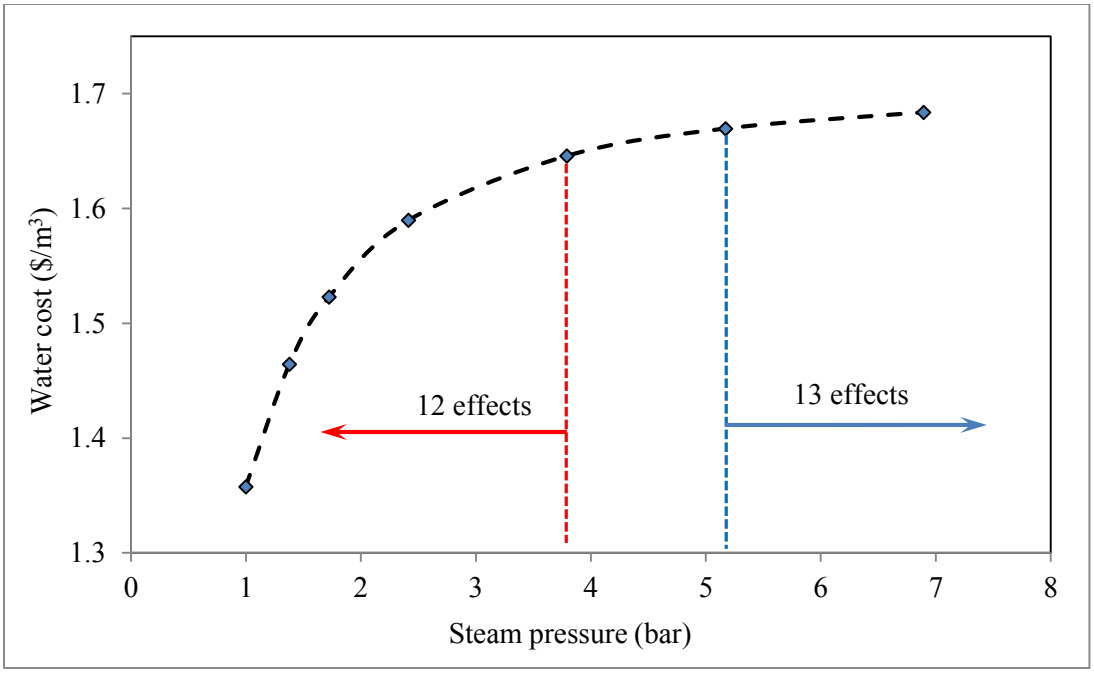

Figure 24 Effects of steam supply pressure on the minimum water cost

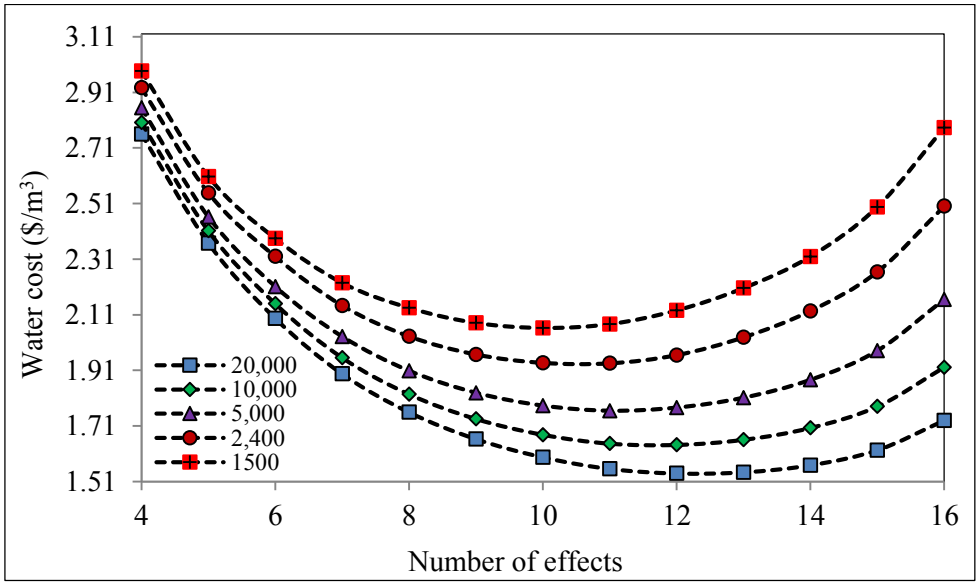

Figure 25 Effects of MED capacity and number of effects on the minimum water cost at 2.4 bar

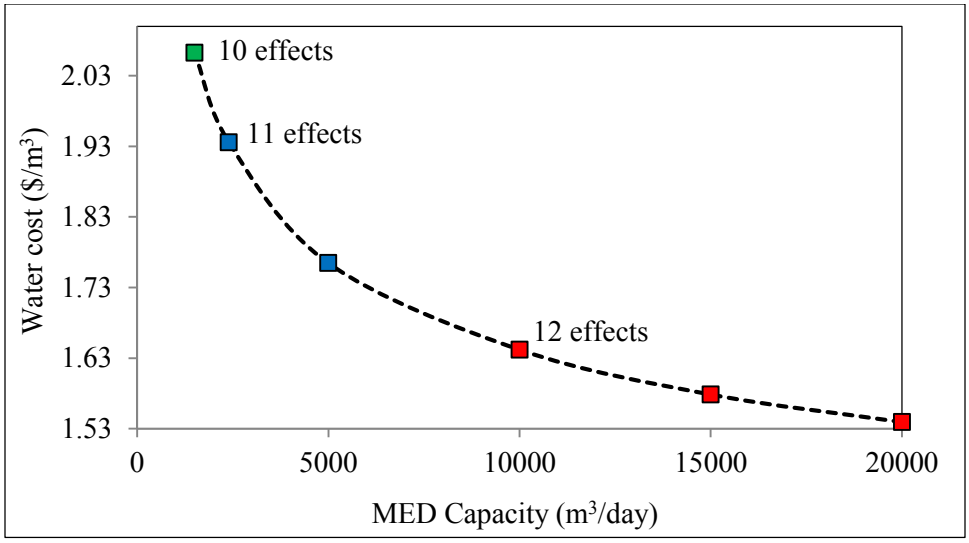

Figure 26 Minimum water cost at various MED plant capacities at 2.4 bar

3.8.3 Seawater salinity effects on cost

A seawater desalination plant can receive feed of various salinities throughout the year. More importantly, the decision to build a desalination plant incorporates the effects of seawater salinity on the economics and reliability of the process. As salinity increases, the potential for water recovery diminishes resulting in an increase required feed flowrate as well as energy for sensible heating. As such a sensitivity analysis on the variation in minimum water cost with salinity would yield an expected nonlinear increasing relationship as shown in Figure 27. In addition, the required number of effects increases to improve GOR thus counteracting the increased power cost for pumping more feed. This result is shown in Figure 28 and Figure 29 for seawater from Eastern Mediterranean (EM), Red Sea (RS) and Arabian Gulf (AG).

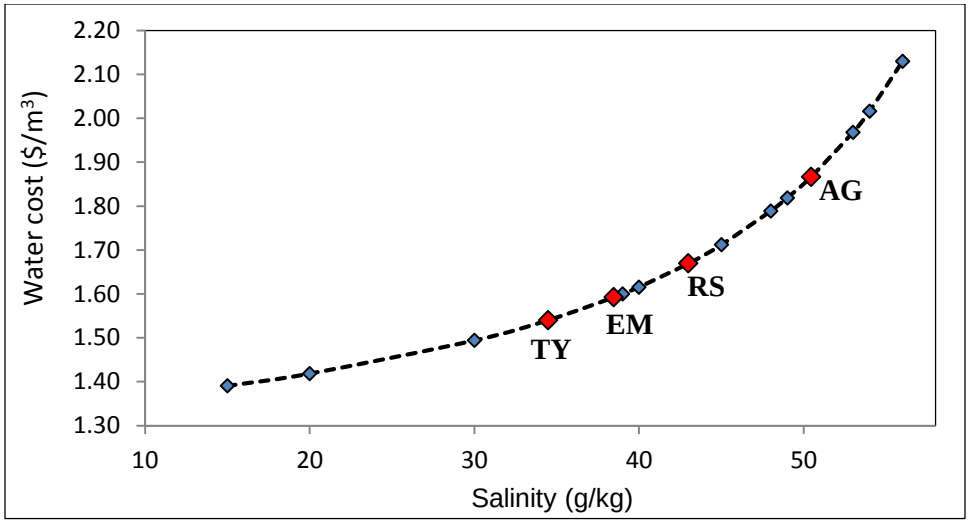

Figure 27 Variation in minimal water cost with salinity for a 20,000 m^3/day MED-TVC plant at 2.4 bar

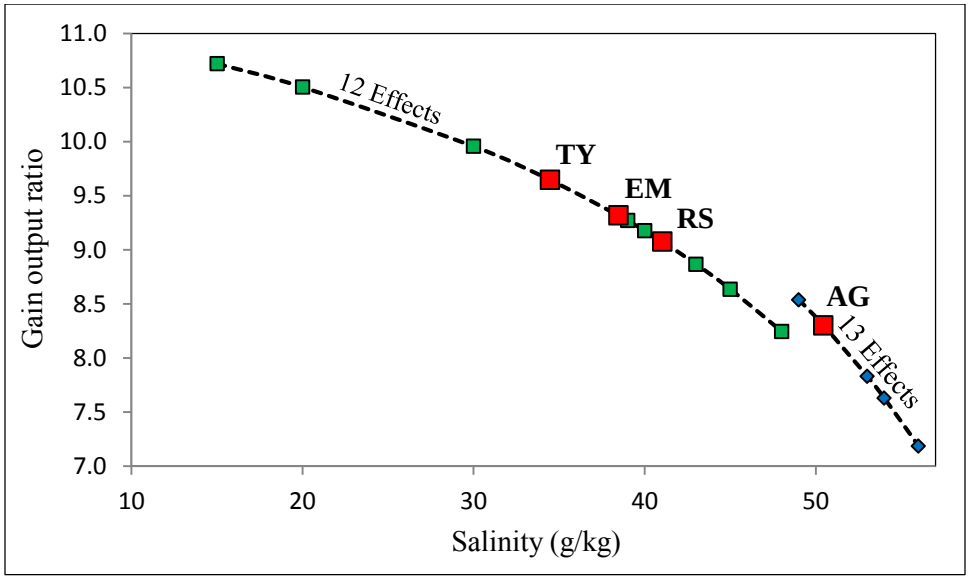

Figure 28 Variation in optimal GOR with salinity for a 20,000 m^3/day MED-TVC plant at 2.4 bar

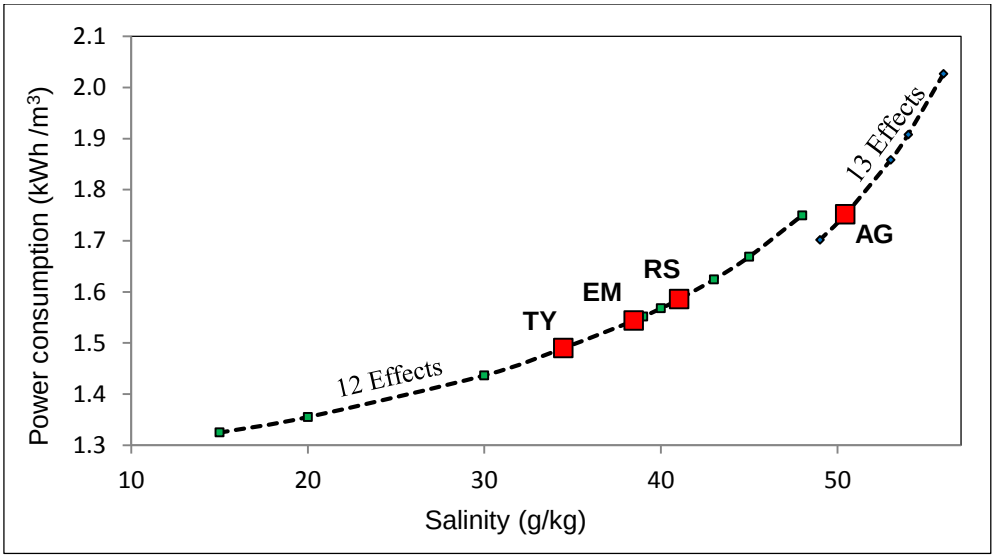

Figure 29 Variation in optimal power consumption with salinity for a 20,000 m^3/day MED-TVC plant

There is an interesting feature in the results illustrated by Figure 28 and Figure 29. Both parameters show a discontinuous relationship with varying salinity. As the salinity increases, the available water for recovery intrinsically decreases thus affecting the optimal gain output ratio (GOR). A decreasing GOR translates to an increasing amount of steam required per unit desalinated water. This represents an increasing cooling requirement manifested as an increasing power consumption for seawater pumping. The discontinuity results from the tradeoff of operating cost for power compared to the capital cost for an additional effect. The additional effect improves GOR thus reducing overall power consumption and minimizes water costs. Another feature worth noting is the optimal number of effects for MED plants receiving seawater from either Eastern Mediterranean or the Red Sea. Both are geographical close but yet optimal plant designs are different. This illustrates that for neighboring countries with similar capital costs, the MED design strategy may vary based on the choice of seawater source.

OPEX effects on MED configuration

Capital and operating cost correlations intrinsically contain some degree of uncertainty [116,117]. A sensitivity analysis of the water price to the capital and operating cost would yield the obvious results of increased price for increased cost. An insight that is not intuitive is the optimal number of effects which actually decreases as price of energy is reduced. This is shown in Figure

30 and is due to the ratio of influence of the capital and operating cost on the overall cost of water. As the operating costs decrease, the optimal configuration would shift to minimize total capital investment. This is manifested as a reduction in the number of effects for the same first and last effect operating temperature. This insight has implications when constructing new MED facilities that are coupled to inexpensive steam sources. While it would be reasonable to take advantage of the increased GOR from a greater number of effects, the decision may be economically suboptimal.

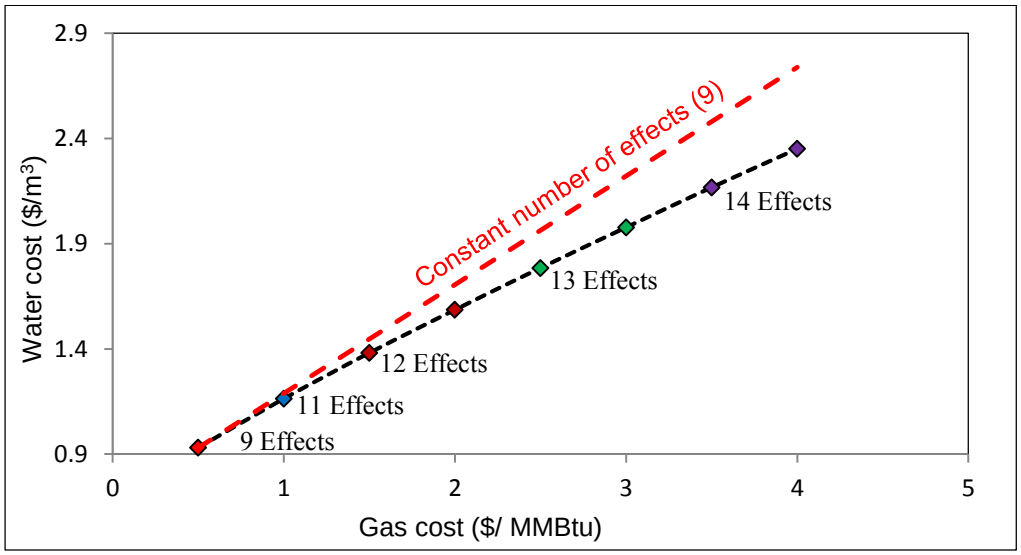

Figure 30 Effects of gas cost on minimum price of water

3.9 Summary

An alternative mathematical formulation for the modeling and optimization of the MED-TVC process has been presented. The model is based on specific enthalpies of seawater which deviates from the conventional specific heat capacity based approach. The model can be solved quickly using deterministic solvers to provide novel configurations and insights for the MED-TVC process. Conceptually, it can also be used to model hybrid MED-MSF structures without having to neglect numerous thermodynamic limitations as done in other studies. In addition, the model can also be used to economically optimize the coupling of power generation systems with thermal desalination processes without having to fix the configuration of both systems.

The results from this study have highlighted potential opportunities for the use of the presented model in future works. Firstly, the results indicate that salinity constraints on the effects can be overcome by novel flow distributions of evaporator condensate. Future work in determining these novel flow distributions and their potential in hybrid MED-MSF plants may be valuable. Secondly, the optimal number of effects consistently changed with varying operating and economic conditions. This changing number of effects is actually a reflection of a changing optimal effect temperature difference. Consequently, there is potential to optimize this value while changing the final effect operating temperature. An approach has been attempted for this concept though the presented model eliminates the need for genetic algorithms and negation of thermodynamic limitations.

Furthermore, the heuristics involved in selecting train capacities for a thermal desalination plant are not known and may yield suboptimal configurations if based on current attainable capacities. With updated economic models for different regions, the presented methodology may be used to assist engineers in feasibility studies for new thermal desalination or dual purpose plants.

CHAPTER IV

THERMOECONOMIC OPTIMIZATION OF THE WATER-ENERGY NEXUS FOR SIMULTANEOUS HEAT, POWER AND WATER GENERATION USING A TOTAL SITE ANALYSIS AND A HYBRID MED-RO DESALINATION PROCESS

4.1 Introduction

The provision of a safe, reliable and sustainable supply of water and energy is required for the health and security of any country's economy. As population grows and standard of living improves, so too would the requirement for access to fresh water and inexpensive energy sources. This demand for water and energy resources has prompted countries to seek alternative routes for supplying both vital resources. In the case of the energy supply, biomass, natural gas and coal to liquid technologies have been explored in great detail to maximize the use of the local carbon resources. This effort has been promoted and driven by the increasing and sometimes capricious crude oil prices. There is a similar parallel for water resources where increased scarcity has prompted countries to consider desalination options as an alternative to the conventional supply of fresh water [118-120].

To date, there are many countries that have adopted desalination technologies for supplying fresh water for domestic, industrial and agricultural use. In particular, many Middle Eastern countries depend on seawater desalination as their major source of fresh water supply. In fact, over 75 million people worldwide obtain their fresh water from seawater and or brackish water desalination[121]. This number is expected to increase as the cost of some desalination technologies further decrease and water scarcity issues continue to hamper economic expansion.

The demand for both water and energy resources cannot be addressed in isolation since they are both inextricably and reciprocally dependent; the treatment and transportation of water requires inexpensive energy while the production of energy requires large amounts of water. This relationship is termed the water-energy nexus and can have numerous implications when developing new processes for either energy or water production.

In countries that are energy rich, the use of thermal and membrane desalination represents the typical standalone solution for fresh water supply [122-124]. For the thermal desalination technologies, this has changed over the past decades due to the appreciation of the water-energy relationship and mounting pressures to reduce GHG emissions and improve process thermal efficiencies. In specific, power plants are now designed to be dual purpose or power and water

cogenerating facilities. This represents an ideal synergy between two energy intensive processes and highlights the benefits of optimizing the water-energy nexus for the water-power tradeoff. This concept is well accepted and established in Middle Eastern countries which are experiencing population growth and a simultaneous demand for water and energy [125-127].

A common approach to the design of processes is to simultaneously consider all integration opportunities with respect to heat, power and water. In most cases, the water integration only includes the existing water sources and sinks in the process without considering the potential for water production via optimizing the water-energy nexus. The concept of dual generation of power and water from some power plants can thus be adopted and extended to any process that has excess energy that can be converted to power and steam for use in membrane and thermal desalination respectively. In essence this approach would be limited to processing facilities that have access to a saline water source that can be purified via either thermal or membrane desalination technologies.

There are numerous studies that have focused on dual purpose plants that utilize the excess energy from power production to drive the thermal desalination process [128-131]. A study by Manesh et al. [106] provided an extension to these works by utilizing excess low pressure steam and power from a plant's utility network to drive thermal and membrane desalination units respectively. The predesigned utility network developed by Aguillar et al. [132] was used as the case study. In this study a systematic framework was developed for which any process could be analyzed and optimized for the production of heat, power and water for use within the process or exported. The developed methodology utilizes a total site analysis approach to determine process targets as well as appropriate steam levels for the process heating. In essence, the developed systematic approach would encompass any process that has excess energy which includes dual purpose plants. In addition, the Gas to liquids (GTL) process utilizing the Autothermal reforming (ATR) option, as presented by Gabriel et al. [133] is used as a case study to illustrate the usefulness of the developed methodology.

4.2 System configuration

A typical processing facility consists of numerous streams that may require either heating or cooling. These energy transfer requirements are satisfied first by process stream heat integration and finally by the site's utility system. With proper heat integration methods, the energy loads on the utility system is reduced thus lowering its capital and operating cost as well as GHG emissions. For processes with a surplus of energy, there is potential to utilize this excess energy for the combined production of power and water. This strategy would be solely dependent on the facility's location, regional demand for either resource, available infrastructure as well as governmental regulations for exporting either commodity. The production of both resources would require a systematic approach to optimizing their mutual dependency.

The interdependent relationship between water and energy creates a fascinating dilemma when considering the location and process design of any facility. The optimal use of this water-energy nexus is not a straightforward task and in some cases has been missed when evaluating and optimizing numerous systems utilizing a cooling water utility [106,134]. The optimization of the water-energy relationship thus requires a systematic methodology for achieving the maximum benefits in the production of either resource.

For this study, the optimization of the water-energy nexus would be considered in isolation from the overall process design. In fact, the globally optimal design of the process and its associated utilities would incorporate a complex relationship of water, energy and mass (process) which may be easier accepted as a concept than realized as a numerically achievable optimization problem. In this study the overall interactions among process, power and water generation sections are shown in Figure 31.

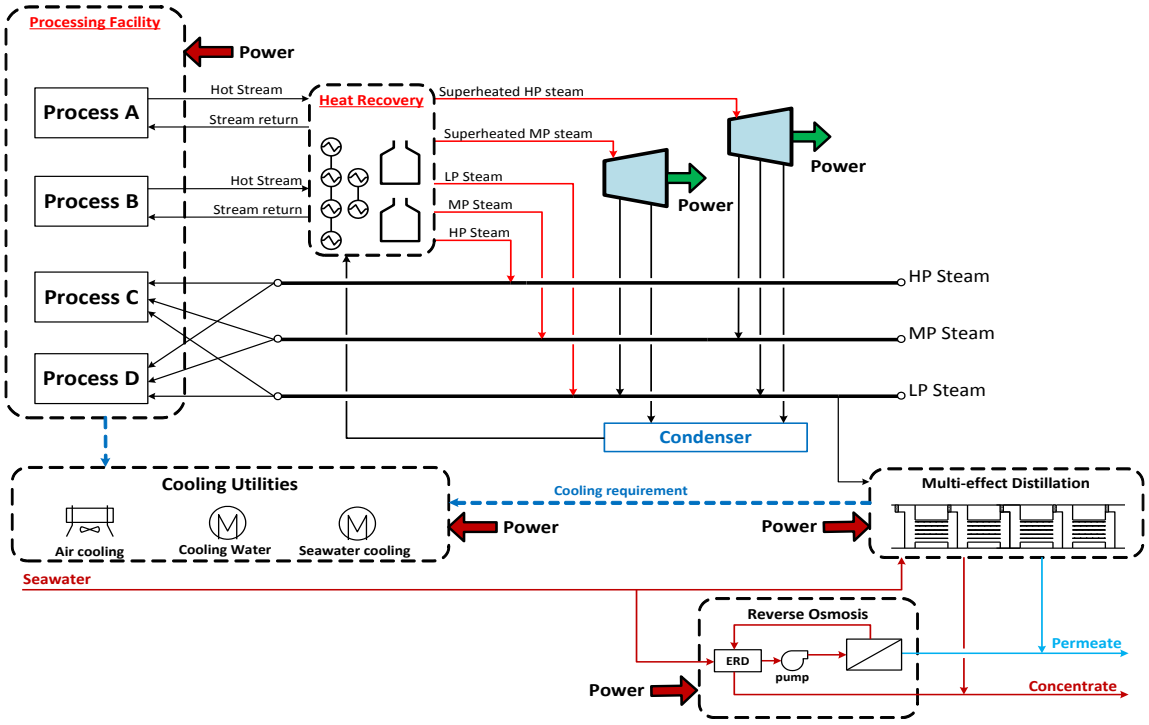

Figure 31 Overall interaction among steam, power and water generation sections

4.3 Problem statement

The objective of this study is to develop such a framework for optimizing the co-generation of both resources from processes that have a surplus of energy at various qualities. In this work, the problem to be addressed is stated as follows with the given information:

- A predesigned process with a given set of hot streams to be cooled and cold streams to be heated. Given also are the heat capacities of each process stream as well as inlet and target outlet temperatures
- Process steam or parasitic steam requirements, if any
- Available fuel gas from the process, if any, that can be used as a heating source in a furnace or boiler. The flow rate and heating value of the fuel is known
- Process power requirements
- Water requirements for the process or external to the process along with their respective concentration constraints
- Thermal and membrane desalination option for water production

The developed methodology for optimizing the usage of available energy sources for the production of process heating, power and excess water while accounting for economic implications should address the following questions:

- What is the target for excess heat from the process, if any?
- What is the configuration of the integrated system that generates heat and power required for the plant as well as for the thermal and membrane desalination technologies
- What is the capacity ratio between thermal and membrane desalination technologies
- What is the water management strategy for the integrated process

4.4 Approach

The study utilizes four (4) building blocks in developing the overall superstructure for optimizing the use of plant surplus energy. These building blocks are -:

1. Heat recovery section inclusive of final cooling requirements
2. Power generation section utilizing steam turbines
3. Water generation via thermal and membrane desalination
4. Water integration strategy via direct recycle

In Figure 31, the water management strategy is not shown though represents the link between the process, utilities and generated water section. In fact, it would dictate the need and source of generated water based on the regional scenario. To determine the overall structure for evaluating this water-energy tradeoff, a systematic method was developed in this study. The holistic approach is as follows with a more in depth approach to the optimization steps given later:-

1. Perform Total site analysis to determine targets for excess energy and appropriate steam levels for the process
2. Evaluate excess heat quality to determine whether power in addition to steam can be produced and supplied to both membrane and thermal desalination technologies respectively
3. Develop a heat recovery system for supplying steam to the process, steam turbine network and thermal desalination technology
4. Develop a steam turbine network that can utilize steam from available levels established by the total site analysis in step 1

5. Utilize existing thermal and membrane desalination models to determine economic tradeoff of producing power and water from overall integrated system
6. Develop direct recycle water management strategy based on process water sources and sinks as well as generated water sources
7. Utilize economic evaluation methods to determine optimal integrated system topology based on interplant water demands and potential export opportunities

Using this approach, a heuristics based superstructure can be developed and solved to determine the optimal configuration for maximizing the benefit of the water-energy nexus.

4.4.1 Total site analysis

The total site analysis method was first introduced by Dhole and Linnhoff [135]. For this methodology, sites are considered as separate processes that are linked via steam lines. Each site is evaluated using thermal pinch analysis to identify targets for minimum heating and cooling then utilized in an overall total site analysis to determine potential heat integration via steam connections. I addition, the analysis also identifies the potential for water and power generation from any excess process heat.

For this study, the total site analysis represents the first step in identifying excess heat targets for potential water and power generation. Given the low grade heating requirements of thermal desalination, the analysis is first performed to identify the potential for water generation via thermal desalination then subsequently evaluated for power generation. For this study, the given total site is segregated into processing sections based on feasibility of integrating process streams. This integration feasibility is determined via the use of a heuristics based approach that considers distance constraints. In essence, the identification of sites is subjected to the experience of the engineer with the process. An alternative approach would be to utilize an optimization framework that targets the minimization of piping and additional infrastructural cost tradeoffs associated with long distance heat transfer options as considered in literature for various processes [136].

The total site analysis also identifies the individual hot process streams that can produce steam for various site heat sinks. For this outlined methodology, these hot streams would be adjusted for heat lost due to process stream integration. In addition, available fuel gas energy is also adjusted for cold streams that cannot be heated to target temperatures using hot streams. The adjustment heuristics would be based on typical rules established for minimizing heat exchange area, number of heat exchangers as well as overall network cost. In essence a separate heat

exchange network would be developed for the process stream integration than that for boiler feed water and steam generation. For this study, the former network would not appear in the optimization framework due to the added numerical complexity of incorporating all these options based on the approach by Yee et al. [137]. For the outlined methodology, process stream integration is prioritized ahead of heat recovery for water and power generation.

4.4.2 Heat recovery model

The heat exchange model is developed using the adjusted hot process streams and the discrete boiler feed water and steam temperature levels. This discrete model allows for the use of fixed enthalpies which can be calculated using the correlations developed by Al-Azri et al. [107] or via the use of the IAPWS-IF97 Industrial formulation for the thermodynamic properties of water and steam [93]. The concept of the discrete temperature levels can be illustrated using the temperature interval diagram shown in Figure 32. The overall structure of the heat exchange network is shown in Figure 33 and is used to develop a linear programming (LP) mathematical model for the heat transfer process given by Equations 138 - 145.

4.4.2.1 Mathematical model development

Overall heat balance of hot process stream (HPS)

$$\left(TIN_i - TOUT_i\right)FCp_i = q_{i,air} + q_{i,cw} + q_{i,sea} + \sum_{j \in CPS} q_{ij} \qquad i \in HPS \tag{138}$$

Heat balance of hot process stream at each utility level

$$\left(TH_{i,j} - TH_{i,j+1}\right)FCp_i = q_{ij} \qquad i \in HPS \tag{139}$$

Heat balance on utility stream (US) for each hot process stream

$$f_{ij}\Delta H_j = q_{ij} \qquad j \in US \tag{140}$$

Mass balance on utility stream flow

In Figure 33, each utility stage (j) represents either boiler feed water (BFW) preheating or steam production. In the case of the j^{th} stage representing steam production then the j+1th stage would be a boiler feed water preheating stage. This alternating pattern is adopted in the development of the overall superstructure. For this approach, the mass balance on the system can be represented by Equation 141, given a steam production operation at stage j. This balance is illustrated in Figure 34.

$$\sum_{i \in HPS} \sum_{j \in US} f_{i,j-1}^{BFW} + f_j^{c} = \sum_{i \in HPS} \sum_{j \in US} \left(f_{i,j+1}^{BFW} + f_{ij}^{stm}\right) \tag{141}$$

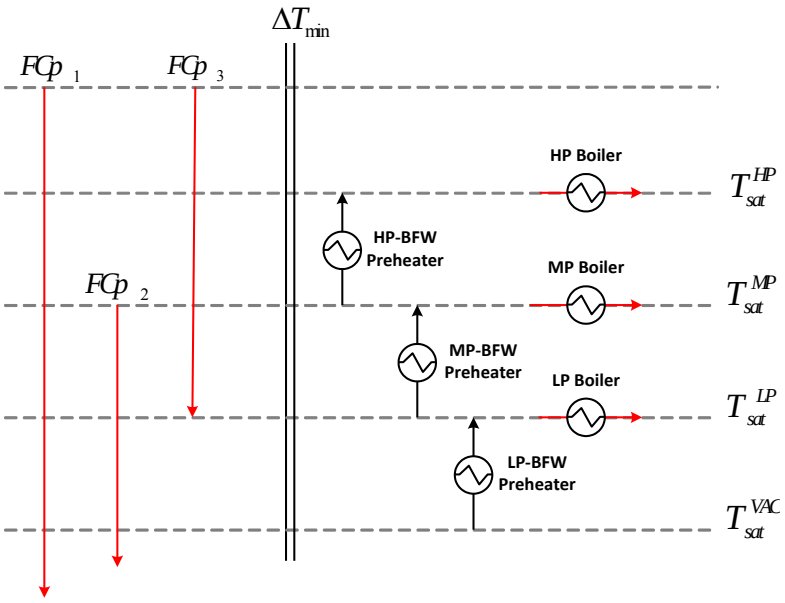

Figure 32 Temperature interval diagram illustrating development concept for steam utilities HEN

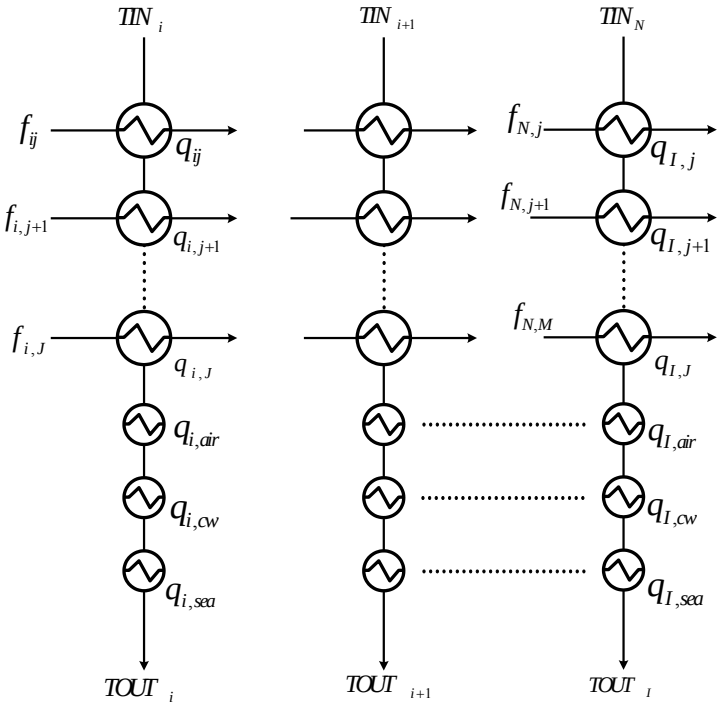

Figure 33 Heat exchange network for maximizing heat recovery from process streams

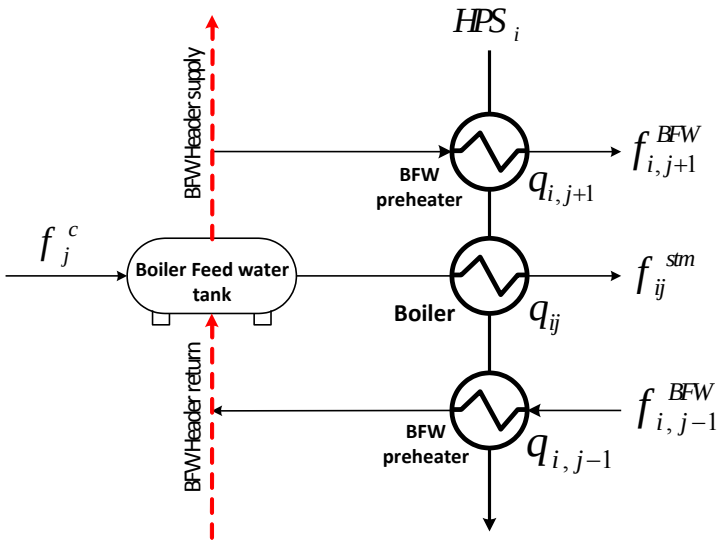

Figure 34 Mass balance for each HEN stage

Assignment of superstructure inlet temperature

The inlet temperature of each hot process stream as well as inlet and outlet temperatures of each utility level is known therefore the inlet temperature assignment for the overall superstructure can be screened based on temperature feasibilities. This approach eliminates the need for binary variables and a Big-M constraint to address issues of temperature crossing. Alternatively, the general formulation presented by Yee et al. [137] can be used. For a hot process stream that can produce steam at the highest level, Equation 142 would be used to assign its inlet temperature for the superstructure. For other hot process streams, the appropriate utility level (j) would be applied.

$$TIN_i = TH_{i,1} \qquad i \in HPS \tag{142}$$

Feasibility of temperatures

$$TH_{i,j} \geq TH_{i,j+1} \qquad i \in HPS \tag{143}$$

$$TOUT_i \leq TH_{i,sea} \qquad i \in HPS \tag{144}$$

Cooling utility overall load

$$\left(TH_{i,air} - TOUT_i\right) FCp_i = q_{i,air} + q_{i,cw} + q_{i,sea} \qquad i \in HPS \tag{145}$$

Calculating approach temperatures

The overall cost of the heat recovery network is incorporated into the objective function via the cost of total heat exchange area. These areas are calculated using the logarithmic mean temperature difference determined from temperature approaches. For this study, the logarithmic temperature difference is calculated using the Chen [99] approximation and incorporated into the optimization model using an exponential transformation described by Equations 146 - 150.

$$LMTD_{ij} \le \exp\left(LMTD_{ij}^{"}\right) \qquad i \in HPS,\ j \in US \tag{146}$$

$$TH_{i,j} - TCOUT_j \ge \exp\left(DT_{i,j}^{in}\right) \qquad i \in HPS,\ j \in US \tag{147}$$

$$TH_{i,j+1} - TCIN_j \ge \exp\left(DT_{i,j}^{out}\right) \qquad i \in HPS,\ j \in US \tag{148}$$

$$TH_{i,j} - TCOUT_j + TH_{i,j+1} - TCIN_j \ge \exp\left(SUMDT_{i,j}\right) \qquad i \in HPS,\ j \in US \tag{149}$$

$$LMTD_{ij}^{"} = 1/3\left\{DT_{i,j}^{in} + DT_{i,j}^{out} + SUMDT_{i,j} - \ln(2)\right\} \qquad i \in HPS,\ j \in US \tag{150}$$

The logarithmic mean temperature difference (LMTD) given in Equation 150 is used along with the overall heat transfer coefficient to determine the required heat exchanger area at each utility level, for each hot process stream. The area calculations for the exchangers are given by Equations 151 - 154 and included in the objective function of the optimization model. For this study the overall heat transfer coefficients are obtained from literature and estimated based on the type of fluids in the heat exchanger [138]. Note that the constraints given by Equations 146 - 149 are expressed as inequalities because the cost of the exchangers is reduced with increasing values of temperature approach.

$$A_{ij}^{WHB/BFW} = \frac{q_{ij}}{U_{ij}^{HEN} LMTD_{ij}} \qquad i \in HPS,\ j \in US \tag{151}$$

$$A_{i,air} = \frac{q_{i,air}}{U_{i,air} LMTD_{i,air}} \qquad i \in HPS \tag{152}$$

$$A_{i,CW} = \frac{q_{i,CW}}{U_{i,CW} LMTD_{i,CW}} \qquad i \in HPS \tag{153}$$

$$A_{i,sea} = \frac{q_{i,sea}}{U_{i,sea} LMTD_{i,sea}} \qquad i \in HPS \tag{154}$$

The represented heat exchange network would be typical for any process with hot streams to be cooled and cold streams to be heated. For systems that exhibit excess energy in the form of fuel gas, the heat exchange network will have a different structure to the one described. In essence, this section of the outlined procedure requires a heuristics based approach to developing the heat exchange network.

For systems with excess fuel gas from the process, priority is given to heating cold streams that cannot attain target temperatures via heat integration with available hot streams. The remaining fuel gas is termed "available fuel" $\left(Q_{fuel}^{available}\right)$ and is utilized in boilers and furnaces to produce superheated steam for the process, for power production or both. The overall heat balances for these units are given by Equations 155 - 157.

$$Q_{fuel}^{available} = \sum_{j=US} Q_j^{boiler} + \sum_{j=US} Q_j^{furnace} \qquad j \in US \tag{155}$$

$$Q_j^{boiler} = F_{j-1}^{BFW,boiler}\left(H_j^{v} - H_{sat,j-1}^{f}\right) \qquad j \in US \tag{156}$$

$$Q_j^{furnace} = F_j^{stm,furnace}\left(H_j^{v} - H_{sat,j}^{v}\right) \qquad j \in US \tag{157}$$

In Equations 155 - 157, the j^{th} term represents the stage at which steam is produced from the heat exchange network. As a result, the boiler feed water used to produce steam at the j^{th} stage would be sourced from the j-1^{th} stage based on superstructure development. In a similar approach, Equation 157 represents the heat balance for superheating steam taken from the j^{th} stage.

The availability of fuel gas can provide numerous alternatives for the design of the overall heat recovery superstructure. In essence, its development would be case specific and require some heuristics based decisions. The final structure would be evaluated and optimized using cost estimates that are included in the overall economic based objective function.

4.4.3 Power generation process configuration

The power generation for this study is achieved via the use of a Rankine cycle as illustrated in Figure 35. For this cycle, fresh boiler feed water is sent to the heat recovery section for conversion to steam at an optimal superheat temperature. The exiting steam is then sent to the turbine network for power extraction. The high kinetic energy of the steam is used to rotate the blades of the turbine thus converting some of this kinetic energy into mechanical energy. The conversion of energy can be ideally described as an isentropic operation though due to

mechanical inefficiencies, the maximum energy extraction cannot be achieved. The relationship between this ideal power extraction and the actual is determined via the isentropic efficiency (η_{is})

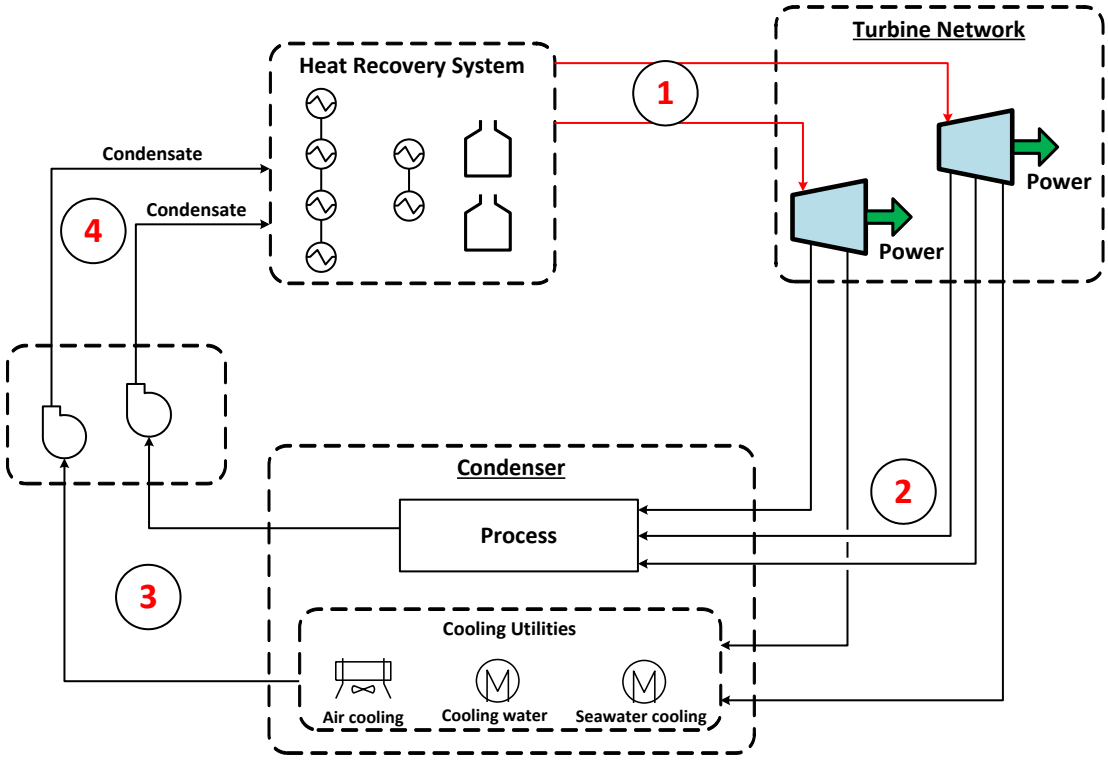

Figure 35 Rankine cycle inclusion in proposed methodology

The steam exiting each turbine in the network can be either slightly superheated steam or wet steam characterized by its quality being less than 100% but greater than some minimum value set by the manufacturer. The former operating approach requires the use of a back pressure turbine while the latter utilizes a condensing turbine. The use of either turbine in the network would depend on the objective. For high power production, condensing turbines would be used since more energy can be extracted due to the allowable saturated steam exit conditions. Back pressure turbines are used when steam has to be transferred across pipelines to be used for process heating thus requiring a small degree of superheating to prevent condensation. For this study we have utilized condensing turbines with steam extraction since this configuration would

provide flexibility for producing superheated steam for thermal desalination and process heating as well as an option for maximizing power generation.

The steam leaving the turbine network should be at the required conditions of temperature and pressure. As a result, extracted steam leaving a back pressure turbine may be above the superheated requirements of the process and would have to be de-superheated. This scenario is illustrated using the entropy-temperature diagram shown by Figure 36 and is remedied by de-superheating exhaust steam to header conditions via the use of boiler feed water from the heat exchange network. This decision provides an intricate connection between the heat exchange network and turbine network thus enhancing the final structure by providing alternative flow options that meet the desired objective function.

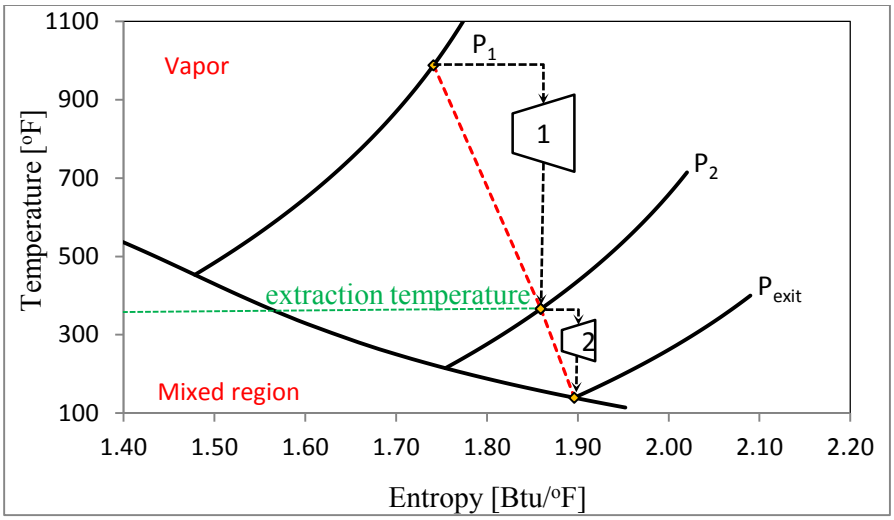

Figure 36 Entropy – temperature properties of steam through extraction turbine

To model the Rankine cycle in this study, thermodynamic correlations of water and steam properties are used. Some of these correlations were developed for this study while others were adopted from literature [107]. These equations are shown in Table 25.

.

Table 25 Correlations for steam and water thermodynamic properties

Equation	Description	
$T_{sat} = 117.66\, P_{sat}^{0.2219}$	Saturation temperature [a] ($14.7 \le P_{sat} \le 2400$ psia) Error = ±0.79%	(158)
$T_{sat} = 102.80 P_{sat}^{0.2741}$	Saturation temperature [a] ($1.5 \le P_{sat} \le 14.7$ psia) Error = ±1.76%	(159)
$s_{sat}^{f} = 1.6308\times10^{-3} T_{sat} - 3.0838\times10^{-2}$	Saturated water entropy [a] ($1.5 \le P_{sat} \le 14.7$ psia) Error = ±0.87%	(160)
$s_{sat}^{v} = -3.9857\times10^{-9} T_{sat}^{3} + 5.4089\times10^{-6} T_{sat}^{2} - 3.3698\times10^{-3} T_{sat} + 2.2658$	Saturated steam entropy [a] ($1.5 \le P_{sat} \le 2400$ psia) Error = ±0.37%	(161)
$s^{v} = s_{sat}^{v} + 0.46883 - 0.46883\exp\left(-k_T \Delta T_{sat}\right)$ $k_T = 1.3845\times10^{-2}\left(\frac{T_{sat}}{1000}\right)^2 - 9.8258\times10^{-3}\left(\frac{T_{sat}}{1000}\right) + 3.1462\times10^{-3}$ $\Delta T_{sat} = T - T_{sat}$	Entropy of steam [a] 14.7 psia < P < 1500 psia $T_{sat} \le T \le 1300$ °F Error = ±1.36%	(162)
$H_{sat}^{f} = 4.2433\times10^{-5} T_{sat}^{2} + 9.8773 T_{sat} - 31.146$	Saturated water enthalpy [a] 1.5 psia < P_{sat} < 14.7 psia Error = ±0.02%	(163)
$H_{sat}^{f} = 4.5395\times10^{-4} T_{sat}^{2} + 0.74207 T_{sat} + 4.8112$	Saturated water enthalpy [a] 14.7 psia < P_{sat} < 1500 psia Error = ±1.26%	(164)
$H_{sat}^{v} = -2.0449\times10^{-4} T_{sat}^{2} + 0.47202 T_{sat} + 1.0595$	Saturated steam enthalpy [a] 1.5 psia < P_{sat} < 14.7 psia Error = ±0.01%	(165)
$H^{v} = 0.2029 T_{sat} \left(s^{v}\right)^{3.647} + 817.35$	Enthalpy steam [b] Error = ±0.66%	(166)

[a] This study; [b] Adopted from work by Al-Azri et al. [107]

4.4.3.1 Turbine modeling

The overall steam turbine efficiency is a function of both its mechanical and isentropic efficiency. The mechanical efficiency is mostly dependent on the structural design set by

manufacturers and can be higher than 95% [107]. In contrast, the isentropic efficiency is dependent on operational parameters such as inlet pressure and temperature, steam mass flow rate as well as desired let down pressure and steam quality. Models have been developed by numerous authors to evaluate the performance of turbines [139,140]. For this study, the model presented by Mavromatis et al. [139] is used to describe the isentropic efficiency of the steam turbines. The model is given by Equations 167 - 169 and relates the isentropic efficiency to the operating $\left(M_{turb}^{stm}\right)$ and maximum mass flowrate of steam $\left(M_{turb}^{stm,\max}\right)$, the isentropic enthalpy difference $\left(\Delta H_{is}\right)$ and constants *A* and *B*. These constants are dependent on the saturation temperature of the inlet steam as well as output power of the turbine. The coefficients used for calculating these constants are given in Table 26.

$$\eta_{is} = \frac{6}{5B}\left(1 - \frac{3.41443\times10^{6} A}{\Delta H_{is} M_{turb}^{stm,\max}}\right)\cdot\left(1 - \frac{M_{turb}^{stm,\max}}{6M_{turb}^{stm}}\right) \tag{167}$$

$$A = a_o + a_1 T_{sat} \tag{168}$$

$$B = b_o + b_1 T_{sat} \tag{169}$$

Table 26 Regression coefficients used in isentropic efficiency equation

Coefficient	Back Pressure turbines		Condensing turbines	
	$W^{\max}$ < 4.1MMBtu/hr	$W^{\max}$ > 4.1 MMBtu/hr	$W^{\max}$ < 5.12 MMBtu/hr	$W^{\max}$ > 5.12 MMBtu/hr
a_o [Btu/hr]	-0.1508	-1.038755556	-0.115877778	-0.062488889
a_1 [Btu/hr-^{o}F]	0.00065	0.003461111	0.000555556	0.000777778
b_o [Btu/hr]	0.961977778	1.111644444	1.195233333	1.166466667
b_1 [Btu/hr-^{o}F]	0.000844444	0.000261111	0.000333333	0.000166667

The coefficients are taken from Varbanov et al. [140] and Mavromatis and Kokosiss [139] with original values expressed in SI units.

In previous studies, the maximum steam flowrate is set as a constant in Equation 167 thus intrinsically fixing the size of steam turbine [107,141]. This approach has been used to optimize the selection of turbine sizes for grassroots processes based on the operating flowrate. For this study, an alternative approach is utilized where the maximum steam flowrate is a function of the

operating flowrate as adopted in standard engineering practice for sizing equipment [36]. In this way, the relationship of the operating flowrate and maximum flowrate is the steam turbine design ratio (DR) and represents the degree of operational flexibility of the unit. In essence, this approach creates an opportunity for optimizing the turbine's operational flexibility via the manipulation of the design ratio. The isentropic efficiency equation can then be represented by Equations 170 - 171 with the use of the design ratio.

$$\eta_{is} = \frac{6}{5B}\left(1 - \frac{3.41443\times10^{6} A}{\Delta H_{is} DR \cdot M_{turb}^{stm}}\right)\cdot\left(1 - \frac{DR}{6}\right) \tag{170}$$

$$DR = \frac{M_{turb}^{stm,\max}}{M_{turb}^{stm}} \tag{171}$$

By including the design ratio (DR), Equation 170 can be rewritten to obtain the turbine shaft power given by Equations 172 - 174.

$$W_{shaft} = C_1 \Delta H_{is} M_{turb}^{stm} - C_2 \tag{172}$$

$$C_1 = \frac{6}{5B}\left(1 - \frac{DR}{6}\right) \tag{173}$$

$$C_2 = \frac{6}{5B}\left(1 - \frac{DR}{6}\right)\cdot\frac{3.41443\times10^{6} A}{DR} \tag{174}$$

The developed turbine network operates within the constraints of the various steam levels determined by the Total site analysis. The inlet and outlet pressure conditions of each turbine in the network is consequently fixed and known. As a result, the maximum power recovered is intuitively obtained via the optimal selection of inlet steam temperature and flowrate to each turbine. The former condition is dependent on the supply temperature of the hot process stream while the latter is restricted by the hot process stream's heat content. An evaluation of Equation 167 would also suggest that there exist an optimal selection of the turbine design ratio to maximize power production. In essence these three variables affect the overall isentropic efficiency which corresponds to a specific optimal inlet steam temperature, given a desired exit condition. This concept is illustrated in Figure 37 where the exit conditions are taken as saturated steam at vacuum. In Figure 37, the steam flowrate at the maximum allowable inlet temperature is less than that at a lower value due to temperature restrictions on the hot process streams. At the optimal isentropic efficiency, the power production is maximized via a tradeoff between inlet steam temperature and operating flowrate.

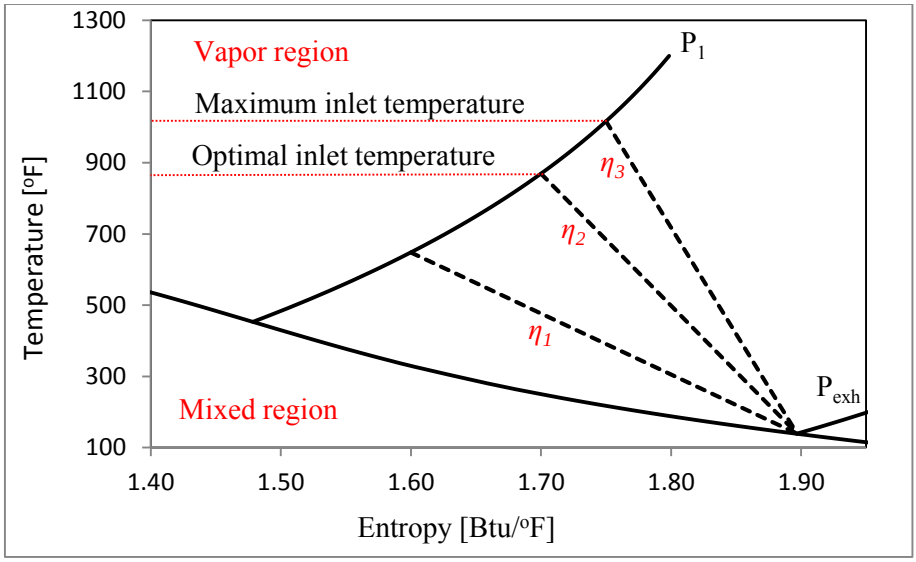

Figure 37 Entropy-Temperature diagram illustrating tradeoff between inlet temperature and isentropic efficiency for maximum power

The optimization model for the turbine network would include the use of Equations 158 - 174 and can be described in eight (8) general steps based on the illustrated Rankine cycle in Figure 35 and the conceptual design of the turbine network in Figure 31.

Step 1: The enthalpy of the steam entering each turbine is determined and illustrated by Equation 175. This equation relates the steam enthalpy to its entropy and saturation temperature. The achievable steam inlet temperature would be dependent on the thermal properties of the hot process streams.

$$H_1^v = 0.2029 T_{sat,1} \left(s_1^v\right)^{3.647} + 817.35 \tag{175}$$

Step 2: The steam inlet entropy and outlet saturation temperature are used to calculate the turbine's exiting isentropic enthalpy and is given by Equation 176. The latter variable is determined using Equation 158 or 159 depending on the outlet pressure of the steam header.

$$H_{2,is}^v = 0.2029 T_{sat,2} \left(s_1^v\right)^{3.647} + 817.35 \tag{176}$$

Step 3: The isentropic enthalpy difference is calculated using the inlet enthalpy and outlet isentropic enthalpy. It is used along with the steam flowrate and design ratio to determine the total shaft power of each turbine given by Equation 177.

Step 4: The actual outlet enthalpy of the turbine is calculated by relating the shaft output power to the product of the actual enthalpy difference and steam flowrate. This outlet enthalpy is then used as the inlet conditions to the subsequent turbine section. Equations 177 - 178 show this step calculation.

$$W_{shaft} = \Delta H_{2,a} M_{turb}^{stm} \tag{177}$$

$$\Delta H_{2,a} = H_1^v - H_{2,a}^v \tag{178}$$

Based on Equation 170, the maximum isentropic efficiency is achieved when the maximum steam flowrate approaches infinite for a given design ratio. The maximum isentropic flowrate is thus a function of the inlet saturated condition only as shown in Equation 179.

$$\eta_{is}^{\max} = \frac{1}{B} \tag{179}$$

With the use of this expression as well as fixed conditions of the final exhaust steam, constraints on the feasible turbine inlet conditions were developed and are given by Equations 180 - 181 and represent an addition of linear constraints.

$$H_{EX,is} = \left(s_1^v - s_{sat,EX}^f\right) \cdot \left(\frac{H_{sat,EX}^v - H_{sat,EX}^f}{s_{sat,EX}^v - s_{sat,EX}^f} \right) + H_{sat,EX}^f \tag{180}$$

$$\eta_{is,1}^{\max} \geq \frac{H_1^v - H_{EX}^v}{H_1^v - H_{EX,is}^v} \tag{181}$$

Step 5: Steam is extracted from the exhaust and sent to a de-superheater while the remainder is sent to the subsequent section. The optimal split would be determined by the overall economic based objective function.

Step 6: The extracted steam with the pressure conditions of the j^{th} stage in the HEN is de-superheated using boiler feed water from the j+1th stage of the HEN. The required boiler feed water for de-superheating would be dictated by the heat balance described by Equation 182 and illustrated in Figure 38.

$$F_{j+1}^{BFW,DS} H_{sat,j+1}^f + S_{j,turb}^{extract} H_{j,turb}^v = \left(F_{j+1}^{BFW,DS} + S_{j,turb}^{extract}\right) \cdot H_{j,header}^v \qquad j \in US \tag{182}$$

$$S_{j,turb}^{in} = S_{j+2,turb}^{extract} + S_{j+4,turb}^{extract} + \ldots + S_{J-2,turb}^{extract} + S_{j,turb}^{exh} \tag{183}$$

Equation 183 represents the overall mass balance on a specific turbine in the network. The first term represents the total inlet steam to the turbine while the second term

represents the total steam extracted. The last term represents the exhaust steam that has to be condensed and pumped back to the heat recovery section.

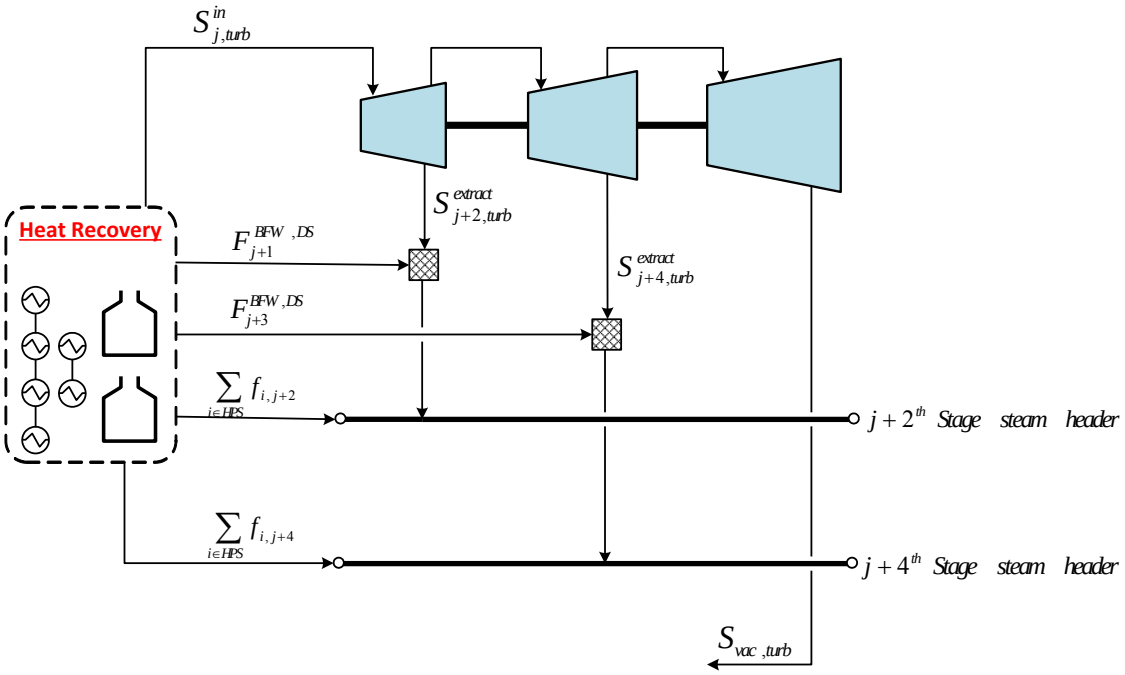

Figure 38 Heat exchange network interconnectivity with turbine network

Step 7: For a back pressure turbine, the maximum power is extracted when the steam exits at saturated conditions. The exhaust steam isentropic enthalpy would thus fall in between saturated vapor and liquid conditions. In this case, the feed entropy is used to determine the steam quality associated with the isentropic enthalpy. This steam quality is then used to calculate the isentropic enthalpy based on the fixed values of saturated liquid and vapor enthalpy at the exit conditions. This calculation is given by Equations 184 - 185.

$$x_{stm} = \frac{\left(s_1^v - s_{sat,2}^f\right)}{\left(s_{sat,2}^v - s_{sat,2}^f\right)} \tag{184}$$

$$H_{is}^{v,vac} = x_{stm}\left(H_{sat}^{v,vac} - H_{sat}^{f,vac}\right) + H_{sat}^{f,vac} \tag{185}$$

Step 8: The exhaust steam from the turbine network is condensed and pumped to the heat recovery section. The cooling requirement is satisfied by using any of the available

cooling utilities. The overall energy balance for the condensed exhaust steam is given by Equation 186.

$$\sum_{j \in US} S_{j,turb}^{exh} \cdot \left(H_{sat}^{v,vac} - H_{sat}^{f,vac} \right) = q_{turb,air}^{exh} + q_{turb,cw}^{exh} + q_{turb,sea}^{exh} \tag{186}$$

To maximize power production from the turbine network, the lowest practical exhaust pressure is chosen. A low exhaust pressure corresponds to a low exhaust saturation temperature thus potentially minimizing the number of cooling utility options. For this study, the selected exhaust saturation temperature was the minimum temperature difference above the operating temperature of the air cooling utility. This approach ensured that all cooling options were available for economic evaluation. A more detailed approach would be to optimize the exhaust pressure though this would introduce more nonlinearities to the overall formulation. Such an approach could be addressed in a later study.

With a fixed exhaust saturation temperature and operating temperatures for each cooling utility, the logarithmic mean temperature difference (LMTD) is a constant thus simplifying the calculation for the required heat transfer area. This heat transfer area is included in the objective function to identify the economically optimal cooling option.

There are numerous alternative structures for the turbine network. For this study, a single option was chosen based on heuristics though a more complex structure may be utilized to explore the full range of network flow options. By increasing network complexity, numerical difficulties would be introduced.

4.4.4 Multi-effect distillation with thermo-vapor compression (MED-TVC) configuration

The MED-TVC configuration adopted in this work is based on the parallel feed forward design described by El-Dessouky et al. [82] with alternative flow routes developed in Chapter III of this thesis. As described in the previous chapter, the MED-TVC system is an aggregation of *n* repeating effects with *n-1* distillate flashing boxes. Seawater is introduced into each effect at a controlled and equal rate depending on the heating provided to the first effect. In the first effect, thermo-compressed vapor is introduced into the tube side and used to sensibly heat and boil a portion of the fed seawater. The vapor formed from boiling is sent to the tube side of the second effect where the sensible heating and boiling process is repeated to produce vapor for the third to the n^{th} effect.

The brine exiting each effect (*i*) is introduced into the brine pool of the subsequent effect (*i+1*). The difference in operating temperature and pressure between the effects results in the

flashing of a small portion of the introduced brine. In addition, the condensed vapor from effects 1 to (n -1) is introduced into the corresponding distillate flashing box, where the reduced operating pressure results in the flashing of a small amount of vapor. The flashed off vapor from both operations are combined and introduced into the tube side of the next effect along with the vapor from the boiling seawater. This additional step improves overall system productivity and thermal efficiency.

The vapor from the last effect is routed to the down condenser where it is partially condensed using a controlled flow of seawater. The remaining vapor is entrained by the steam ejector which thermo-compresses it the desired pressure using motive steam. In a similar fashion, the brine leaving the last effect is cooled to the desired temperature using a controlled flow of seawater. An overall heat balance indicates that most of the heat load introduced into the system via motive steam, is rejected to the cooling seawater.

The MED-TVC process has been mathematically modeled and evaluated for its performance by various authors. For this study, the modeling approach detailed in Chapter III and summarized by Equations 187 - 222 would be adopted. This linear based enthalpy model for the MED-TVC process includes all the thermodynamic limitations presented by the various authors while ensuring accuracy in the developed heat and mass balances. In addition, the model allows for the optimization of heat transfer areas as well as flow routes within the system.

The following assumptions are utilized when developing this model:

- Condensed vapor from each effect is salt free
- Environmental heat losses from the desalination process is negligible
- Brine discharge concentration is 71,800 ppm
- Equal flow of seawater feed to each effect
- Equal temperature difference between effects with the top brine temperature (T_1) and reject brine temperature (T_N) being fixed

The general mass and salt component balance equations for all effects, the down condenser and the distillate flashing boxes are given by Equations 187 - 192 and are summarized in Table 27. In addition, the corresponding energy balances are given by Equations 193 - 201 for all the effects as well as the condenser, distillate flashing boxes and steam ejector. These energy balances are described in more detail in Chapter III of this document. They represent an alternative approach to modeling the MED-TVC process from the previously utilized specific heat capacity model.

Table 27 Mass and energy balance equations for MED-TVC process

Equations	Descriptions	
$F^{MED} = \sum_{i \in N_{eff}} F_i^{MED}$	Total MED feed flow	(187)
$F_i^{MED} = V_i + B_i$	Mass balance on effect 1	(188)
$F_i^{MED} + B_{i-1} = V_i + B_i$	Mass balance on effect 2 to N_{eff}	(189)
$M_{sea}^{cond} = \frac{\left(V_N + M_{pot,N_{eff}-1}^{stm} - Dr\right) \cdot \lambda_{cond}}{Cp \cdot \left(T_f - T_{sea}^{IN}\right)}$	Cooling seawater balance on condenser	(190)
$M_{feed}^{salt} = M_1^{salt}$	Salt balance on effect 1	(191)
$M_{feed}^{salt} + M_{i-1}^{salt} = M_i^{salt}$	Salt balance on effect 2 to N_{eff}	(192)
$Q_i^{EVAP} + M_{feed} H_{feed} + \frac{Q^{PRE}}{N_{eff}} = M_{feed,i}^{stm} H_i^{v} + M_{feed,i}^{brine} H_i^{brine}$	Energy balance on effect evaporator	(193)
$Q_i^{EVAP} = Q_i^{vap} + Q_i^{sens}$	Energy distribution of effect evaporator	(194)
$Q_i^{vap} = M_{feed,i}^{stm} H_i^{v}$		(195)
$M_{feed,i-1}^{brine} H_{feed,i-1}^{brine} + M_{BF,i-1}^{brine} H_{BF,i-1}^{brine} = M_{BF,i}^{brine} H_{BF,i}^{brine} + M_{BF,i}^{stm} H_i^{v'}$	Energy balance on brine flashing (BF)	(196)
$M_{brine}^{MED} = M_{BF,N_{eff}}^{brine}$	MED brine flow	(197)
$D_{i-1} H_{i-1}^{f''} + M_i^{c} H_{i-1}^{c} = M_{pot,i}^{stm} H_i^{v''} + M_{pot,i}^{water} H_i^{f''}$	Distillate (D) flashing pot balance	(198)
$M_{pot,i}^{water} = M_{DS,i}^{water} + M_{BFW,i} + D_i$	Mass balance on flash pot outflow (W)	(199)
$M_{perm}^{MED} = D_{N-1} + \left(V_{N_{eff}} + M_{pot,N_{eff}-1}^{stm}\right) - Dr$	MED permeate flow	(200)
$S_{mot} \cdot H_{mot}^{v} + Dr \cdot H_{N_{eff}}^{v} + \sum_{i=1}^{N} M_{DS,i}^{water} H_i^{f''} = M_{DS}^{stm} H_{DS}^{v} + M_{DS}^{c} H_{DS}^{f}$	De-superheater balance	(201)

The steam ejector represents the section of the process that improves the thermal performance of the overall MED process. To model the steam ejector, the semi-empirical correlation developed by El-Dessouky et al. [142] was adopted. This correlation was developed using field data collected over 35 years and relates the vapor entrainment ratio (mass of entrained vapor to motive steam) to the entrained vapor pressure (P_{ent}), motive steam pressure (P_{mot}) and ejector exhaust pressure (P_{exh}). This relationship is given by Equations 202 - 204 for the entrainment ratio (ε) and is valid for compressions ratios (Cr) greater than 1.81 and less than 6.

$$\varepsilon = 0.65 Er^{-1.54} P_{ent}^{1.72} P_{cxh}^{0.0679} \frac{\left(22.82 + 0.000421 P_{mot}^{1.34}\right)}{\left(9.32 + 0.128 P_{cxh}^{1.14}\right)} \tag{202}$$

$$Er = \frac{P_{mot}}{P_{ent}} \tag{203}$$

$$Cr = \frac{P_{exh}}{P_{ent}} \tag{204}$$

The entrainment vapor pressure (P_{ent}), ejector exhaust pressure (P_{exh}) and steam motive pressure (P_{mot}) are measured in kPa. The equation is valid for $\varepsilon \leq 4$ and 100 kPa $\leq P_{mot} \leq$ 3500 kPa.

The heat transfer areas for each effect and condenser are determined using Equations 205 - 208. The logarithmic mean temperature difference for each heat exchanger is calculated using Equations 209 - 210 while the heat transfer coefficient is determined using correlations developed by El-Dessouky [82] and given by Equations 211 - 212.

The operating temperature of each effect is determined using the constant temperature difference approach described by Equation 213 and used in other studies [88-90]. The temperature profile for each effect's saturated vapor temperature and condensation temperature as well as brine and distillate flashing temperature are determined using Equations 214 – 222 and are given in Table 29. For this study the MED-TVC process is represented by Figure 39 with the corresponding modeling data given in Table 30.

Table 28 Equations for calculating the heat transfer area, logarithmic mean temperature difference and overall heat transfer coefficients for MED-TVC process

Equations	Descriptions	
$A_i^{vap} = \frac{Q_i^{vap}}{U_i^{eff}\left(T_{i-1}^{c} - T_i^{eff}\right)}$	Vaporization heat transfer area for each evaporator	(205)
$A_i^{sens} = \frac{Q_i^{sens}}{U_i^{eff}\left(LMTD\right)_i^{sens}}$	Sensible heat transfer area for each evaporator	(206)
$A_i^{Total} = A_i^{vap} + A_i^{sens}$	Total heat transfer area for each evaporator	(207)
$A_{cond} = \frac{Q_{total}^{COND}}{U_{cond}\left(LMTD\right)_{cond}}$	Condenser heat transfer area	(208)
$\left(LMTD\right)_i^{sens} = \left[\left(T_{i-1}^{c} - T_f\right)\cdot\left(T_{i-1}^{c} - T_i^{eff}\right)\cdot\left(T_{i-1}^{c} - \frac{T_f + T_i^{eff}}{2}\right)\right]^{1/3}$	Logarithmic mean temperature difference for each effect based on Chen approximation [99]	(209)
$\left(LMTD\right)_{cond} = \left[\left(T_{N_{eff}}^{c} - T_f\right)\cdot\left(T_{N_{eff}}^{c} - T_{sea}^{IN}\right)\cdot\left(T_{N_{eff}}^{c} - \frac{T_f + T_{sea}^{IN}}{2}\right)\right]^{1/3}$	Logarithmic mean temperature difference for condenser based on Chen approximation [99]	(210)
$U_i^{eff} = 2.318\times10^{-6}\left(T_i^{eff}\right)^3 - 2.0752\times10^{-4}\left(T_i^{eff}\right)^2 + 1.4056\times10^{-3}\left(T_i^{eff}\right) + 1.9394$	Overall heat transfer coefficient for evaporator	(211)
$U_{cond} = -8.026\times10^{-8}\left(T_{N_{eff}}^{c}\right)^3 + 1.825\times10^{-4}\left(T_N^{c}\right)^2 + 1.537\times10^{-4}\left(T_{N_{eff}}^{c}\right) + 1.6175$	Overall heat transfer coefficient for condenser	(212)

Overall heat transfer coefficients for evaporator and condenser are presented in their original units as described in work by El-Dessouky et al. [82]

Table 29 Equations for calculating the heat transfer area, logarithmic mean temperature difference and overall heat transfer coefficients for MED-TVC process

Equations	Description	
$\Delta T^{eff} = \frac{T_1^{eff} - T_N^{eff}}{N_{eff} - 1}$	Temperature difference of all effects	(213)
$T^{DS} = T_1^{eff} + \Delta T^{eff}$	Temperature of steam from de-superheater	(214)
$T_{i+1}^{eff} = T_i^{eff} - \Delta T^{eff}$	Temperature of effects 2 to N_{eff}	(215)
$T_f \le T_N^c - \Delta T_{\min}^{cond}$	Feed seawater temperature constraint	(216)
$T_i^v = T_i^{eff} - BPE_i$	Temperature of vapor formed in each effect	(217)
$T_i^{brine} = T_i^{eff} + NEA_i^{brine}$	Temperature of flashed brine	(218)
$T_i^{flash} = T_i^v + NEA_i^{flash}$	Temperature of flashed distillate	(219)
$BPE = C\left(X_{sal}^{eff}\right)^2 + D\left(X_{sal}^{eff}\right)$ $C = -4.584 \times 10^{-4}\left(T^{eff}\right)^2 + 0.2823\left(T^{eff}\right) + 17.95$ $D = 1.536 \times 10^{-4}\left(T^{eff}\right)^2 + 5.267 \times 10^{-2}\left(T^{eff}\right) + 6.56$	Boiling point elevation [95].	(220)
$NEA_i^{brine} = \frac{33 \cdot \left(T_{i-1}^{eff} - T_i^{eff}\right)^{0.55}}{T_i^v}$	Non-equilibrium allowance for flashing brine	(221)
$NEA_i^{flash} = \frac{0.33 \cdot \left(T_{i-1}^c - T_i^v\right)}{T_i^v}$	Non-equilibrium allowance for flashing distillate	(222)

Table 30 Design and operating parameter used for MED-TVC process

Parameter	Unit	Value
Number of effects		4 - 16
Temperature of sea water inlet	^{o}F	77
Operating temperature of first effect	^{o}F	158
Operating temperature of last effect	^{o}F	104

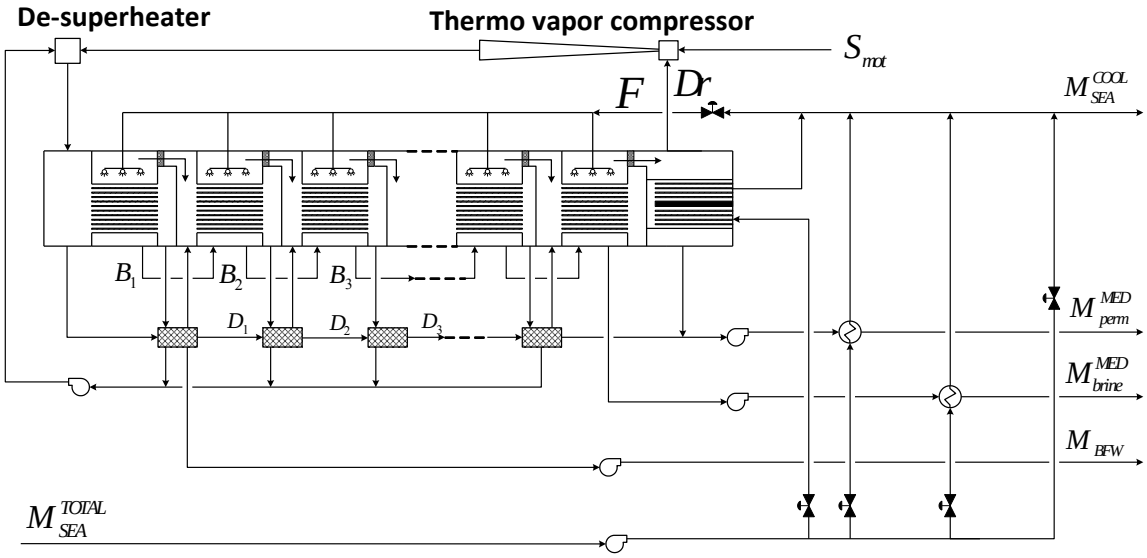

Figure 39 Process flow diagram of Multi-effect desalination with thermo vapor compression

4.4.5 Reverse osmosis

The natural process of osmosis occurs when a solvent moves from a region of low solute concentration to a region of high solute concentration, across a membrane. This is due to a difference in chemical potential which translates to what is known as the system's osmotic pressure. Conceivably, reverse osmosis (RO) occurs when the system is subjected to a pressure greater than the osmotic pressure thus forcing the direction of diffusion across the membrane to be occur in reverse. This transport phenomena has been exploited for decades in seawater desalination applications that utilize RO semipermeable membranes for the production of fresh water.

To achieve economically competitive water production flowrates, the applied pressures for RO systems range from 55 to 70 bar [143,144] and can reach as high as 80 bar [143,145] depending on membrane characteristics and seawater salinity. To increase the efficiency of seawater reverse osmosis (SWRO) systems, research has focused on both improving membrane water selectivity as well as RO network optimization via mathematical modeling. For the latter effort, there have been numerous contributions by various authors [146-150] in the specific area of reverse osmosis networks (RON). For this study, the mathematical modeling and economic evaluation described by Alnouri et al. [100] was used. The membrane modeling equations as well as system balances are described by Equations 223 - 233 and shown in Table 31. These equations are in fact adopted from models developed by DOW and utilized in their Reverse Osmosis Systems Analysis (ROSA) Filmtec software [151].

For this study, the RO process shown in Figure 40 was used as the building block for the RON. The quality requirements of the desalinated water would dictate the required number of RO units as well as structural orientation of the RON. A systematic approach to synthesizing these networks has been presented by various authors [150,152]. In addition, the data used for evaluating the optimal inclusion of RO desalination technology is shown in Table 32.

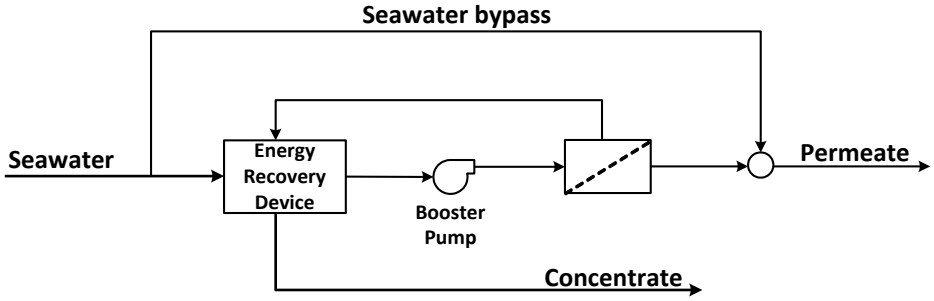

Figure 40 Process flow diagram of single stage reverse osmosis desalination

Table 31 General modeling equations for reverse osmosis (RO) unit

Equations	Descriptions	
$NM = \dfrac{M_{feed}^{RO}}{SM \cdot \overline{A}(\overline{\pi}) \cdot TCF \cdot FF \cdot \rho_f \cdot \left[P_f - \dfrac{\overline{\Delta P}_{fc}}{2} - P_p - \pi_{pf} \right]}$	Number of modules	(223)

Table 31 (*continued*)

Equations	Descriptions	
$\pi_{pf} = \pi_f \left(\frac{\overline{C}_{fc}}{C_f} pf + \overline{R} - 1 \right)$		
$if\ \pi_f \le 2 \qquad \overline{A}(\overline{\pi}) = 0.125$	Membrane permeability at 25°C	(224)
$if\ 25 \le \pi_f \le 200 \qquad \overline{A}(\overline{\pi}) = 0.125 - 0.011 \cdot \left(\frac{\pi_f - 25}{35} \right)$		
$if\ 200 \le \pi_f \le 400 \qquad \overline{A}(\overline{\pi}) = 0.070 - 0.0001 \cdot (\pi_f - 200)$		
$if\ T \ge 25, \quad TCF = \exp\left[2640 \cdot \left(\frac{1}{298} - \frac{1}{273+T} \right) \right]$	Temperature correction factor	(225)
$if\ T \le 25, \quad TCF = \exp\left[3020 \cdot \left(\frac{1}{298} - \frac{1}{273+T} \right) \right]$		
$\overline{\Delta P}_{fc} = 0.04 \cdot \left(\frac{M_{feed}^{RO} + M_{brine}^{RO}}{2 \cdot NM \cdot \overline{\rho}} \right)^2$	Average concentrate side system pressure drop	(226)
$\frac{\overline{C}_{fc}}{C_f} = -\frac{\ln(1-Y)}{Y}$	Approximate log-mean concentrates side to feed concentration ratio for system	(227)
$\pi_{feed} = 1.12 \cdot (273+T) \cdot \sum_{i=1}^{Nc} m_i \qquad i \in Nc$	Feed osmotic pressure	(228)
$pf = \exp(0.7Y)$	Concentration polarization factor	(229)
$F^{RO} = M_{perm}^{RO} + M_{brine}^{RO}$	Mass balance on RO unit	(230)
$X_{feed}^{RO} F^{RO} = X_{perm}^{RO} M_{perm}^{RO} + X_{brine}^{RO} M_{brine}^{RO}$	Salt balance on RO unit	(231)
$X_{feed}^{RO} = \sum_{i \in Nc} X_{feed,i}^{RO}$		
$X_{perm}^{RO} = \sum_{i \in Nc} X_{perm,i}^{RO}$		
$X_{brine}^{RO} = \sum_{i \in Nc} X_{brine,i}^{RO} \qquad i \in Nc$		
$Y = \frac{M_{perm}^{RO}}{F^{RO}}$	RO unit recovery	(232)
$\overline{R} = 1 - \frac{X_{perm}^{RO}}{X_{feed}^{RO}}$	Average salt rejection	(233)

Table 32 Design and operating parameters for Reverse osmosis network (RON)

Parameter	Unit	Value
Final permeate pressure	psia	14.5
Final reject pressure	psia	14.5
Energy recovery device efficiency	%	80
Pump efficiency	%	80
Seawater feed temperature	^{o}F	77
Maximum pressure drop across RO unit	psia	18.9
Maximum feed pressure to RO unit	psia	1015
Maximum number of modules in one unit		1000
Membrane area per module (6 elements/module)	ft^2	2641

4.4.6 Water management strategy

The concept of water management in the integrated facility is based on the established mass integration methodology by El-Halwagi [54]. This approach is conceptually straightforward and easily implemented into an optimization framework, though represents a critical constraint on the utilized water sources based on sink concentration requirements. In essence, these constraints would also directly affect the ratio of generated water produced from either technology thus affecting influencing optimal distribution of surplus energy to power or steam. To implement this water integration strategy into the overall integrated model, a linear based mathematical model can be used. These equations balance both overall and impurity mass flow rates and constrain them to the requirements of the sinks. The relationships are given by Equations 234 - 244. The overall mass integration strategy can be described by Figure 41.

4.4.6.1 Mathematical model for water management

Water source (m) overall mass balance

$$W_m = \sum_{n \in SINK} w_{m,n} \qquad m \in SOURCE \tag{234}$$

$$W_{MED} = \sum_{n \in SINK} w_{MED,n} + w_{MED,Export} \tag{235}$$

$$W_{RO} = \sum_{n \in SINK} w_{RO,n} + w_{RO,Export} \tag{236}$$

$$W_{sea} = \sum_{n \in SINK} w_{sea,n} + w_{sea,Export} \tag{237}$$

For this study the sources of water are from the processing facility, the desalination processes as well as from seawater. The seawater is included due to the potentially high purity of water from the desalination processes which creates an opportunity for increased water export based on export water concentration constraints. In addition, Equation 239 implies that exportable water would exclusively originate from desalination processes as well as seawater. This approach is by design since for this study we consider potable water for export. The formulation can be changed to include the use of process water for external plant uses within the boundaries of the regional regulations.

Water sink (n) overall mass balance (m)

$$G_n = \sum_{m \in SOURCE} w_{m,n} + w_{MED,n} + w_{RO,n} + w_{sea,n} \qquad n \in SINK \tag{238}$$

$$G_{Export} = w_{MED,Export} + w_{RO,Export} + w_{sea,Export} \tag{239}$$

$$G_{waste} = \sum_{m \in SOURCE} w_{m,waste} \tag{240}$$

Overall component (k) balance for each sink (n)

$$G_n z_{n,k}^{in} = \sum_{m \in SOURCE} w_{m,n} y_{m,k} + w_{MED,n} y_{MED,k} + w_{RO,n} y_{RO,k} + w_{sea,n} y_{sea,k} \qquad n \in SINK, k \in IMPURITY \tag{241}$$

$$G_{Export} z_{Export,k}^{in} = w_{MED,Export} y_{MED,k} + w_{RO,Export} y_{RO,k} + w_{sea,Export} y_{sea,k} \tag{242}$$

Constraints on sink contaminant composition

$$z_{n,k}^{\min} \le z_{n,k}^{in} \le z_{n,k}^{\max} \tag{243}$$

$$z_{Export,k}^{\min} \le z_{Export,k}^{in} \le z_{Export,k}^{\max} \tag{244}$$

The overall implementation is linear since all source and sink concentrations information are known. For an optimization study inclusive of the process design, available water sources can conceivably have varying water source concentrations. In essence this would increase the level of numerical difficulty of the optimization problem by introducing bilinear terms.

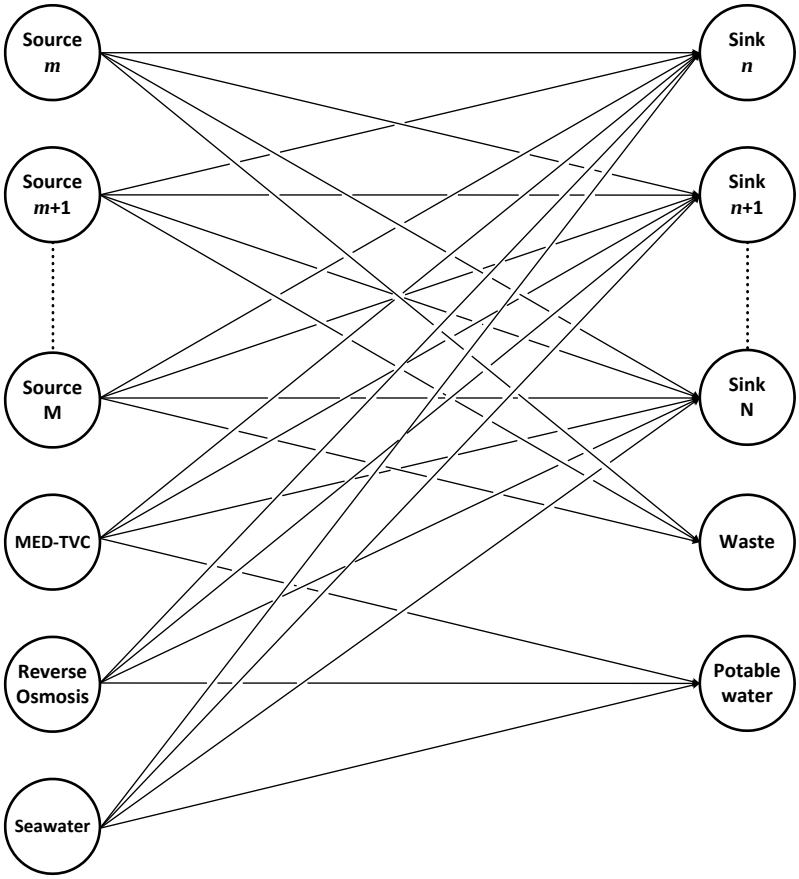

Figure 41 Source-sink mapping diagram for interplant water usage and export

4.4.7 Process cooling and pumping requirements

The minimum cooling requirements for the overall process is satisfied via various utility options. For the outlined methodology, air cooling, cooling water and seawater are used to remove any excess heat from the process. Each utility can operate within a specific temperature range [36,108,153]. For this study, the selected ranges are shown in Table 33.

Each cooling utility option has an associated capital (CAPEX) and operating expense (OPEX). For the air cooling option, the associated CAPEX includes the cost of the heat exchange unit while the OPEX is simply the cost associated with the draft fan power requirements. In the case of the cooling water utility, the CAPEX includes the cost of the circulation pumps, cooling tower and heat exchange unit. The OPEX incudes the cost for powering the pumps, cooling tower draft fans and cooling tower make-up water. For the

seawater cooling option, the CAPEX represents the cost of the heat exchange unit and pumps while the OPEX captures the power cost for pumping the seawater.

Table 33 Selected temperature range for cooling utilities

Cooling utility	Inlet temperature (ºF)	Outlet temperature (ºF)
Air cooling	113	131
Circulating cooling water	86	104
Once through seawater cooling	77	86 [a]

[a] Maximum allowable rejection temperature [108,153]

To determine the pumping power requirements, Equation 245 is used to determine the appropriate cooling fluid flow while Equation 246 is used to calculate the overall pumping power. For the draft fan power requirement as well as make-up water requirements, the parameters shown in Table 34 were used [36].

$$M_{Cool\ fluid}^{Total} = \frac{Q_{Cool\ fluid}^{Total}}{Cp_{Cool\ fluid}\Delta T_{Cool\ fluid}} \tag{245}$$

$$PW_{pump} = {}^{1}\!/_{\eta_{pump}}\ 0.1 \cdot \left(P^{Sink} - P^{Source}\right)\frac{M_{Cool\ fluid}^{Total}}{\rho_{Cool\ fluid}} \tag{246}$$

Table 34 Cooling utility power and water requirement factors

Cooling parameter	Value
Air cooler draft fan power [kW/MMBtu/hr]	1.000
Cooling tower daft fan power [kW/MMBtu/hr]	0.092
Cooling tower water makeup [lb/MMBtu/hr]	1.000

To calculate the pump power requirement for other operations within the integrated process, Equations 245 - 246 were suitably adapted. Such pumping requirements would include boiler feed water (BFW) pumps, RO feed pumps as well as MED seawater feed pumps. For details on

additional pumping requirements, Chapter III should be consulted for the MED-TVC process while the studies on reverse osmosis networks should be referenced.

4.4.8 Economics

The optimal design of a process can be dependent on factors such as capital and operating cost, environmental responsibility, safety or even job growth stimulation. In most cases, the overall objective in process design is to minimize cost thus improving overall economics. As a result, a similar approach is taken for this study where cost estimate equations were developed to aid in the selection of the economically optimal utilities design. These cost estimates are shown in Table 35 and given by Equations 247 - 269. In addition, cost estimate equations for the MED-TVC process were taken from Chapter III while respective cost estimates for the RO process were adopted from the study by Alnouri et al. [100]. The equations in Table 35 capture both capital (CAPEX) and operating expenditures (OPEX) for the heat recovery and power production sections. In addition, costs associated with project engineering services, project development, financing and contingency are obtained from literature and included in the overall economic evaluation [101,104,154,155]. These soft costs are determined as a percentage of the overall direct equipment cost.

In this study, the heat recovery system may include the use of non-conventional heating sources such as oil, gas or biomass. In the case with heating oil or natural gas, the associated boiler or furnace maintenance cost is estimated as a function of the fuel cost [156]. For this study, excess fuel may not have and intrinsic value if the original option involved flaring. As a result, the maintenance cost of the steam generation system within the heat recovery section would be evaluated using as similar concept on an energy equivalency basis to natural gas.

To evaluate the overall cost of a product from a facility, the Total annualized cost (TAC) is determined by annualizing the contributing CAPEX and OPEX. For a basic system such as a steam cycle, it is easy to identify the equipment that contribute to the production of the commodity – power. For large integrated systems, this identification can be difficult depending on the perspective of the evaluator. In this study, steam can be produced by either extraction from a turbine or directly from the heat recovery system. If the steam originates solely from the heat recover system, then the profits associated with steam production is unambiguously dependent on the CAPEX and OPEX for the heat recovery system as well as the sales price of the steam. In contrast, the production of steam from both the heat recovery system and extraction from the steam turbine introduces some ambiguity in assigning CAPEX. The additional CAPEX

for a larger capacity turbine could benefit both the production of power as well as steam thus two perspectives on CAPEX assignment can be developed. As a result, this study considers a holistic evaluation of the integrated system since it cannot be easily decoupled by economically optimizing individual systems then integrating using cost correlations.

The economic optimality of the system is evaluated by maximizing the total profits. To determine the profits associated with the integrated system, the regional cost of power and water is used along with the TAC of each section. An evaluation dependent on minimizing the cost of power and water would not be effective due to the water-energy relationship. In other words, minimizing the production cost of one commodity would result in an increase in the cost of the other due to economies of scale. As a result, this study balances the production of either commodity via profits. The use of regional commodity cost only serves to aid in finding this balance.

Table 35 Cost estimate equations for combined heat recovery system and turbine network (HRS-TN)

Category	Equation	
Total annualized cost	$TAC^{HRS-TN} = \frac{1}{L} TCI + TOC$	(247)
Total capital investment	$TCI = DCC + SC + CC_{contingency}$	(248)
Direct capital costs	$DCC = CC_{Boiler\ /\ furnace} + CC_{Des} + CC_{HEX} + CC_{CT} + CC_{Turbine} + CC_{Pumps}$	(249)
Fuel gas boiler/ furnace	$CC_{Boiler\ /\ furnace} = 3.13 \times N_P N_T Q_{boil\ /\ furnace}^{0.77}$ $N_P = 1.015 \times 10^{-2} \times P_{gauge} + 0.6$ $N_T = 4.63 \times 10^{-7} T_{sh}^2 + 6.28 \times 10^{-4} T_{sh} + 1$	(250)
De-superheater	$CC_{Des} = 34158 \times \left(\dot{m}_j^{BFW} \right)^{0.3}$	(251)
Boiler feed water tank	$CC_{BFW-Tank} = 68154 \times \left(\sum_{i \in HPS} \sum_{j \in US} f_{jj}^{BFW} \right)^{0.3}$	(252)
Heat exchangers	$CC_{HEX} = CC_{WHB} + CC_{BFW-preheater} + CC_{air} + CC_{CW} + CC_{sea}$	(253)

Table 35 (*continued*)

Category	Equation	
Waste heat boiler	$CC_{WHB} = \sum_{i \in HPS} \sum_{j \in US} 1720 \cdot \left(A_{ij}^{WHB}\right)^{0.7}$	(254)
	$CC_{BFW-preheater} = \sum_{i \in HPS} \sum_{j \in US} 479 \cdot \left(A_{ij}^{BFW}\right)^{0.7}$	(255)
	$CC_{air} = \sum_{i \in HPS} 29 \cdot \left(A_{i,air}\right)^{0.7}$	(256)
	$CC_{CW} = \sum_{i \in HPS} 479 \cdot \left(A_{i,CW}\right)^{0.7}$	(257)
	$CC_{sea} = \sum_{i \in HPS} 719 \cdot \left(A_{i,sea}\right)^{0.7}$	(258)
Cooling Tower (CT)	$CC_{CT} = 3714 \cdot \left(M_{CW}^{Total}\right)^{0.7}$	
Steam turbine	$CC_{Turbine} = 304793 \cdot \left(DR \cdot W_{shaft,i}\right)^{0.7}$	
Process Pumps	$CC_{Pumps} = CC_{Sea-pump} + CC_{CW-pump} + CC_{BFW-pump}$	(259)
	$CC_{Pumps} = 3516 \times \left(PW_{pumps}\right)^{0.65}; if\ PW_{pumps} \le 224\,kW$	
	$CC_{Pumps} = 50000 + 234.5 \times PW_{pumps}; if\ PW_{pumps} \ge 224\,kW$	
Soft costs	$SC = CC_{Financing}$	(260)
Project financing	$CC_{Financing} = 0.04 \times DCC$	(261)
Contingency	$CC_{Contingency} = 0.05 \times DCC$	(262)
Total operating costs	$TOC = VOC + FOC$	(263)
Variable operating costs	$VOC = OC_{CT-makeup} + OC_{Boil} + OC_{Power}$	(264)
CT make-up water	$OC_{CT-makeup} = 0.5 \cdot C_{water} Q_{Total}^{CW}$	(265)
Boiler auxiliaries	$OC_{Boil} = 2.63 \times 10^{-3} NGC \times Q_{boil}$	(266)
Power	$OC_{Power} = 8760 \times PWC \times PW_{Net};\ if\ PW_{Net} \ge 0$	(267)
	$OC_{Power} = 0;\ if\ PW_{Net} \le 0$	
Fixed operating cost	$FOC = OC_{Spare}$	(268)
Spare cost	$OC_{Spare} = 0.01 \times DCC$	(269)

4.4.8.1 Objective function

The objective function for evaluating the integrated system would be to maximize total annual profits (TAP). This general concept is described by Equation 270.

$$\max \quad TAP = C_{power} PW_{Total} + C_{water} \cdot \left(M_{perm}^{RO} + M_{perm}^{MED} \right) - TAC^{HRS-TN} - TAC^{MED-TVC} - TAC^{RO} \tag{270}$$

For this objective function the total annualized cost of the MED-TVC and RO processes are taken from Chapter III and the study by Alnouri et al. [100] respectively. These annualized costs capture the capital and operating expenditures of the respective unit. It should also be noted that the power requirements of the GTL process is not included in the objective function. This decision is based on the selected boundaries of economic evaluation which is considered to be isolated from the overall GTL process. The profits in this case represents the difference between the sales from produced power and water to the overall capital and operating cost of the isolated process; the integrated heat recovery system and turbine network as well as MED-TVC and RO desalination technology.

4.4.9 Optimization approach

The optimization of this integrated system requires the manipulation of numerous variables included in highly non-linear equations. To reduce the time and improve efficiency of finding an optimal solution, the integrated system is strategically decoupled. In the case of the reverse osmosis network, this process is only linked to the overall integrated system via a power connection. Conceivably, it can be optimized independently to obtain the optimal operating variables that maximize the use of power.

For the MED-TVC process, the optimal water cost is attained via the manipulation of the motive steam pressure as well as the number of effects. Based on the study done in Chapter III, the lowest water cost is obtained at the lowest stable operating steam ejector pressure. This indicates that the lowest water cost would be dependent on the number of effects which is turn is a function of the desalinated water flow rate.

The overall procedure for optimizing the integrated system is shown in Figure 42 and described in the following steps. The methodical approach captures the various impacts of specific variables on attaining an optimal process configuration.

Step 1: Categorize processing facility into “sites”. The criteria for developing each site would be based on the potential for practical process stream heat integration. This can be a heuristics based approach or optimization based task where pipe routing and spatial

constraints are considered Alnouri et al. [136]. The latter based approach represents an extension to the outlined framework.

Step 2: Develop Grand composite curves (GCC) for each site using respective process heating and cooling information. Utilize grand composite curves to perform a Total site analysis on the process and to identify appropriate steam levels that minimize heat exchanger areas as well as maximizes heat recovery for water and power production. The identification of steam levels can be a heuristics based or optimization based approach.

Step 3: Adjust hot streams and excess process fuel gas in each site to account for process stream heat integration. Heat for column reboilers in a site should be via steam supply. For suitable hot stream integration with column reboilers, matching would be included in overall process heat exchange network.

In this study process heat integration is performed as a separate task from heat recovery for water and power generation. The approach for obtaining an optimal configuration for this task is not covered in this study though can be explored to expand the boundaries of the optimization framework.

Step 4: Determine remaining site heat loads from each steam level after process integration of site hot and cold stream is performed (Step 3).

Step 5: Develop a heat recovery system using all adjusted hot streams and "available fuel gas" post heat integration. The heat recovery system should be designed to include the selected steam levels from step 2 as well as steam level for the thermal desalination process. In addition, each process and desired operational objective is unique thus requiring a heuristics based approach to developing the overall superstructure.

Step 6: Develop a turbine network that incorporates the selected steam levels and can be merged with the heat recovery network to provide options for multiple flow configurations and novel system topologies. The design of this superstructure can be complex or simple depending on the choices of the evaluator.

Step 7: Merge the heat exchange network and turbine network and optimize for maximum power generation using incremental values of the maximum allowable design ratio. At the point where the maximum power generation does not increase, fix this design ratio as the maximum allowable.

Step 8: Evaluate process water source and sink data to determine the quality requirements of the MED-TVC and RO processes. Since water quality from the MED-TVC process has a typical consistent range of 2 - 16 ppm [59], select an appropriate quality constraint for which the RON should operate.

Step 9: Utilize existing RO models to determine the optimal configuration that satisfies the quality requirements at the minimum cost based on the seawater salinity, power regional cost and other system input data. These optimal design and operating parameters would be fixed for the optimization of the overall integrated system.

Step 10: Merge heat recovery system and turbine network with RO process, MED-TVC process and water integration model and optimize integrated system for a fixed number of MED-TVC effects.

Step 11: Validate the optimal flowrate of the MED-TVC process in the integrated system with its optimal number of effects. Optimize the standalone MED-TVC model using the same cost of fuel gas and obtained flowrate from integrated system.

It should be noted that the optimal number of effects can be the same for a range of flowrates. This trend is highlighted in the Chapter III.

The developed model in this study contains nonlinear, non-convex equations with additional mixed integer variables. It is a Mixed Integer Nonlinear Programming problem (MINLP) that may require advanced methodologies for obtaining a globally optimal system configuration. In this study, the globally optimal solution cannot be guaranteed though the methodology represents a systematic approach to coupling all water-energy linked processes.

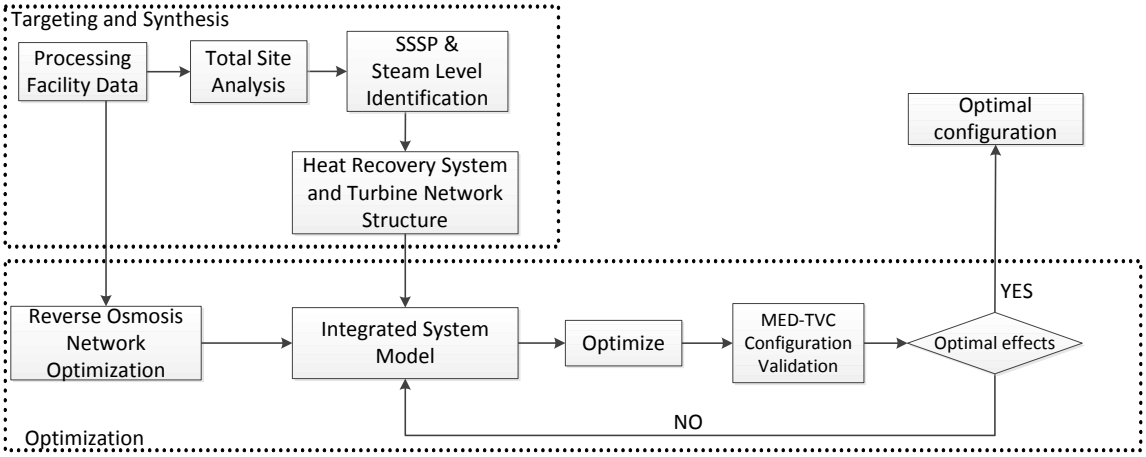

Figure 42 Optimization algorithm for obtaining an optimal integrated system

4.5 Case study

The proposed methodology and optimization model was demonstrated using the Autothermal reforming (ATR), Gas to liquid (GTL) process described by Gabriel et al. [133]. In that study, the potential for water and power generation from excess process heat was illustrated via the development of system targets. These water and power targets were achieved using MED based thermal desalination and power generation from a single steam level. In contrast, this study explores the use of both MED-TVC and RO desalination technologies and expands on the options for power generation at various steam levels as dictated by a total site analysis.

The associated ATR based GTL process data used in this study was taken from Gabriel et al. [133] and are summarized in Table 36 - Table 39. In addition, other parameters required for developing the optimization model are given in Table 40.

Table 36 GTL process requirements and excess fuel gas heating value

Parameter	Unit	Value
ATR reforming steam requirement	ton/hr	228
Power requirement	MMBtu/hr	729
Fuel gas heating value	MMBtu/hr	3393.6 [a]

[a] Total fuel heating value not accounting for boiler or furnace efficiencies

Table 37 Water integration sink data for GTL process

Sink	**Flow Rate [tons/hr]**	**Max. conc. Of Oil [ppm]**	**Max. conc. Of TDS [ppm]**
Natural gas saturator	51	1.0	2.0
Natural gas reformer	228	1.0	2.0
CO_2 removal unit	4	1.0	500
Cooling tower	[a]-	1.0	500

[a] Variable flowrate

Table 38 Water integration sink data for GTL process

Source	**Flow Rate** [tons/hr]	**Conc. Of Oil** [ppm]	**Conc. Of TDS** [ppm]
Pretreated water	705	0.1	0.06
MED-TVC process	[a]-	0.001	10
RO process	[a]-	0.001	500
Seawater	[a]-	-	34,483

[a] Variable flowrate

The ATR based GTL process represented in this case study provides an example of a process with multiple heat sources for water and power generation. To explore the range of configurations for water and power production, three (3) scenarios were evaluated. These case study scenarios are:-

1. Maximum power exportation while satisfying water and power interplant requirements
2. Zero exportation of power with maximum production of potable water while satisfying internal water and power requirements
3. Fixed demand for potable water with maximum limits on technology capacity and allowed power exportation. The additional data for this scenario is shown in Table 41.

Table 39 Stream data for ATR-based GTL process

Process stream	Duty (MMBtu/hr)	T_{supply} (°F)	T_{target} (°F)
Syngas production (Site 1) [a]			
E-101	93	138	300
E-102	49	212	392
E-103	263	581	787
E-104	395	342	700
Syngas conditioning (Site 2)			
E-201	-4002	1949	122
E-204	1093	-	254
E-205	-444	-	122
E-206	-497	173	122
FT Reaction (Site 3)			
E-301	-2550	410	365
E-302	-1051	428	122
Upgrading (Site 4)			
E-401	55	140	662
E-402	65	430	662
E-403	-191	705	400
E-404	-3	404	122
E-405	266	402	733
E-406	-240	-	302
E-407	-55	302	122
Water pretreatment (Site 5)			
E-501	124	-	230
E-502	-0.2	-	227

[a] Exchanger E-106 is excluded as a cold stream and included in the required HP steam requirements

For every region there exits various regulations that may restrict or permit the exportation of water and power. In addition, some plant locations may be restricted by access to infrastructure for distributing either commodity. Therefore these scenarios were designed to demonstrate the

optimal topology that may satisfy the constraints of the region. In particular, this study was done to reflect the regulations in Qatar which has a restriction on the discharge of liquids from facilities. As a result all three scenarios highlighted were optimized with a zero liquid discharge constraint.

Table 40 Input data and parameters used in integrated system model

Parameter	Unit	Value
Salinity of inlet seawater	ppm	34,483
Salinity limit on brine discharge	ppm	71,800
Boiler / Furnace efficiency	%	75
Power generation efficiency	%	2.0
Turbine exhaust pressure	psia	3.0
Maximum turbine inlet temperature	°F	1049
ΔT_{min} for steam production/heating	°F	9.0 [a]
ΔT_{min} for BFW production	°F	18.0
Plant life	years	20
Fuel gas value	$/MMBtu	2.0 [b]
Water sale price	$/ton	1.08
Power cost ($/kWh)	$/kWh	0.05

[a] Overall temperature driving force between hot and cold stream maintained at 18°F
[b] Comparable cost of natural gas [105,109]

Table 41 Scenario three (3) data input

Parameter	Unit	Value
Required potable water	ton/day	314,301
Maximum MED-TVC capacity	ton/day	146,667
Maximum RO capacity	ton/day	837,8111

Maximum capacities based on commercially established plants [157]

4.6 Results and discussion

4.6.1 Targeting and synthesis

The sites for the GTL facility were based on the processing sections identified in the study by Gabriel et al. [133]. For these sites, the individual grand composite curves (GCC) are shown in Figure 43.

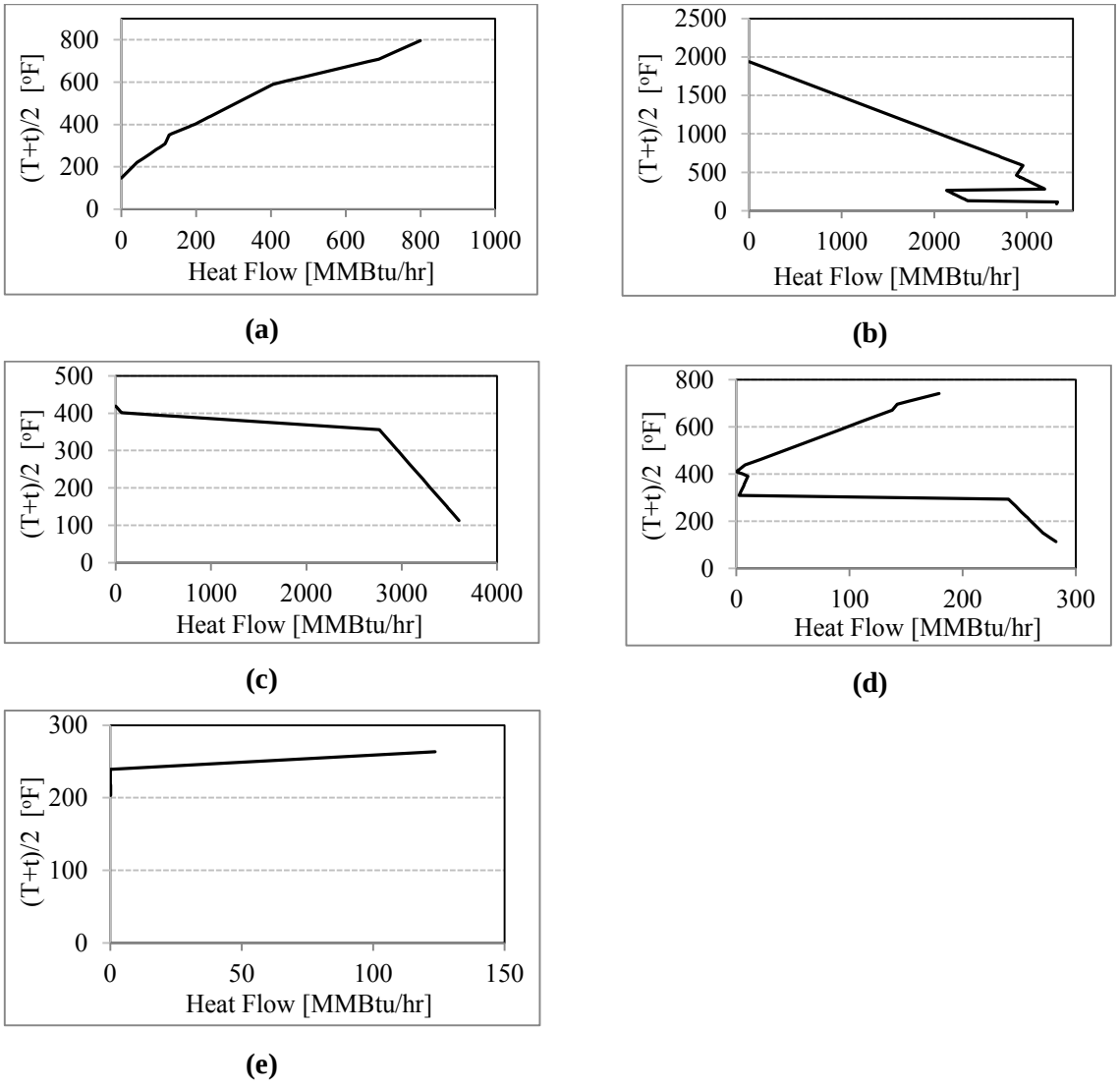

Figure 43 Grand composite curve for (a) Syngas production, (b) Syngas conditioning, (c) FT reaction, (d) Upgrading, (e) Water pretreatment

By eliminating the non-monotonic sections or "pockets" in each site's GCC, the site source-sink profile (SSSP) was developed and is shown in Figure 44. The SSSP indicates that the GTL process exhibits a significant amount of surplus heat that can be utilized for both water and power generation.

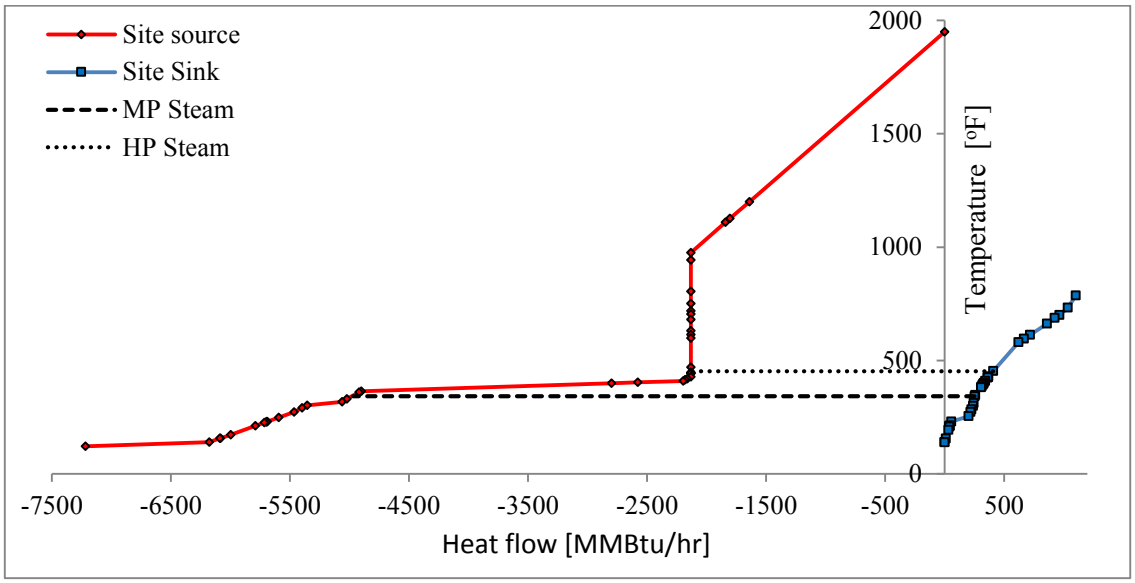

Figure 44 Site source-sink profile (SSSP) for ATR based GTL process

To satisfy the heating demands of the site sink, the appropriate steam levels were determined based on a heuristics approach. The process requirement for high pressure (HP) steam in the autothermal reformer dictated the selection of one of the steam levels. The medium pressure (MP) steam level was chosen to capture the significant amount of heat provided by the Fischer-Tropsch (FT) reactor as represented by the long horizontal line on the site source profile in Figure 44. To determine the appropriate steam level for the MED-TVC process, water cost trends developed in Chapter III were referenced. These trends indicate a minimum water cost at the lowest stable motive steam pressure for the ejector in the MED-TVC process. Hence this pressure was chosen.

With steam levels identified, each site was reevaluated to determine the total steam heating requirements. This was done after heat integration of hot and cold streams in each site. For the

upgrading section (site 4), the basic heat exchange network was developed as shown in Figure 45. Similar networks were developed for other applicable sites to determine the adjusted characteristics of each hot process stream. For sites with column reboilers represented as cold streams, process stream heat integration was replaced by steam heating. In addition, excess fuel gas from the GTL process was used as a heating source for process streams that could not be heated to target temperatures using available site hot streams. The total excess fuel was adjusted accordingly.

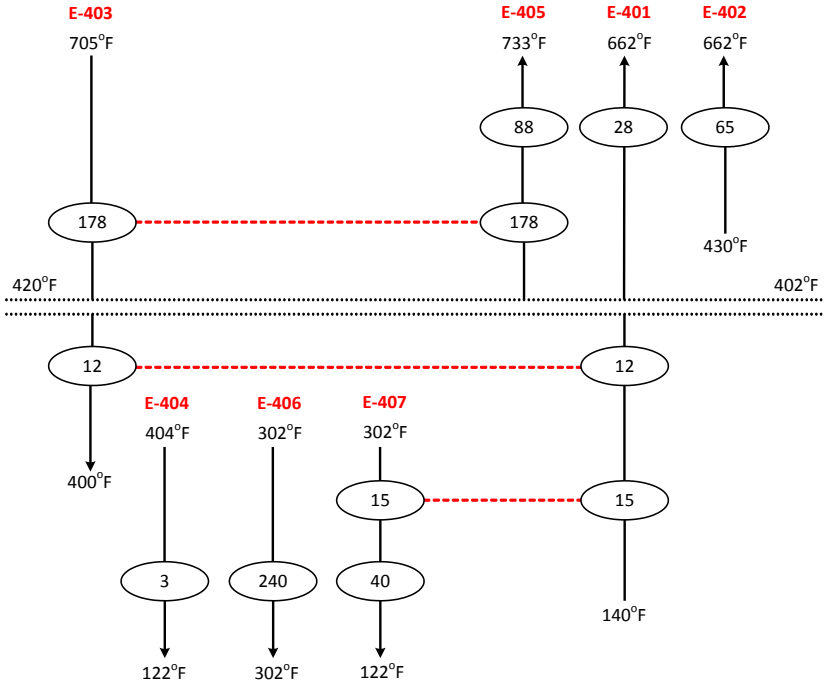

Figure 45 Process stream heat integration for syncrude upgrading section (site 4)

The final adjusted hot process streams, required steam flowrates and fuel gas are shown in Table 42 and Table 43. These data were used to develop the appropriate heat recovery superstructure and turbine network.

Table 42 Hot process stream data used for development of heat recovery system model

Process stream	Duty [MMBtu/hr]	T_{supply} [°F]	T_{target} [°F]
E-201	-4002	1949	122
E-205	-444	-	122
E-206	-497	173	122
E-301	-2550	410	365
E-302	-1051	428	122
E-404	-3	404	122
E-406	-240	-	302
E-407	-40	252	122
E-502	-0.2	-	227

Table 43 Cold stream heating requirements

Stream Heat exchanger	Fuel gas [MMBtu/hr]	HP Steam [MMBtu/hr]	MP Steam [MMBtu/hr]
E-101	-	93	-
E-102	-	49	-
E-103	263	-	-
E-104	293	102	-
E-204	-	-	1093 [b]
E-401	28 [a]	-	-
E-402	65	-	-
E-405	88 [a]	-	-
E-501	-	-	124 [b]
Total heating requirements	737	244	1217

[a] Remaining heating requirements not fulfilled via process stream heat integration
[b] Column reboiler heating requirement

The steam heating requirements were converted to mass flowrates for inclusion in the overall mass balance of the HEN model. In addition, the HP steam requirement for the autothermal reactor is added to the total shown in Table 43 to capture the overall HP steam requirement. To

calculate the logarithmic mean temperature difference for exchangers in the HEN, the operating temperatures based on steam level pressures are used and given in Table 44. The overall heat transfer coefficient used in the area calculation of each exchanger is shown in Table 45.

Table 44 Selected steam level and associated boiler feed water operating conditions

Utility Stream	**Pressure** [psia]	**Supply temp.** [°F]	**Target Temp.** [°F]	**Description**
HP_{Steam}	435	453	453	Saturated HP steam
HP_{BFW}	435	344	453	Preheating MP_{BFW} to HP_{BFW}
MP_{Steam}	125	344	344	Saturated MP steam
MP_{BFW}	125	213	344	Preheating LP_{BFW} to MP_{BFW}
LP_{Steam}	15	213	213	Saturated LP steam
LP_{BFW}	15	140	213	Preheating Cond. To LP_{BFW} [a]

[a] Supply temperature taken as lowest return temperature

The last stage in the HEN is used to preheat a mixture of fresh water, return condensate from the MED-TVC process and turbine network. The heat balance for this stage was determined using source enthalpies as well as final LP boiler feed water enthalpy. For the supply temperature of the combined stream, the turbine network condensate temperature was used.

For this case study, the heat recovery system was developed in conjunction with the steam turbine network. The overall superstructure was designed for an efficient use of heat sources. For instance, the fuel gas was considered a high quality heating source and consequently used for the operation of boilers and furnaces only. For this case, the heat exchange network was developed to produce only saturated steam while furnaces were used for superheating steam by 18°F before sending to the appropriate headers. This approach was convenient for the GTL case though may be different for other processes. In addition, the heat recovery system's superstructure captures various flow options for the generation of steam at the different levels. The developed structure is shown in Figure 46.

Table 45 Overall heat transfer coefficients used in developing HEN model

Utility Stream	Heat transfer coefficient [Btu/ft^2-h-^{o}F]								
	E-201	E-205	E-206	E-301	E-302	E-404	E-406	E-407	E-502
HP_{Steam}	35	-	-	-	-	-	-	-	-
HP_{BFW}	28	-	-	-	-	-	-	-	-
MP_{Steam}	35	-	-	145	35	53	-	-	-
MP_{BFW}	28	-	-	110	28	32	-	-	-
LP_{Steam}	35	-	-	145	35	53	132	53	-
LP_{BFW}	28	-	-	110	28	32	150	32	-
AIR	18	66	66	35	18	18	79	18	66
CW	28	176	140	110	28	32	150	32	137
SEA	25	153	122	98	25	28	131	28	118

Heat transfer coefficients not shown for hot process streams that cannot heat specific utility streams

For this study, the turbine network has LP steam as an extraction option. This structural feature introduces a true tradeoff between steam generation for thermal desalination and power for membrane desalination. In other studies, this option is not often considered. In the discussion of scenario 2, the effect of this design feature would be highlighted.

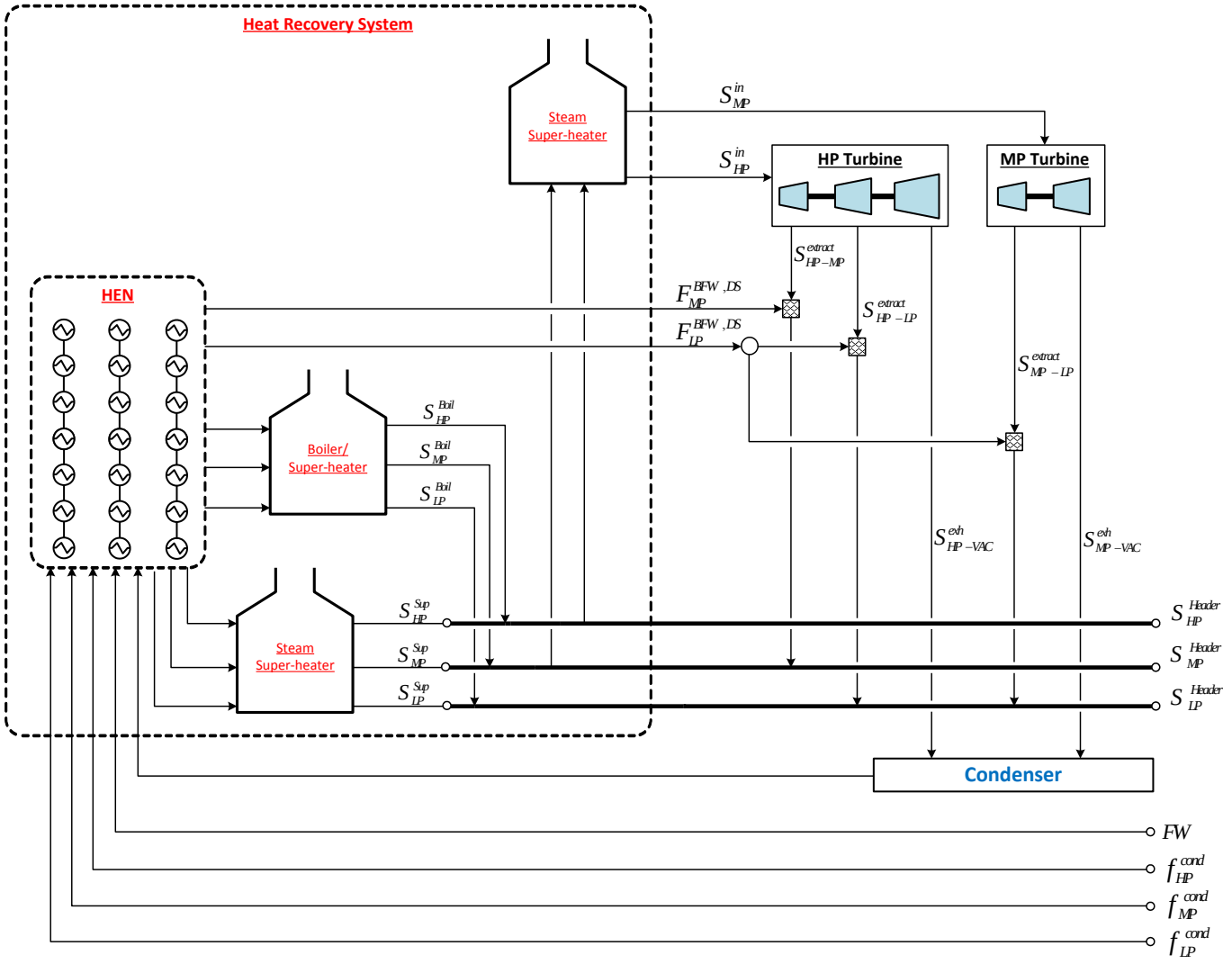

Figure 46 Integrated heat exchange network and turbine network for case study

4.6.2 Scenario 1

For the maximum power scenario, a target for the system was first determined. In this targeting approach, the model is solved for maximum power generation using the combined heat exchange network and turbine network models. For this modeling effort, performance equations for the turbine network were included thus a mixed integer nonlinear programming problem (MINLP) was developed. The optimization model was solved using LINGO and run on a desktop PC (Intel® Core™ Duo, 2.27 GHz, 4 GB RAM, 64-bit operating system). The results of this targeting approach are shown in Table 46 - Table 49. These results represent the maximum generated power within the constraints of the turbine correlations and water management constraints while excluding the use of economic estimations for process equipment.

Table 46 Heat transfer matrix between adjusted hot process streams and utility streams at maximum power target

Utility Stream	**Heat transferred** [MMBtu/hr]								
	E-201	E-205	E-206	E-301	E-302	E-404	E-406	E-407	E-502
HP_{Steam}	3036	-	-	-	-	-	-	-	-
HP_{BFW}	441	-	-	-	-	-	-	-	-
MP_{Steam}	-	-	-	2527	228	0.5	-	-	-
MP_{BFW}	282	-	-	23	444	1.4	-	-	-
LP_{Steam}	-	-	-	-	-	-	-	-	-
LP_{BFW}	166	-	-	-	30	-	240	29	-
AIR	57	-	-	-	319	-	-	8	0.2
CW	20	-	-	-	31	-	-	3	-
SEA	-	444	497	-	-	1.2	-	-	-
Total	4002	444	497	2550	1051	3	240	40	0.2

Table 47 Total cooling requirements for maximum power target

Utility	**Cooling requirements** [MMBtu/hr]	
	Heat exchange network	Turbine network
Air cooling	384	4,576
Cooling water	53	791
Seawater	942	-
Total	1,379	5,367

Table 48 Power distribution for GTL process and integrated system at maximum power target

System	Power [MMBtu/hr]
Produced	
HP turbine	741
MP turbine	967
Usage	
GTL process	729
Cooling tower draft fan	0.3
Air cooler draft fan	17
Integrated system pumping [a]	15
Total Export Power	947

[a] Includes power for seawater, cooling water and boiler feed water pumps for HEN and turbine network

Table 49 Steam flowrates for integrated Heat exchange network and turbine network at maximum power target

Stream	Parameter	Temperature [ºF]	Flowrate [ton/hr]
Boiler HP steam from HEN HP-BFW	S_{HP}^{Boil}	471	-
Boiler MP steam from HEN MP-BFW	S_{MP}^{Boil}	362	-
Boiler LP steam from HEN LP-BFW	S_{LP}^{Boil}	233	-
Superheated HEN HP steam	S_{HP}^{Sup}	471	1982
Superheated HEN MP steam	S_{MP}^{Sup}	362	1570
Superheated HEN LP steam	S_{LP}^{Sup}	233	-
HP turbine steam feed	S_{HP}^{in}	988	1597
MP turbine steam feed	S_{MP}^{in}	768	1884
MP-BFW for de-superheating	$F_{MP}^{BFW,DS}$	344	164
LP-BFW for de-superheating	$F_{LP}^{BFW,DS}$	215	-
Extracted MP steam from HP turbine	$S_{HP-MP}^{extract}$	700	836
Extracted LP steam from HP turbine	$S_{HP-LP}^{extract}$	323	-
Extracted LP steam from MP turbine	$S_{MP-LP}^{extract}$	340	-
Fresh water makeup for ATR reforming	FW	77	228

A comparison of the maximum power target obtained by Gabriel et al. [133] and this study indicated a disparity between both results. This difference is an artifact of the assumptions used in the previous study whereby a single steam level and turbine efficiency were adopted. In contrast, this study expands the steam level options for power generation, incorporates turbine performance equations to estimate efficiencies at various flow options and allows for an optimal inlet temperature to the turbines to be determined. These options impact the attainable maximum power significantly as shown by the results. In specific, the data indicate that the generation of medium pressure (MP) steam for the process is optimally obtained via turbine extraction only. In addition, the properties of the steam through the turbine network to achieve these results is shown in Figure 47 and validates the need for a comprehensive turbine network structure to capture the unique options for maximizing power.

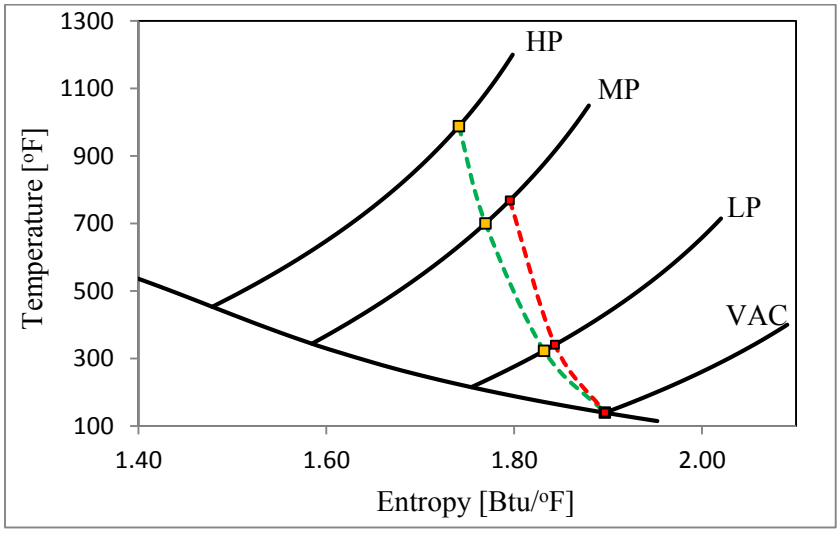

Figure 47 Entropy – Temperature diagram for turbine network

With the targets for maximum power established, the system was optimized within economic constraints. In comparison to the target power, the maximum power configuration was similar to the target in terms of power generated and optimal steam flow routing. In contrast, the economic optimization approach results in an expected change in the overall heat exchange network which

sought to minimize total heat transfer area cost. These heat transfer option differences are shown in Table 50 - Table 51.

Table 50 Heat transfer matrix between adjusted hot process streams and utility streams for maximum power

Utility Stream	**Heat transferred** [MMBtu/hr]								
	E-201	E-205	E-206	E-301	E-302	E-404	E-406	E-407	E-502
HP_{Steam}	3036	-	-	-	-	-	-	-	-
HP_{BFW}	441	-	-	-	-	-	-	-	-
MP_{Steam}	-	-	-	2550	206	-	-	-	-
MP_{BFW}	282	-	-	-	466	1.9	-	-	-
LP_{Steam}	-	-	-	-	-	-	-	-	-
LP_{BFW}	72	-	-	-	152	-	240	-	-
AIR	-	-	-	-	-	1.1	-	-	0.2
CW	170	-	-	-	228	0.1	-	40	-
SEA	-	444	497	-	-	-	-	-	-
Total	4002	444	497	2550	1051	3	240	40	0.2

Table 51 Total cooling requirements for maximum power

Utility	**Cooling requirements** [MMBtu/hr]	
	Heat exchange network	Turbine network
Air cooling	1.3	4960
Cooling water	438	407
Seawater	941	-
Total	1,380	5,367

With the use of this study's cost estimations, an economic comparison of cooling water and seawater cooling cost would highlight the advantage of the seawater option. The identified cost difference between both options were the capital expenditure for the cooling tower and operating expenditure associated with cooling tower make-up water cost. This cost advantage was not realized in the overall system topology where cooling water was greatly used as an option over seawater. This result can be attributed to the zero liquid discharge constraint imposed on the overall integrated system. In essence, the cooling tower losses water via evaporation and serves

as an ideal sink for minimizing waste water discharge. As a result, the use of the cooling water option was maximized to minimize the discharge of waste water from the integrated system. This is reflected in the cooling water requirement being exactly matched by the amount of excess process water. The summary of the scenario's economics is shown in Table 52 which highlight a favorable cost for power from the recovered energy.

Table 52 Economics for maximum power

Description	Parameter	Units	Value
Total capital investment	TCI	$	300,000,000
Total operating cost	TOC	$/yr	12,000,000
Total annualized cost	TAC^{HRS-TN}	$	28,000,000
Effective power cost		$/kWh	0.01
Sales		$/yr	220,000,000
Profits	AP^{HRS-TN}	$/yr	192,000,000

4.6.3 Scenario 2

The mirror image of the maximum power case would be the maximum water generation scenario. This scenario was developed to reflect processes in regions that restrict power exportation to the grid or are inaccessible to infrastructure to facilitate this distribution. In that case, power generated from the process would be for interplant use only while excess energy would be converted to the optimal form to generate water via a suitable combination of both desalination technologies. The optimal ratio of water supply from either technology would be based on economics. The detailed results of this scenario are shown in Table 53 - Table 56.

Table 53 Heat transfer matrix between adjusted hot process streams and utility streams for maximum water

Utility Stream	Heat transferred [MMBtu/hr]								
	E-201	E-205	E-206	E-301	E-302	E-404	E-406	E-407	E-502
HP_{Steam}	3036	-	-	-	-	-	-	-	-
HP_{BFW}	441	-	-	-	-	-	-	-	-
MP_{Steam}	-	-	-	2550	196	-	-	-	-
MP_{BFW}	272	-	-	-	475	1.9	-	-	-
LP_{Steam}	-	-	-	-	-	-	228	-	-
LP_{BFW}	176	-	-	-	260	-	11	29	-
AIR	-	-	-	-	-	1.1	-	8	0.2
CW	76	-	-	-	120	0.1	-	3	-
SEA	-	444	497	-	-	-	-	-	-
Total	4002	444	497	2550	1051	3	240	40	0.2

Table 54 Total cooling requirements for integrated system for maximum water

Utility	Cooling requirements [MMBtu/hr]		
	Heat exchange network	Turbine network	MED-TVC
Air cooling	9.3	4711	-
Cooling water	199	645	-
Seawater	941	-	199
Total	1,149	5,357	199

Table 55 Power distribution for GTL process and integrated system for maximum water

System		Power [MMBtu/hr]
Produced		
	HP turbine	741
	MP turbine	965
Usage		
	GTL process	729
	Cooling tower draft fan	0.3
	Air cooler draft fan	16
	Integrated system pumping [a]	20
	RO desalination	940
Total Export Power		0

[a] Includes power for seawater, cooling water and boiler feed water pumps for HEN, turbine network and MED-TVC where applicable

Table 56 Steam flowrates for integrated Heat exchange network and turbine network for maximum water

Stream	**Parameter**	**Temperature** [ºF]	**Flowrate** [ton/hr]
Boiler HP steam from HEN HP-BFW	S_{HP}^{Boil}	471	-
Boiler MP steam from HEN MP-BFW	S_{MP}^{Boil}	362	-
Boiler LP steam from HEN LP-BFW	S_{LP}^{Boil}	233	-
Superheated HEN HP steam	S_{HP}^{Sup}	471	1982
Superheated HEN MP steam	S_{MP}^{Sup}	362	1564
Superheated HEN LP steam	S_{LP}^{Sup}	233	118
HP turbine steam feed	S_{HP}^{in}	988	1597
MP turbine steam feed	S_{MP}^{in}	768	1879
MP-BFW for de-superheating	$F_{MP}^{BFW,DS}$	344	164
LP-BFW for de-superheating	$F_{LP}^{BFW,DS}$	215	-
Extracted MP steam from HP turbine	$S_{HP-MP}^{extract}$	700	836
Extracted LP steam from HP turbine	$S_{HP-LP}^{extract}$	323	-
Extracted LP steam from MP turbine	$S_{MP-LP}^{extract}$	340	-
Fresh water makeup for ATR reforming	FW	77	228

For this study, the outlined approach to economically evaluating the overall system was based on an aggregated assessment of the individual systems. Table 57 - Table 59 illustrate the individual economics surrounding each system based on the selected market value of power and water given in Table 40.

Table 57 Heat exchange network and turbine network economics for maximum water

Description	Parameter	Units	Value
Total capital investment	TCI	$	301,000,000
Total operating cost	TOC	$/yr	12,000,000
Total annualized cost	TAC^{HRS-TN}	$	26,000,000 [a]
Effective power cost		$/kWh	0.01
Sales		$/yr	218,000,000
Profits	AP^{HRS-TN}	$/yr	192,000,000

[a] Price inclusive of LP steam generation costs

Table 58 Optimal reverse osmosis process for maximum water

Description	Parameter	Units	Value
Water flowrate [a]		ton/day	2,520,873
Number of modules	NM		27,251
Feed pressure	P_f	psia	919
Power usage		kWh/m^3	2.9
Recovery		%	52.3
Total annualized cost	TAC^{RO}	$	473,000,000
Effective water cost		$/ton	0.51
Sales		$/yr	992,000,000
Profits	AP^{RO}	$/yr	519,000,000

[a] Includes seawater flowrate to meet potable water specifications

Table 59 Optimal MED-TVC process for maximum water

Description	Parameter	Units	Value
Water flowrate [a]		ton/day	33,167
Number of effects	N_{eff}		11
Gain output ratio	GOR		11.6
Power usage		kWh/m^3	1.2
Heat usage		kWh/m^3	57.8
Recovery		%	54.0
Total annualized cost	$TAC^{MED-TVC}$	$	6,000,000
Effective water cost [b]		$/ton	0.49
Sales		$/yr	13,000,000
Profits	$AP^{MED-TVC}$	$/yr	7,000,000

[a] Includes seawater flowrate to meet potable water specifications

[b] Price not inclusive of steam costs. This cost is captured in TAC^{HRS-TN}

The results for this scenario indicated that the majority of the desalinated water was generated using RO technology. This contradicts previous studies that suggest a fairly even distribution in fresh water supply from both technologies [106]. In fact these results highlight the conditions that determine the optimal distribution of the hybrid desalination plant.

The differences in the results from scenario 1 and 2 were a reduced required cooling of the hot process streams as well as the utilization of excess power for RO desalination. The former result indicated that low grade heat from the hot process streams was not suitable for power production but could be used for LP steam generation for the MED-TVC process. As a result, the minimum cooling for the hot process streams was transferred to the cooling requirement of the MED-TVC process. In fact, this was the only energy used for thermal desalination which illustrates the impact of energy utilization efficiency of either desalination technology.

With the MED and RO processes considered as black boxes with intrinsic energy requirements for water production, the tradeoff of selecting either process would depend on the source of the energy and the conversion efficiency pathway. Based on the developed superstructure in this study, the recovered energy can either be converted to steam via a simple path or power via a more complicated cycle. The former process provides a path with minimal inefficiencies and loss of energy therefore it would be favorable. The latter pathway results in energy losses via turbine operation, pump inefficiencies as well as latent heat wastage at the end

of the Rankine cycle. Hence every unit of recovered energy is more favorably used for steam generation. The tradeoff between the MED-TVC and RO process is therefore dictated by the overall energy requirement of the process as well as the capital cost associated with producing that form of energy.

Based on this study and validated by literature [49,131], the aggregated heat and power energy requirement for producing desalinated water is approximately 59 and 2.9 kWh/m^3 for MED-TVC and RO respectively. These values are an order of magnitude different and as such the selection of either technology is inherently biased to the RO process. In contrast the cost of heat exchangers, turbines and pumps may result in MED-TVC technology having the economic advantage. In essence the optimal ratio of MED-TVC and RO technology would be dependent on the combined impact of the technology's energy utilization, energy conversion efficiency and capital cost for generating the required form of energy.

Another factor that contributed to the lack of a balanced hybrid desalination process was the configuration of the turbine network. In this study, the exhaust steam from the turbine network was fixed at vacuum conditions while there was an extraction option to provide low pressure (LP) steam to the MED-TVC process. The embedded structural design created a natural tradeoff between maximum generation of power with RO based desalination and balanced power generation with the incorporation of MED-TVC desalination. This approach to coupling both desalination technologies was not adopted often. In comparison to typical designs in literature, the thermal desalination process was designated as a permanent heat sink for the turbine exhaust steam. In these cases, the exhaust pressure was fixed to the allowable operating pressure of the thermo vapor compressor thus intrinsically reducing the potential power generation from the cycle. By utilizing the MED-TVC as a permanent heat sink, it would always appear in the optimal hybrid desalination topology since latent heat from the exhaust steam would have to be removed regardless of the presence of the integrated desalination process. In essence the exhaust steam in that case would economically advantage the MED-TVC process.

The final and more encompassing factor that limits the balanced selection of both technologies is the concept of economies of scale. The selected turbine network, inefficient energy pathways as well as capital cost for required equipment all contribute to the overall cost of water from either technology. The overall capital cost naturally reduces due to economies of scale. The initial cost at low capacity and rate of reduction in cost is different for either technology therefore a single technology could be selected in one particular capacity range while

another in a different range. With a maximum profits based objective function and no restrictions on technology capacities, only a single desalination process would dominate as indicated by the results.

4.6.4 Scenario 3

This scenario would represent the ideal case of a fixed water demand with no restrictions on power exportation. In this case, there is a tradeoff in maximizing power generation for profits while satisfying the water requirements. With RO desalination requiring more power than the MED-TVC process, an interesting tradeoff between both technologies was obtained. These results are shown in Table 60- Table 63 and indicate that the water supply from MED-TVC increases from that shown in scenario 2.

Table 60 Heat transfer matrix between adjusted hot process streams and utility streams for fixed water demand

Utility Stream	**Heat transferred** [MMBtu/hr]								
	E-201	E-205	E-206	E-301	E-302	E-404	E-406	E-407	E-502
HP_{Steam}	2994	-	-	-	-	-	-	-	-
HP_{BFW}	483	-	-	-	-	-	-	-	-
MP_{Steam}	-	-	-	2550	184	-	-	-	-
MP_{BFW}	267	-	-	-	482	-	-	-	-
LP_{Steam}	-	-	-	-	-	-	240	-	-
LP_{BFW}	181	-	-	-	265	2.7	-	29	-
AIR	-	-	-	-	-	-	-	-	0.2
CW	76	-	-	-	120	0.4	-	11	-
SEA	-	444	497	-	-	-	-	-	-
Total	4002	444	497	2550	1051	3	240	40	0.2

Table 61 Total cooling requirements for integrated system for fixed water demand

Utility	**Cooling requirements** [MMBtu/hr]		
	Heat exchange network	Turbine network	MED-TVC
Air cooling	0.2	4,722	-
Cooling water	208	637	-
Seawater	941	-	208
Total	1,149	5,359	208

Table 62 Power distribution for GTL process and integrated system for fixed water demand

System		Power [MMBtu/hr]
Produced		
	HP turbine	1245
	MP turbine	448
Usage		
	GTL process	729
	Cooling tower draft fan	0.3
	Air cooler draft fan	16
	Integrated system pumping [a]	125
Total Export Power		822

[a] Includes power for seawater, cooling water and boiler feed water pumps for HEN, turbine network, MED-TVC and RO where applicable

The results from scenario 2 would suggest that the MED-TVC process was only selected based on the inability to utilize low grade heat to generate power for the more energy efficient RO process. In this scenario, a similar trend as in scenario 2 was expected where the flowrate from the MED-TVC would have remained the same with the remaining water supplemented by the power driven RO desalination. This would reduce the power output but would conceivably be the more energy efficient choice. In fact, the flowrate from MED-TVC increases and can be attributed to the complex tradeoff of profits from each section per unit of energy required. This profits per unit energy parameter changes with unit capacity and as such, there is an optimized economic balance based on the capacity of each unit as well as their profits and energy utilization efficiencies. A summary of the economic evaluation of each section is given in Table 64 - Table 66.

Table 63 Steam flowrates for integrated Heat exchange network and turbine network for fixed water demand

Stream	Parameter	Temperature [ºF]	Flowrate [ton/hr]
Boiler HP steam from HEN HP-BFW	S_{HP}^{Boil}	471	199
Boiler MP steam from HEN MP-BFW	S_{MP}^{Boil}	362	-
Boiler LP steam from HEN LP-BFW	S_{LP}^{Boil}	233	-
Superheated HEN HP steam	S_{HP}^{Sup}	471	1955
Superheated HEN MP steam	S_{MP}^{Sup}	362	1558
Superheated HEN LP steam	S_{LP}^{Sup}	233	123
HP turbine steam feed	S_{HP}^{in}	988	1769
MP turbine steam feed	S_{MP}^{in}	768	872
MP-BFW for de-superheating	$F_{MP}^{BFW,DS}$	344	-
LP-BFW for de-superheating	$F_{LP}^{BFW,DS}$	215	-
Extracted MP steam from HP turbine	$S_{HP-MP}^{extract}$	700	-
Extracted LP steam from HP turbine	$S_{HP-LP}^{extract}$	322	-
Extracted LP steam from MP turbine	$S_{MP-LP}^{extract}$	341	-
Fresh water makeup for ATR reforming	FW	77	228

Table 64 Heat exchange network and turbine network economics for fixed water demand

Description	Parameter	Units	Value
Total capital investment	TCI	$	303,000,000
Total operating cost	TOC	$/yr	12,000,000
Total annualized cost	TAC^{HRS-TN}	$	28,000,000[a]
Effective power cost		$/kWh	0.01
Sales		$/yr	217,000,000
Profits	AP^{HRS-TN}	$/yr	189,000,000

[a] Price inclusive of LP steam generation costs for MED-TVC

Table 65 Optimal reverse osmosis process for fixed water demand

Description	Parameter	Units	Value
Water flowrate [a]		ton/day	278,995
Number of modules	NM		3016
Feed pressure	P_f	psia	919
Power usage		kWh/m^3	2.89
Recovery		%	52.3
Total annualized cost	TAC^{RO}	$	44,000,000
Effective water cost		$/ton	0.43
Sales		$/yr	110,000,000
Profits	AP^{RO}	$/yr	66,000,000

[a] Includes seawater flowrate to meet potable water specifications

Table 66 Optimal MED-TVC process for fixed water demand

Description	Parameter	Units	Value
Water flowrate [a]		ton/day	35,306
Number of effects	N_{eff}		11
Gain output ratio	GOR		11.8
Power usage		kWh/m^3	1.19
Heat usage		kWh/m^3	56.9
Recovery		%	54.0
Total annualized cost	$TAC^{MED-TVC}$	$	6,000,000
Effective water cost [b]		$/ton	0.47
Sales		$/yr	14,000,000
Profits	$AP^{MED-TVC}$	$/yr	8,000,000

[a] Includes seawater flowrate to meet potable water specifications

[b] Price not inclusive of steam costs. This cost is captured in TAC^{HRS-TN}

4.6.5 Overall water management

For all scenarios, the water integration strategy among process water sources (M) and sinks (N) was represented by Figure 48. This strategy was consistently chosen as the optimal configuration based on the scenario constraints. For scenarios 2 and 3 the flows between desalination technology and export sink are given in data presented earlier and illustrated in Figure 49 and Figure 50. It should be noted that the overall strategy is different to that outlined

in the study by Gabriel at al. [133]. In this case, the water-nexus is economically optimized to minimize fresh water being sent to the cooling tower sink. This illustrates the applicability of the presented methodology for optimizing the tradeoff of generating water and energy.

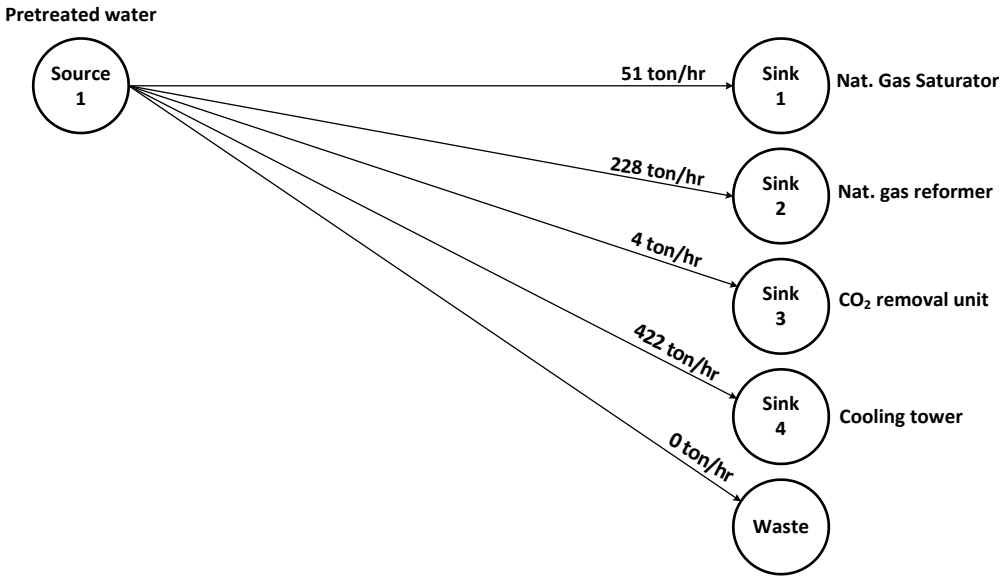

Figure 48 Interplant water source-sink diagram for the ATR based GTL process

In this case study, the process water is within the impurity constraints required by all sinks therefore there is no need for fresh water. The zero liquid discharge strategy consistently forces the routing of excess process water to the cooling tower. For a change in process water specifications, the overall scheme would be altered thus requiring an optimal tradeoff of water sourcing from both MED-TVC and RO processes. This scenario would be investigated in a later study.

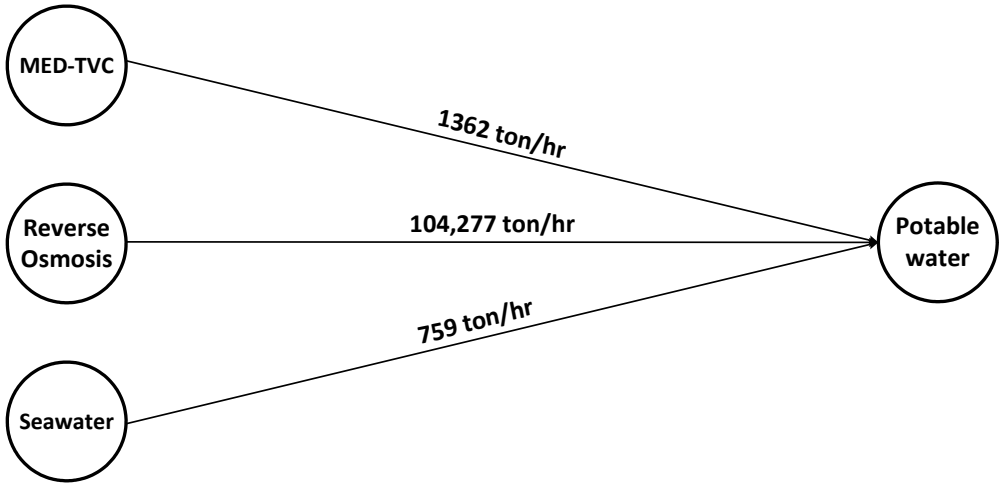

Figure 49 Export water source-sink diagram for scenario 2

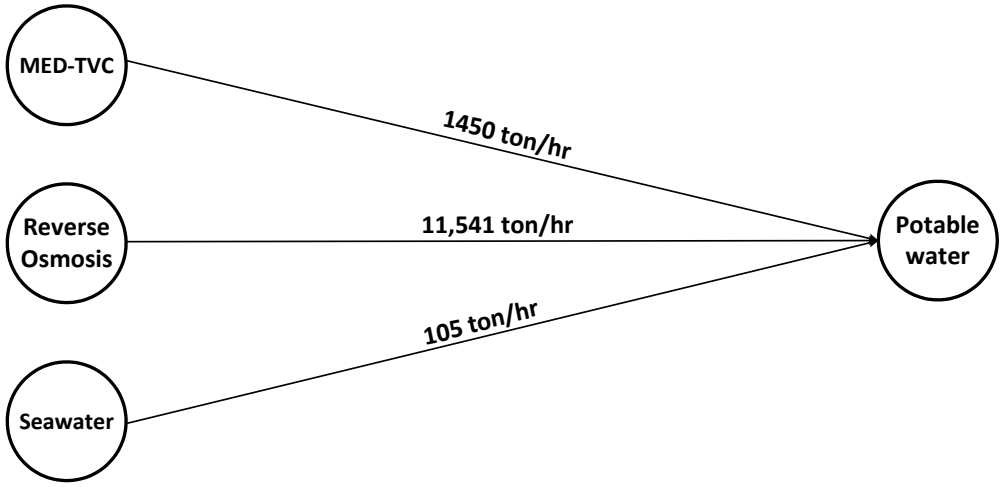

Figure 50 Export water source-sink diagram for scenario 3

4.7 Summary

A new systematic procedure has been proposed for optimizing the benefits of the water-energy nexus in processes with a surplus of energy. In addition, the procedure provides a suitable framework for which the utilities section of these processes can be developed to maximize the benefits of generating power and water in regions that can benefit from the exportation of both commodities.

This new methodology included the use of Total site analysis to first identify the potential for excess energy as well as the appropriate steam levels for the utility system. In the following steps, heat integration of process hot and cold streams was done to adjust the available energy content and temperature quality of hot streams. The adjusted hot streams were then used to develop the combined heat recovery system and turbine network for generation of steam and power for thermal and membrane desalination technologies respectively. Existing models for reverse osmosis networks as well as multi-effect desalination with thermo vapor compression were used in the overall integrated system model. Finally, economic optimization was carried out on the overall system to identify process configuration tradeoffs for various scenarios.

The procedure was strategically demonstrated using the Gas-to-liquids process to highlight its potential for producing fuels, power and potable water. The results from the case study indicated that the RO desalination option is more economical provided the quality of surplus energy is suitable for power production. In addition, thermal desalination processes are included in the overall configuration when there is surplus heat suitable for generating low pressure steam only or when the technology is used as a designated heat sink for exhaust steam.

With some regions having abundant natural gas resources, the outlined methodology provides an ideal framework for which GTL processes can be exploited to satisfy the mutually linked energy and water demands. In general the developed procedure provides a new systematic approach to improving the thermal efficiency of net energy producing processes by introducing a new commodity into the production portfolio – water.

CHAPTER V
CONCLUSION

In this research a systematic approach to optimizing the benefits of the water-energy nexus in energy surplus processes was developed. The following novel tools associated with the methodical framework were proposed.

In chapter II, a targeting approach was adopted to identify potential quantities and qualities of surplus energy in a given process. These targets were used to benchmark the process for generation of water and power. This was achieved via the use of thermal pinch analysis and water integration techniques.

With desalination becoming an increasingly popular alternative for water production, a new formulation for developing flexible and novel thermal desalination processes was introduced (chapter III). The inclusion of this study provided an additional configuration option in the overall approach to optimizing the use of surplus energy in processes for water and power generation.

In the final chapter (IV), total site analysis, heat exchange network synthesis, turbine network development, thermal and membrane desalination as well as water integration via direct recycle were used as building blocks to develop the overall superstructure for optimizing the benefits of the water-energy nexus. A thermoeconomic evaluation of the superstructure was performed to obtain novel configurations that balanced the tradeoff between water and power generation.

The developed tools were demonstrated using the Gas-to-liquids process. This process was strategically chosen to highlight its advantage in producing a diverse portfolio of intertwined resources – water and energy. In general, the proposed tools represent an integrated and strategic approach to guiding researchers and decision makers in addressing water-energy issues.

REFERENCES

1. International-Energy-Agency. Golden Rules for a Golden Age of Gas. *A Special Report Published by the IEA*2012: http://www.worldenergyoutlook.org/media/weowebsite/2012/goldenrules/WEO2012_GoldenRulesReport.pdf.

2. Wood DA, Nwaoha C, Towler BF. Gas-to-liquids (GTL): A review of an industry offering several routes for monetizing natural gas. *Journal of Natural Gas Science and Engineering.* 2012;9(0):196-208.

3. Hall KR. A new gas to liquids (GTL) or gas to ethylene (GTE) technology. *Catalysis Today.* 2005;106(1–4):243-246.

4. Reddy Keshav T, Basu S. Gas-to-liquid technologies: India's perspective. *Fuel Processing Technology.* 2007;88(5):493-500.

5. De Klerk A. *Fischer-Tropsch Refining*. Weinheim, Germany: Wiley-VCH Verlag & Co. KGaA, Boschstr; 2011.

6. Senden MMG, Martens FJA, Steenge WDE, Nagelvoort RK. Shell's GTL: Its Technology and Design, Its Operation and Products. *International Petroleum Technology Conference*. Doha, Qatar: International Petroleum Technology Conference 2005.

7. Fiato RA, Sibal PW. ExxonMobil's Advanced Gas-to-Liquids Technology - AGC21. *SPE Middle East Oil and Gas Show and Conference*. Kingdom of Bahrain: Society of Petroleum Engineers; 2005.

8. Godorr S. GTL Technology Advancements: World Petroleum Conference; 2011.

9. Ha K-S, Bae JW, Woo K-J, Jun K-W. Efficient Utilization of Greenhouse Gas in a Gas-to-Liquids Process Combined with Carbon Dioxide Reforming of Methane. *Environmental Science & Technology.* 2010/02/15 2010;44(4):1412-1417.

10. Rafiee A, Hillestad M. Techno-Economic Analysis of a Gas-to-Liquid Process with Different Placements of a CO2 Removal Unit. *Chemical Engineering & Technology.* 2012;35(3):420-430.

11. Gandrik AM, Patterson MW, Mills PM. *HTGR-Integrated Coal and Gas to Liquids Production Analysis*: Idaho National Laboratory;2011. Project No. 23843.

12. Bao B, El-Halwagi MM, Elbashir NO. Simulation, integration, and economic analysis of gas-to-liquid processes. *Fuel Processing Technology.* 2010;91(7):703-713.

13. Martínez DY, Jiménez-Gutiérrez A, Linke P, Gabriel KJ, Noureldin MMB, El-Halwagi MM. Water and Energy Issues in Gas-to-Liquid Processes: Assessment and Integration

of Different Gas-Reforming Alternatives. *ACS Sustainable Chemistry & Engineering.* 2014/02/03 2013;2(2):216-225.

14. Bourbonneux G. Conversion Processes. *Petroleum Refining.* Vol 3. Paris: Editions Technip; 2001:451-501.

15. Aasberg-Petersen K, Christensen TS, Dybkjaer I, et al. Chapter 4 - Synthesis gas production for FT synthesis. In: André S, Mark D, eds. *Studies in Surface Science and Catalysis.* Vol Volume 152: Elsevier; 2004:258-405.

16. Noureldin MMB, Elbashir NO, El-Halwagi MM. Optimization and Selection of Reforming Approaches for Syngas Generation from Natural/Shale Gas. *Industrial & Engineering Chemistry Research.* 2014/02/05 2013;53(5):1841-1855.

17. Kuipers EW, Scheper C, Wilson JH, Vinkenburg IH, Oosterbeek H. Non-ASF Product Distributions Due to Secondary Reactions during Fischer–Tropsch Synthesis. *Journal of Catalysis.* 1996;158(1):288-300.

18. Puskas I, Hurlbut RS. Comments about the causes of deviations from the Anderson–Schulz–Flory distribution of the Fischer–Tropsch reaction products. *Catalysis Today.* 2003;84(1–2):99-109.

19. Van Der Laan GP, Beenackers AACM. Kinetics and Selectivity of the Fischer–Tropsch Synthesis: A Literature Review. *Catalysis Reviews.* 1999/01/10 1999;41(3-4):255-318.

20. Botes FG. Proposal of a New Product Characterization Model for the Iron-Based Low-Temperature Fischer−Tropsch Synthesis. *Energy & Fuels.* 2007/05/01 2007;21(3):1379-1389.

21. Anderson RB. Hydrocarbon Synthesis, Hydrogenation and Cyclization. *Catalysis.* Vol IV. New York: Reinhold; 1956:29-255.

22. Anderson RB, Ralek M, Kolbel H. *The Fischer-Tropsch Synthesis*. Orlando, FL.: Academic Press; 1984.

23. Dry ME. Catalysis Science and Technology. In: Anderson JR, Boudart M, eds. Vol 1. Berlin: Springer-Verlag; 1981:159-255.

24. Dry ME. Chapter 7 - FT catalysts. In: André S, Mark D, eds. *Studies in Surface Science and Catalysis.* Vol Volume 152: Elsevier; 2004:533-600.

25. Perego C, Bortolo R, Zennaro R. Gas to liquids technologies for natural gas reserves valorization: The Eni experience. *Catalysis Today.* 2009;142(1–2):9-16.

26. Storch HH, Golumbic N, Anderson RB. *The Fischer-Tropsch and Related Syntheses*. New York: John Wiley & Sons, Inc.; 1951.

27. Van Steen E, Claeys M. Fischer-Tropsch Catalysts for the Biomass-to-Liquid (BTL)-Process. *Chemical Engineering & Technology.* 2008;31(5):655-666.

28. Gamba S, Pellegrini LA, Calemma V, Gambaro C. Liquid fuels from Fischer–Tropsch wax hydrocracking: Isomer distribution. *Catalysis Today.* 2010;156(1–2):58-64.

29. Leckel D. Selectivity Effect of Oxygenates in Hydrocracking of Fischer−Tropsch Waxes. *Energy & Fuels.* 2007/03/01 2007;21(2):662-667.

30. Leckel D. Noble Metal Wax Hydrocracking Catalysts Supported on High-Siliceous Alumina. *Industrial & Engineering Chemistry Research.* 2007/05/01 2007;46(11):3505-3512.

31. Leckel D, Liwanga-Ehumbu M. Diesel-Selective Hydrocracking of an Iron-Based Fischer−Tropsch Wax Fraction (C15−C45) Using a MoO3-Modified Noble Metal Catalyst. *Energy & Fuels.* 2006/11/01 2006;20(6):2330-2336.

32. Sánchez S, Rodríguez MA, Ancheyta J. Kinetic Model for Moderate Hydrocracking of Heavy Oils. *Industrial & Engineering Chemistry Research.* 2005/12/01 2005;44(25):9409-9413.

33. Smith R, Asaro M. Fuels of the future: technology intelligence for gas to liquids strategies. *SRI Consulting, Menlo Park.* 2005.

34. Aasberg-Petersen K, Stub Nielsen C, Perregaard J. *Large Scale Methanol Production from Natural Gas*: Haldor Topsoe.

35. Steynberg A, Dry M. *Fischer-Tropsch Technology*: Access Online via Elsevier; 2004.

36. Processors G. Suppliers Association (GPSA) Engineering Data book, Gas Processors and Suppliers Association. *Tulsa, OK, USA.* 2004.

37. MTR. Hydrogen Separation in Syngas Processes. 2013; http://www.mtrinc.com/hydrogen_separation_in_syngas_processes.html. Accessed Nov. 11th 2013.

38. Ockwig NW, Nenoff TM. Membranes for Hydrogen Separation. *Chemical Reviews.* 2007/10/01 2007;107(10):4078-4110.

39. Yang S-I, Choi D-Y, Jang S-C, Kim S-H, Choi D-K. Hydrogen separation by multi-bed pressure swing adsorption of synthesis gas. *Adsorption.* 2008/10/01 2008;14(4-5):583-590.

40. Stocker J, Whysall M, Miller G. *30 Years of PSA Technology for Hydrogen Purification.* UOP LLC1998.

41. Davis BH, Occelli ML. *Advances in Fischer-Tropsch synthesis, catalysts, and catalysis*: CRC Press; 2010.

42. Jager B, Espinoza R. Advances in low temperature Fischer-Tropsch synthesis. *Catalysis Today.* 1995;23(1):17-28.

43. Dry ME. High quality diesel via the Fischer–Tropsch process – a review. *Journal of Chemical Technology & Biotechnology.* 2002;77(1):43-50.

44. Saib AM, Borgna A, van de Loosdrecht J, van Berge PJ, Niemantsverdriet JW. XANES study of the susceptibility of nano-sized cobalt crystallites to oxidation during realistic Fischer–Tropsch synthesis. *Applied Catalysis A: General.* 2006;312(0):12-19.

45. Dancuart LP, de Haan R, de Klerk A. Chapter 6 - Processing of Primary Fischer-Tropsch Products. In: André S, Mark D, eds. *Studies in Surface Science and Catalysis.* Vol Volume 152: Elsevier; 2004:482-532.

46. Calemma V, Correra S, Perego C, Pollesel P, Pellegrini L. Hydroconversion of Fischer–Tropsch waxes: Assessment of the operating conditions effect by factorial design experiments. *Catalysis Today.* 2005;106(1–4):282-287.

47. Calemma V, Peratello S, Pavoni S, Clerici G, Perego C. Hydroconvesion of a mixture of long chain n-paraffins to middle distillate: effect of the operating parameters and products properties. In: E. Iglesia JJS, Fleisch TH, eds. *Studies in Surface Science and Catalysis.* Vol Volume 136: Elsevier; 2001:307-312.

48. Minnie R, Knottenbelt C, Clur J, Grond W, Karodia M, De Wet H. Fundamentals of Gas to Liquids. 2nd ed. London: Petroleum Economist; 2005.

49. Zander A, Elimelech M, Furukawa D, et al. Desalination: A national perspective. *National Research Council, The National Academies.* 2008.

50. El-Halwagi M, Harell D, Dennis Spriggs H. Targeting cogeneration and waste utilization through process integration. *Applied Energy.* 2009;86(6):880-887.

51. El-Halwagi M, Gabriel F, Harell D. Rigorous graphical targeting for resource conservation via material recycle/reuse networks. *Industrial & Engineering Chemistry Research.* 2003;42(19):4319-4328.

52. Gabriel FB, El-Halwagi MM. Simultaneous synthesis of waste interception and material reuse networks: problem reformulation for global optimization. *Environmental progress.* 2005;24(2):171-180.

53. Biegler LT, Grossmann IE, Westerberg AW. *Systematic methods for chemical process design*. New Jersey: Prentice Hall; 1997.

54. El-Halwagi MM. *Sustainable Design through Process Integration: Fundamentals and Applications to Industrial Pollution Prevention, Resource Conservation, and Profitability Enhancement*. Amsterdam: Butterworth-Heinemann/Elsevier; 2012.

55. Seider WD, Seader JD, Lewin DR. *Product and Process Design Principles: Synthesis, Analysis, and Evaluation*. 3rd ed: Wiley; 2009.

56. Smith R. *Chemical Process Design and Integration*. New York: Wiley 2005.

57. Towler GP, Sinnott RK. *Chemical Engineering Design: Principles, Practice, and Economics of Plant and Process Design*. Amsterdam: Elsevier; 2008.

58. Beysel G. Enhanced Cryogenic Air Separation: A proven Process applied to Oxyfuel. Paper presented at: 1st Oxyfuel Combustion Conference2009; Cottbus.

59. Ophir A, Lokiec F. Advanced MED process for most economical sea water desalination. *Desalination.* 2005;182(1):187-198.

60. Lenntech. Water Treatment Solutions. 2014; http://www.lenntech.com/applications/process/process.htm. Accessed Mar. 20th 2014.

61. Schiermeier Q. Water: purification with a pinch of salt. *Nature.* 2008;452(7185):260-261.

62. El-Dessouky H, Alatiqi I, Bingulac S, Ettouney H. Steady-state analysis of the multiple effect evaporation desalination process. *Chemical Engineering & Technology.* 1998;21(5):437.

63. El-Dessouky HT, Ettouney HM, Mandani F. Performance of parallel feed multiple effect evaporation system for seawater desalination. *Applied Thermal Engineering.* 2000;20(17):1679-1706.

64. Jernqvist A, Jernqvist M, Aly G. Simulation of thermal desalination processes. *Desalination.* 2001;134(1–3):187-193.

65. Sen PK, Sen PV, Mudgal A, Singh SN. A small scale multi-effect distillation (MED) unit for rural micro enterprises: Part II — Parametric studies and performance analysis. *Desalination.* 2011;279(1–3):27-37.

66. Zhao D, Xue J, Li S, Sun H, Zhang Q-d. Theoretical analyses of thermal and economical aspects of multi-effect distillation desalination dealing with high-salinity wastewater. *Desalination.* 2011;273(2–3):292-298.

67. Aly G. Computer simulations of multiple-effect FFE-VC systems for water desalination. *Desalination.* 1983;45(1–3):119-131.

68. El-Dessouky HT, Assassa GM. Computer simulation of the horizontal falling film desalination plant. *Desalination.* 1985;55:119-138.

69. Hanbury W. An analytical simulation of multiple effect distillation plant. Paper presented at: Proc IDA World Conf Desalination and Water Science, Abu Dhabi, UAE1995.

70. Wade NM. Technical and economic evaluation of distillation and reverse osmosis desalination processes. *Desalination.* 1993;93(1):343-363.

71. Darwish M, El-Dessouky H. The heat recovery thermal vapour-compression desalting system: A comparison with other thermal desalination processes. *Applied Thermal Engineering.* 1996;16(6):523-537.

72. Morin OJ. Design and operating comparison of MSF and MED systems. *Desalination.* 1993;93(1–3):69-109.

73. Hamed O, Zamamiri A, Aly S, Lior N. Thermal performance and exergy analysis of a thermal vapor compression desalination system. *Energy conversion and management.* 1996;37(4):379-387.

74. Lambert RN, Joye DD, Koko FW. Design calculations for multiple-effect evaporators. 1. Linear method. *Industrial & Engineering Chemistry Research.* 1987;26(1):100-104.

75. Al-Shayji K, Al-Wadyei S, Elkamel A. Modelling and optimization of a multistage flash desalination process. *Engineering optimization.* 2005;37(6):591-607.

76. Dahdah TH, Mitsos A. Structural optimization of seawater desalination: I. A flexible superstructure and novel MED–MSF configurations. *Desalination.* 2014;344:252-265.

77. Sayyaadi H, Saffari A, Mahmoodian A. Various approaches in optimization of multi effects distillation desalination systems using a hybrid meta-heuristic optimization tool. *Desalination.* 2010;254(1):138-148.

78. Sayyaadi H, Saffari A. Thermoeconomic optimization of multi effect distillation desalination systems. *Applied Energy.* 2010;87(4):1122-1133.

79. Khademi M, Rahimpour M, Jahanmiri A. Simulation and optimization of a six-effect evaporator in a desalination process. *Chemical Engineering and Processing: Process Intensification.* 2009;48(1):339-347.

80. Ettouney H. Design of single-effect mechanical vapor compression. *Desalination.* 2006;190(1):1-15.

81. El-Dessouky HT, Ettouney H. Multiple-effect evaporation desalination systems. thermal analysis. *Desalination.* 1999;125(1):259-276.

82. El-Dessouky HT, Ettouney HM, Al-Juwayhel F. Multiple Effect Evaporation—Vapour Compression Desalination Processes. *Chemical Engineering Research and Design.* 2000;78(4):662-676.

83. Shakib SE, Amidpour M, Aghanajafi C. A new approach for process optimization of a METVC desalination system. *Desalination and Water Treatment.* 2012;37(1-3):84-96.

84. El-Sayed YM. Designing desalination systems for higher productivity. *Desalination.* 2001;134(1–3):129-158.

85. Shakouri M, Ghadamian H, Sheikholeslami R. Optimal model for multi effect desalination system integrated with gas turbine. *Desalination.* 9/30/ 2010;260(1–3):254-263.

86. Sharaf MA, Nafey AS, García-Rodríguez L. Thermo-economic analysis of solar thermal power cycles assisted MED-VC (multi effect distillation-vapor compression) desalination processes. *Energy.* 5// 2011;36(5):2753-2764.

87. Al-Najem NM, Darwish M, Youssef F. Thermovapor compression desalters: energy and availability—analysis of single-and multi-effect systems. *Desalination.* 1997;110(3):223-238.

88. Darwish M, Al-Juwayhel F, Abdulraheim HK. Multi-effect boiling systems from an energy viewpoint. *Desalination.* 2006;194(1):22-39.

89. Aly NH, El-Figi AK. Thermal performance of seawater desalination systems. *Desalination.* 2003;158(1):127-142.

90. Ansari K, Sayyaadi H, Amidpour M. Thermoeconomic optimization of a hybrid pressurized water reactor (PWR) power plant coupled to a multi effect distillation desalination system with thermo-vapor compressor (MED-TVC). *Energy.* 2010;35(5):1981-1996.

91. Singh D, Bromley LA. Relative enthalpies of sea salt solutions at 0. deg. to 75. deg. *Journal of Chemical and Engineering Data.* 1973;18(2):174-181.

92. Millero F. The thermodynamics of seawater. II. Thermochemical properties. *Ocean science and engineering.* 1983;8.

93. Wagner W, Cooper J, Dittmann A, et al. The IAPWS industrial formulation 1997 for the thermodynamic properties of water and steam. *Journal of engineering for gas turbines and power.* 2000;122(1):150-184.

94. Cooper J, Dooley R. International Association for the Properties of Water and Steam, Release on the IAPWS formulation for the thermodynamic properties of seawater. 2008:19.

95. Sharqawy MH, Lienhard JH, Zubair SM. Thermophysical properties of seawater: A review of existing correlations and data. *Desalination and Water Treatment.* 2010;16(1-3):354-380.

96. Connors DN. On the enthalpy of seawater. *Limnology and Oceanography.* 1970;15(4):587-594.

97. Mandani F, Ettouney H, El-Dessouky H. LiBr□H2O absorption heat pump for single-effect evaporation desalination process. *Desalination.* 2000;128(2):161-176.

98. Miyatake O, Murakami K, Kawata Y, Fujii T. Fundamental experiments with flash evaporation. *Heat Transfer-Jpn. Res.* 1973;2(4):89-100.

99. Chen J. Comments on improvements on a replacement for the logarithmic mean. *Chemical Engineering Science.* 1987;42(10):2488-2489.

100. Alnouri SY, Linke P. Optimal SWRO desalination network synthesis using multiple water quality parameters. *Journal of Membrane Science.* 2013;444:493-512.

101. Seawater Desalination Costs. White Paper. Alexandria, VA, USA: Water Reuse Association; 2011.

102. Awerbuch L. Future Directions in Integration of Desalination. Paper presented at: Energy and the Environment. International Desalinaiton Association Seminar, Boston2009.

103. Khawaji AD, Kutubkhanah IK, Wie J-M. Advances in seawater desalination technologies. *Desalination.* 2008;221(1):47-69.

104. URS. *Bay Area Regional Desalination Project Feasibility Study* 2007.

105. Brinded M. Natural Gas: Changing the Middle East Energy Landscape2010.

106. Khoshgoftar Manesh M, Ghalami H, Amidpour M, Hamedi M. Optimal coupling of site utility steam network with MED-RO desalination through total site analysis and exergoeconomic optimization. *Desalination.* 2013;316:42-52.

107. Al-Azri N, Al-Thubaiti M, El-Halwagi M. An algorithmic approach to the optimization of process cogeneration. *Clean Technologies and Environmental Policy.* 2009;11(3):329-338.

108. Roberts DA, Johnston EL, Knott NA. Impacts of desalination plant discharges on the marine environment: A critical review of published studies. *Water Research.* 2010;44(18):5117-5128.

109. GCC natural gas prices in need of review. http://www.arabianoilandgas.com/article-12349-gcc-natural-gas-prices-in-need-of-review/. Accessed 5th August, 2014.

110. Wade NM. Distillation plant development and cost update. *Desalination.* 2001;136(1):3-12.

111. Tian J, Shi G, Zhao Z, Cao D. Economic analyses of a nuclear desalination system using deep pool reactors. *Desalination.* 1999;123(1):25-31.

112. Andrianne J, Alardin F. Thermal and membrane processe economics: Optimized selection for seawater desalination. *Desalination.* 2003;153(1):305-311.

113. Ettouney H. Visual basic computer package for thermal and membrane desalination processes. *Desalination.* 2004;165:393-408.

114. Karagiannis IC, Soldatos PG. Water desalination cost literature: review and assessment. *Desalination.* 2008;223(1):448-456.

115. El-Dessouky HT, Ettouney HM. *Fundamentals of salt water desalination*: Elsevier; 2002.

116. Amer AOB. Development and optimization of ME-TVC desalination system. *Desalination.* 2009;249(3):1315-1331.

117. Al-Sahali M, Ettouney H. Developments in thermal desalination processes: Design, energy, and costing aspects. *Desalination.* 2007;214(1):227-240.

118. *IDA Desalination Inventory Report, No. 17.* Topsfield, MA, USA: Internation Desalination Association.

119. Alawadhi A. Regional Report on Desalination-GCC Countries. Paper presented at: Proceedings of the IDA World Congress on Desalination and Water Reuse, Manama, Bahrain, March2002.

120. Bremere I, Kennedy M, Stikker A, Schippers J. How water scarcity will effect the growth in the desalination market in the coming 25 years. *Desalination.* 2001;138(1):7-15.

121. *IDA Desalting Inventory 2004: Desalination Business Stabilized on a High Level*: Internationl Desalination Water Reuse, 14 (2) (2004).

122. Siddiqi A, Anadon LD. The water–energy nexus in Middle East and North Africa. *Energy Policy.* 2011;39(8):4529-4540.

123. Lattemann S, Kennedy MD, Schippers JC, Amy G. Global desalination situation. *Sustainability Science and Engineering.* 2010;2:7-39.

124. Ericsson B, Hallmans B. A comparative study of the economics of RO and MSF in the Middle East. *Desalination.* 1985;55:441-459.

125. Wade NM. Energy and cost allocation in dual-purpose power and desalination plants. *Desalination.* 1999;123(2):115-125.

126. Starr JR. Water wars. *Foreign policy.* 1991:17-36.

127. Kamal I. Integration of seawater desalination with power generation. *Desalination.* 2005;180(1):217-229.

128. El-Nashar AM. Cogeneration for power and desalination—state of the art review. *Desalination.* 2001;134(1):7-28.

129. Ludwig H. Hybrid systems in seawater desalination—practical design aspects, present status and development perspectives. *Desalination.* 2004;164(1):1-18.

130. Kronenberg G, Lokiec F. Low-temperature distillation processes in single-and dual-purpose plants. *Desalination.* 2001;136(1):189-197.

131. Cardona E, Piacentino A, Marchese F. Performance evaluation of CHP hybrid seawater desalination plants. *Desalination.* 2007;205(1):1-14.

132. Aguillar O. Design and optimisation of flexible utility systems. *Centre for process integration. Manchester, University of Manchester.* 2005.

133. Gabriel K, Linke P, Jimenez-Gutierrez A, Martinez DY, Noureldin M, El-Halwagi MM. Targeting of the Water-Energy Nexus in Gas-to-Liquid Processes: A Comparison of Syngas Technologies. *Industrial & Engineering Chemistry Research.* 2014.

134. Manan ZA, Tea SY, Alwi SRW. A new technique for simultaneous water and energy minimisation in process plant. *Chemical Engineering Research and Design.* 11// 2009;87(11):1509-1519.

135. Dhole VR, Linnhoff B. Total site targets for fuel, co-generation, emissions, and cooling. *Computers & chemical engineering.* 1993;17:S101-S109.

136. Alnouri SY, Linke P, El-Halwagi M. Water integration in industrial zones: a spatial representation with direct recycle applications. *Clean Technologies and Environmental Policy.* 2014:1-23.

137. Yee TF, Grossmann IE. Simultaneous optimization models for heat integration—II. Heat exchanger network synthesis. *Computers & Chemical Engineering.* 10// 1990;14(10):1165-1184.

138. Sinnott RK. *Chemical engineering design: SI Edition*: Elsevier; 2009.

139. Mavromatis S, Kokossis A. Conceptual optimisation of utility networks for operational variations—I. Targets and level optimisation. *Chemical Engineering Science.* 1998;53(8):1585-1608.

140. Varbanov P, Doyle S, Smith R. Modelling and optimization of utility systems. *Chemical Engineering Research and Design.* 2004;82(5):561-578.

141. Bamufleh HS, Ponce-Ortega JM, El-Halwagi MM. Multi-objective optimization of process cogeneration systems with economic, environmental, and social tradeoffs. *Clean Technologies and Environmental Policy.* 2013;15(1):185-197.

142. El-Dessouky H, Ettouney H, Alatiqi I, Al-Nuwaibit G. Evaluation of steam jet ejectors. *Chemical Engineering and Processing: Process Intensification.* 2002;41(6):551-561.

143. Dow Water & Process Solutions, Midland MI, USA, FILMTEC Reverse Osmosis Membranes: Technical Manual Form No. 609-00071-1009.

144. Fritzmann C, Löwenberg J, Wintgens T, Melin T. State-of-the-art of reverse osmosis desalination. *Desalination.* 2007;216(1):1-76.

145. Wilf M, Awerbuch L. The guidebook to membrane desalination technology. *Balaban Desalination Publication, L'Aquila, Italy.* 2007.

146. Marcovecchio MG, Aguirre PA, Scenna NJ. Global optimal design of reverse osmosis networks for seawater desalination: modeling and algorithm. *Desalination.* 2005;184(1):259-271.

147. Saif Y, Elkamel A, Pritzker M. Global optimization of reverse osmosis network for wastewater treatment and minimization. *Industrial & Engineering Chemistry Research.* 2008;47(9):3060-3070.

148. Vince F, Marechal F, Aoustin E, Breant P. Multi-objective optimization of RO desalination plants. *Desalination.* 2008;222(1):96-118.

149. Zhu M, El-Halwagi MM, Al-Ahmad M. Optimal design and scheduling of flexible reverse osmosis networks. *Journal of membrane science.* 1997;129(2):161-174.

150. El-Halwagi MM. Synthesis of reverse-osmosis networks for waste reduction. *AIChE journal.* 1992;38(8):1185-1198.

151. Dow Water & Process Solutions FILMTEC™ Reverse Osmosis Membranes Technical Manual. http://www.dowwaterandprocess.com/en/resources/reverse-osmosis-technical-manual.

152. Alnouri SY, Linke P. A systematic approach to optimal membrane network synthesis for seawater desalination. *Journal of Membrane Science.* 2012;417:96-112.

153. *Environmental Protection Agency (1999), "Seawater Cooling Overboard Discharge: Nature of Discharge".* Reference Number: EPA-842-R-99-001.

154. Black J. *Capital Cost Scaling Methodology*: National Energy Technology Laboratory 2013.

155. Peters M, Timmerhaus KD. Plant Design and Economics for Chemical Engineers. 5th ed: New York: McGraw-Hill; 2003.

156. *Kumana & Associates (2003), How to calculate the true cost of steam.* Rep. No. DOE/GO-102003-1736. US Department of Energy, Washington, DC.

157. IDE. Sorek Project: The World's Largest and Most Advanced SWRO Desalination Plant. http://www.ide-tech.com/case-study/sorek-israel-project/. Accessed 5th August, 2014.

APPENDIX A

DATA FOR THE TARGETING OF THE WATER-ENERGY NEXUS IN GTL PROCESSES

Table A.1 Simulation parameters for each syngas configuration

Simulation Parameter		ATR	POx	SMR
Operating pressure	[psia]	435	435	300
Operating temperature	[^{o}F]	1949	2372	1600
Steam to Carbon ratio		0.41[a]	0.1[a]	2.5
Saturator water to gas	[mol/mol]	0.1	0.1	0.1
Saturator water temperature	[^{o}F]	230	230	230

[a] Represents the final steam to carbon ratio to adjust syngas ratio to required 2.15

Table A.2 Simulation parameters for cooling utilities

Simulation Parameter		Value
Air cooler power [a]	[kW/ MMBtu/hr]	1.00
Cooling Tower power [a]	[kW/ MMBtu/hr]	1.32

[a] Represents power requirement for cooling 1 MMBtu/hr

Table A.3 Stoichiometric coefficients for hydrocracking of C_{20} and C_{21} paraffin

Hydrocarbon	$C_{20}H_{42}$	$C_{21}H_{44}$
C_7H_{16}	0.0026366	0.0026366
C_8H_{18}	0.0428032	0.0428032
C_9H_{20}	0.2718275	0.2718275
$C_{10}H_{22}$	1.3654655	0.6827327
$C_{11}H_{24}$	0.2718275	0.6827327
$C_{12}H_{26}$	0.0428032	0.2718275
$C_{13}H_{28}$	0.0026366	0.0428032
$C_{14}H_{30}$		0.0026366

Table A.3 coefficients are repeated for similar even or odd carbon number hydrocarbons

Table A.4 Stoichiometric coefficients for FT reaction with alpha value (α) = 0.92

Carbon #	ψ_{Cn}	ψ_{H2}
1	0.0059	0.0178
2	0.0055	0.0273
3	0.0050	0.0353
4	0.0047	0.0419
5	0.0043	0.0473
6	0.0040	0.0516
7	0.0037	0.0550
8	0.0034	0.0575
9	0.0031	0.0593
10	0.0029	0.0605
11	0.0027	0.0612
12	0.0025	0.0614
13	0.0023	0.0612
14	0.0021	0.0607
15	0.0019	0.0599
16	0.0018	0.0588
17	0.0016	0.0576
18	0.0015	0.0562
19	0.0014	0.0547
20	0.0013	0.0530
21	0.0012	0.0513
22	0.0011	0.0496
23	0.0010	0.0478
24	0.0009	0.0460
25	0.0009	0.0442
26	0.0008	0.0424
27	0.0007	0.0406
28	0.0007	0.0389
29	0.0006	0.0371
30	0.0106	0.6439

Equation A.1 represents the overall conversion of one (1) mole of CO to GTL product.

$$CO + (\sum \psi_{H2})H_2 \xrightarrow{yields} \psi_{Cn} C_n H_{2n+2} + H_2O \quad \text{(A.1)}$$

The following linear programming (LP) mathematical model is used in LINGO® to determine the minimum MED water requirement and consequent maximum excess water from the GTL process, for each reforming technology.

Total flow from MED water source to each sink (*j*):

$$F_{MED} = \sum_{j=1}^{N_{sinks}} f_{MED,j} + f_{MED,excess} \quad \text{(A.2)}$$

Total flow from pretreated water source to each sink (*j*) including waste:

$$W_{pre} = \sum_{j=1}^{N_{sinks}} w_{pre,j} + w_{pre,waste} \quad \text{(A.3)}$$

Overall water balance for each sink (*j*):

$$G_j = w_{pre,j} + f_{MED,j} \quad \text{(A.4)}$$

Overall component (*k*) balance for each sink (*j*):

$$G_j z_{j,k}^{in} = w_{pre,j} y_{pre,k} + f_{MED,j} x_{MED,k} \quad \text{(A.5)}$$

Constraints on sink contaminant composition:

$$z_{j,k}^{min} \leq z_{j,k}^{in} \leq z_{j,k}^{max} \quad \text{(A.6)}$$

Where:
j = [gas saturator unit, reforming reactor, CO_2 removal unit, cooling tower]
k = [oil, TDS]

LINGO® Model for ATR based GTL process:

```
[_1]   MAX = F_MED_EXCESS;
[_2]   12860 – F_MED_1 – F_MED_2 – F_MED_3 – F_MED_4 – F_MED_EXCESS = 0;
[_3]   705 – W_PRE_1 – W_PRE_2 – W_PRE_3 – W_PRE_4 – W_PRE_WASTE = 0;
[_4]   51 – W_PRE_1 – F_MED_1 = 0;
[_5]   228 – W_PRE_2 – F_MED_2 = 0;
[_6]   4 – W_PRE_3 – F_MED_3 = 0;
[_7]   514 – W_PRE_4 – F_MED_4 = 0;
[_8]    51*Z_IN_1_1 – W_PRE_1*0.1 – F_MED_1*0.001 = 0;
[_9]   228* Z_IN_2_1 – W_PRE_2*0.1 – F_MED_2*0.001 = 0;
[_10]    4* Z_IN_3_1 – W_PRE_3*0.1 – F_MED_3*0.001 = 0;
[_11]  514* Z_IN_4_1 – W_PRE_4*0.1 – F_MED_4*0.001 = 0;
[_12]   51*Z_IN_1_2 – W_PRE_1*0.06 – F_MED_1*10 = 0;
[_13]  228* Z_IN_2_2 – W_PRE_2*0.06 – F_MED_2*10 = 0;
[_14]    4* Z_IN_3_2 – W_PRE_3*0.06 – F_MED_3*10 = 0;
```

[_15] 514* Z_IN_4_2 – W_PRE_4*0.06 – F_MED_4*10 = 0;
[_16] Z_IN_1_1 <= 1.0;
[_17] Z_IN_2_1 <= 1.0;
[_18] Z_IN_3_1 <= 1.0;
[_19] Z_IN_4_1 <= 1.0;
[_20] Z_IN_1_2 <= 2.0;
[_21] Z_IN_2_2 <= 2.0;
[_22] Z_IN_3_2 <= 500;
[_23] Z_IN_4_2 <= 500;

This LINGO model was appropriately altered and used to determine the maximum excess water for all three GTL process configurations.

APPENDIX B

OPTIMIZATION MODEL FOR MULTI-EFFECT DISITLLATION PROCESS

```
DATA:
P_MOT          = 35;     ! Pressure of motive steam [psia] 14.5038 PSIA = 100 bar;

N_EFF          = 11;     ! Number effect;
N_C            = 8;      ! Number of chemicals;

CAP_ADJ        = 100;    ! Capital cost adjustment for equipment [%];

T_EFF_FIRST    = 158;    ! Temperature of first effect [F];
T_EFF_LAST     = 104;    ! Temperature of last effect [F];

F_PERM_MED  = 289.35185;! Total flow of fresh desalinated water [L/s] equivalent to 20,000 cum/day;
T_SEA          = 77;     !Temperature of inlet seawater [F];
T_SEA_MAX      = 86;     ! Max. temp. of seawater outlet [F];
X_BRINE_MAX = 71.8;  ! Maximum salt concentration return [g/kg];
X_EFF_MIN      = 60;     ! Minimum potential salt concentration in each effect [g/kg];

MED_LINE_DP  = 30;     ! Pressure drop of seawater in MED process. Assumes dP across exchangers,
                          solids filters, line losses etc [psi];
MED_STORE_P = 30;     ! Storage tank pressure including 10 m head in tank [psia];
P_ATM          = 14.6959;! Atmospheric pressure [psia];
PUMP_EFF       = 80;     ! Pump efficiency [%];
BOIL_EFF       = 75;     ! Nat. gas boiler efficiency [%];

DP_LOSSES      = 0.071117;! Constant pressure drop across demister, vapor transfer line and condenser
                            tubes @10 cmH2O [psia];
DTMIN          = 9;      ! Minimum delta T for HEX [F];
DT_SUPER       = 18;     ! Superheated temperature of steam to the MED unit [F];

PLANT_LIFE     = 20;     ! Plant life [yrs];
COST_WATER  = 1.21;   ! Cost of desalinated water for industrial purposes [$/cum];
PW_COST        = 0.05;   ! Power cost [$/kWh];

GAS_COST       = 2.0;    ! Nat. gas cost [$/MMBtu];

BOIL_MAIN      = 30;     ! Boiler maintenance factor based on natural gas usage [%];

CO_HEX_1       = 718.5;
CO_EVAP_1      = 492.28;
CO_EJECTOR_1= 2470;
CO_POT_1       = 41233;

BOIL_EXP       = 0.77;
POT_EXP        = 0.3;
EVAP_EXP       = 0.7;
HEX_EXP        = 0.7;
EJ_EXP         = 0.3;
```

```
CF_FIN          = 0.04;   ! Fraction of Direct Capital Cost used for financing;
CF_PERM         = 0.1;    ! Fraction of Direct Capital Cost used for permitting;
CF_CONTIN       = 0.05;   ! Fraction of Direct Capital Cost used for contingency costs;
CF_FOC          = 0.01;   !Fraction of Direct Capital Cost used for Fixed operating costs/ spare parts;
ENDDATA

!**** ********************* SETS INTILIALIZATION SECTION ************************;

SETS:
EFFECTS/1..N_EFF/;
COMP/1..N_C/;

COMP_STREAM(COMP) : X_FEED;
ENTHALPY(EFFECTS)   : HV, HV_I, HV_II, HF, HF_I, HF_II, HS, HS_I, HS_II, HC;
FLOW(EFFECTS)       : M_BRINE_STM, M_SEA_STM, M_BRINE_WATER, M_SEA_WATER,
                      M_WATER, M_BRINE_SALT, M_SEA_SALT, M_SALT, M_DS, M_BFW,
                      M_DIST, MV_POT, MF_POT;
TEMP(EFFECTS)       : T_V, T_EFF, DT_LOSSES, T_EFF_CEL, T_EFF_I, T_EFF_II, T_C,
                      T_BFW, BPE_AVG, NEA_BRINE, NEA_DIST;
PRESS(EFFECTS)      : P_EFF;
CONC(EFFECTS)       : X_EFF_MAX, X_EFF_MINMAX, X_EFF_AVG;
HEX(EFFECTS)        : Q_EFF, Q_EFF_VAP, Q_EFF_SENS, A_EFF_VAP, DT_EFF_VAP,
                      U_EFF, DT_EFF_SENS, DT1_EFF_SENS;
ENDSETS

!************************ PARAMTER CALCULATION SECTION ************************;

DATA:
X_FEED          = @ole('H:\Desalination paper\LINGO and EXCEL
Files\MED_OPT.XLSM','MED_X_FEED');
X_BRINE_AVG = @ole('H:\Desalination paper\LINGO and EXCEL
Files\MED_OPT.XLSM','MED_X_BRINE_AVG');
ENDDATA

CALC:

TSAT_MOT = 117.664*P_MOT^0.2219;

DT_EFF          = (T_EFF_FIRST - T_EFF_LAST)/(N_EFF-1);!Temperature difference of effects [F];
T_EFF(1)        = T_EFF_FIRST;
T_EFF(N_EFF)= T_EFF_LAST;
TSAT_TVC        = T_EFF(1) + DT_EFF;
P_TVC           = (TSAT_TVC/102.799)^(1/0.2741);          !Equation for P_sat at vacuum conditions;
TC_TVC          = 102.799*(P_TVC - DP_LOSSES)^0.2741;
T_EX            = T_SEA + DTMIN;

@FOR(EFFECTS(I)|I#GE#2 #AND# I#LE#N_EFF: T_EFF(I) = T_EFF(I-1) - DT_EFF);

!Boiling point elevation calc;
@FOR(EFFECTS(I): T_EFF_CEL(I) = (T_EFF(I) - 32)/1.8);
@FOR(EFFECTS(I): X_EFF_MAX(I)       = 0.9*(457628.5 - 11304.11*T_EFF_CEL(I) +
107.5781*T_EFF_CEL(I)^2 - 0.360747*T_EFF_CEL(I)^3)*1E-3); !Effect max Xbrine [g/kg];
@FOR(EFFECTS(I): X_EFF_MINMAX(I) = @SMIN(X_EFF_MAX(I), X_BRINE_AVG));
```

```
@FOR(EFFECTS(I): X_EFF_AVG(I) = 0.5*(X_EFF_MIN + X_EFF_MINMAX(I)));
@FOR(EFFECTS(I): BPE_AVG(I)             = (-4.584E-4*T_EFF_CEL(I)^2 + 2.823E-1*T_EFF_CEL(I)
+ 17.95)*(X_EFF_MINMAX(I)/1000)^2 + (1.536E-4*T_EFF_CEL(I)^2 + 5.267E-2*T_EFF_CEL(I) +
6.56)*X_EFF_MINMAX(I)/1000);             !Max. BPE in [K];

!Enthalpy calc for vaporized seawater;
@FOR(EFFECTS(I): T_V(I)   = T_EFF(I) - 1.8*BPE_AVG(I));!Effect vapor temp. [F];
@FOR(EFFECTS(I): P_EFF(I) = (T_V(I)/102.799)^(1/0.2741));!Effect pressure as function of Tv [psia];
@FOR(EFFECTS(I): DT_LOSSES(I) = T_V(I) - 102.799*(P_EFF(I) - DP_LOSSES)^0.2741);
!DT_LOSSES across each effect [F];

@FOR(EFFECTS(I): T_C(I) = T_V(I) - DT_LOSSES(I));      !Condensing temp. of effect vapor [F];
@FOR(EFFECTS(I): HV(I)  = -2.044854E-04*T_V(I)^2 + 0.4720204*T_V(I) + 1.059540E3);!Enthalpy
of effect vapor [Btu/lb];

@FOR(EFFECTS(I): HC(I)  = 4.243328E-5*T_C(I)^2 + 0.9877278*T_C(I) - 31.14636); !Enthalpy of
condensed steam [Btu/lb];

@FOR(EFFECTS(I): HF(I)  = 4.243328E-5*T_EFF(I)^2 + 0.9877278*T_EFF(I) - 31.14636);!Enthalpy
of effect water from sea [Btu/lb];

@FOR(EFFECTS(I): HS(I)  = -9.00786E-5*T_EFF_CEL(I)^3 + 0.0148023*T_EFF_CEL(I)^2 -
0.8640971*T_EFF_CEL(I) - 7.8738015); !Enthalpy of effect salt from sea [Btu/lb];

!Enthalpy calc for flashing brine;
@FOR(EFFECTS(I): NEA_BRINE(I) = 1.8*33*((DT_EFF/1.8)^0.55)/((T_V(I)-32)/1.8));!Non-
equilibrium allowance [F];
@FOR(EFFECTS(I): T_EFF_I(I)   = T_EFF(I) + NEA_BRINE(I));
@FOR(EFFECTS(I): HV_I(I)      = -2.044854E-04*T_EFF_I(I)^2 + 0.4720204*T_EFF_I(I) +
1.059540E3);
@FOR(EFFECTS(I): HF_I(I)      = 4.243328E-5*T_EFF_I(I)^2 + 0.9877278*T_EFF_I(I) - 31.14636);
@FOR(EFFECTS(I): HS_I(I)      = -9.00786E-5*((T_EFF_I(I)-32)/1.8)^3 + 0.0148023*((T_EFF_I(I)-
32)/1.8)^2 - 0.8640971*((T_EFF_I(I)-32)/1.8) - 7.8738015);

!Enthalpy calc for flashing distillate;
NEA_DIST(1) = 1.8*0.33*((TC_TVC - T_V(1))/1.8)/((T_V(1) - 32)/1.8);
@FOR(EFFECTS(I)|I#GE#2: NEA_DIST(I)  = 1.8*0.33*((T_C(I-1) - T_V(I))/1.8)/((T_V(I) - 32)/1.8));
!Non-equilibrium allowance [F];

@FOR(EFFECTS(I): T_EFF_II(I)  = T_V(I) + NEA_DIST(I));
@FOR(EFFECTS(I): HV_II(I)     = -2.044854E-04*T_EFF_II(I)^2 + 0.4720204*T_EFF_II(I) +
1.059540E3);
@FOR(EFFECTS(I): HF_II(I)     = 4.243328E-5*T_EFF_II(I)^2 + 0.9877278*T_EFF_II(I) -
31.14636);
@FOR(EFFECTS(I): HS_II(I)     = -9.00786E-5*((T_EFF_II(I)-32)/1.8)^3 + 0.0148023*((T_EFF_II(I)-
32)/1.8)^2 - 0.8640971*((T_EFF_II(I)-32)/1.8) - 7.8738015);


!Enthalpy calculations for motive steam and TVC exit steam / condensate;
SV_MOT  = -4.144273E-9*TSAT_MOT^3 + 5.639936E-6*TSAT_MOT^2 - 3.47771E-3*TSAT_MOT +
2.281821;
K_S_MOT = 1.3845E-2*(TSAT_MOT/1000)^2 -9.8258E-3*(TSAT_MOT/1000) + 3.1462E-3;
S_MOT   = SV_MOT + 0.46883*(1 - @EXP(-K_S_MOT*DT_SUPER));
```

```
HV_MOT = (0.2029*TSAT_MOT)*S_MOT^3.647 + 817.35;
HV_TVC = -2.044854E-04*TSAT_TVC^2 + 0.4720204*TSAT_TVC + 1.059540E3;
HF_TVC = 4.243328E-5*TSAT_TVC^2 + 0.9877278*TSAT_TVC - 31.14636;
HC_TVC = 4.243328E-5*TC_TVC^2 + 0.9877278*TC_TVC - 31.14636;


!Enthalpy calculation for inlet seawater components (water and salt);
HF_SEA = 4.708284E-5*T_SEA^2 + 9.888650E-1*T_SEA - 31.44198;
HS_SEA = -9.00786E-5*((T_SEA - 32)/1.8)^3 + 0.0148023*((T_SEA - 32)/1.8)^2 - 0.8640971*((T_SEA
- 32)/1.8) - 7.8738015;


!Enthalpy calculation for outlet distillate / brine components (water and salt);
HF_EX  = 4.708284E-5*T_EX^2 + 9.888650E-1*T_EX - 31.44198;
HS_EX  = -9.00786E-5*((T_EX - 32)/1.8)^3 + 0.0148023*((T_EX - 32)/1.8)^2 - 0.8640971*((T_EX -
32)/1.8) - 7.8738015;



!Calculation for entrainment ratio;
C_R  = P_TVC/P_EFF(N_EFF);                    !Compression ratio;
EX_R = P_MOT/P_EFF(N_EFF);

P_E = P_EFF(N_EFF)*6.89476;
P_C = P_TVC*6.89476;
P_P = P_MOT*6.89476;

ENT_K1 = (0.65*(P_E^3.26)*(P_C^6.79E-2)/(9.32 + 0.128*(P_C^1.14)))*22.82;
ENT_K2 = (0.65*(P_E^3.26)*(P_C^6.79E-2)/(9.32 + 0.128*(P_C^1.14)))*4.21E-4;

ENT_R = ENT_K1*(P_P^-1.54) + ENT_K2*(P_P^-0.2);

!Calculation for average Cp of seawater feed;
X_SALT = 0.99886*@SUM(COMP(K): X_FEED(K)); !Seawater conc.   (0.99886*ppm/1000) [g/L];
X_SAL  = @SUM(COMP(K): X_FEED(K));          !Seawater salinity (ppm/1000)  [g/kg];

T_SEA_CEL = (T_SEA - 32)/1.8;
TEFF_CEL = (T_EFF(N_EFF) - 32)/1.8;
DENS_WATER     = 1E-3*(1E3 + 2.7099E-2*T_SEA_CEL - 6.6452E-3*T_SEA_CEL^2 + 2.97035E-
5*T_SEA_CEL^3 - 7.62746E-8*T_SEA_CEL^4);     !Water density [kg/L];
DENS_WATER_EFF = 1E-3*(1E3 + 2.7099E-2*TEFF_CEL - 6.6452E-3*TEFF_CEL^2 + 2.97035E-
5*TEFF_CEL^3 - 7.62746E-8*TEFF_CEL^4);         !Water density [kg/L];


!Calculation of seawater Cp [Btu/lb-F];
CP_A = (5.328 - 9.76E-2*X_SAL + 4.04E-4*X_SAL^2)*0.238846; CP_B = (-6.913E-3 + 7.351E-
4*X_SAL - 3.15E-6*X_SAL^2)*0.238846;
CP_C = (9.6E-6 - 1.927E-6*X_SAL + 8.23E-9*X_SAL^2)*0.238846;
CP_D = (2.5E-9 + 1.666E-9*X_SAL - 7.125E-12*X_SAL^2)*0.238846;

CP_T_SEA_MIN  = ((T_SEA - 32)/1.8) + 273.15;
CP_T_SEA_MAX  = ((T_EFF(N_EFF) - DTMIN - 32)/1.8) + 273.15;
```

```
CP_SEA_MIN = CP_A + CP_B*CP_T_SEA_MIN + CP_C*CP_T_SEA_MIN^2 +
CP_D*CP_T_SEA_MIN^3;
CP_SEA_MAX = CP_A + CP_B*CP_T_SEA_MAX + CP_C*CP_T_SEA_MAX^2 +
CP_D*CP_T_SEA_MAX^3;

CP_SEA_AVG = 0.5*(CP_SEA_MIN + CP_SEA_MAX);

!Heat transfer coefficient of evaporator and condenser;
@FOR(EFFECTS(I): U_EFF(I) = 176.11*(1.9394 + 1.40562E-3*((T_EFF(I) - 32)/1.8) - 2.0752E-
4*((T_EFF(I) - 32)/1.8)^2 + 2.3186E-6*((T_EFF(I) - 32)/1.8)^3));
U_COND = 176.11*(1.6175 + 0.1537E-3*((T_C(N_EFF) - 32)/1.8) + 0.1825E-3*((T_C(N_EFF) -
32)/1.8)^2 - 8.026E-8*((T_C(N_EFF) - 32)/1.8)^3);
U_BRINE = 176.11*(1.262650391 + 1.0945838E-2*((0.5*(T_EFF(N_EFF) + T_EFF_I(N_EFF)) -
32)/1.8) + 1.1928024E-2*((T_SEA - 32)/1.8));
U_DIST  = 176.11*(1.418251642 + 1.1383865E-2*((0.5*(T_C(N_EFF) + T_EFF_II(N_EFF - 1)) -
32)/1.8) + 1.3381501E-2*((T_SEA - 32)/1.8));

DT_EFF_VAP(1) = TC_TVC - T_EFF(1);
@FOR(EFFECTS(I)|I#GE#2: DT_EFF_VAP(I) = T_C(I-1) - T_EFF(I));


NP_BOIL   = 7E-4*(P_MOT - 14.6959) + 0.6;
NT_BOIL_1 = 1.5E-6*DT_SUPER^2 + 1.13E-3*DT_SUPER + 1;


CO_HEX        = (CAP_ADJ/100)*CO_HEX_1;
CO_EVAP       = (CAP_ADJ/100)*CO_EVAP_1;
CO_EJECTOR    = (CAP_ADJ/100)*CO_EJECTOR_1;
CO_POT        = (CAP_ADJ/100)*CO_POT_1;
NT_BOIL       = (CAP_ADJ/100)*NT_BOIL_1;

ENDCALC


!**************************** OBJECTIVE FUNCTION *********************************;

! Objective function;

MIN = TAC_DESAL + (1 + CF_FIN + CF_PERM + CF_CONTIN +
CF_FOC*PLANT_LIFE)*(CC_COND + CC_BRINE + CC_DIST + CC_EVAP + CC_EJECT +
CC_DES + CC_POTS + CC_BOIL);

CC_COND  >= (1E-
3*CO_EVAP/PLANT_LIFE)*(Q_COND/((U_COND/3600)*(0.5*DT_COND_PRE*DT1_COND_PRE*
(DT_COND_PRE + DT1_COND_PRE))^(1/3)))^EVAP_EXP;
CC_BRINE >= (1E-
3*CO_HEX/PLANT_LIFE)*(Q_BRINE/((U_BRINE/3600)*(0.5*DT_BRINE_PRE*DT1_BRINE_PRE*
(DT_BRINE_PRE + DT1_BRINE_PRE))^(1/3)))^HEX_EXP;
CC_DIST  >= (1E-
3*CO_HEX/PLANT_LIFE)*(Q_DIST/((U_DIST/3600)*(0.5*DT_DIST_PRE*DT1_DIST_PRE*(DT_DI
ST_PRE + DT1_DIST_PRE))^(1/3)))^HEX_EXP;
```

```
CC_EVAP  >= @SUM(EFFECTS(I):(1E-3*CO_EVAP/PLANT_LIFE)*(A_EFF_VAP(I) +
Q_EFF_SENS(I)/((U_EFF(I)/3600)*(0.5*DT_EFF_SENS(I)*DT1_EFF_SENS(I)*(DT_EFF_SENS(I) +
DT1_EFF_SENS(I)))^(1/3)))^EVAP_EXP);

CC_EJECT >= (1E-3*CO_EJECTOR/PLANT_LIFE)*(3600*M_STM_DIS)^EJ_EXP;
CC_DES   >= (1E-3*CO_POT/PLANT_LIFE)*(60*M_COND_TVC/62.43)^POT_EXP;
CC_POTS  >= @SUM(EFFECTS(I): (1E-
3*CO_POT/PLANT_LIFE)*(60*M_DIST(I)/62.43)^POT_EXP);
CC_BOIL  >=  1E-
3*(3*NP_BOIL*NT_BOIL)/PLANT_LIFE*(3600*(BOIL_EFF/100)*Q_MED_BOIL)^BOIL_EXP;



! THESE CONSTRAINTS ARE FOR THE BASE CASE CONVENTION FOR MED_TVC;
M_COND_TVC = 0;

! Boiler feed water only comes from first effect condensate;
@FOR(EFFECTS(I)|I#GE#2 #AND# I#LE#(N_EFF - 1): M_BFW(I) = 0)

@FOR(EFFECTS(I)|I#LE#(N_EFF-2): M_DS(I) = 0);

!Max. conc. constraint in effect;
M_SALT(1)*(1000 - X_EFF_MAX(1)) <= X_EFF_MAX(1)*M_WATER(1);

@FOR(EFFECTS(I)|I#GE#2: M_SALT(I)*(1000 - X_EFF_MAX(I))  <=
X_EFF_MAX(I)*M_WATER(I));                                    !Max. conc. constraint in effect;


!***************************** MED OVERALL MODEL ******************************;
!Required product flow;
M_DESAL = 2.20462*DENS_WATER*F_PERM_MED;

!Seawater feed balance;
SEA_WATER*N_EFF = 2.20462*DENS_WATER*F_FEED_MED; !Flow rate of water in seawater to
each effect assuming water density (1kg/L) [lb/s];
SEA_SALT*(1000 - X_SAL) = X_SAL*SEA_WATER;!Flow rate of salt in seawater to each effect [lb/s];


!TVC balance;
M_STM_MOT + M_STM_SUC = M_STM_DIS;
M_STM_SUC = ENT_R*M_STM_MOT;


!Desuperheater balance;
M_STM_MOT*HV_MOT + M_STM_SUC*HV(N_EFF) + @SUM(EFFECTS(I): M_DS(I)*HF_II(I)) =
M_STM_TVC*HV_TVC + M_COND_TVC*HF_TVC;
M_STM_MOT + M_STM_SUC + @SUM(EFFECTS(I): M_DS(I)) = M_STM_TVC + M_COND_TVC;


!Effect one balance;
Q_EFF(1) = M_STM_TVC*(HV_TVC - HC_TVC);              !Latent energy into first effect [Btu/s];
Q_EFF(1) = Q_EFF_VAP(1) + Q_EFF_SENS(1);
```

```
Q_EFF(1) + SEA_WATER*HF_SEA + SEA_SALT*HS_SEA + Q_SEA_PRE/N_EFF =
M_SEA_STM(1)*HV(1) + M_SEA_WATER(1)*HF(1) + M_SEA_SALT(1)*HS(1);
Q_EFF_VAP(1) = M_SEA_STM(1)*(HV(1) - HF(1));
Q_EFF_SENS(1)= SEA_WATER*HF(1) + SEA_SALT*HS(1) - (SEA_WATER*HF_SEA +
SEA_SALT*HS_SEA + Q_SEA_PRE/N_EFF);

!Mass balance on first effect;
SEA_WATER + SEA_SALT = M_SEA_STM(1) + M_SEA_WATER(1)+ M_SEA_SALT(1);

SEA_WATER = M_SEA_STM(1) + M_SEA_WATER(1);     !Water balance;
SEA_SALT  = M_SEA_SALT(1);                     !Salt balance;

M_SEA_SALT(1) = M_SALT(1);
M_SEA_WATER(1)= M_WATER(1);


M_BRINE_STM(1)     = 0;          !No brine entering first effect therefore no flashing occurs;
M_BRINE_WATER(1)   = 0;
M_BRINE_SALT(1)    = 0;


!Effect 2 - N balance;
!Latent energy into effect[Btu/hr];
@FOR(EFFECTS(I)|I#GE#2: Q_EFF(I) = M_SEA_STM(I-1)*HV(I-1) + M_BRINE_STM(I-1)*HV_I(I-
1) + MV_POT(I-1)*HV_II(I-1)-(M_SEA_STM(I-1) + M_BRINE_STM(I-1) + MV_POT(I-1))*HC(I-1));
@FOR(EFFECTS(I)|I#GE#2: Q_EFF(I) = Q_EFF_VAP(I) + Q_EFF_SENS(I));

!Vaporization of seawater balance;
@FOR(EFFECTS(I)|I#GE#2: Q_EFF(I) + SEA_WATER*HF_SEA + SEA_SALT*HS_SEA +
Q_SEA_PRE/N_EFF = M_SEA_STM(I)*HV(I) + M_SEA_WATER(I)*HF(I) +
M_SEA_SALT(I)*HS(I));
@FOR(EFFECTS(I)|I#GE#2: Q_EFF_VAP(I) = M_SEA_STM(I)*(HV(I) - HF(I)));
@FOR(EFFECTS(I)|I#GE#2: Q_EFF_SENS(I)= SEA_WATER*HF(I) + SEA_SALT*HS(I) -
(SEA_WATER*HF_SEA + SEA_SALT*HS_SEA + Q_SEA_PRE/N_EFF));

@FOR(EFFECTS(I)|I#GE#2: SEA_WATER + SEA_SALT = M_SEA_STM(I) + M_SEA_WATER(I)+
M_SEA_SALT(I));                    !Mass balance on effect HEX;
@FOR(EFFECTS(I)|I#GE#2: SEA_WATER = M_SEA_STM(I) + M_SEA_WATER(I));
                                   !Water balance on effect HEX;
@FOR(EFFECTS(I)|I#GE#2: SEA_SALT = M_SEA_SALT(I));  !Salt balance on effect HEX;

!Brine flashing in effect balance;
@FOR(EFFECTS(I)|I#GE#2: M_BRINE_WATER(I-1)*HF_I(I-1) + M_BRINE_SALT(I-1)*HS_I(I-1) +
M_SEA_WATER(I-1)*HF(I-1) + M_SEA_SALT(I-1)*HS(I-1) =
                                   M_BRINE_WATER(I)*HF_I(I) + M_BRINE_SALT(I)*HS_I(I) +
M_BRINE_STM(I)*HV_I(I));

@FOR(EFFECTS(I)|I#GE#2: M_BRINE_WATER(I-1) + M_BRINE_SALT(I-1) + M_SEA_WATER(I-
1) + M_SEA_SALT(I-1) = M_BRINE_WATER(I) + M_BRINE_SALT(I) + M_BRINE_STM(I));
@FOR(EFFECTS(I)|I#GE#2: M_BRINE_WATER(I-1) + M_SEA_WATER(I-1) =
M_BRINE_WATER(I) + M_BRINE_STM(I)); !Water balance on brine flashing;
@FOR(EFFECTS(I)|I#GE#2: M_BRINE_SALT(I-1)  + M_SEA_SALT(I-1)  = M_BRINE_SALT(I));
                                   !Salt balance on brine flashing;
```

```
@FOR(EFFECTS(I)|I#GE#2: M_BRINE_WATER(I) + M_SEA_WATER(I) = M_WATER(I));
@FOR(EFFECTS(I)|I#GE#2: M_BRINE_SALT(I)  + M_SEA_SALT(I)  = M_SALT(I));


!Effect N steam balance;
M_SEA_STM(N_EFF) = M_STM_SUC + M_STM_COND;
M_SALT(N_EFF)*(1000 - X_BRINE_MAX)   <= X_BRINE_MAX*M_WATER(N_EFF);


!Condenser balance;
Q_COND = M_STM_COND*(HV(N_EFF) - HC(N_EFF)) + M_BRINE_STM(N_EFF)*(HV_I(N_EFF)
- HC(N_EFF));


!Condensate for desuperheater balance;
M_STM_MOT + M_STM_SUC + @SUM(EFFECTS(I):M_DS(I)) = M_DIST(1);
M_STM_TVC + M_COND_TVC = M_DIST(1);

@FOR(EFFECTS(I)|I#GE#2: M_SEA_STM(I-1) + M_BRINE_STM(I-1) + MV_POT(I-1) + MF_POT(I-
1) = M_DIST(I));


!Flash Pot balance;
M_STM_TVC + M_COND_TVC = MV_POT(1) + MF_POT(1) + M_DS(1) + M_BFW(1);
M_STM_TVC*HC_TVC + M_COND_TVC*HF_TVC = MV_POT(1)*HV_II(1) +
MF_POT(1)*HF_II(1) + M_DS(1)*HF_II(1) + M_BFW(1)*HF_II(1);

@FOR(EFFECTS(I)|I#GE#2 #AND# I#LE#(N_EFF-1): M_DIST(I) = MV_POT(I) + MF_POT(I) +
M_DS(I) + M_BFW(I));
@FOR(EFFECTS(I)|I#GE#2 #AND# I#LE#(N_EFF-1): (M_SEA_STM(I-1) + M_BRINE_STM(I-1) +
MV_POT(I-1))*HC(I-1) + MF_POT(I-1)*HF_II(I-1) =
                                                    MV_POT(I)*HV_II(I) +
MF_POT(I)*HF_II(I) + M_DS(I)*HF_II(I) + M_BFW(I)*HF_II(I));

MV_POT(N_EFF) = 0;
MF_POT(N_EFF) = 0;

M_DS(1)          = 0;          !Desuperheating condensate does not come from first or last flash pot;
M_DS(N_EFF)   = 0;
M_BFW(N_EFF) = 0;


!BFW return balance;
@SUM(EFFECTS(I):M_BFW(I)) = M_STM_MOT;
@FOR(EFFECTS(I): T_BFW(I) = T_EFF_II(I));!Defines BFW return temperatures from each flash pot;


!BFW Heating requirement from Nat. gas Boiler;
Q_MED_BOIL = (100/BOIL_EFF)*@SUM(EFFECTS(I): M_BFW(I)*(HV_MOT - HF_II(I))); !Boiler
heat req. [Btu/s];
```

```
!Condensate line;
M_DESAL = M_DIST(N_EFF) + M_STM_COND + M_BRINE_STM(N_EFF);!Sea stm was used to
balance stmsuc and stmcond so add brine_stm;

(M_SEA_STM(N_EFF-1) + M_BRINE_STM(N_EFF-1) + MV_POT(N_EFF-1))*HC(N_EFF-1) +
MF_POT(N_EFF-1)*HF_II(N_EFF-1) + (M_STM_COND + M_BRINE_STM(N_EFF))*HC(N_EFF) =
HF_EX*M_DESAL + Q_DIST;


!Brine line;
M_BRINE = M_WATER(N_EFF) + M_SALT(N_EFF);

M_BRINE_WATER(N_EFF)*HF_I(N_EFF) + M_BRINE_SALT(N_EFF)*HS_I(N_EFF) +
M_SEA_WATER(N_EFF)*HF(N_EFF) + M_SEA_SALT(N_EFF)*HS(N_EFF) =
M_WATER(N_EFF)*HF_EX + M_SALT(N_EFF)*HS_EX + Q_BRINE;


!Overall MED heat & material balance;
H_IN  = M_STM_MOT*HV_MOT + (SEA_WATER*HF_SEA + SEA_SALT*HS_SEA)*N_EFF;
H_OUT = @SUM(EFFECTS(I): M_BFW(I)*HF_II(I)) + Q_COND_XS + Q_BRINE_XS + Q_DIST_XS
+ (M_WATER(N_EFF) + M_DESAL)*HF_EX + M_SALT(N_EFF)*HS_EX;


M_IN    = (SEA_WATER + SEA_SALT)*N_EFF;
M_OUT = M_WATER(N_EFF) + M_SALT(N_EFF) + M_DESAL;



!Seawater preheater balance;
Q_COND  = Q_COND_PRE  + Q_COND_XS;
Q_BRINE = Q_BRINE_PRE + Q_BRINE_XS;
Q_DIST  = Q_DIST_PRE  + Q_DIST_XS;

CP_SEA_AVG*M_SEA_PRE*(TH_SEA - T_SEA) = Q_COND + Q_BRINE + Q_DIST;

Q_SEA_PRE       = Q_COND_PRE + Q_BRINE_PRE + Q_DIST_PRE;
Q_SEA_PRE       = (SEA_WATER + SEA_SALT)*N_EFF*CP_SEA_AVG*(TH_SEA - T_SEA);

M_SEA_HOT       = M_SEA_PRE - N_EFF*(SEA_WATER + SEA_SALT);

TH_SEA <= T_C(N_EFF) - DTMIN;
TH_SEA <= T_EFF(N_EFF) - DTMIN;
TH_SEA >= T_SEA;


!Seawater flow rate for cooling;
M_SEA_BYPASS*CP_SEA_AVG*(T_SEA_MAX - T_SEA) = Q_COND_XS + Q_BRINE_XS +
Q_DIST_XS;


!Seawater pumping energy requirement;
M_SEA_TOTAL = M_SEA_PRE + M_SEA_BYPASS;
```

```
!DT calculations for seawater preheaters;
DT_COND_PRE  = T_C(N_EFF) - TH_SEA;
DT1_COND_PRE = T_C(N_EFF) - T_SEA;

DT_BRINE_PRE  = 0.5*(T_EFF(N_EFF) + T_EFF_I(N_EFF)) - TH_SEA;
        !Average of boiling seawater and flashing brine temperatures;
DT1_BRINE_PRE = T_EX - T_SEA;

DT_DIST_PRE  = 0.5*(T_C(N_EFF) + T_EFF_II(N_EFF - 1)) - TH_SEA;
        !Average temperature between condensate and flashing temp of previous pot;
DT1_DIST_PRE = T_EX - T_SEA;

!DT calculations for evaporators;
@FOR(EFFECTS(I): Q_EFF_VAP(I) = U_EFF(I)/3600*A_EFF_VAP(I)*DT_EFF_VAP(I)); !Evap. area
req. for vaporization;

DT_EFF_SENS(1)  = TC_TVC - TH_SEA;
DT1_EFF_SENS(1) = TC_TVC - T_EFF(1);

@FOR(EFFECTS(I)|I#GE#2: DT_EFF_SENS(I)  = T_C(I-1) - TH_SEA);
@FOR(EFFECTS(I)|I#GE#2: DT1_EFF_SENS(I) = T_C(I-1) - T_EFF(I));

! Pumping power requirements;
(PUMP_EFF/100)*145.038*MED_BRINE_PUMP = 1/(2.20462*DENS_WATER_EFF)*(P_ATM -
P_EFF(N_EFF))*M_WATER(N_EFF);       !Discharge of brine to 1 atm;
(PUMP_EFF/100)*145.038*MED_DIST_PUMP  =
1/(2.20462*DENS_WATER_EFF)*(MED_STORE_P - P_EFF(N_EFF))*M_DESAL;
(PUMP_EFF/100)*145.038*MED_FEED_PUMP  = 1/(2.20462*DENS_WATER)*MED_LINE_DP*(1 -
X_SAL/1000)*M_SEA_TOTAL;
(PUMP_EFF/100)*145.038*MED_BFW_PUMP   = 1/(2.20462*DENS_WATER)*(P_MOT - (P_TVC -
DP_LOSSES))*M_STM_MOT;
(PUMP_EFF/100)*145.038*MED_DS_PUMP    = 1/(2.20462*DENS_WATER)*(P_TVC -
P_EFF(N_EFF))*@SUM(EFFECTS(I):M_DS(I));

MED_PUMP_PW = MED_BRINE_PUMP + MED_DIST_PUMP + MED_FEED_PUMP +
MED_BFW_PUMP + MED_DS_PUMP;     ! Pumping power requirement [kW];

! DESAL SYSTEM BALANCE ----------------------------------------------------------------------------------------;
DESAL_FEED    = F_FEED_RO + F_FEED_MED;
F_DESAL       = F_PERM_RO + F_PERM_MED;
!-------------------------------------------------------------------------------------------------------------;

! OVERALL DESALINATION PLANT COSTING --------------------------------------------------------------------------;
ACI_DESAL = DCC_RO + DCC_MED + DCC_DESAL + CONTIN_DESAL + SC_DESAL;
TAC_DESAL = ACI_DESAL + TOC_RO + TOC_MED + OC_DESAL + FOC_DESAL;
!-------------------------------------------------------------------------------------------------------------;


! MED COSTING -------------------------------------------------------------------------------------------------;
DCC_MED       = CC_MED_PUMP + CC_MED_CLEAN + CC_MED_SOLIDS;
TOC_MED       = OC_MED_GAS + OC_MED_PW;
```

```
! MED UNIT SPECIFIC COSTS ----------------------------------------------------------------------------------------;
1E3*CC_MED_PUMP = (50000/PLANT_LIFE) + (234.5/PLANT_LIFE)*MED_PUMP_PW;

1/(1E-3*432/PLANT_LIFE)*CC_MED_CLEAN  = F_FEED_MED;
1/(1E-3*432/PLANT_LIFE)*CC_MED_SOLIDS = F_FEED_MED;

!---------------------------------------------------------------------------------------------------------------;
OC_MED_PW = OC_MED_INT + OC_MED_PRE + OC_MED_PUMP + OC_MED_POST +
OC_MED_CLEAN + OC_MED_SERVICE;
1/(1E-3*0.191*(24*PW_COST*365)/3.38)*OC_MED_INT       = MED_PUMP_PW;
1/(1E-3*0.013*(24*PW_COST*365)/3.38)*OC_MED_PRE       = MED_PUMP_PW;
1/(1E-3*24*PW_COST*365)*OC_MED_PUMP                   = MED_PUMP_PW;
1/(1E-3*0.177*(24*PW_COST*365)/3.38)*OC_MED_POST      = MED_PUMP_PW;
1/(1E-3*0.027*(24*PW_COST*365)/3.38)*OC_MED_CLEAN     = MED_PUMP_PW;
1/(1E-3*0.130*(24*PW_COST*365)/3.38)*OC_MED_SERVICE = MED_PUMP_PW;

1E3*OC_MED_GAS = 1E-6*(3600*24*365)*(100 + BOIL_MAIN)/100*GAS_COST*Q_MED_BOIL;

! AUXILLIARY COSTS FOR THE REST OF PLANT ------------------------------------------------------------------;
DCC_DESAL     = CC_SITE + CC_INTAKE + CC_PRETREAT + CC_PIPING + CC_POST +
CC_DISPOSE + CC_BUILD + CC_ELEC + CC_AUX + CC_START;
1/(1E-3*432/PLANT_LIFE)*CC_SITE         = DESAL_FEED;
1/(1E-3*1963.6/PLANT_LIFE)*CC_INTAKE  = DESAL_FEED;
1/(1E-3*2700/PLANT_LIFE)*CC_PRETREAT  = DESAL_FEED;
1/(1E-3*1369.61/PLANT_LIFE)*CC_PIPING = DESAL_FEED;
1/(1E-3*785.45/PLANT_LIFE)*CC_POST    = DESAL_FEED;
1/(1E-3*1296/PLANT_LIFE)*CC_DISPOSE             = DESAL_FEED;
1E3*CC_BUILD = 49.369/PLANT_LIFE*F_DESAL + 12185/PLANT_LIFE +
1728/PLANT_LIFE*DESAL_FEED;
1/(1E-3*614/PLANT_LIFE*(86.4^0.65))*CC_ELEC = F_DESAL^0.65;
1/(1E-3*785.45/PLANT_LIFE)*CC_AUX   = DESAL_FEED;
1/(1E-3*785.45/PLANT_LIFE)*CC_START            = DESAL_FEED;
!---------------------------------------------------------------------------------------------------------------;
SC_DESAL        = CC_FINANCE + CC_PERMIT;
(1/CF_FIN)*CC_FINANCE = DCC_DESAL + DCC_RO + DCC_MED;
(1/CF_PERM)*CC_PERMIT = DCC_DESAL + DCC_RO + DCC_MED;
!---------------------------------------------------------------------------------------------------------------;
(1/CF_CONTIN)*CONTIN_DESAL          = DCC_DESAL + DCC_RO + DCC_MED;
!---------------------------------------------------------------------------------------------------------------;
OC_DESAL        = OC_CHEM + OC_DISPOSE;
1/(1E-3*1576.8)*OC_CHEM           = F_DESAL;
1/(1E-3*315.36)*OC_DISPOSE = DESAL_FEED;
!---------------------------------------------------------------------------------------------------------------;
FOC_DESAL     = FOC_LABOR + FOC_MAIN + FOC_ENVIRON + FOC_IND + FOC_SPARE;
1/(1E-3*473.04)*FOC_LABOR  = F_DESAL;
1/(1E-3*630.72)*FOC_MAIN          = DESAL_FEED;
1/(1E-3*50.46)*FOC_ENVIRON      = DESAL_FEED;
1/(1E-3*756.86)*FOC_IND             = DESAL_FEED;
1/(CF_FOC*PLANT_LIFE)*FOC_SPARE = DCC_DESAL + DCC_RO + DCC_MED;
!---------------------------------------------------------------------------------------------------------------;
```

APPENDIX C

LINGO MODEL FOR OPTIMIZAING THE WATER-ENERGY NEXUS IN A GTL PROCESS

```
!Stream labels:                                    Description
                    FW      -       Fresh water to the system to replace steam to ATR reactor
                    VAC     -       Vaccuum exhaust conditions of steam returning to HEN
                    LP      -       LP Steam to Process
                    MPS     -       MP Steam to Process
                    HPS     -       HP Steam to Process
                    MPL_R   -       Saturated MP-BFW returning to HEN
                    HPL_R   -       Saturated HP-BFW returning to HEN
                    LP_MP   -       LP-BFW to be heated to MP saturated liquid conditions
                    MP_HP   -       MP-BFW to be heated to HP saturated liquid conditions
                    HP_VHP-         HP-BFW to be heated to VHP saturated liquid conditions
                    ATR     -       Steam to be sent to ATR Reformer
Exchanger layout:
1 - HP SAT. STEAM VAPORIZER
2 - MP-HP BFW PREHEATER
3 - MP SAT. STEAM VAPORIZER
4 - LP-MP BFW PREHEATER
5 - LP SAT. STEAM VAPORIZER
6 - COMB. VAC/FW/MED-COND TO LP BFW PREHEATER
7 - AIR COOLER
8 - CW COOLER
9 - SEA WATER COOLER;

DATA:
N_COLD = 9;
N_HOT   = 6;
N_MP    = 3;            !HEX # for MPS production;
N_LP    = 5;            !HEX # for LPS production;
N_EFF   = 11;           !Number effect;
N_C     = 8;            !Number of chemicals;
N_RO    = 1;            !Nunmber of RO units;
ENDDATA


SETS:
!COGEN-HEN SETS;
C_STREAM/1..N_COLD/;
H_STREAM/1..N_HOT/;

HOT_TEMP(C_STREAM, H_STREAM)    : TH, TH1;
COLD_TEMP(C_STREAM)             : TC, TC1;
ENTHALPY(H_STREAM)              : FCP;
FLOW(H_STREAM)                  : M_HP_SUP, M_HP_SAT, M_MP_HP, M_MP_SAT,
M_LP_MP, M_LP_SAT, M_FW, M_MED_COND, M_VAC;
HEX_HEAT(C_STREAM, H_STREAM)    : Q_HEN, U_HEN, DTLM_HEX, DTMIN_HEX,
LOG_DTLM, LOG_DTH, LOG_DTH1, LOG_SUMDTH;
COSTING(C_STREAM, H_STREAM)     : CO_HEX, EXP_HEX;
```

```
!MED MODEL SETS;
EFFECTS/1..N_EFF/;
COMP/1..N_C/;

COMP_STREAM(COMP): X_FEED, X_BRINE, X_PERM;!CONTAINS SETS FOR RO MODEL;
EFF_ENTH(EFFECTS) : HV, HV_I, HV_II, HF, HF_I, HF_II, HS, HS_I, HS_II, HC;
EFF_FLOW(EFFECTS)    : M_BRINE_STM, M_SEA_STM, M_BRINE_WATER, M_SEA_WATER,
M_WATER, M_BRINE_SALT, M_SEA_SALT, M_SALT, M_DS, M_BFW, M_DIST, MV_POT,
MF_POT;
TEMP(EFFECTS)           : T_V, T_EFF, DT_LOSSES, T_EFF_CEL, T_EFF_I, T_EFF_II, T_C,
T_BFW, BPE_AVG, NEA_BRINE, NEA_DIST;
PRESS(EFFECTS)          : P_EFF;
CONC(EFFECTS)           : X_EFF_MAX, X_EFF_MINMAX, X_EFF_AVG;
HEX(EFFECTS) : Q_EFF, Q_EFF_VAP, Q_EFF_SENS, A_EFF_VAP, DT_EFF_VAP, U_EFF,
DT_EFF_SENS, DT1_EFF_SENS;


!RO MODEL SETS;
SOURCE/1..N_RO/;
SINK/1..N_RO/;

FEED_SPLIT(SINK):       F_F, BIN_F_POW, F_POWER, F_POW1, F_POW2, F_CC_PUMP1,
F_CC_PUMP2 ;
RO_FEED(SINK):                  F_RO;
RO_BRINE(SOURCE):    F_B;
RO_PERM(SOURCE):                F_P, F_P_MOD;
BRINE_SPLIT(SOURCE,SINK): F_BS, BIN_BS_POW, BIN_BS_ERD, BS_POWER, BS_ERD,
BS_POW1, BS_POW2, BS_ERD1, BS_ERD2, BS_CC_PUMP1, BS_CC_PUMP2, BS_CC_ERD1,
                                                        BS_CC_ERD2;
PERM_SPLITS(SOURCE,SINK): F_PS, BIN_PS_POW, PS_POWER, PS_POW1, PS_POW2,
PS_CC_PUMP1, PS_CC_PUMP2;
BRINE_STREAM(SOURCE):       F_BS_BRINE, BIN_BRINE, BRINE_ERD, BRINE_ERD1,
BRINE_ERD2, BRINE_CC_ERD1, BRINE_CC_ERD2;
PERM_STREAM(SOURCE):        F_PS_PERM;

COMP_SINK(SINK,COMP):           X_RO;
COMP_SOURCE(SOURCE,COMP):  X_BS, X_PS;

MODULES(SINK):                  N_MOD;
RO_PROPS(SINK):                 RO_A_PI, RO_PI, RO_PSI, RO_PI_PSI, RO_PSI_MAX;
MOD_PRESS(SINK):                RO_P_FEED, RO_P_B, RO_P_P, RO_MOD_DP;
RO_PERM_PROP(SINK):             RO_A_PI1, RO_A_PI2, RO_A_PI3, RO_PI1, RO_PI2, RO_PI3,
RO_PERM_BIN1, RO_PERM_BIN2, RO_PERM_BIN3;
RO_FLOW_DP(SINK):               DP_FEED, DP_BRINE;
RO_FLOW2_DP(SOURCE, SINK): DP_PS, DP_BS1, DP_BS2, DP_BS3, DP_BS_BIN1, DP_BS_BIN2,
DP_BS_BIN3;
REJECT(COMP):                   REJ;
RECOVERY(SINK):                 REC;
M_WEIGHT(COMP):                 RO_FEED_MW;

ENDSETS
```

```
DATA:
!COGEN-HEN DATA IMPORT;
U_HEN      = @ole('C:\Users\Kerron-Gabriel\Desktop\CASE_3\HEN-COGEN.XLSX','U_HEN');
U_VAC_AIR  = @ole('C:\Users\Kerron-Gabriel\Desktop\CASE_3\HEN-
COGEN.XLSX','U_VAC_AIR');
U_VAC_CW   = @ole('C:\Users\Kerron-Gabriel\Desktop\CASE_3\HEN-
COGEN.XLSX','U_VAC_CW');
U_VAC_SEA  = @ole('C:\Users\Kerron-Gabriel\Desktop\CASE_3\HEN-
COGEN.XLSX','U_VAC_SEA');
DTMIN_HEX  = @ole('C:\Users\Kerron-Gabriel\Desktop\CASE_3\HEN-
COGEN.XLSX','DTMIN_HEX');
CO_CT      = @ole('C:\Users\Kerron-Gabriel\Desktop\CASE_3\HEN-COGEN.XLSX','CO_CT');
CO_TANK    = @ole('C:\Users\Kerron-Gabriel\Desktop\CASE_3\HEN-COGEN.XLSX','CO_TANK');
CO_HEX     = @ole('C:\Users\Kerron-Gabriel\Desktop\CASE_3\HEN-COGEN.XLSX','CO_HEX');
C_REF_TURB = @ole('C:\Users\Kerron-Gabriel\Desktop\CASE_3\HEN-
COGEN.XLSX','C_REF_TURB');
EXP_HEX    = @ole('C:\Users\Kerron-Gabriel\Desktop\CASE_3\HEN-COGEN.XLSX','EXP_HEX');
EXP_TURB   = @ole('C:\Users\Kerron-Gabriel\Desktop\CASE_3\HEN-COGEN.XLSX','EXP_TURB');
EXP_BOIL   = @ole('C:\Users\Kerron-Gabriel\Desktop\CASE_3\HEN-COGEN.XLSX','EXP_BOIL');
EXP_CT     = @ole('C:\Users\Kerron-Gabriel\Desktop\CASE_3\HEN-COGEN.XLSX','EXP_CT');
EXP_TANK   = @ole('C:\Users\Kerron-Gabriel\Desktop\CASE_3\HEN-COGEN.XLSX','EXP_TANK');

!MED MODEL DATA IMPORT;
X_FEED           = @ole('C:\Users\Kerron-
Gabriel\Desktop\CASE_3\COGEN_MED_OPT.XLSM','MED_X_FEED');
X_BRINE_AVG = @ole('C:\Users\Kerron-
Gabriel\Desktop\CASE_3\COGEN_MED_OPT.XLSM','MED_X_BRINE_AVG');

!RO MODEL DATA IMPORT;
REJ              = @ole('C:\Users\Kerron-Gabriel\Desktop\CASE_3\RO_OPT.XLSM','REJ_ROSA');
RO_FEED_MW  = @ole('C:\Users\Kerron-Gabriel\Desktop\CASE_3\RO_OPT.XLSM','MW');
ENDDATA

!RO MODEL BINARY VARIABLE INITIALIZE;
@FOR(SINK(J): @BIN(RO_PERM_BIN1(J)));
@FOR(SINK(J): @BIN(RO_PERM_BIN2(J)));
@FOR(SINK(J): @BIN(RO_PERM_BIN3(J)));

@FOR(SINK(J)  : @BIN(BIN_F_POW(J)));
@FOR(SOURCE(I): @FOR(SINK(J): @BIN(BIN_BS_POW(I,J))));
@FOR(SOURCE(I): @FOR(SINK(J): @BIN(BIN_BS_ERD(I,J))));
@FOR(SOURCE(I): @FOR(SINK(J): @BIN(BIN_PS_POW(I,J))));
@FOR(SOURCE(I): @BIN(BIN_BRINE(I)));

@FOR(SOURCE(I): @FOR(SINK(J): @BIN(DP_BS_BIN1(I,J))));
@FOR(SOURCE(I): @FOR(SINK(J): @BIN(DP_BS_BIN2(I,J))));
@FOR(SOURCE(I): @FOR(SINK(J): @BIN(DP_BS_BIN3(I,J))));
```

```
DATA:
!****** ****************** CASE SCENARIO DATA **********************************;
F_DESAL_EXP = 3310.185387;    ! Largest desalination plant output approx. 682,000 cum/day [L/s];
M_WASTE     = 0;
Q_FUEL_XS   = 0;

!************************ COGEN-HEN DATA ************************************;
!Steam level data (LP AND VAC ENTHALPY HAS TO BE ADJUSTED MANUALLY);
P_HP    = 435.113;        !High pressure steam level [psia];
P_MP    = 125;            !Medium pressure steam level that can be produced from HO [psia];
P_LP    = 15;             !Lower pressure steam level [psia];
P_VAC   = 3;              !Turbine exhaust pressure [psia];

!Turbine and furnace data;
T_MAX          = 1049;        !Maximum turbine inlet temperature [F];
P_MAX          = 2465;        !Max turbine inlet pressure [psia];
STM_QUAL_MIN = 90;            !Min. exhaust steam quality [%];

GEN_EFF        = 90;   !Generator efficiency;
FURN_EFF       = 75;   !Furnace efficiency for superheating steam;
BOIL_EFF       = 75;   !Boiler efficiency for superheating steam;
PUMP_EFF       = 80;   !Pump efficiency [%];
K_DR_MAX       = 1.8;  !Max over design ratio;

!Heat Exchange operating data;
DT_SUPER       = 18;   !Superheat for transported steam [F];

!Hot stream data;
FCP_SYN        = 2.190413;          !FCp of syngas stream [MMBtu/hr-F]   2.190413;
FCP_HO         = 56.67247;          !FCp of FT Hot Oil stream [MMBtu/hr-F];
FCP_FT_VAP     = 3.435997;          !FCp of FT reactor vapor [MMBtu/hr-F];
FCP_C_SEP      = 0.010848;          !FCp of feed to cold separator pre-cooler [MMBtu/hr-F];
FCP_P_COOL     = 0.307203;          !FCp of product stream [MMBtu/hr-F];

T_SYN_IN       = 1949;        T_SYN_OUT      = 122;
T_FT_VAP_IN    = 428;         T_FT_VAP_OUT = 122;
T_C_SEP_IN     = 404;         T_C_SEP_OUT    = 122;
T_P_COOL_IN    = 252;         T_P_COOL_OUT = 122;
T_FRAC_IN      = 302;         T_FRAC_OUT     = 302;
T_HO_IN        = 410;         T_HO_OUT       = 365;

!Process power requirements;
PW_PROCESS_REQ = 213.7;       !Process power requirements [MW];

!Fuel gas Distribution properties;
Q_HPS_REQ = 243.99093;        !Total required HPS energy [MMBtu/hr];
Q_MPS_REQ = 1216.791469;!Total required MPS energy [MMBtu/hr];
Q_FUR_REQ = 735.122543;       !Total required heating for furnaces [MMBtu/hr];
M_ATR     = 227.6335;     !HP steam requirement for ATR [ton/hr];

Q_FUEL     = 3393.5712; !Total energy from the fuel [MMBtu/hr];
Q_FRAC_COND = 239.688294;    !Total energy from Fractionator condenser @302 degF [MMBtu/hr];
Q_E_205_TOT    = 444.193422;
```

```
Q_E_206_TOT   = 496.570810;
Q_E_502_TOT   = 0.205153;

T_SEA_IN          = 77;  ! Seawater supply temp [F];
T_SEA_OUT         = 86;  ! Seawater return temp [F];
T_CWS             = 86;  ! Cooling water supply temp [F];
T_CWR             = 104;! Cooling water return temp [F];
T_AIR_IN          = 113;! Amb Air inlet temp [F];
T_AIR_OUT         = 131;! Amb Air outlet temp [F];
T_FW              = 77;  ! Fresh water feed temperature [F];
T_MED_COND    = 158;! Temperature return of condensate from MED [F];
PWREQ_AIR_FAN= 1.00;! Power requirement in air cooling [kW/MMBtu/hr];
PWREQ_CT_FAN  = 0.0922;! Cooling Tower fan power requirement [kW/MMBtu/hr];

HEX_DP          = 7.5;   ! HEX pressure drop [psia]  0.5 bar;
DP_SEA          = 14.7;  ! Pressure drop across sea water cooling circuit [psia];
DP_CW           = 14.7;  ! Pressure drop across cooling water cooling circuit [psia];
COND_DP         = 5;     ! Condensate return line DP [psia];

!*************************** MED DATA ******************************************;
T_EFF_FIRST   = 158;   ! Temperature of first effect [F];
T_EFF_LAST    = 104;   ! Temperature of last effect [F];

T_SEA           = 77;    !Temperature of inlet seawater [F];
T_SEA_MAX     = 86;    !Max. temp. of seawater outlet [F];
X_BRINE_MAX= 71.8;  !Maximum salt concentration return [g/kg];
X_EFF_MIN     = 60;    !Minimum potential salt concentration in each effect [g/kg];

F_PERM_MED_MAX= 2314.81;!Largest MED desalination plant output approx. 200,000 cum/day [L/s];

MED_LINE_DP  = 30;     !Pressure drop of seawater in MED process. Assumes dP across exchangers,
solids filters, line losses etc [psi];
MED_STORE_P = 30;              !Storage tank pressure including 10 m head in tank [psia];
P_ATM           = 14.6959;       !Atmospheric pressure [psia];

DP_LOSSES     = 0.071117; !Constant pressure drop across demister, vapor transfer line and condenser
tubes @10 cmH2O [psia];
DTMIN = 9;                  !Minimum delta T for HEX [F];


!********* ********************** RO  DATA ***************************************;
RO_FF           = 1;               !RO fouling factor (1 = new installations);
P_FEED = 14.5038;       !Pressure of permeate [psi];
AREA_MEM      = 245.4;!Surface area in 6-membrane module [sqm];
RO_P_MAX      = 1015.26;       !Maximum RO feed pressure [psi];
RO_DP_MAX     = 18.8549;       !Maximum pressure drop in RO module [psi];
MOD_PERM_MAX = 3.15;           !Maximum module permeate flow [L/s];
MOD_FEED_MIN = 0.6944;         !Minimum feed flow to module [L/s];
N_MOD_MAX    = 1000; !Maximum number of modules;
PERM_REC_MAX = 0.30;           !Maximum element recovery for RO permeate feed;
BRINE_REC_MAX= 0.15;           !Maximum element recovery for open seawater feed;

F_PERM_RO_MAX= 7893.519;!Largest RO desalination plant output approx. 682,000 cum/day [L/s];
```

```
ERD_EFF          = 80;    !ERD efficiency [%];
ERD_DP_MIN       = 14.5038;       !Minimum DP for using an ERD [psi];

X_PERM_MAX   = 0.50;  !Maximum Permeate TDS concentration leaving RO network [*1000 ppm];
X_PERM_MG    = 0.030;!Required Mg concentration in permeate [*1000 ppm];
X_PERM_CA    = 0.010;!Required Mg concentration in permeate [*1000 ppm];


!********************** DIRECT RECYCLE NETWORK DATA *************************;
M_PRE_WATER   = 705;          !Pretreated water from ATR based GTL process [ton/hr];
M_SAT_WATER   = 51;           !Process water required for Nat. Gas Saturator [ton/hr];
M_CO2_WATER   = 4;            !Process water required for CO2 removal unit [ton/hr];

X_POT_WATER  = 500;           !TDS conc. for potable water [ppm];

X_ATR_PWATER_OIL = 0.1;       !Conc. of oil in pretreated water [ppm];
X_ATR_PWATER_TDS = 0.06;      !Conc. of TDS in pretreated water [ppm];

X_PWATER_OIL  = 1.0;          !Allowable conc. of oil in process water [ppm];
X_PWATER_TDS  = 500;          !Allowable conc. of TDS in process water [ppm];

X_BFW_OIL       = 1.0;        !Allowable conc. of oil in Boiler feed water [ppm];
X_BFW_TDS       = 2.0;        !Allowable conc. of TDS in Boiler feed  water [ppm];

X_DESAL_OIL    = 0.001;       !Conc. of oil in desalination water [ppm];
X_MED_TDS      = 10;          !Conc. of TDS in MED desalinated water [ppm];

!********************** COST FACTORS FOR BOTH MODELS *************************;
C_ELECT          = 0.05;      !Electricity cost  in Qatar [$/kWh];
C_FUEL           = 2.0;       !Fuel cost  in Qatar [$/MMBtu];
C_WATER          = 1.0778;    !Cost of water in Qatar [$/ton];


CO_EVAP          = 492.28;
CO_EJECTOR    = 2470;

EVAP_EXP         = 0.7;
EJ_EXP           = 0.3;

PLANT_LIFE     = 20;          !Plant life for estimating annualized capital [yrs];

CF_PERM          = 0.1;   !Fraction of Direct Capital Cost used for permitting;
CF_FIN           = 0.04;  !Financing cost factor;
CF_CONTIN        = 0.05;  !Contingency cost factor;
CF_FOC           = 0.01;  !Fixed operating cost factor;

CF_RO_CONTIN = 0.05; !Contingency cost factor for RO;
CF_RO_FOC        = 0.02; !Fixed operating cost factor;

ENDDATA
```

```
CALC:
!********************** CALC SECTION FOR COGEN-HEN MODEL **********************;
!Saturation temperature calculation for various pressure levels;
TSAT_VAC      = 102.799*P_VAC^0.2741;          !Saturation temp at Vaccuum [F];
TSAT_LP       = 117.664*(P_LP^0.2219);         !Saturation temp at LP conditions [F];
TSAT_MP       = 117.664*(P_MP^0.2219);         !Saturation temp at MP conditions [F];
TSAT_HP       = 117.664*(P_HP^0.2219);         !Saturation temp at HP conditions [F];

TC(1) = TSAT_HP;                    TC1(1) =  TSAT_HP;
TC(2) = TSAT_MP;                    TC1(2) =  TSAT_HP;
TC(3) = TSAT_MP;                    TC1(3) =  TSAT_MP;
TC(4) = TSAT_LP;                    TC1(4) =  TSAT_MP;
TC(5) = TSAT_LP;                    TC1(5) =  TSAT_LP;
TC(6) = TSAT_VAC;                   TC1(6) =  TSAT_LP;
TC(7) = T_AIR_IN;                   TC1(7) =  T_AIR_OUT;
TC(8) = T_CWS;                      TC1(8) =  T_CWR;
TC(9) = T_SEA_IN;                   TC1(9) =  T_SEA_OUT;

!Saturated liquid enthalpy calculation for various pressure levels;
HF_FW = 4.708284E-5*T_FW^2 + 9.888650E-1*T_FW - 31.44198;                    !Enthalpy of FW
[Btu/lb];
HFSAT_VAC = 4.243328E-5*TSAT_VAC^2 + 0.9877278*TSAT_VAC - 31.14636;     !Enthalpy of sat
VAC stream [Btu/lb[;
HFSAT_LP  = 4.243328E-5*TSAT_LP^2  + 0.9877278*TSAT_LP  - 31.14636;          !Enthalpy of sat
LP stream [Btu/lb];
HFSAT_MP = 4.539463E-4*TSAT_MP^2 + 7.420701E-1*TSAT_MP + 4.811173;       !Enthalpy of sat
MP stream [Btu/lb];
HFSAT_HP = 4.539463E-4*TSAT_HP^2 + 7.420701E-1*TSAT_HP + 4.811173;       !Enthalpy of sat
HP stream [Btu/lb];

!Saturated and Superheated steam entropy calculations;
SV_VAC = -3.985674E-9*TSAT_VAC^3 + 5.408928E-6*TSAT_VAC^2 - 3.369786E-3*TSAT_VAC +
2.265838;
SV_LP  = -3.985674E-9*TSAT_LP^3  + 5.408928E-6*TSAT_LP^2  - 3.369786E-3*TSAT_LP  +
2.265838;
SV_MP  = -3.985674E-9*TSAT_MP^3  + 5.408928E-6*TSAT_MP^2  - 3.369786E-3*TSAT_MP  +
2.265838;
SV_HP  = -3.985674E-9*TSAT_HP^3  + 5.408928E-6*TSAT_HP^2  - 3.369786E-3*TSAT_HP  +
2.265838;

!Saturated liquid entropy calculations;
SF_VAC = 1.630830E-3*TSAT_VAC - 3.083814E-2;

!Saturated vapor enthalpy calculations;
HV_HP  = (0.2029*TSAT_HP)*SV_HP^3.647 + 817.35;
HV_MP  = (0.2029*TSAT_MP)*SV_MP^3.647 + 817.35;
HV_LP  = (0.2029*TSAT_LP)*SV_LP^3.647 + 817.35;
HV_VAC = -2.044854E-04*TSAT_VAC^2 + 0.4720204*TSAT_VAC + 1.059540E3;

!Saturated and Superheated steam entropy calculations;
K_S_LP = 1.3845E-2*(TSAT_LP/1000)^2 -9.8258E-3*(TSAT_LP/1000) + 3.1462E-3;
S_LP     = SV_LP + 0.46883*(1 - @EXP(-K_S_LP*DT_SUPER));
H_LP   = (0.2029*TSAT_LP)*S_LP^3.647 + 817.35;
```

```
K_S_MP = 1.3845E-2*(TSAT_MP/1000)^2 -9.8258E-3*(TSAT_MP/1000) + 3.1462E-3;
S_MP     = SV_MP + 0.46883*(1 - @EXP(-K_S_MP*DT_SUPER));
H_MP   = (0.2029*TSAT_MP)*S_MP^3.647 + 817.35;

K_S_HP   = 1.3845E-2*(TSAT_HP/1000)^2 -9.8258E-3*(TSAT_HP/1000) + 3.1462E-3;
S_HP       = SV_HP + 0.46883*(1 - @EXP(-K_S_HP*DT_SUPER));
H_HP     = (0.2029*TSAT_HP)*S_HP^3.647 + 817.35;

!Max entropy into turbine based on Turbine max temp restriction;
S_HP_MAX    = SV_HP + 0.46883*(1 - @EXP(-K_S_HP*(T_MAX - TSAT_HP)));
S_MP_MAX    = SV_MP + 0.46883*(1 - @EXP(-K_S_MP*(T_MAX - TSAT_MP)));
S_LP_MAX    = SV_LP + 0.46883*(1 - @EXP(-K_S_LP*(T_MAX - TSAT_LP)));

!Steam turbine constant calculations;
TURB_A_HP = -1.038755556 + 0.003461111*TSAT_HP;          !A factor for turbine 2     W>4.1
MMBtu/hr;
TURB_B_HP =  1.111644444 + 0.000261111*TSAT_HP;          !B factor for turbine 2     W>4.1
MMBtu/hr;

TURB_A_MP = -1.038755556 + 0.003461111*TSAT_MP;          !A factor for turbine 3     W>4.1
MMBtu/hr;
TURB_B_MP =  1.111644444 + 0.000261111*TSAT_MP;          !B factor for turbine 3     W>4.1
MMBtu/hr;

TURB_A_LP = -1.038755556 + 0.003461111*TSAT_LP;          !A factor for turbine 3     W>4.1
MMBtu/hr;
TURB_B_LP =  1.111644444 + 0.000261111*TSAT_LP;          !B factor for turbine 3     W>4.1
MMBtu/hr;

K_IS_FACTOR = (HV_VAC - HFSAT_VAC)/(SV_VAC - SF_VAC);

K1_HP_MAX = (6/(5*TURB_B_HP))*(3.41214E6*TURB_A_HP)*(1/K_DR_MAX) -
(1/(5*TURB_B_HP))*(3.41214E6*TURB_A_HP) ;
K1_MP_MAX = (6/(5*TURB_B_MP))*(3.41214E6*TURB_A_MP)*(1/K_DR_MAX) -
(1/(5*TURB_B_MP))*(3.41214E6*TURB_A_MP) ;
K1_LP_MAX = (6/(5*TURB_B_LP))*(3.41214E6*TURB_A_LP)*(1/K_DR_MAX) -
(1/(5*TURB_B_LP))*(3.41214E6*TURB_A_LP) ;

!Hot stream FCP;
FCP(1) = FCP_SYN;
FCP(2) = FCP_HO;
FCP(3) = FCP_FT_VAP;
FCP(4) = FCP_C_SEP;
FCP(5) = FCP_P_COOL;

!Hot Stream temperature initialize;
TH(1,1)    = T_SYN_IN;
TH(N_MP,2) = T_HO_IN;
TH(N_MP,3) = T_FT_VAP_IN;
TH(N_MP,4) = T_C_SEP_IN;
TH(N_LP,5) = T_P_COOL_IN;
TH(N_LP,6) = T_FRAC_IN;
```

```
TH1(N_COLD,1) = T_SYN_OUT;
TH1(N_COLD,2) = T_HO_OUT;
TH1(N_COLD,3) = T_FT_VAP_OUT;
TH1(N_COLD,4) = T_C_SEP_OUT;
TH1(N_COLD,5) = T_P_COOL_OUT;
TH1(N_COLD,6) = T_FRAC_OUT;

!Required Process steam flows;
M_MPS_REQ  = Q_MPS_REQ*500/(H_MP - HFSAT_MP);  !Flowrate of req. Process MPS [ton/hr];
M_HPS_REQ  = Q_HPS_REQ*500/(H_HP - HFSAT_HP);    !Flowrate of req. Process HPS [ton/hr];

Q_FUEL_AVAIL = (FURN_EFF/100)*Q_FUEL - Q_FUR_REQ; !Heat avaialable from FT tail gas
[MMBtu/hr];

!Logic constraints on steam and BFW preheating for hot stream;
@FOR(H_STREAM(J)|J#GE#2: M_HP_SAT(J) = 0);
@FOR(H_STREAM(J)|J#GE#2: M_MP_HP(J)  = 0);

@FOR(H_STREAM(J)|J#GE#5: M_MP_SAT(J) = 0);
@FOR(H_STREAM(J)|J#GE#5: M_LP_MP(J)  = 0);

!Logic constraints on steam and BFW preheating for hot stream;
@FOR(C_STREAM(I)|I#LE#2: @FOR(H_STREAM(J)|J#GE#2: Q_HEN(I,J) = 0));
@FOR(C_STREAM(I)|I#LE#4: @FOR(H_STREAM(J)|J#GE#5: Q_HEN(I,J) = 0));

DTLM_VAC_AIR = (0.5*(TSAT_VAC - T_AIR_IN)*(TSAT_VAC - T_AIR_OUT)*(TSAT_VAC -
T_AIR_IN + TSAT_VAC - T_AIR_OUT))^(1/3);
DTLM_VAC_CW  = (0.5*(TSAT_VAC - T_CWS)*(TSAT_VAC - T_CWR)*(TSAT_VAC - T_CWS +
TSAT_VAC - T_CWR))^(1/3);
DTLM_VAC_SEA = (0.5*(TSAT_VAC - T_SEA_IN)*(TSAT_VAC - T_SEA_OUT)*(TSAT_VAC -
T_SEA_IN + TSAT_VAC - T_SEA_OUT))^(1/3);

A_E_205 = 1E6*Q_E_205_TOT/(153*(0.5*(122 - T_SEA_IN)*(122 - T_SEA_OUT)*(2*122 -
T_SEA_IN - T_SEA_OUT))^(1/3));
A_E_206 = 1E6*Q_E_206_TOT/(122*(0.5*(122 - T_SEA_IN)*(173.21 - T_SEA_OUT)*(122 + 173.21 -
T_SEA_IN - T_SEA_OUT))^(1/3));
A_E_502 = 1E6*Q_E_502_TOT/(66* (0.5*(225.88 - T_AIR_IN)*(225.88 - T_AIR_OUT)*(2*225.88 -
T_AIR_IN - T_AIR_OUT))^(1/3));


!********************** CALC SECTION FOR MED MODEL ****************************;
P_MOT          = P_LP;                    !Pressure of motive steam [psia] 14.5038 PSIA = 100 bar;
TSAT_MOT       = TSAT_LP;
DT_EFF         = (T_EFF_FIRST - T_EFF_LAST)/(N_EFF-1);!Temperature difference of effects [F];
T_EFF(1)       = T_EFF_FIRST;
T_EFF(N_EFF)= T_EFF_LAST;
TSAT_TVC       = T_EFF(1) + DT_EFF;
P_TVC          = (TSAT_TVC/102.799)^(1/0.2741);          !Equation for P_sat at vacuum conditions;
TC_TVC         = 102.799*(P_TVC - DP_LOSSES)^0.2741;
T_EX           = T_SEA + DTMIN;

@FOR(EFFECTS(I)|I#GE#2 #AND# I#LE#N_EFF: T_EFF(I) = T_EFF(I-1) - DT_EFF);
```

```
!Boiling point elevation calc;
@FOR(EFFECTS(I): T_EFF_CEL(I) = (T_EFF(I) - 32)/1.8);
@FOR(EFFECTS(I): X_EFF_MAX(I)        = 0.9*(457628.5 - 11304.11*T_EFF_CEL(I) +
107.5781*T_EFF_CEL(I)^2 - 0.360747*T_EFF_CEL(I)^3)*1E-3); !Effect max Xbrine [g/kg];
@FOR(EFFECTS(I): X_EFF_MINMAX(I) = @SMIN(X_EFF_MAX(I), X_BRINE_AVG));
@FOR(EFFECTS(I): X_EFF_AVG(I) = 0.5*(X_EFF_MIN + X_EFF_MINMAX(I)));
@FOR(EFFECTS(I): BPE_AVG(I)  = (-4.584E-4*T_EFF_CEL(I)^2 + 2.823E-1*T_EFF_CEL(I) +
17.95)*(X_EFF_MINMAX(I)/1000)^2 + (1.536E-4*T_EFF_CEL(I)^2 + 5.267E-2*T_EFF_CEL(I) +
6.56)*X_EFF_MINMAX(I)/1000);              !Max. BPE in [K];

!Enthalpy calc for vaporized seawater;
@FOR(EFFECTS(I): T_V(I)   = T_EFF(I) - 1.8*BPE_AVG(I));!Effect vapor temp. [F];
@FOR(EFFECTS(I): P_EFF(I) = (T_V(I)/102.799)^(1/0.2741));!Effect pressure as function of Tv [psia];
@FOR(EFFECTS(I): DT_LOSSES(I) = T_V(I) - 102.799*(P_EFF(I) -
DP_LOSSES)^0.2741);!DT_LOSSES across each effect [F];
@FOR(EFFECTS(I): T_C(I)          = T_V(I) - DT_LOSSES(I));!Condensing temp. of effect vapor [F];
@FOR(EFFECTS(I): HV(I)  = -2.044854E-04*T_V(I)^2 + 0.4720204*T_V(I) + 1.059540E3);!Enthalpy
of effect vapor [Btu/lb];
@FOR(EFFECTS(I): HC(I)  = 4.243328E-5*T_C(I)^2 + 0.9877278*T_C(I) - 31.14636); !Enthalpy of
condensed steam [Btu/lb];
@FOR(EFFECTS(I): HF(I)  = 4.243328E-5*T_EFF(I)^2 + 0.9877278*T_EFF(I) - 31.14636);!Enthalpy
of effect water from sea [Btu/lb];
@FOR(EFFECTS(I): HS(I)  = -9.00786E-5*T_EFF_CEL(I)^3 + 0.0148023*T_EFF_CEL(I)^2 -
0.8640971*T_EFF_CEL(I) - 7.8738015); !Hs of effect salt from sea [Btu/lb];

!Enthalpy calc for flashing brine;
@FOR(EFFECTS(I): NEA_BRINE(I) = 1.8*33*((DT_EFF/1.8)^0.55)/((T_V(I)-32)/1.8));!Non-
equilibrium allowance [F];
@FOR(EFFECTS(I): T_EFF_I(I)   = T_EFF(I) + NEA_BRINE(I));
@FOR(EFFECTS(I): HV_I(I)         = -2.044854E-04*T_EFF_I(I)^2 + 0.4720204*T_EFF_I(I) +
1.059540E3);
@FOR(EFFECTS(I): HF_I(I)         = 4.243328E-5*T_EFF_I(I)^2 + 0.9877278*T_EFF_I(I) - 31.14636);
@FOR(EFFECTS(I): HS_I(I)         = -9.00786E-5*((T_EFF_I(I)-32)/1.8)^3 + 0.0148023*((T_EFF_I(I)-
32)/1.8)^2 - 0.8640971*((T_EFF_I(I)-32)/1.8) - 7.8738015);


!Enthalpy calc for flashing distillate;
NEA_DIST(1) = 1.8*0.33*((TC_TVC - T_V(1))/1.8)/((T_V(1) - 32)/1.8);
@FOR(EFFECTS(I)|I#GE#2: NEA_DIST(I)  = 1.8*0.33*((T_C(I-1) - T_V(I))/1.8)/((T_V(I) -
32)/1.8));!Non-equilibrium allowance [F];
@FOR(EFFECTS(I): T_EFF_II(I)  = T_V(I) + NEA_DIST(I));
@FOR(EFFECTS(I): HV_II(I)        = -2.044854E-04*T_EFF_II(I)^2 + 0.4720204*T_EFF_II(I) +
1.059540E3);
@FOR(EFFECTS(I): HF_II(I)        = 4.243328E-5*T_EFF_II(I)^2 + 0.9877278*T_EFF_II(I) -
31.14636);
@FOR(EFFECTS(I): HS_II(I)        = -9.00786E-5*((T_EFF_II(I)-32)/1.8)^3 + 0.0148023*((T_EFF_II(I)-
32)/1.8)^2 - 0.8640971*((T_EFF_II(I)-32)/1.8) - 7.8738015);

!Enthalpy calculations for motive steam and TVC exit steam / condensate;
HV_MOT = H_LP;
HV_TVC = -2.044854E-04*TSAT_TVC^2 + 0.4720204*TSAT_TVC + 1.059540E3;
HF_TVC = 4.243328E-5*TSAT_TVC^2 + 0.9877278*TSAT_TVC - 31.14636;
HC_TVC = 4.243328E-5*TC_TVC^2 + 0.9877278*TC_TVC - 31.14636;
```

```
!Enthalpy calculation for inlet seawater components (water and salt);
HF_SEA = 4.708284E-5*T_SEA^2 + 9.888650E-1*T_SEA - 31.44198;
HS_SEA = -9.00786E-5*((T_SEA - 32)/1.8)^3 + 0.0148023*((T_SEA - 32)/1.8)^2 - 0.8640971*((T_SEA
- 32)/1.8) - 7.8738015;

!Enthalpy calculation for outlet distillate / brine components (water and salt);
HF_EX  = 4.708284E-5*T_EX^2 + 9.888650E-1*T_EX - 31.44198;
HS_EX  = -9.00786E-5*((T_EX - 32)/1.8)^3 + 0.0148023*((T_EX - 32)/1.8)^2 - 0.8640971*((T_EX -
32)/1.8) - 7.8738015;

!Calculation for entrainment ratio;
C_R  = P_TVC/P_EFF(N_EFF);                    !Compression ratio;
EX_R = P_MOT/P_EFF(N_EFF);

P_E = P_EFF(N_EFF)*6.89476;
P_C = P_TVC*6.89476;
P_P = P_MOT*6.89476;

ENT_K1 = (0.65*(P_E^3.26)*(P_C^6.79E-2)/(9.32 + 0.128*(P_C^1.14)))*22.82;
ENT_K2 = (0.65*(P_E^3.26)*(P_C^6.79E-2)/(9.32 + 0.128*(P_C^1.14)))*4.21E-4;

ENT_R = ENT_K1*(P_P^-1.54) + ENT_K2*(P_P^-0.2);

!Calculation for average Cp of seawater feed;
X_SALT = 0.99886*@SUM(COMP(K): X_FEED(K));!Seawater conc.   (0.99886*ppm/1000) [g/L];
X_SAL  = @SUM(COMP(K): X_FEED(K));          !Seawater salinity (ppm/1000)  [g/kg];

T_SEA_CEL = (T_SEA - 32)/1.8;
TEFF_CEL = (T_EFF(N_EFF) - 32)/1.8;
DENS_WATER     = 1E-3*(1E3 + 2.7099E-2*T_SEA_CEL - 6.6452E-3*T_SEA_CEL^2 + 2.97035E-
5*T_SEA_CEL^3 - 7.62746E-8*T_SEA_CEL^4);    !Water density [kg/L];
DENS_WATER_EFF = 1E-3*(1E3 + 2.7099E-2*TEFF_CEL - 6.6452E-3*TEFF_CEL^2 + 2.97035E-
5*TEFF_CEL^3 - 7.62746E-8*TEFF_CEL^4);      !Water density [kg/L];


CP_A = (5.328 - 9.76E-2*X_SAL + 4.04E-4*X_SAL^2)*0.238846;      !Seawater Cp [Btu/lb-F];
CP_B = (-6.913E-3 + 7.351E-4*X_SAL - 3.15E-6*X_SAL^2)*0.238846;
CP_C = (9.6E-6 - 1.927E-6*X_SAL + 8.23E-9*X_SAL^2)*0.238846;
CP_D = (2.5E-9 + 1.666E-9*X_SAL - 7.125E-12*X_SAL^2)*0.238846;

CP_T_SEA_MIN  = ((T_SEA - 32)/1.8) + 273.15;
CP_T_SEA_MAX  = ((T_EFF(N_EFF) - DTMIN - 32)/1.8) + 273.15;

CP_SEA_MIN = CP_A + CP_B*CP_T_SEA_MIN + CP_C*CP_T_SEA_MIN^2 +
CP_D*CP_T_SEA_MIN^3;
CP_SEA_MAX = CP_A + CP_B*CP_T_SEA_MAX + CP_C*CP_T_SEA_MAX^2 +
CP_D*CP_T_SEA_MAX^3;

CP_SEA_AVG = 0.5*(CP_SEA_MIN + CP_SEA_MAX);

!Heat transfer coefficient of evaporator and condenser;
@FOR(EFFECTS(I): U_EFF(I) = 176.11*(1.9394 + 1.40562E-3*((T_EFF(I) - 32)/1.8) - 2.0752E-
4*((T_EFF(I) - 32)/1.8)^2 + 2.3186E-6*((T_EFF(I) - 32)/1.8)^3));
```

```
U_COND  = 176.11*(1.6175 + 0.1537E-3*((T_C(N_EFF) - 32)/1.8) + 0.1825E-3*((T_C(N_EFF) -
32)/1.8)^2 - 8.026E-8*((T_C(N_EFF) - 32)/1.8)^3);
U_BRINE = 176.11*(1.262650391 + 1.0945838E-2*((0.5*(T_EFF(N_EFF) + T_EFF_I(N_EFF)) -
32)/1.8) + 1.1928024E-2*((T_SEA - 32)/1.8));
U_DIST  = 176.11*(1.418251642 + 1.1383865E-2*((0.5*(T_C(N_EFF) + T_EFF_II(N_EFF - 1)) -
32)/1.8) + 1.3381501E-2*((T_SEA - 32)/1.8));

DT_EFF_VAP(1) = TC_TVC - T_EFF(1);
@FOR(EFFECTS(I)|I#GE#2: DT_EFF_VAP(I) = T_C(I-1) - T_EFF(I));


!****************************** CALC SECTION FOR RO MODEL **********************;
RO_FEED_TEMP = (T_SEA_IN - 32)/1.8;
PERM_PSI_MAX  = @LOG(91.345/(91.345- (100 - 100*(1 - PERM_REC_MAX)^6)))/0.8265;
BRINE_PSI_MAX = @LOG(91.345/(91.345- (100 - 100*(1 - BRINE_REC_MAX)^6)))/0.8265;

RO_TCF = @EXP(3020*((1/298) - (1/(273 + RO_FEED_TEMP))));
@FOR(SINK(J): RO_MOD_DP(J) = RO_DP_MAX);
@FOR(SINK(J): RO_P_P(J)    = P_FEED);

! RO CONFIGURATION ----------------------------------------------------------------------------------------------------;
!Configuration 1.;
RO_PSI_MAX(1)     = BRINE_PSI_MAX;
RO_PERM_BIN3(1) = 1;

@FOR(SOURCE(I):@FOR(SINK(J)|I#EQ#J: F_BS(I,J) = 0));
@FOR(SOURCE(I):@FOR(SINK(J)|I#EQ#J: F_PS(I,J) = 0));

!********************** BOILER CALC FOR COGEN-HEN MODEL **********************;
NP_BOIL_HP   = 7E-4*(P_HP - 14.6959) + 0.6;
NT_BOIL_HP   = 1.5E-6*DT_SUPER^2 + 1.13E-3*DT_SUPER + 1;
NT_BOIL_SUP  = 1.5E-6*(T_MAX - TSAT_HP)^2 + 1.13E-3*(T_MAX - TSAT_HP) + 1;

!Calculation section for objective function coefficients;
CO_TURB        = C_REF_TURB/PLANT_LIFE*(0.293071E-3)^EXP_TURB;
CO_POT         = CO_TANK;
POT_EXP        = EXP_TANK;
HEX_EXP        = EXP_HEX (9,1);
CO_HEX_MED  = CO_HEX(9,1);
ENDCALC

!-------------------------------------------------------------------------------------------------------------------;
!***************************** Objective function to minimize cost *****************************;
!-------------------------------------------------------------------------------------------------------------------;
CALC:
KOBJ1 = C_ELECT*1E-3*24*365;
KOBJ2 = C_WATER*1E-3*24*365;
KOBJ3 = 0.3*1E-3*24*365*C_FUEL;
KOBJ4 = (1 + CF_FIN + CF_CONTIN + CF_FOC*PLANT_LIFE)*1E-3;
ENDCALC
```

```
MAX = KOBJ1*AVAIL_PW_TOT + KOBJ2*(M_RO_EXPORT + M_MED_EXPORT) -
KOBJ3*(Q_BOIL_TOT + Q_FURN_SUP + Q_FURN_TURB) - KOBJ4*(
@SUM(C_STREAM(I):@SUM(H_STREAM(J)| J#EQ#1:
(CO_HEX(I,J)/PLANT_LIFE)*((1E6/U_HEN(I,J))*Q_HEN(I,J)/DTLM_HEX(I,J))^EXP_HEX(I,J) )) +
@SUM(C_STREAM(I)|I#GE#N_MP: @SUM(H_STREAM(J)|J#GE#2 #AND# J#LE#4:
(CO_HEX(I,J)/PLANT_LIFE)*((1E6/U_HEN(I,J))*Q_HEN(I,J)/DTLM_HEX(I,J))^EXP_HEX(I,J) )) +
@SUM(C_STREAM(I)|I#GE#N_LP: @SUM(H_STREAM(J)|J#GE#5:
(CO_HEX(I,J)/PLANT_LIFE)*((1E6/U_HEN(I,J))*Q_HEN(I,J)/DTLM_HEX(I,J))^EXP_HEX(I,J) )) +

(CO_HEX(7,1)/PLANT_LIFE)*A_VAC_AIR^EXP_HEX(7,1) +
(CO_HEX(8,1)/PLANT_LIFE)*A_VAC_CW^EXP_HEX(8,1) +
(CO_HEX(9,1)/PLANT_LIFE)*A_VAC_SEA^EXP_HEX(9,1) +

(CO_HEX(9,1)/PLANT_LIFE)*A_E_205^EXP_HEX(9,1) +
(CO_HEX(9,1)/PLANT_LIFE)*A_E_206^EXP_HEX(9,1) +
(CO_HEX(7,1)/PLANT_LIFE)*A_E_502^EXP_HEX(7,1) +


CO_TURB*(K_DR_HP*W_SHAFT_HP_MP)^EXP_TURB +
CO_TURB*(K_DR_HPMP*W_SHAFT_HP_LP)^EXP_TURB +
CO_TURB*(K_DR_HPLP*W_SHAFT_HP_VAC)^EXP_TURB +
CO_TURB*(K_DR_MP*W_SHAFT_MP_LP)^EXP_TURB +
CO_TURB*(K_DR_MPLP*W_SHAFT_MP_VAC)^EXP_TURB +

(3*NP_BOIL_HP*NT_BOIL_HP)/PLANT_LIFE*(1E6*Q_BOIL_TOT)^EXP_BOIL +
(3*NP_BOIL_HP*NT_BOIL_HP)/PLANT_LIFE*(1E6*Q_FURN_SUP)^EXP_BOIL +
(3*NP_BOIL_HP*NT_BOIL_SUP)/PLANT_LIFE*(1E6*Q_FURN_TURB)^EXP_BOIL +

CO_CT/PLANT_LIFE*(2000/62.43*M_CW_COGEN)^EXP_CT +

CO_TANK/PLANT_LIFE*(2000/60/62.43*M_LP_BFW)^EXP_TANK +
CO_TANK/PLANT_LIFE*(2000/60/62.43*M_MP_BFW)^EXP_TANK +
CO_TANK/PLANT_LIFE*(2000/60/62.43*10*LP_BFW_HOLD)^EXP_TANK +
CO_TANK/PLANT_LIFE*(2000/60/62.43*10*MP_BFW_HOLD)^EXP_TANK +
CO_TANK/PLANT_LIFE*(2000/60/62.43*10*HP_BFW_HOLD)^EXP_TANK + CC_COGEN_PUMP )


!MED TOTAL ANNUALIZED COST;
- TAC_DESAL - (1 + CF_FIN + CF_PERM + CF_CONTIN + CF_FOC*PLANT_LIFE)*(
(1E-
3*CO_EVAP/PLANT_LIFE)*(Q_COND/((U_COND/3600)*(0.5*DT_COND_PRE*DT1_COND_PRE*
(DT_COND_PRE + DT1_COND_PRE))^(1/3)))^EVAP_EXP +
(1E-
3*CO_HEX_MED/PLANT_LIFE)*(Q_BRINE/((U_BRINE/3600)*(0.5*DT_BRINE_PRE*DT1_BRINE
_PRE*(DT_BRINE_PRE + DT1_BRINE_PRE))^(1/3)))^HEX_EXP +
(1E-
3*CO_HEX_MED/PLANT_LIFE)*(Q_DIST/((U_DIST/3600)*(0.5*DT_DIST_PRE*DT1_DIST_PRE*(
DT_DIST_PRE + DT1_DIST_PRE))^(1/3)))^HEX_EXP +
@SUM(EFFECTS(I):(1E-3*CO_EVAP/PLANT_LIFE)*(A_EFF_VAP(I) +
Q_EFF_SENS(I)/((U_EFF(I)/3600)*(0.5*DT_EFF_SENS(I)*DT1_EFF_SENS(I)*(DT_EFF_SENS(I) +
DT1_EFF_SENS(I)))^(1/3)))^EVAP_EXP) +

(1E-3*CO_EJECTOR/PLANT_LIFE)*(3600*M_STM_DIS)^EJ_EXP +
```

```
(1E-3*CO_POT/PLANT_LIFE)*(60*M_COND_TVC/62.43)^POT_EXP +
@SUM(EFFECTS(I): (1E-3*CO_POT/PLANT_LIFE)*(60*M_DIST(I)/62.43)^POT_EXP) )

- TAC_DESAL_RO;

M_SALT(1)*(1000 - X_EFF_MAX(1)) <= X_EFF_MAX(1)*M_WATER(1); !Max. conc. constraint in
effect;
@FOR(EFFECTS(I)|I#GE#2: M_SALT(I)*(1000 - X_EFF_MAX(I))  <=
X_EFF_MAX(I)*M_WATER(I)); !Max. conc. constraint in effect;

!=========================================================================
************************ COGEN-HEN MODELING SECTION ************************
=========================================================================;
!Hot stream HEX heat balance;
@FOR(C_STREAM(I): @FOR(H_STREAM(J)|J#EQ#1: FCP(J)*(TH(I,J)-TH1(I,J)) = Q_HEN(I,J)));
@FOR(C_STREAM(I)|I#GE#N_MP: @FOR(H_STREAM(J)|J#EQ#2: FCP(J)*(TH(I,J)-TH1(I,J)) =
Q_HEN(I,J)));

@FOR(C_STREAM(I)|I#GE#N_MP: @FOR(H_STREAM(J)|J#EQ#3: FCP(J)*(TH(I,J)-TH1(I,J)) =
Q_HEN(I,J)));
@FOR(C_STREAM(I)|I#GE#N_MP: @FOR(H_STREAM(J)|J#EQ#4: (TH(I,J)-TH1(I,J)) =
(1/FCP(J))*Q_HEN(I,J)));
@FOR(C_STREAM(I)|I#GE#N_LP: @FOR(H_STREAM(J)|J#EQ#5: (TH(I,J)-TH1(I,J)) =
(1/FCP(J))*Q_HEN(I,J)));

!Hot stream overall heat balance;
@FOR(H_STREAM(J)|J#EQ#1: @SUM(C_STREAM(I): @SUM(H_STREAM(J)|J#EQ#1:
Q_HEN(I,J))) = FCP(J)*(T_SYN_IN - T_SYN_OUT));

@FOR(H_STREAM(J)|J#EQ#2: @SUM(C_STREAM(I)|I#GE#N_MP: @SUM(H_STREAM(J)|J#EQ#2:
Q_HEN(I,J))) = FCP(J)*(T_HO_IN - T_HO_OUT));

@FOR(H_STREAM(J)|J#EQ#3: @SUM(C_STREAM(I)|I#GE#N_MP: @SUM(H_STREAM(J)|J#EQ#3:
Q_HEN(I,J))) = FCP(J)*(T_FT_VAP_IN - T_FT_VAP_OUT));
@FOR(H_STREAM(J)|J#EQ#4: @SUM(C_STREAM(I)|I#GE#N_MP: @SUM(H_STREAM(J)|J#EQ#4:
Q_HEN(I,J))) = FCP(J)*(T_C_SEP_IN - T_C_SEP_OUT));
@FOR(H_STREAM(J)|J#EQ#5: @SUM(C_STREAM(I)|I#GE#N_LP: @SUM(H_STREAM(J)|J#EQ#5:
Q_HEN(I,J))) = FCP(J)*(T_P_COOL_IN - T_P_COOL_OUT));
@SUM(C_STREAM(I)|I#GE#N_LP: @SUM(H_STREAM(J)|J#EQ#6: Q_HEN(I,J))) =
Q_FRAC_COND;

!Cold stream heat balances;
@FOR(H_STREAM(J)|J#EQ#1: 1000*Q_HEN(1,J) = 2*(HV_HP -
HFSAT_HP)*M_HP_SAT(J));!Vaporizing HP-BFW;
@FOR(H_STREAM(J)|J#EQ#1: 1000*Q_HEN(2,J) = 2*(HFSAT_HP -
HFSAT_MP)*M_MP_HP(J));!Preheating MP-HP BFW;

@FOR(H_STREAM(J)|J#LE#4: 1000*Q_HEN(3,J) = 2*(HV_MP -
HFSAT_MP)*M_MP_SAT(J));!Vaporizing MP-BFW;
@FOR(H_STREAM(J)|J#LE#4: 1000*Q_HEN(4,J) = 2*(HFSAT_MP -
HFSAT_LP)*M_LP_MP(J));!Preheating LP-MP BFW;
@FOR(H_STREAM(J): 1000*Q_HEN(N_LP,J)     = 2*(HV_LP -
HFSAT_LP)*M_LP_SAT(J));!Vaporizing LP-BFW;
```

```
!Preheating VAC/FW/MED-COND;
HFSAT_MED*M_MED_LP = (3600/2000)*@SUM(EFFECTS(I): M_BFW(I)*HF_II(I));
@FOR(H_STREAM(J): 1000*Q_HEN(6,J) = 2*HFSAT_LP*(M_MED_COND(J) + M_FW(J) +
M_VAC(J)) - 2*(HFSAT_MED*M_MED_COND(J) + HF_FW*M_FW(J) +
HFSAT_VAC*M_VAC(J)));

!Utilities cooling requirements;
@SUM(H_STREAM(J): Q_HEN(7,J)) = Q_AIR_PROC;        !Cooling requirement [MMBtu/hr];
@SUM(H_STREAM(J): Q_HEN(8,J)) = Q_CW_PROC;
@SUM(H_STREAM(J): Q_HEN(9,J)) = Q_SEA_PROC;

Q_COOL_PROC_TOT = Q_AIR_PROC + Q_CW_PROC + Q_SEA_PROC;

!Mass balance on HEN;
@SUM(H_STREAM(J): M_MED_COND(J) + M_FW(J) + M_VAC(J)) =  @SUM(H_STREAM(J):
M_LP_SAT(J)) + @SUM(H_STREAM(J): M_LP_MP(J)) + M_LP_BFW + M_LP_BOIL;
@SUM(H_STREAM(J): M_LP_MP(J))   + M_MPC_RET =  @SUM(H_STREAM(J): M_MP_SAT(J)) +
@SUM(H_STREAM(J): M_MP_HP(J)) + M_MP_BFW + M_MP_BOIL ;
@SUM(H_STREAM(J): M_MP_HP(J))   + M_HPC_RET =  @SUM(H_STREAM(J): M_HP_SAT(J)) +
M_HP_BOIL;

@SUM(H_STREAM(J): M_VAC(J))  = M_HP_VAC + M_MP_VAC;
@SUM(H_STREAM(J): M_FW(J))    = M_ATR;
@SUM(H_STREAM(J): M_MED_COND(J)) = M_MED_LP;
@SUM(H_STREAM(J): M_MED_COND(J)) = (3600/2000)*@SUM(EFFECTS(I): M_BFW(I));
@SUM(H_STREAM(J): M_LP_SAT(J))   = M_LPS_HEN;
@SUM(H_STREAM(J): M_MP_SAT(J))   = M_MPS_HEN;
@SUM(H_STREAM(J): M_HP_SAT(J))   = M_HPS_HEN;

!BFW HOLD-UP;
LP_BFW_HOLD = @SUM(H_STREAM(J): M_MED_COND(J) + M_FW(J) + M_VAC(J));
MP_BFW_HOLD = @SUM(H_STREAM(J): M_LP_MP(J))   + M_MPC_RET;
HP_BFW_HOLD = @SUM(H_STREAM(J): M_MP_HP(J))   + M_HPC_RET;

!HPS HEADER BALANCE;
M_HPS_HEADER = M_HPS_HEN + M_HP_BOIL;
M_HPS_HEADER = M_ATR + M_HPS_REQ + M_HPS_TURB;
M_HPS_REQ    = M_HPC_RET;

!MPS HEADER BALANCE;
M_MPS_HEADER = M_MPS_HEN + M_MP_BOIL + M_HPS_MP_TURB + M_MP_BFW;
M_MPS_HEADER = M_MPS_REQ + M_MPS_TURB;
M_MPS_REQ    = M_MPC_RET;

!LPS HEADER BALANCE;
M_LPS_HEADER = M_LPS_HEN + M_LP_BOIL + M_HPS_LP_TURB + M_MPS_LP_TURB +
M_LP_BFW;
M_LPS_HEADER = M_MED_LP;

!De-superheating of turbine exhaust steam for LP steam to MED plant;
M_HPS_MP_TURB*H_HP_MP + M_MP_BFW*HFSAT_MP = (M_HPS_MP_TURB +
M_MP_BFW)*H_MP;
```

```
!De-superheating of turbine exhaust steam for LP steam to MED plant;
M_HPS_LP_TURB*H_HP_VAC  + M_MPS_LP_TURB*H_MP_VAC + M_LP_BFW*HFSAT_LP =
(M_HPS_LP_TURB + M_MPS_LP_TURB + M_LP_BFW)*H_LP;

!Furnace/ Boiler Superheating balance;
Q_FUEL_AVAIL = Q_HPS_SUP + Q_MPS_SUP + Q_LPS_SUP + Q_HPS_TURB + Q_MPS_TURB +
Q_HP_BOIL + Q_MP_BOIL + Q_LP_BOIL + Q_FUEL_XS;

!Superheated steam for process heat balance;
500*Q_HPS_SUP = (H_HP - HV_HP)* M_HPS_HEN;
500*Q_MPS_SUP = (H_MP - HV_MP)* M_MPS_HEN;
500*Q_LPS_SUP = (H_LP - HV_LP)* M_LPS_HEN;

!Superheated steam for turbines heat balance;
500*Q_HPS_TURB = M_HPS_TURB*H_HP_TURB - M_HPS_TURB*H_HP;!Balance for superheating
HPS for LP let down turbines;
H_HP_TURB       = (0.2029*TSAT_HP)*S_HP_TURB^3.647 + 817.35;
S_HP_TURB    <= S_HP_MAX;

500*Q_MPS_TURB = M_MPS_TURB*H_MP_TURB - M_MPS_TURB*H_MP;!Balance for
superheating MPS for LP let down turbines;
H_MP_TURB       = (0.2029*TSAT_MP)*S_MP_TURB^3.647 + 817.35;
S_MP_TURB    <= S_MP_MAX;

!Steam from boilers;
500*Q_HP_BOIL = (H_HP - HFSAT_HP)*M_HP_BOIL;   !HP BOILER/SUPERHAETER BALANCE;
500*Q_MP_BOIL = (H_MP - HFSAT_MP)*M_MP_BOIL;!MP BOILER/SUPERHAETER BALANCE;
500*Q_LP_BOIL = (H_LP - HFSAT_LP)*M_LP_BOIL;    !MP BOILER/SUPERHAETER BALANCE;

!HEAT BALANCE FOR BOILER AND FURNACE;
Q_BOIL_TOT    = Q_HP_BOIL  + Q_MP_BOIL + Q_LP_BOIL;
Q_FURN_SUP    = Q_HPS_SUP  + Q_MPS_SUP + Q_LPS_SUP;
Q_FURN_TURB = Q_HPS_TURB + Q_MPS_TURB;

!Temperature feasibility;
@FOR(C_STREAM(I):@FOR(H_STREAM(J)| J#EQ#1: TH(I,J) >= TH1(I,J)));
@FOR(C_STREAM(I)|I#GE#N_MP: @FOR(H_STREAM(J)|J#LE#4: TH(I,J)   >= TH1(I,J)));
@FOR(C_STREAM(I)|I#GE#N_LP: @FOR(H_STREAM(J)|J#GE#5: TH(I,J)   >= TH1(I,J)));

!End temperature feasibility;
TH(N_COLD,1) >= T_SYN_OUT;
TH(N_COLD,2) >= T_HO_OUT;
TH(N_COLD,3) >= T_FT_VAP_OUT;
TH(N_COLD,4) >= T_C_SEP_OUT;
TH(N_COLD,5) >= T_P_COOL_OUT;
TH(N_COLD,6) >= T_FRAC_OUT;

!Matching of stage(I) outlet temperature TH with stage(I+1) inlet temperature based on notation;
@FOR(C_STREAM(I)|I#GE#2 #AND# I#LE#N_COLD:@FOR(H_STREAM(J)|J#EQ#1: TH(I,J) =
TH1(I-1,J)));
@FOR(C_STREAM(I)|I#GE#N_MP+1 #AND# I#LE#N_COLD:@FOR(H_STREAM(J)|J#LE#4: TH(I,J)
= TH1(I-1,J)));
```

```
@FOR(C_STREAM(I)|I#GE#N_LP+1 #AND# I#LE#N_COLD:@FOR(H_STREAM(J)|J#GE#5: TH(I,J)
= TH1(I-1,J)));

!HEX temperature approaches and constraints;
@FOR(C_STREAM(I):@FOR(H_STREAM(J)|J#EQ#1: @EXP(LOG_DTH(I,J))  <= TH(I,J)  - TC1(I)));
@FOR(C_STREAM(I):@FOR(H_STREAM(J)|J#EQ#1: @EXP(LOG_DTH1(I,J)) <= TH1(I,J) - TC(I)));

@FOR(C_STREAM(I)|I#GE#N_MP:@FOR(H_STREAM(J)|J#LE#4: @EXP(LOG_DTH(I,J))  <=
TH(I,J)  - TC1(I)));
@FOR(C_STREAM(I)|I#GE#N_MP:@FOR(H_STREAM(J)|J#LE#4: @EXP(LOG_DTH1(I,J)) <=
TH1(I,J) - TC(I)));

@FOR(C_STREAM(I)|I#GE#N_LP:@FOR(H_STREAM(J)|J#GE#5: @EXP(LOG_DTH(I,J))  <=
TH(I,J)  - TC1(I)));
@FOR(C_STREAM(I)|I#GE#N_LP:@FOR(H_STREAM(J)|J#GE#5: @EXP(LOG_DTH1(I,J)) <=
TH1(I,J) - TC(I)));

!HEX temperature approaches and constraints;
@FOR(C_STREAM(I):@FOR(H_STREAM(J)|J#EQ#1: @EXP(LOG_SUMDTH(I,J)) <= TH1(I,J) -
TC(I) + TH(I,J)  - TC1(I)));
@FOR(C_STREAM(I)|I#GE#N_MP:@FOR(H_STREAM(J)|J#LE#4:   @EXP(LOG_SUMDTH(I,J)) <=
TH1(I,J) - TC(I) + TH(I,J)  - TC1(I)));
@FOR(C_STREAM(I)|I#GE#N_LP:@FOR(H_STREAM(J)|J#GE#5:   @EXP(LOG_SUMDTH(I,J)) <=
TH1(I,J) - TC(I) + TH(I,J)  - TC1(I)));

!Approach temperature constraints;
@FOR(C_STREAM(I):@FOR(H_STREAM(J)|J#EQ#1: LOG_DTH(I,J)  >=
@LOG(DTMIN_HEX(I,J))));
@FOR(C_STREAM(I):@FOR(H_STREAM(J)|J#EQ#1: LOG_DTH1(I,J) >=
@LOG(DTMIN_HEX(I,J))));

@FOR(C_STREAM(I)|I#GE#N_MP:@FOR(H_STREAM(J)|J#LE#4: LOG_DTH(I,J)  >=
@LOG(DTMIN_HEX(I,J))));
@FOR(C_STREAM(I)|I#GE#N_MP:@FOR(H_STREAM(J)|J#LE#4: LOG_DTH1(I,J) >=
@LOG(DTMIN_HEX(I,J))));

@FOR(C_STREAM(I)|I#GE#N_LP:@FOR(H_STREAM(J)|J#GE#5: LOG_DTH(I,J)  >=
@LOG(DTMIN_HEX(I,J))));
@FOR(C_STREAM(I)|I#GE#N_LP:@FOR(H_STREAM(J)|J#GE#5: LOG_DTH1(I,J) >=
@LOG(DTMIN_HEX(I,J))));

!HEX DTLM CALCULATION;
@FOR(C_STREAM(I):@FOR(H_STREAM(J)|J#EQ#1: 3*LOG_DTLM(I,J) = LOG_DTH(I,J) +
LOG_DTH1(I,J) + LOG_SUMDTH(I,J) - @LOG(2)));
@FOR(C_STREAM(I)|I#GE#N_MP:@FOR(H_STREAM(J)|J#LE#4:   3*LOG_DTLM(I,J) =
LOG_DTH(I,J) + LOG_DTH1(I,J) + LOG_SUMDTH(I,J) - @LOG(2)));!ADJUST HOT STREAM;
@FOR(C_STREAM(I)|I#GE#N_LP:@FOR(H_STREAM(J)|J#GE#5:   3*LOG_DTLM(I,J) =
LOG_DTH(I,J) + LOG_DTH1(I,J) + LOG_SUMDTH(I,J) - @LOG(2)));

!HEX DTLM CALCULATION;
@FOR(C_STREAM(I):@FOR(H_STREAM(J)|J#EQ#1:                DTLM_HEX(I,J) <=
@EXP(LOG_DTLM(I,J))));
```

```
@FOR(C_STREAM(I)|I#GE#N_MP:@FOR(H_STREAM(J)|J#LE#4:   DTLM_HEX(I,J) <=
@EXP(LOG_DTLM(I,J))));
@FOR(C_STREAM(I)|I#GE#N_LP:@FOR(H_STREAM(J)|J#GE#5:   DTLM_HEX(I,J) <=
@EXP(LOG_DTLM(I,J))));

!=========================================================================
********************** TURBINE CONFIGURATION SECTION **********************
=========================================================================;
@FREE(K1_HP);
@FREE(K2_HP);
@FREE(K1_HPMP);
@FREE(K2_HPMP);
@FREE(K1_HPLP);
@FREE(K2_HPLP);

@FREE(K1_MP);
@FREE(K2_MP);
@FREE(K1_MPLP);
@FREE(K2_MPLP);

K1_HP   = (6/(5*TURB_B_HP))*(3.41214E6*TURB_A_HP)*(1/K_DR_HP) -
(1/(5*TURB_B_HP))*(3.41214E6*TURB_A_HP) ;
K2_HP   = (6/(5*TURB_B_HP)) - (1/(5*TURB_B_HP))*K_DR_HP;
K1_HPMP = (6/(5*TURB_B_MP))*(3.41214E6*TURB_A_MP)*(1/K_DR_HPMP) -
(1/(5*TURB_B_MP))*(3.41214E6*TURB_A_MP) ;
K2_HPMP = (6/(5*TURB_B_MP)) - (1/(5*TURB_B_MP))*K_DR_HPMP;
K1_HPLP = (6/(5*TURB_B_LP))*(3.41214E6*TURB_A_LP)*(1/K_DR_HPLP) -
(1/(5*TURB_B_LP))*(3.41214E6*TURB_A_LP) ;
K2_HPLP = (6/(5*TURB_B_LP)) - (1/(5*TURB_B_LP))*K_DR_HPLP;

K1_MP   = (6/(5*TURB_B_MP))*(3.41214E6*TURB_A_MP)*(1/K_DR_MP) -
(1/(5*TURB_B_MP))*(3.41214E6*TURB_A_MP) ;
K2_MP   = (6/(5*TURB_B_MP)) - (1/(5*TURB_B_MP))*K_DR_MP;
K1_MPLP = (6/(5*TURB_B_LP))*(3.41214E6*TURB_A_LP)*(1/K_DR_MPLP) -
(1/(5*TURB_B_LP))*(3.41214E6*TURB_A_LP) ;
K2_MPLP = (6/(5*TURB_B_LP)) - (1/(5*TURB_B_LP))*K_DR_MPLP;

K_DR_HP       >= 1;                    !The minimum design ratio is 100%;
K_DR_HPMP     >= 1;
K_DR_HPLP     >= 1;
K_DR_MP       >= 1;
K_DR_MPLP     >= 1;

K_DR_HP       <= K_DR_MAX;             !The maximum design ratio;
K_DR_HPMP     <= K_DR_MAX;
K_DR_HPLP     <= K_DR_MAX;
K_DR_MP       <= K_DR_MAX;
K_DR_MPLP     <= K_DR_MAX;

!------------------------------------ (HP--MP-LP-VAC TURBINE) ----------------------------------------------;
!HP to MP STEAM TURBINE;
H_IS_HP_MP  = (0.2029*TSAT_MP)*S_HP_TURB^3.647 + 817.35;
```

```
0.5*W_SHAFT_HP_MP + (K1_HP/2E3)  = K2_HP*M_HPS_TURB*DH_IS_HP_MP; !Power scaled in
1000Btu/hr;
W_SHAFT_HP_MP = 2*M_HPS_TURB*DH_A_HP_MP;

DH_IS_HP_MP = H_HP_TURB - H_IS_HP_MP;
DH_A_HP_MP  = H_HP_TURB - H_HP_MP;                                  !Exit enthalpy;

H_HP_MP         = (0.2029*TSAT_MP)*S_HP_MP^3.647 + 817.35;          !Exit entropy;

M_HPS_TURB   = M_HPS_MP_TURB + M_HP_LP;


H_IS_HP = K_IS_FACTOR*(S_HP_TURB - SF_VAC) + HFSAT_VAC; !Constraints to ensure
isentropic efficiency does not exceed max;
(TURB_B_HP - 1)*H_HP_TURB <= TURB_B_HP*HV_VAC - H_IS_HP; !Constraints to ensure
isentropic efficiency does not exceed max;


!MP to LP STEAM TURBINE;
H_IS_HP_LP  = (0.2029*TSAT_LP)*S_HP_MP^3.647 + 817.35;

0.5*W_SHAFT_HP_LP + (K1_HPMP/2E3)  = K2_HPMP*M_HP_LP*DH_IS_HP_LP;  !Power scaled in
1000Btu/hr;
W_SHAFT_HP_LP = 2*M_HP_LP*DH_A_HP_LP;

DH_IS_HP_LP = H_HP_MP - H_IS_HP_LP;
DH_A_HP_LP  = H_HP_MP - H_HP_VAC;                                   !Exit enthalpy;

H_HP_VAC        = (0.2029*TSAT_LP)*S_HP_VAC^3.647 + 817.35;         !Exit entropy;

M_HP_LP         = M_HPS_LP_TURB + M_HP_VAC;


H_IS_HPMP = K_IS_FACTOR*(S_HP_MP - SF_VAC) + HFSAT_VAC;!Constraints to ensure
isentropic efficiency does not exceed max;
(TURB_B_MP - 1)*H_HP_MP <= TURB_B_MP*HV_VAC - H_IS_HPMP;!Constraints to ensure
isentropic efficiency does not exceed max;


!LP to VAC STEAM TURBINE;
STM_QUAL_IS_HP*(SV_VAC - SF_VAC) = 100*S_HP_VAC - 100*SF_VAC;
H_IS_HP_VAC = (STM_QUAL_IS_HP/100)*(HV_VAC - HFSAT_VAC) + HFSAT_VAC;

0.5*W_SHAFT_HP_VAC + (K1_HPLP/2E3) = K2_HPLP*M_HP_VAC*DH_IS_HP_VAC;!Power
scaled in 1000Btu/hr;
W_SHAFT_HP_VAC = 2*M_HP_VAC*DH_A_HP_VAC;

DH_IS_HP_VAC = H_HP_VAC - H_IS_HP_VAC;
DH_A_HP_VAC  = H_HP_VAC - HV_VAC;                                   !Exit enthalpy;

STM_QUAL_IS_HP >= STM_QUAL_MIN;
```

```
H_IS_HPLP = K_IS_FACTOR*(S_HP_VAC - SF_VAC) + HFSAT_VAC;!Constraints to ensure
isentropic efficiency does not exceed max;
(TURB_B_LP - 1)*H_HP_VAC <= TURB_B_LP*HV_VAC - H_IS_HPLP;!Constraints to ensure
isentropic efficiency does not exceed max;

S_HP_TURB <= S_HP_MP;
S_HP_MP   <= S_HP_VAC;
S_HP_VAC  <= SV_VAC;

!---------------------------------------- (MP-LP-VAC TURBINE) ----------------------------------------------------;
!MP to LP STEAM TURBINE;
H_IS_MP_LP  = (0.2029*TSAT_LP)*S_MP_TURB^3.647 + 817.35;

0.5*W_SHAFT_MP_LP + (K1_MP/2E3)  = K2_MP*M_MPS_TURB*DH_IS_MP_LP;  !Power scaled in
1000Btu/hr;
W_SHAFT_MP_LP = 2*M_MPS_TURB*DH_A_MP_LP;

DH_IS_MP_LP = H_MP_TURB - H_IS_MP_LP;
DH_A_MP_LP  = H_MP_TURB - H_MP_VAC;                                    !Exit enthalpy;

H_MP_VAC       = (0.2029*TSAT_LP)*S_MP_VAC^3.647 + 817.35;             !Exit entropy;

M_MPS_TURB  = M_MPS_LP_TURB + M_MP_VAC;


H_IS_MP = K_IS_FACTOR*(S_MP_TURB - SF_VAC) + HFSAT_VAC;!Constraints to ensure
isentropic efficiency does not exceed max;
(TURB_B_MP - 1)*H_MP_TURB <= TURB_B_MP*HV_VAC - H_IS_MP;!Constraints to ensure
isentropic efficiency does not exceed max;


!LP to VAC STEAM TURBINE;
STM_QUAL_IS_MP*(SV_VAC - SF_VAC) = 100*S_MP_VAC - 100*SF_VAC;
H_IS_MP_VAC = (STM_QUAL_IS_MP/100)*(HV_VAC - HFSAT_VAC) + HFSAT_VAC;

0.5*W_SHAFT_MP_VAC + (K1_MPLP/2E3) = K2_MPLP*M_MP_VAC*DH_IS_MP_VAC;!Power
scaled in 1000Btu/hr;
   W_SHAFT_MP_VAC = 2*M_MP_VAC*DH_A_MP_VAC;

DH_IS_MP_VAC = H_MP_VAC - H_IS_MP_VAC;
DH_A_MP_VAC  = H_MP_VAC - HV_VAC;                                      !Exit enthalpy;

STM_QUAL_IS_MP >= STM_QUAL_MIN;


H_IS_MPLP = K_IS_FACTOR*(S_MP_VAC - SF_VAC) + HFSAT_VAC; !Constraints to ensure
isentropic efficiency does not exceed max;
(TURB_B_LP - 1)*H_MP_VAC <= TURB_B_LP*HV_VAC - H_IS_MPLP; !Constraints to ensure
isentropic efficiency does not exceed max;

S_MP_TURB <= S_MP_VAC;
S_MP_VAC  <= SV_VAC;
```

```
!Condensing turbine exhaust cooling;
(HV_VAC - HFSAT_VAC)*(M_HP_VAC + M_MP_VAC)  = 500*(Q_VAC_AIR + Q_VAC_CW +
Q_VAC_SEA);

A_VAC_AIR = Q_VAC_AIR*1E6/(U_VAC_AIR*DTLM_VAC_AIR);
A_VAC_CW  = Q_VAC_CW*1E6 /(U_VAC_AIR*DTLM_VAC_CW);
A_VAC_SEA = Q_VAC_SEA*1E6/(U_VAC_AIR*DTLM_VAC_SEA);

!Total cooling requirement of each option;
Q_AIR_TOTAL = Q_AIR_PROC + Q_VAC_AIR + Q_E_502_TOT;
Q_CW_TOTAL  = Q_CW_PROC  + Q_VAC_CW;
Q_SEA_TOTAL = Q_SEA_PROC + Q_VAC_SEA + Q_E_205_TOT + Q_E_206_TOT;

!Cooling Tower (CT) water loss / make-up;
2*CT_WATER_LOSS = Q_CW_TOTAL;
                  !Water make-up is 1 lb/1000Btu cooling [ton/hr];
(T_CWR - T_CWS)*M_CW_COGEN = (1E6/2000)*Q_CW_TOTAL;
          !Assumes CW SHC = 1 Btu/lb-F;
(PUMP_EFF/100)*145.038*CW_COOL_PUMP  =
1/(2.20462*DENS_WATER)*DP_CW*(2000/3600)*M_CW_COGEN;

!Seawater cooling for Cogen-HEN unit;
CP_SEA_AVG*(T_SEA_OUT - T_SEA_IN)*M_SEA_COGEN = (1E6/2000)*Q_SEA_TOTAL;

(PUMP_EFF/100)*145.038*SEA_COOL_PUMP  = 1/(2.20462*DENS_WATER)*DP_SEA*(1 -
X_SAL/1000)*(2000/3600)*M_SEA_COGEN;

!pumping requirements for BFW and HEN;
!NOTE THAT CONDENSATE FROM VAC CONDITIONS WOULD HAVE ACTUALLY BE AT
ATM CONDITIONS DUE TO DIPLEG PRESSURE HEAD;
(PUMP_EFF/100)*145.038*HEN_VAC_PUMP   = 1/(2.20462*DENS_WATER)*(P_LP -
P_ATM)*(2000/3600)*@SUM(H_STREAM(J): M_FW(J) + M_VAC(J));
(PUMP_EFF/100)*145.038*HEN_LPMP_PUMP  = 1/(2.20462*DENS_WATER)*(P_MP - P_LP)
*(2000/3600)*@SUM(H_STREAM(J): M_LP_MP(J));
(PUMP_EFF/100)*145.038*HEN_MPHP_PUMP  = 1/(2.20462*DENS_WATER)*(P_HP - P_MP)
*(2000/3600)*@SUM(H_STREAM(J): M_MP_HP(J));

(PUMP_EFF/100)*145.038*MPCOND_PUMP          =
1/(2.20462*DENS_WATER)*COND_DP*(2000/3600)*M_MPC_RET;
(PUMP_EFF/100)*145.038*HPCOND_PUMP    =
1/(2.20462*DENS_WATER)*COND_DP*(2000/3600)*M_HPC_RET;


AVAIL_PW_TOT = 0.293071*(GEN_EFF/100)*(W_SHAFT_HP_MP + W_SHAFT_HP_LP +
W_SHAFT_HP_VAC + W_SHAFT_MP_LP + W_SHAFT_MP_VAC);          !Total power produced
[kW];

!Total power balance for process;
PW_BFW_PUMP  = HEN_VAC_PUMP + HEN_LPMP_PUMP + HEN_MPHP_PUMP +
MPCOND_PUMP + HPCOND_PUMP;
PW_AIR_FAN   = PWREQ_AIR_FAN*Q_AIR_TOTAL;
                                                !Total power requirement [kW];
PW_CT_FAN      = PWREQ_CT_FAN*Q_CW_TOTAL;
```

```
PW_CT_PUMP    = CW_COOL_PUMP;
PW_SEA_PUMP  = SEA_COOL_PUMP;

REQ_PW_PUMP              = PW_BFW_PUMP + PW_CT_PUMP + PW_SEA_PUMP;
PW_HEN_TOTAL = PW_BFW_PUMP + PW_AIR_FAN + PW_CT_FAN + PW_CT_PUMP +
PW_SEA_PUMP;

!Pump costs;
CC_COGEN_PUMP = (50000/PLANT_LIFE) + (234.5/PLANT_LIFE)*REQ_PW_PUMP;

!=========================================================================
********************** MED MODEL CONFIGURATION SECTION **********************
=========================================================================;
!Required product flow;
M_MED_DESAL = 2.20462*DENS_WATER*F_PERM_MED;                    !Mass flow rate [lb/s];
F_PERM_MED  <= F_PERM_MED_MAX;!Largest MED based desalination facility approx 200,000
sum/day [L/s];

!Seawater feed balance;
SEA_WATER*N_EFF = 2.20462*DENS_WATER*F_FEED_MED;                !Flow rate of water in
seawater to each effect assuming water density (1kg/L) [lb/s];
SEA_SALT*(1000 - X_SAL) = X_SAL*SEA_WATER;                      !Flow rate of salt in
seawater to each effect [lb/s];

!TVC balance;
M_STM_MOT = (2000/3600)*M_MED_LP;
M_STM_MOT + M_STM_SUC = M_STM_DIS;
M_STM_SUC = ENT_R*M_STM_MOT;

!Desuperheater balance;
M_STM_MOT*HV_MOT + M_STM_SUC*HV(N_EFF) + @SUM(EFFECTS(I): M_DS(I)*HF_II(I)) =
M_STM_TVC*HV_TVC + M_COND_TVC*HF_TVC;
M_STM_MOT + M_STM_SUC + @SUM(EFFECTS(I): M_DS(I)) = M_STM_TVC + M_COND_TVC;

!Effect one balance;
Q_EFF(1) = M_STM_TVC*(HV_TVC - HC_TVC);              !Latent energy into first effect [Btu/s];
Q_EFF(1) = Q_EFF_VAP(1) + Q_EFF_SENS(1);
Q_EFF(1) + SEA_WATER*HF_SEA + SEA_SALT*HS_SEA + Q_SEA_PRE/N_EFF =
M_SEA_STM(1)*HV(1) + M_SEA_WATER(1)*HF(1) + M_SEA_SALT(1)*HS(1);
Q_EFF_VAP(1) = M_SEA_STM(1)*(HV(1) - HF(1));
Q_EFF_SENS(1)= SEA_WATER*HF(1) + SEA_SALT*HS(1) - (SEA_WATER*HF_SEA +
SEA_SALT*HS_SEA + Q_SEA_PRE/N_EFF);
SEA_WATER + SEA_SALT = M_SEA_STM(1) + M_SEA_WATER(1)+ M_SEA_SALT(1); !Mass
balance on first effect;
SEA_WATER = M_SEA_STM(1) + M_SEA_WATER(1);                      !Water balance;
SEA_SALT  = M_SEA_SALT(1);                                      !Salt balance;

M_SEA_SALT(1) = M_SALT(1);
M_SEA_WATER(1)= M_WATER(1);


M_BRINE_STM(1)        = 0;              !No brine entering first effect therefore no flashing occurs;
M_BRINE_WATER(1)    = 0;
```

```
M_BRINE_SALT(1)        = 0;

!Effect 2 - N balance;
@FOR(EFFECTS(I)|I#GE#2: Q_EFF(I) = M_SEA_STM(I-1)*HV(I-1) + M_BRINE_STM(I-1)*HV_I(I-
1) + MV_POT(I-1)*HV_II(I-1) - (M_SEA_STM(I-1) + M_BRINE_STM(I-1) + MV_POT(I-1))*HC(I-
1));!Latent energy into effect[Btu/hr];
@FOR(EFFECTS(I)|I#GE#2: Q_EFF(I) = Q_EFF_VAP(I) + Q_EFF_SENS(I));

!Vaporization of seawater balance;
@FOR(EFFECTS(I)|I#GE#2: Q_EFF(I) + SEA_WATER*HF_SEA + SEA_SALT*HS_SEA +
Q_SEA_PRE/N_EFF = M_SEA_STM(I)*HV(I) + M_SEA_WATER(I)*HF(I) +
M_SEA_SALT(I)*HS(I));
@FOR(EFFECTS(I)|I#GE#2: Q_EFF_VAP(I) = M_SEA_STM(I)*(HV(I) - HF(I)));
@FOR(EFFECTS(I)|I#GE#2: Q_EFF_SENS(I)= SEA_WATER*HF(I) + SEA_SALT*HS(I) -
(SEA_WATER*HF_SEA + SEA_SALT*HS_SEA + Q_SEA_PRE/N_EFF));

@FOR(EFFECTS(I)|I#GE#2: SEA_WATER + SEA_SALT = M_SEA_STM(I) + M_SEA_WATER(I)+
M_SEA_SALT(I)); !Mass balance on effect HEX;
@FOR(EFFECTS(I)|I#GE#2: SEA_WATER = M_SEA_STM(I) + M_SEA_WATER(I)); !Water balance
on effect HEX;
@FOR(EFFECTS(I)|I#GE#2: SEA_SALT = M_SEA_SALT(I));          !Salt balance on effect HEX;

!Brine flashing in effect balance;
@FOR(EFFECTS(I)|I#GE#2: M_BRINE_WATER(I-1)*HF_I(I-1) + M_BRINE_SALT(I-1)*HS_I(I-1) +
M_SEA_WATER(I-1)*HF(I-1) + M_SEA_SALT(I-1)*HS(I-1) =
                                    M_BRINE_WATER(I)*HF_I(I) + M_BRINE_SALT(I)*HS_I(I) +
M_BRINE_STM(I)*HV_I(I));

@FOR(EFFECTS(I)|I#GE#2: M_BRINE_WATER(I-1) + M_BRINE_SALT(I-1) + M_SEA_WATER(I-
1) + M_SEA_SALT(I-1) = M_BRINE_WATER(I) + M_BRINE_SALT(I) + M_BRINE_STM(I));
@FOR(EFFECTS(I)|I#GE#2: M_BRINE_WATER(I-1) + M_SEA_WATER(I-1) =
M_BRINE_WATER(I) + M_BRINE_STM(I)); !Water balance on brine flashing;
@FOR(EFFECTS(I)|I#GE#2: M_BRINE_SALT(I-1)  + M_SEA_SALT(I-1)  = M_BRINE_SALT(I));
                                          !Salt balance on brine flashing;

@FOR(EFFECTS(I)|I#GE#2: M_BRINE_WATER(I) + M_SEA_WATER(I) = M_WATER(I));
@FOR(EFFECTS(I)|I#GE#2: M_BRINE_SALT(I)  + M_SEA_SALT(I)  = M_SALT(I));

!Effect N steam balance;
M_SEA_STM(N_EFF) = M_STM_SUC + M_STM_COND;
M_SALT(N_EFF)*(1000 - X_BRINE_MAX)   <= X_BRINE_MAX*M_WATER(N_EFF);

!Condenser balance;
Q_COND = M_STM_COND*(HV(N_EFF) - HC(N_EFF)) + M_BRINE_STM(N_EFF)*(HV_I(N_EFF)
- HC(N_EFF));

!Condensate for desuperheater balance;
M_STM_MOT + M_STM_SUC + @SUM(EFFECTS(I):M_DS(I)) = M_DIST(1);
M_STM_TVC + M_COND_TVC = M_DIST(1);

@FOR(EFFECTS(I)|I#GE#2: M_SEA_STM(I-1) + M_BRINE_STM(I-1) + MV_POT(I-1) + MF_POT(I-
1) = M_DIST(I));
```

```
!Flash Pot balance;
M_STM_TVC + M_COND_TVC = MV_POT(1) + MF_POT(1) + M_DS(1) + M_BFW(1);
M_STM_TVC*HC_TVC + M_COND_TVC*HF_TVC = MV_POT(1)*HV_II(1) +
MF_POT(1)*HF_II(1) + M_DS(1)*HF_II(1) + M_BFW(1)*HF_II(1);

@FOR(EFFECTS(I)|I#GE#2 #AND# I#LE#(N_EFF-1): M_DIST(I) = MV_POT(I) + MF_POT(I) +
M_DS(I) + M_BFW(I));
@FOR(EFFECTS(I)|I#GE#2 #AND# I#LE#(N_EFF-1): (M_SEA_STM(I-1) + M_BRINE_STM(I-1) +
MV_POT(I-1))*HC(I-1) + MF_POT(I-1)*HF_II(I-1) = MV_POT(I)*HV_II(I) + MF_POT(I)*HF_II(I) +
M_DS(I)*HF_II(I) + M_BFW(I)*HF_II(I));

MV_POT(N_EFF) = 0;
MF_POT(N_EFF) = 0;

M_DS(1)      = 0;    !Desuperheating condensate does not come from first or last flash pot;
M_DS(N_EFF)  = 0;
M_BFW(N_EFF) = 0;

!BFW return balance;
@SUM(EFFECTS(I):M_BFW(I)) = M_STM_MOT;
@FOR(EFFECTS(I): T_BFW(I) = T_EFF_II(I)); !BFW return temperatures from each flash pot [F];

 !Condensate line;
M_MED_DESAL = M_DIST(N_EFF) + M_STM_COND + M_BRINE_STM(N_EFF); !Sea stm was
used to balance stmsuc and stmcond so add brine_stm;

(M_SEA_STM(N_EFF-1) + M_BRINE_STM(N_EFF-1) + MV_POT(N_EFF-1))*HC(N_EFF-1) +
MF_POT(N_EFF-1)*HF_II(N_EFF-1) + (M_STM_COND + M_BRINE_STM(N_EFF))*HC(N_EFF) =
HF_EX*M_MED_DESAL + Q_DIST;

!Brine line;
M_BRINE = M_WATER(N_EFF) + M_SALT(N_EFF);

M_BRINE_WATER(N_EFF)*HF_I(N_EFF) + M_BRINE_SALT(N_EFF)*HS_I(N_EFF) +
M_SEA_WATER(N_EFF)*HF(N_EFF) + M_SEA_SALT(N_EFF)*HS(N_EFF) =
M_WATER(N_EFF)*HF_EX + M_SALT(N_EFF)*HS_EX + Q_BRINE;

!Overall MED heat & material balance;
H_IN  = M_STM_MOT*HV_MOT + (SEA_WATER*HF_SEA + SEA_SALT*HS_SEA)*N_EFF;
H_OUT = @SUM(EFFECTS(I): M_BFW(I)*HF_II(I)) + Q_COND_XS + Q_BRINE_XS + Q_DIST_XS
+ (M_WATER(N_EFF) + M_MED_DESAL)*HF_EX + M_SALT(N_EFF)*HS_EX;

M_IN  = (SEA_WATER + SEA_SALT)*N_EFF;
M_OUT = M_WATER(N_EFF) + M_SALT(N_EFF) + M_MED_DESAL;

!Seawater preheater balance;
Q_COND  = Q_COND_PRE  + Q_COND_XS;
Q_BRINE = Q_BRINE_PRE + Q_BRINE_XS;
Q_DIST  = Q_DIST_PRE  + Q_DIST_XS;

CP_SEA_AVG*M_SEA_PRE*(TH_SEA - T_SEA) = Q_COND + Q_BRINE + Q_DIST;

Q_SEA_PRE    = Q_COND_PRE + Q_BRINE_PRE + Q_DIST_PRE;
```

```
Q_SEA_PRE       = (SEA_WATER + SEA_SALT)*N_EFF*CP_SEA_AVG*(TH_SEA - T_SEA);

M_SEA_HOT       = M_SEA_PRE - N_EFF*(SEA_WATER + SEA_SALT);

TH_SEA <= T_C(N_EFF) - DTMIN;
TH_SEA <= T_EFF(N_EFF) - DTMIN;
TH_SEA >= T_SEA;

!Seawater flow rate for cooling;
M_SEA_BYPASS*CP_SEA_AVG*(T_SEA_MAX - T_SEA) = Q_COND_XS + Q_BRINE_XS +
Q_DIST_XS;

(1E6/3600)*Q_MED_TOTAL = Q_COND_XS + Q_BRINE_XS + Q_DIST_XS;

!Seawater pumping energy requirement;
M_SEA_TOTAL = M_SEA_PRE + M_SEA_BYPASS;

!DT calculations for seawater preheaters;
DT_COND_PRE  = T_C(N_EFF) - TH_SEA;
DT1_COND_PRE = T_C(N_EFF) - T_SEA;
DT_BRINE_PRE  = 0.5*(T_EFF(N_EFF) + T_EFF_I(N_EFF)) - TH_SEA; !Average of boiling seawater
and flashing brine temperatures;
DT1_BRINE_PRE = T_EX - T_SEA;
DT_DIST_PRE  = 0.5*(T_C(N_EFF) + T_EFF_II(N_EFF - 1)) - TH_SEA; !Average temperature
between condensate and flashing temp of previous pot;
DT1_DIST_PRE = T_EX - T_SEA;

!DT calculations for evaporators;
@FOR(EFFECTS(I): Q_EFF_VAP(I) = U_EFF(I)/3600*A_EFF_VAP(I)*DT_EFF_VAP(I)); !Evap. area
req. for vaporization;

DT_EFF_SENS(1)  = TC_TVC - TH_SEA;
DT1_EFF_SENS(1) = TC_TVC - T_EFF(1);

@FOR(EFFECTS(I)|I#GE#2: DT_EFF_SENS(I)  = T_C(I-1) - TH_SEA);
@FOR(EFFECTS(I)|I#GE#2: DT1_EFF_SENS(I) = T_C(I-1) - T_EFF(I));

!Pumping power requirements;
(PUMP_EFF/100)*145.038*MED_BRINE_PUMP = 1/(2.20462*DENS_WATER_EFF)*(P_ATM -
P_EFF(N_EFF))*M_WATER(N_EFF);       !Discharge of brine to 1 atm;
(PUMP_EFF/100)*145.038*MED_DIST_PUMP  =
1/(2.20462*DENS_WATER_EFF)*(MED_STORE_P - P_EFF(N_EFF))*M_MED_DESAL;
(PUMP_EFF/100)*145.038*MED_FEED_PUMP  = 1/(2.20462*DENS_WATER)*MED_LINE_DP*(1 -
X_SAL/1000)*M_SEA_TOTAL;
(PUMP_EFF/100)*145.038*MED_DS_PUMP    = 1/(2.20462*DENS_WATER)*(P_TVC -
P_EFF(N_EFF))*@SUM(EFFECTS(I):M_DS(I));
(PUMP_EFF/100)*145.038*MED_BFW_PUMP   = 1/(2.20462*DENS_WATER)*(P_MOT - (P_TVC -
DP_LOSSES))*M_STM_MOT;

PW_PUMP_MED = MED_BRINE_PUMP + MED_DIST_PUMP + MED_FEED_PUMP +
MED_BFW_PUMP + MED_DS_PUMP;     !Pumping power requirement [kW];
```

```
! OVERALL MED DESALINATION PLANT COSTING ----------------------------------------------------;
ACI_DESAL = DCC_MED + DCC_DESAL + CONTIN_DESAL + SC_DESAL;
TAC_DESAL = ACI_DESAL + TOC_MED + OC_DESAL + FOC_DESAL;
!-------------------------------------------------------------------------------------------------------------------;

! MED COSTING ---------------------------------------------------------------------------------------------------;
DCC_MED        = CC_MED_PUMP + CC_MED_CLEAN + CC_MED_SOLIDS;
TOC_MED        = OC_MED_PW;

!MED UNIT SPECIFIC COSTS ---------------------------------------------------------------------------------------;
1E3*CC_MED_PUMP = (50000/PLANT_LIFE) + (234.5/PLANT_LIFE)*PW_PUMP_MED;

1/(1E-3*432/PLANT_LIFE)*CC_MED_CLEAN  = F_FEED_MED;
1/(1E-3*432/PLANT_LIFE)*CC_MED_SOLIDS = F_FEED_MED;
!-------------------------------------------------------------------------------------------------------------------;
OC_MED_PW = OC_MED_INT + OC_MED_PRE + OC_MED_PUMP + OC_MED_POST +
OC_MED_CLEAN + OC_MED_SERVICE;
1/(1E-3*0.191*(24*C_ELECT*365)/3.38)*OC_MED_INT        = PW_PUMP_MED;
1/(1E-3*0.013*(24*C_ELECT*365)/3.38)*OC_MED_PRE        = PW_PUMP_MED;
1/(1E-3*24*C_ELECT*365)*OC_MED_PUMP                    = PW_PUMP_MED;
1/(1E-3*0.177*(24*C_ELECT*365)/3.38)*OC_MED_POST    = PW_PUMP_MED;
1/(1E-3*0.027*(24*C_ELECT*365)/3.38)*OC_MED_CLEAN   = PW_PUMP_MED;
1/(1E-3*0.130*(24*C_ELECT*365)/3.38)*OC_MED_SERVICE = PW_PUMP_MED;

! AUXILLIARY COSTS FOR THE REST OF PLANT -----------------------------------------------------------------------;
DCC_DESAL     = CC_SITE + CC_INTAKE + CC_PRETREAT + CC_PIPING + CC_POST +
CC_DISPOSE + CC_BUILD + CC_ELEC + CC_AUX + CC_START;
1/(1E-3*432/PLANT_LIFE)*CC_SITE         = F_FEED_MED;
1/(1E-3*1963.6/PLANT_LIFE)*CC_INTAKE  = F_FEED_MED ;
1/(1E-3*2700/PLANT_LIFE)*CC_PRETREAT  = F_FEED_MED ;
1/(1E-3*1369.61/PLANT_LIFE)*CC_PIPING = F_FEED_MED ;
1/(1E-3*785.45/PLANT_LIFE)*CC_POST    = F_FEED_MED ;
1/(1E-3*1296/PLANT_LIFE)*CC_DISPOSE             = F_FEED_MED ;
1E3*CC_BUILD = 49.369/PLANT_LIFE*F_PERM_MED + 12185/PLANT_LIFE +
1728/PLANT_LIFE*(F_FEED_MED );
1/(1E-3*614/PLANT_LIFE*(86.4^0.65))*CC_ELEC = F_PERM_MED^0.65;
1/(1E-3*785.45/PLANT_LIFE)*CC_AUX   = F_FEED_MED;
1/(1E-3*785.45/PLANT_LIFE)*CC_START           = F_FEED_MED;
!-------------------------------------------------------------------------------------------------------------------;
SC_DESAL       = CC_FINANCE + CC_PERMIT;
(1/CF_FIN)*CC_FINANCE = DCC_DESAL + DCC_MED;
(1/CF_PERM)*CC_PERMIT = DCC_DESAL + DCC_MED;
!-------------------------------------------------------------------------------------------------------------------;
 (1/CF_CONTIN)*CONTIN_DESAL         = DCC_DESAL + DCC_MED;

!-------------------------------------------------------------------------------------------------------------------;
OC_DESAL       = OC_CHEM + OC_DISPOSE;
1/(1E-3*1576.8)*OC_CHEM           = F_PERM_MED;
1/(1E-3*315.36)*OC_DISPOSE = F_FEED_MED;
!-------------------------------------------------------------------------------------------------------------------;
FOC_DESAL     = FOC_LABOR + FOC_MAIN + FOC_ENVIRON + FOC_IND + FOC_SPARE;
1/(1E-3*473.04)*FOC_LABOR  = F_PERM_MED;
```

```
1/(1E-3*630.72)*FOC_MAIN        = F_FEED_MED;
1/(1E-3*50.46)*FOC_ENVIRON   = F_FEED_MED;
1/(1E-3*756.86)*FOC_IND          = F_FEED_MED;
1/(CF_FOC*PLANT_LIFE)*FOC_SPARE = DCC_DESAL + DCC_MED;
!-------------------------------------------------------------------------------------------------------------------------------------;

!=============================================================================
********************** RO MODEL CONFIGURATION SECTION **********************
!=============================================================================
M_RO_DESAL = 2.20462*DENS_WATER*F_PERM_RO;              !Mass flow rate [lb/s];

! FEED BALANCE ------------------------------------------------------------------------------------------------------------------;
F_FEED_RO = @SUM(SINK(J): F_F(J)) + F_F_RO_PERM;
!-------------------------------------------------------------------------------------------------------------------------------------;

! RO FEED MIXER BALANCE ---------------------------------------------------------------------------------------------------------;
@FOR(SINK(J):F_RO(J) = @SUM(SOURCE(I):F_BS(I,J)) + @SUM(SOURCE(I):F_PS(I,J)) + F_F(J));
                    !Total Balance;
@FOR(SINK(J):@FOR(COMP(K): F_RO(J)*X_RO(J,K) = @SUM(SOURCE(I): F_BS(I,J)*X_BS(I,K))
+ @SUM(SOURCE(I):F_PS(I,J)*X_PS(I,K)) + F_F(J)*X_FEED(K))); !Component;
!-------------------------------------------------------------------------------------------------------------------------------------;

! RO SEPARATION BALANCE ---------------------------------------------------------------------------------------------------------;
@FOR(SOURCE(I): F_RO(I) = F_B(I) + F_P(I));                                    !RO unit balance;
@FOR(SOURCE(I): @FOR(COMP(K): F_RO(I)*X_RO(I,K) = F_B(I)*X_BS(I,K) +
F_P(I)*X_PS(I,K))); !RO unit component balance;

@FOR(SOURCE(I): @FOR(COMP(K): X_RO(I,K) = 100/(100 - REJ(K))* X_PS(I,K))); !Relationship
between inlet composition on oulet conc.;
@FOR(SOURCE(I): 100*F_P(I) = REC(I)*F_RO(I));                                  !Recovery of permeate;

@FOR(SINK(J): N_MOD(J)*F_P_MOD(J) = F_P(J));                        !Number of modules per unit ;
@FOR(SINK(J): N_MOD(J)*MOD_PERM_MAX >= F_P(J));!Maximum permeate flow from module ;
@FOR(SINK(J): (1/MOD_FEED_MIN)*F_RO(J) >= N_MOD(J));       !Minimum feed flow to module;


!Max number of modules increases for the single stage RO unit
!=============================================================================
@FOR(SINK(J): N_MOD(J) <= N_MOD_MAX*N_SKIDS); !Maximum number of modules per skid;
!=============================================================================

@FOR(SINK(J): RO_PI1(J) >= 0);                      !Lower range for RO membrane permeability;
@FOR(SINK(J): RO_PI1(J) <= 25*RO_PERM_BIN1(J));


@FOR(SINK(J): RO_PI2(J) >= 25*RO_PERM_BIN2(J));!Middle range for RO membrane permeability;
@FOR(SINK(J): RO_PI2(J) <= 200*RO_PERM_BIN2(J));

@FOR(SINK(J): RO_PI3(J) >= 200*RO_PERM_BIN3(J));!Upper range for RO membrane permeability;
@FOR(SINK(J): RO_PI3(J) <= 1000*RO_PERM_BIN3(J));

@FOR(SINK(J): RO_A_PI1(J) = 125*RO_PERM_BIN1(J));  !RO membrane permeability;
```

```
@FOR(SINK(J): RO_A_PI2(J) = 125*RO_PERM_BIN2(J) -  11*(RO_PI2(J) -
25*RO_PERM_BIN2(J))/35);
@FOR(SINK(J): RO_A_PI3(J) =  70*RO_PERM_BIN3(J) - 0.1*(RO_PI3(J) -
200*RO_PERM_BIN3(J)));

@FOR(SINK(J): RO_A_PI(J) = RO_A_PI1(J) + RO_A_PI2(J) + RO_A_PI3(J));!Addition of
permeability based on ranges and Big-M consrt.;
@FOR(SINK(J): RO_PI(J)  = RO_PI1(J) + RO_PI2(J) + RO_PI3(J));   !Addition of osmotic press. Big-M
consrt.;
@FOR(SINK(J): RO_PERM_BIN1(J) + RO_PERM_BIN2(J) + RO_PERM_BIN3(J) = 1); !Select ONLY
ONE range for osmotic pressure;

@FOR(SINK(J): RO_PI(J) = 0.99886*1.12*(273 + RO_FEED_TEMP)*@SUM(COMP(K):
X_RO(J,K)/RO_FEED_MW(K)));  !Feed osmotic press. calc. NOTICH: ppm - mg/L;

@FOR(SINK(J): F_P_MOD(J)*22824.432/(10.7639*AREA_MEM) = 1E-
3*RO_A_PI(J)*RO_TCF*RO_FF*(RO_P_FEED(J) - 0.5*RO_MOD_DP(J) - RO_P_P(J) - RO_PI_PSI(J)
- 1.12*(273 + RO_FEED_TEMP)*@SUM(COMP(K):
(0.99886*X_RO(J,K))*(REJ(K)/100)/RO_FEED_MW(K))));

@FOR(SINK(J): @LOG(RO_PI_PSI(J)) = @LOG(RO_PI(J)) + @LOG(RO_PSI(J)));
@FOR(SINK(J): RO_PSI(J) <= RO_PSI_MAX(J)); !Max. module recovery permissible based on feed
conc.;
@FOR(SINK(J): REC(J) = 91.345 - 91.345*@EXP(-0.8265*RO_PSI(J)));
@FOR(SINK(J): RO_DP_MAX*(N_MOD(J))^2 = (0.04*(15.8503*0.5)^2)*(F_RO(J) + F_B(J))^2);

@FOR(SINK(J): RO_P_FEED(J) <= RO_P_MAX);              !RO feed pressure maximum constraint;
@FOR(SINK(J): RO_P_B(J)  = RO_P_FEED(J) - RO_DP_MAX);
@FOR(SINK(J): DP_FEED(J) = RO_P_FEED(J) - P_FEED);

@FOR(SOURCE(I): @FOR(SINK(J)|I#NE#J: RO_P_FEED(J) - RO_P_B(I) = DP_BS1(I,J) -
DP_BS2(I,J) - DP_BS3(I,J)));
@FOR(SOURCE(I): @FOR(SINK(J)|I#NE#J: DP_BS1(I,J) <= (RO_P_MAX -
P_FEED)*DP_BS_BIN1(I,J)));
@FOR(SOURCE(I): @FOR(SINK(J)|I#NE#J: DP_BS2(I,J) <= ERD_DP_MIN*DP_BS_BIN2(I,J)));
@FOR(SOURCE(I): @FOR(SINK(J)|I#NE#J: DP_BS3(I,J) >= ERD_DP_MIN*DP_BS_BIN3(I,J)));
@FOR(SOURCE(I): @FOR(SINK(J)|I#NE#J: DP_BS3(I,J) <= (RO_P_MAX -
P_FEED)*DP_BS_BIN3(I,J)));
@FOR(SOURCE(I): @FOR(SINK(J)|I#NE#J: DP_BS_BIN1(I,J) + DP_BS_BIN2(I,J) +
DP_BS_BIN3(I,J) = 1));

@FOR(SOURCE(I): @FOR(SINK(J)|I#NE#J: DP_PS(I,J) = RO_P_FEED(J) - P_FEED));
@FOR(SINK(J): DP_BRINE(J) = RO_P_B(J) - P_FEED);

@FOR(SINK(J)  :                                          145.038*F_POWER(J) =
(100/PUMP_EFF)*F_F(J)*DP_FEED(J));
@FOR(SOURCE(I): @FOR(SINK(J)|I#NE#J: 145.038*BS_POWER(I,J) =
(100/PUMP_EFF)*F_BS(I,J)*DP_BS1(I,J)));
@FOR(SOURCE(I): @FOR(SINK(J)|I#NE#J: 145.038*(100/ERD_EFF)*BS_ERD(I,J)  =
F_BS(I,J)*DP_BS3(I,J)));
@FOR(SOURCE(I): @FOR(SINK(J)|I#NE#J: 145.038*PS_POWER(I,J) =
(100/PUMP_EFF)*F_PS(I,J)*DP_PS(I,J)));
```

```
@FOR(SOURCE(I):                                    145.038*(100/ERD_EFF)*BRINE_ERD(I)  =
F_BS_BRINE(I)*DP_BRINE(I));

PW_PUMP_RO = @SUM(SINK(J): F_POWER(J)) + @SUM(SOURCE(I): @SUM(SINK(J)|I#NE#J:
BS_POWER(I,J) + PS_POWER(I,J)));
PW_ERD_RO  = @SUM(SOURCE(I): BRINE_ERD(I)) + @SUM(SOURCE(I):
@SUM(SINK(J)|I#NE#J: BS_ERD(I,J)));
!-------------------------------------------------------------------------------------------------------------------------;

! RO EFFLUENT SPLIT ------------------------------------------------------------------------------------------------------;
@FOR(SOURCE(I): F_B(I) = @SUM(SINK(J): F_BS(I,J)) + F_BS_BRINE(I));!Brine splitter balance;
@FOR(SOURCE(I): F_P(I) = @SUM(SINK(J): F_PS(I,J)) + F_PS_PERM(I));  !Permeate splitter
balance;
!-------------------------------------------------------------------------------------------------------------------------;


! PRODUCT MIXER BALANCE --------------------------------------------------------------------------------------------------;
F_BRINE_RO = @SUM(SOURCE(I): F_BS_BRINE(I));                    !Final brine stream balance;
@FOR(COMP(K): F_BRINE_RO*X_BRINE(K) =
@SUM(SOURCE(I):F_BS_BRINE(I)*X_BS(I,K)));!Component balance on final Brine stream;

F_PERM_RO = @SUM(SOURCE(I):F_PS_PERM(I)) + F_F_RO_PERM;!Final permeate stream
balance;
@FOR(COMP(K): F_PERM_RO*X_PERM(K) = @SUM(SOURCE(I):F_PS_PERM(I)*X_PS(I,K)) +
F_F_RO_PERM*X_FEED(K));      !Component balance on final Permeater stream;

!Mg and Ca concentration requirements after POST Treatment;
F_PERM_RO*X_PERM(2) + (1/0.99886)*M_POST_MG = F_PERM_RO*X_PERM_MG;!Post
Treatment adjustment of Mg;
F_PERM_RO*X_PERM(3) + (1/0.99886)*M_POST_CA = F_PERM_RO*X_PERM_CA;!Post
Treatment adjustment of Ca;
M_POST_MGCO3 = (RO_FEED_MW(2) + 60.008)/RO_FEED_MW(2)*M_POST_MG; !Final flow req.
of MgCO3;
M_POST_CACO3 = (RO_FEED_MW(3) + 60.008)/RO_FEED_MW(3)*M_POST_CA; !Final flow req.
of CaCO3;

@SUM(COMP(K): F_PERM_RO*X_PERM(K)) + (1/0.99886)*M_POST_MGCO3 +
(1/0.99886)*M_POST_CACO3 = F_PERM_RO*X_PERM_MAX;      !Post Treatment constraint on
conc.;
!-------------------------------------------------------------------------------------------------------------------------;

! OVERALL RO SYSTEM BALANCE ----------------------------------------------------------------------------------------------;
F_FEED_RO = F_BRINE_RO + F_PERM_RO;
@FOR(COMP(K): F_FEED_RO*X_FEED(K) = F_BRINE_RO*X_BRINE(K) +
F_PERM_RO*X_PERM(K));
!-------------------------------------------------------------------------------------------------------------------------;

! RO COSTING -------------------------------------------------------------------------------------------------------------;
DCC_RO          = CC_RO_SKID + CC_RO_FILTER + CC_RO_MOD + CC_RO_PUMP +
CC_RO_ERD + CC_RO_CLEAN + CC_RO_SOLIDS + CC_RO_INSTR;
TOC_RO          = OC_RO_PW + OC_RO_MEM;

! CAPITAL COST FOR RO NETWORK --------------------------------------------------------------------------------------------;
```

```
CC_RO_SKID                = 1E-3*250000/PLANT_LIFE*N_RO*N_SKIDS;
CC_RO_FILTER= 1E-
3*112836/PLANT_LIFE*(F_FEED_RO^0.831)*(1.2*N_RO*N_SKIDS)*(86.4/(3600*24*N_RO*N_SKI
DS))^0.831;
1/(1E-3*5000/PLANT_LIFE)*CC_RO_MOD = @SUM(SINK(J): N_MOD(J));

CC_RO_PUMP = @SUM(SINK(J): F_CC_PUMP1(J) + F_CC_PUMP2(J)) +
@SUM(SOURCE(I):@SUM(SINK(J)|I#NE#J: BS_CC_PUMP1(I,J) + BS_CC_PUMP2(I,J) +
PS_CC_PUMP1(I,J) + PS_CC_PUMP2(I,J)));
CC_RO_ERD  = @SUM(SOURCE(I): BRINE_CC_ERD1(I) + BRINE_CC_ERD2(I)) +
@SUM(SOURCE(I):@SUM(SINK(J)|I#NE#J: BS_CC_ERD1(I,J) + BS_CC_ERD2(I,J)));

@FOR(SINK(J): 1/(0.2345/PLANT_LIFE)*F_CC_PUMP2(J) = 50/0.2345 + F_POWER(J));
@FOR(SOURCE(I): @FOR(SINK(J)|I#NE#J: 1/(0.2345/PLANT_LIFE)*BS_CC_PUMP2(I,J) =
50/0.2345 + BS_POWER(I,J)));
@FOR(SOURCE(I): @FOR(SINK(J)|I#NE#J: 1/(0.2345/PLANT_LIFE)*PS_CC_PUMP2(I,J) =
50/0.2345 + PS_POWER(I,J)));
@FOR(SOURCE(I): @FOR(SINK(J)|I#NE#J: BS_CC_ERD2(I,J) =
85/PLANT_LIFE*(BS_ERD(I,J)*0.0134)^0.65));
@FOR(SOURCE(I): BRINE_CC_ERD2(I) = 85/PLANT_LIFE*(BRINE_ERD(I)*0.0134)^0.65);

1/(1E-3*432/PLANT_LIFE)*CC_RO_CLEAN  = F_FEED_RO;
1/(1E-3*432/PLANT_LIFE)*CC_RO_SOLIDS = F_FEED_RO;
CC_RO_INSTR  = 1E-3/PLANT_LIFE*(300000 + 65000*N_RO*N_SKIDS);
!-------------------------------------------------------------------------------------------------------------;
OC_RO_PW = OC_RO_INT + OC_RO_PRE + OC_RO_PUMP + OC_RO_POST + OC_RO_CLEAN +
OC_RO_SERVICE;
1/(1E-3*0.191*(24*C_ELECT*365)/3.38)*OC_RO_INT          = PW_PUMP_RO - PW_ERD_RO;
1/(1E-3*0.013*(24*C_ELECT*365)/3.38)*OC_RO_PRE          = PW_PUMP_RO - PW_ERD_RO;
1/(1E-3*1.000*24*C_ELECT*365)*OC_RO_PUMP                = PW_PUMP_RO - PW_ERD_RO;
1/(1E-3*0.177*(24*C_ELECT*365)/3.38)*OC_RO_POST    = PW_PUMP_RO - PW_ERD_RO;
1/(1E-3*0.027*(24*C_ELECT*365)/3.38)*OC_RO_CLEAN   = PW_PUMP_RO - PW_ERD_RO;
1/(1E-3*0.130*(24*C_ELECT*365)/3.38)*OC_RO_SERVICE = PW_PUMP_RO - PW_ERD_RO;
!-------------------------------------------------------------------------------------------------------------;
OC_RO_MEM      = OC_RO_MEMBRANE + OC_RO_FILTER;
1/(1E-3*2.5*AREA_MEM)*OC_RO_MEMBRANE = @SUM(SINK(J): N_MOD(J));
1/(1E-3*23.097*2.94)*OC_RO_FILTER    = N_RO*N_SKIDS*F_FEED_RO;
!-------------------------------------------------------------------------------------------------------------;

! OVERALL RO DESALINATION PLANT COSTING ------------------------------------------------------;
ACI_RO_DESAL = DCC_RO + DCC_RO_DESAL + CONTIN_RO_DESAL + SC_RO_DESAL;
TAC_DESAL_RO = ACI_RO_DESAL + TOC_RO + OC_RO_DESAL + FOC_RO_DESAL;
!-------------------------------------------------------------------------------------------------------------;
DCC_RO_DESAL = CC_RO_SITE + CC_RO_INTAKE + CC_RO_PRETREAT + CC_RO_PIPING +
CC_RO_POST + CC_RO_DISPOSE + CC_RO_BUILD + CC_RO_ELEC + CC_RO_AUX +
CC_RO_START;
1/(1E-3*432/PLANT_LIFE)*CC_RO_SITE                      = F_FEED_RO;
1/(1E-3*1963.6/PLANT_LIFE)*CC_RO_INTAKE          = F_FEED_RO;
1/(1E-3*2700/PLANT_LIFE)*CC_RO_PRETREAT                 = F_FEED_RO;
1/(1E-3*1369.61/PLANT_LIFE)*CC_RO_PIPING         = F_FEED_RO;
1/(1E-3*785.45/PLANT_LIFE)*CC_RO_POST            = F_FEED_RO;
1/(1E-3*1296/PLANT_LIFE)*CC_RO_DISPOSE           = F_FEED_RO;
1/(1E-3*785.45/PLANT_LIFE)*CC_RO_AUX             = F_FEED_RO;
```

```
1/(1E-3*785.45/PLANT_LIFE)*CC_RO_START                = F_FEED_RO;
1/(1E-3*614/PLANT_LIFE*(86.4^0.65))*CC_RO_ELEC  = F_PERM_RO^0.65;
1E3*CC_RO_BUILD = 49.369/PLANT_LIFE*F_PERM_RO + 12185/PLANT_LIFE +
1728/PLANT_LIFE*F_FEED_RO;
!-------------------------------------------------------------------------------------------------------------------------------;
SC_RO_DESAL  = CC_RO_SERVICE + CC_RO_DEVELOP + CC_RO_FINANCE +
CC_RO_PERMIT;
1/(1E-3*2304/PLANT_LIFE)*CC_RO_SERVICE     = F_FEED_RO;
1/(1E-3*1944/PLANT_LIFE)*CC_RO_DEVELOP   = F_FEED_RO;
(1/CF_FIN)*CC_RO_FINANCE    = DCC_RO_DESAL + DCC_RO;
(1/CF_PERM)*CC_RO_PERMIT   = DCC_RO_DESAL + DCC_RO;
!-------------------------------------------------------------------------------------------------------------------------------;
 (1/CF_RO_CONTIN)*CONTIN_RO_DESAL         = DCC_RO_DESAL + DCC_RO;
!-------------------------------------------------------------------------------------------------------------------------------;
OC_RO_DESAL = OC_RO_CHEM + OC_RO_DISPOSE;
1/(1E-3*378.4)*OC_RO_CHEM    = F_FEED_RO;
1/(1E-3*315.36)*OC_RO_DISPOSE = F_FEED_RO;
!-------------------------------------------------------------------------------------------------------------------------------;
FOC_RO_DESAL = FOC_RO_LABOR + FOC_RO_MAIN + FOC_RO_ENVIRON + FOC_RO_IND +
FOC_RO_MISC;
1/(1E-3*378.43)*FOC_RO_LABOR    = F_FEED_RO;
1/(1E-3*630.72)*FOC_RO_MAIN     = F_FEED_RO;
1/(1E-3*50.46)*FOC_RO_ENVIRON   = F_FEED_RO;
1/(1E-3*756.86)*FOC_RO_IND      = F_FEED_RO;
1/(CF_RO_FOC*PLANT_LIFE)*FOC_RO_MISC = DCC_RO_DESAL + DCC_RO;
!-------------------------------------------------------------------------------------------------------------------------------;

!=============================================================================
********************* WATER INTEGRATION VIA DIRECT RECYCLE ********************
!=============================================================================
M_RO_PERM  = 3.6/2*2.20462*DENS_WATER*F_F_RO_PERM;!Mass flow of bypass seawater for
RO outlet to meet desired conc. [ton/hr];
M_MED_PERM = 3.6/2*2.20462*DENS_WATER*F_F_MED_PERM;!Mass flow of bypass seawater
for MED outlet to meet pot. water conc. [ton/hr];

!WATER SOURCES;
M_SR1     = M_PRE_WATER;                    !Pretreated water from process [ton/hr];
M_SR2     = 3.6/2*M_RO_DESAL;               !Desalinated water from RO process [ton/hr];
M_SR3     = 3.6/2*M_MED_DESAL;              !Desalinated water from MED process [ton/hr];
M_SR4      = M_RO_PERM + M_MED_PERM;        !Seawater bypass for mixing [ton/hr];

!WATER SINKS;
M_SK1     = M_SAT_WATER;            !Nat. Gas saturator water requirement [ton/hr];
M_SK2     = M_ATR;                  !ATR reactor steam requirement [ton/hr];
M_SK3     = M_CO2_WATER;            !CO2 removal unit water make-up requirement [ton/hr];
M_SK4     = CT_WATER_LOSS;          !Cooling Tower water make-up requirement [ton/hr];

CALC:
!WATER SOURCE CONC.;
Z_SR1_OIL = X_ATR_PWATER_OIL;
Z_SR1_TDS = X_ATR_PWATER_TDS;

Z_SR2_OIL = X_DESAL_OIL;
```

```
Z_SR2_TDS = 1000*X_PERM_MAX;

Z_SR3_OIL = X_DESAL_OIL;
Z_SR3_TDS = X_MED_TDS;

Z_SR4_TDS = 1E3*X_SAL;

!WATER SINK MAX. CONC.;
Z_SK1_OIL = X_BFW_OIL;
Z_SK1_TDS = X_BFW_TDS;

Z_SK2_OIL = X_BFW_OIL;
Z_SK2_TDS = X_BFW_TDS;

Z_SK3_OIL = X_PWATER_OIL;
Z_SK3_TDS = X_PWATER_TDS;

Z_SK4_OIL = X_PWATER_OIL;
Z_SK4_TDS = X_PWATER_TDS;

ENDCALC

!SOURCE BALANCES;
M_SR1 = M_SR1_SK1 + M_SR1_SK2 + M_SR1_SK3 + M_SR1_SK4 + M_WASTE;
M_SR2 = M_SR2_SK1 + M_SR2_SK2 + M_SR2_SK3 + M_SR2_SK4 + M_RO_EXPORT;
M_SR3 = M_SR3_SK1 + M_SR3_SK2 + M_SR3_SK3 + M_SR3_SK4 + M_MED_EXCESS;

!SINK OVERALL MASS BALANCES;
M_SK1 = M_SR1_SK1 + M_SR2_SK1 + M_SR3_SK1;
M_SK2 = M_SR1_SK2 + M_SR2_SK2 + M_SR3_SK2;
M_SK3 = M_SR1_SK3 + M_SR2_SK3 + M_SR3_SK3;
M_SK4 = M_SR1_SK4 + M_SR2_SK4 + M_SR3_SK4;

!SINK OIL BALANCES;
Z_SK1_OIL*M_SK1 >= Z_SR1_OIL*M_SR1_SK1 + Z_SR2_OIL*M_SR2_SK1 +
Z_SR3_OIL*M_SR3_SK1;
Z_SK2_OIL*M_SK2 >= Z_SR1_OIL*M_SR1_SK2 + Z_SR2_OIL*M_SR2_SK2 +
Z_SR3_OIL*M_SR3_SK2;
Z_SK3_OIL*M_SK3 >= Z_SR1_OIL*M_SR1_SK3 + Z_SR2_OIL*M_SR2_SK3 +
Z_SR3_OIL*M_SR3_SK3;
Z_SK4_OIL*M_SK4 >= Z_SR1_OIL*M_SR1_SK4 + Z_SR2_OIL*M_SR2_SK4 +
Z_SR3_OIL*M_SR3_SK4;

!SINK TDS BALANCES;
Z_SK1_TDS*M_SK1 >= Z_SR1_TDS*M_SR1_SK1 + Z_SR2_TDS*M_SR2_SK1 +
Z_SR3_TDS*M_SR3_SK1;
Z_SK2_TDS*M_SK2 >= Z_SR1_TDS*M_SR1_SK2 + Z_SR2_TDS*M_SR2_SK2 +
Z_SR3_TDS*M_SR3_SK2;
Z_SK3_TDS*M_SK3 >= Z_SR1_TDS*M_SR1_SK3 + Z_SR2_TDS*M_SR2_SK3 +
Z_SR3_TDS*M_SR3_SK3;
Z_SK4_TDS*M_SK4 >= Z_SR1_TDS*M_SR1_SK4 + Z_SR2_TDS*M_SR2_SK4 +
Z_SR3_TDS*M_SR3_SK4;
```

```
M_MED_EXPORT = M_MED_EXCESS + M_MED_PERM;

(2.20462*DENS_WATER)*F_DESAL_EXP = 2/3.6*(M_RO_EXPORT + M_MED_EXPORT);

!SEAWATER BYPASS FLOW FOR MED WATER TO MEET POTABLE WATER SPECS.;
Z_SR2_TDS*M_RO_EXPORT + Z_SR3_TDS*M_MED_EXCESS  + Z_SR4_TDS*M_MED_PERM =
X_POT_WATER*(M_RO_EXPORT + M_MED_EXCESS + M_MED_PERM);

!=========================================================================
********************** POWER DISTRIBUTION SECTION ***************************
!=========================================================================

1E-3*AVAIL_PW_TOT = PW_PROCESS_REQ + 1E-3*PW_HEN_TOTAL + 1E-3*PW_PUMP_MED
+ 1E-3*PW_PUMP_RO - 1E-3*PW_ERD_RO + 1E-3*PW_EXPORT;

1E3*SYS_PUMP_PW = REQ_PW_PUMP + PW_PUMP_RO - PW_ERD_RO + PW_PUMP_MED;
```